



Mark-1 PB-FHR Technical Description

Technical Description of the “Mark 1” Pebble-Bed Fluoride-Salt-Cooled High-Temperature Reactor (PB-FHR) Power Plant

Charalampos “Harry” Andreades
Anselmo T. Cisneros
Jae Keun Choi
Alexandre Y.K. Chong
Massimiliano Fratoni
Sea Hong
Lakshana R. Huddar
Kathryn D. Huff
David L. Krumwiede
Michael R. Laufer
Madicken Munk
Raluca O. Scarlat
Nicolas Zweibaum
Ehud Greenspan
Per F. Peterson

UCBTH-14-002

September 30, 2014
Department of Nuclear Engineering
University of California, Berkeley

This research is being performed using funding received from the U.S. Department of Energy Office of Nuclear Energy’s Nuclear Energy University Programs.



Executive Summary

This report describes the results of work at the University of California, Berkeley (UCB) to develop an initial pre-conceptual design for a small, modular 236-MWth pebble-bed fluoride-salt-cooled, high-temperature reactor (PB-FHR). This design study contributes to a larger U.S. Department of Energy Integrated Research Project (IRP) collaboration with the Massachusetts Institute of Technology and the University of Wisconsin, Madison to establish the technical basis to design, license, and commercially deploy FHRs.

The Mark-1 (Mk1) PB-FHR design described here differs from previous FHR designs developed and published by UCB and others. It uses a nuclear air-Brayton combined cycle (NACC) based upon a modified General Electric 7FB gas turbine, designed to produce 100 MWe of base-load electricity when operated with only nuclear heat, and to increase this power output to 242 MWe using gas co-firing for peak electricity generation. Due to the high thermal efficiency of the NACC system, the steam-bottoming condenser of the Mk1 PB-FHR requires only 40% of the cooling water supply that is required for a conventional light water reactor (LWR), for each MWh of base-load generation. As with conventional natural-gas combined cycle (NGCC) plants, this makes the efficiency penalty of using dry cooling with air-cooled condensers much smaller, enabling economic operation in regions where water is scarce.

The primary purpose of the Mk1 design, with its co-firing capability, is to provide a new value proposition for nuclear power. The new value proposition for NACC arises from additional revenues earned by providing flexible grid support services to handle the ever-increasing demand for dispatchable peak power, in addition to traditional base-load electrical power generation. Because under base-load operation NACC power conversion has lower fuel costs than NGCC, and under peaking operation has higher efficiency in converting natural gas to electricity than NGCC, NACC plants will always dispatch before conventional NGCC plants.

The reference configuration for the Mk1 site uses 12 Mk1 units, as shown in Fig. ES-1, capable of producing 1200 MWe of base load electricity, and ramping to a peak power output of 2900 MWe. The Mk1 design uses the same steel-plate composite wall modular construction methods as the Westinghouse AP1000, and its modular components can be manufactured in the same factories. A Mk1 reactor uses 10 structural modules, so the total number of structural modules needed to build a 12-unit station is quite similar to the ~120 structural modules used to build an AP1000 reactor. Estimated quantities of steel and concrete needed to construct a Mk1 station compare favorably, per MWe, with requirements for LWRs. The major difference between construction of a Mk1 station and an AP1000 is the highly repetitive construction tasks for the Mk1 station, arising from the construction of 12 identical units.

PB-FHR fuel pebbles are 3.0 cm in diameter, smaller than golf balls (4.3 cm). Four Mk1 pebbles can provide electricity for a full year for an average U.S. household, which in 2011 consumed 11.3 MWe-hr. These four small pebbles are far less than the 8.1 tons of anthracite coal, or 17 tons of lignite coal, needed to produce the same amount of electricity using a coal power plant.

Each Mk1 pebble contains 1.5 g of uranium encapsulated inside 4730 coated particles. This is only slightly more than the 0.9 g of uranium in 4150 particles in cylindrical, 1.25-cm diameter, 2.54-cm long Advanced Gas Reactor fuel compacts that have provided outstanding performance

in recent irradiation tests in the Idaho National Laboratory Advanced Test Reactor. Due to the high power density of the Mk1 core compared to modular helium-cooled reactors (MHRs), Mk1 pebbles reach full depletion in 1.4 years, compared to 2.5 years in a MHR and over 3 years for LWR fuel, so fuel testing and qualification can be performed more rapidly than for conventional LWR and MHR fuels. This fact has important programmatic implications, because it means that fuel testing and qualification, which would normally be time consuming, is unlikely to occupy the critical path for development of FHRs that use pebble fuel.

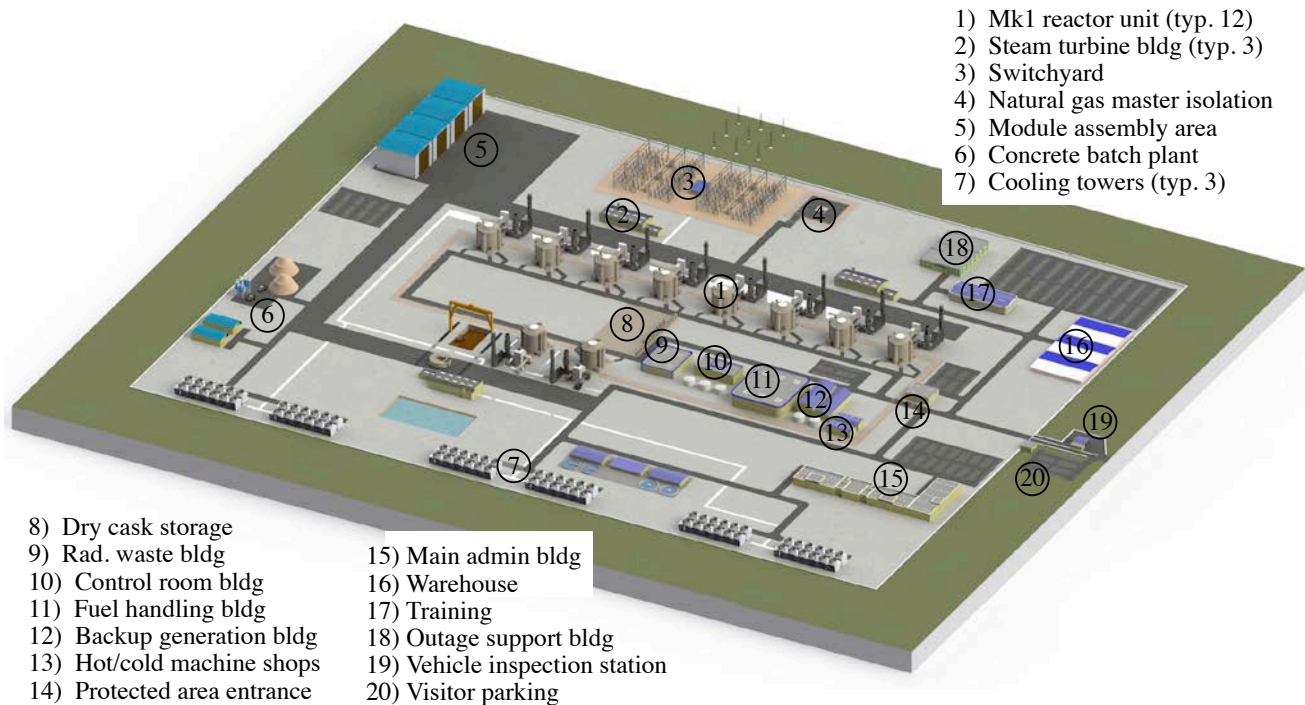


Figure ES-1 Reference site arrangement for a 12-unit PB-FHR plant, capable of producing 1200 MWe base load and 2900 MWe peak.

FHRs produce significantly more tritium than current LWRs, but less than current heavy water reactors. Analysis of the Mk1 design, with its well-defined core and heat exchanger surface areas, shows that graphite surfaces will be the most important sink to recover and remove this tritium. This conclusion generalizes to all FHRs, which will have much larger graphite surface areas than molten-salt-fueled reactors. The key goal for FHR tritium control is to limit tritium losses to heat exchangers. In the Mk1 design, tritium diffusion through heat exchangers is controlled by the use of an aluminized metal coating on the outside of heat exchanger tubes, which forms an impermeable aluminum oxide layer that self-heals via oxidation with the high-temperature air contacting the outside of the tubes.

The Mk1 design implements several other innovative features. The Mk1 PB-FHR does not use an intermediate coolant loop and instead directly heats the power conversion fluid. It eliminates the conventional reactor guard vessel used in sodium fast reactors and instead uses a refractory reactor cavity liner system. All components for the Mk1 design are rail-transportable. As with previous FHR conceptual designs, the new Mk1 PB-FHR design presented here provides a basis to develop safety models, perform fuel cycle analyses, and assess the potential economics of FHRs compared to other reactor technologies.

Contents

1	Mark-1 PB-FHR Design Overview	12
1.1	Mk1 Reactor Design Overview	15
1.2	Mk1 Reactor Building Arrangement	16
1.3	Mk1 Reference 12-Unit Site Arrangement	20
1.4	Mk1 Modular Design and Construction	23
1.5	Mk1 Materials Quantities	26
1.6	Mk1 Structural Materials Selection	29
1.6.1	Mk1 structural design approach	30
1.6.2	Mk1 structural material selection criteria	31
1.7	Mk1 Fuel Development and Qualification	32
1.8	Comparison with Other Reactors	33
1.9	Organization of Report	35
2	Mark-1 Nuclear Heat Supply	36
2.1	Reactor Internals System	36
2.1.1	Fuel and reflector pebbles	36
2.1.2	Core design	39
2.1.3	Pebble injection subsystem	41
2.1.4	Graphite structures	43
2.1.5	Core barrel and upper core support structures	47
2.1.6	Primary coolant flow path description	48
2.2	Reactivity Control and Monitoring System	55
2.2.1	Buoyant control rod subsystem	55
2.2.2	Shutdown blade subsystem	57
2.2.3	Drive subsystem	58
2.2.4	Anticipated Transient With Scram (ATWS)	59
2.2.5	Reactivity monitoring	61
2.3	Direct Reactor Auxiliary Cooling System	62
2.4	Reactor Vessel and Cavity/Containment Systems	67
2.4.1	Thermal expansion and stress management	68
2.4.2	Reactor vessel and support skirt	69
2.4.3	Reactor cavity insulation subsystem	70
2.4.4	Reactor cavity cooling subsystem	73
2.4.5	Reactor containment penetration subsystem	75
2.4.6	Electrical heating subsystem	76
2.4.7	Steel-plate composite walls	77
2.4.8	Considerations for reactor vessel replacement and plant decommissioning	77
3	Mark-1 Heat Transport	79
3.1	Primary Loop “Gas-Gap” Subsystem	79
3.1.1	Hot well “gas-gap” subsystem	81
3.1.2	Cold-leg stand pipe “gas-gap” subsystem	82
3.1.3	Additional regulatory considerations	84
3.2	Main Salt Piping System	84
3.2.1	Hot leg and cross-over legs subsystems	84
3.2.2	Cold legs subsystem	85
3.2.3	Drain tank subsystem	85
3.3	Main Salt Pump System	85
3.4	Coiled Tube Air Heater System	87

3.5	Main salt freeze protection and recovery	93
3.5.1	Prior experience with freeze protection and recovery	93
3.5.2	Main salt piping insulation and trace heating subsystem.....	93
3.5.3	Freeze protection and recovery in Mk1 heat exchangers.....	94
3.6	Warm and Hot Air Duct System.....	94
3.7	Normal Shutdown Cooling and Maintenance Heat Removal System	96
4	Mark-1 Main Support Systems.....	97
4.1	Tritium Control and Recovery.....	97
4.1.1	Tritium absorption by graphite	97
4.1.2	Tritium permeation barrier.....	99
4.1.3	Tritium mass transfer in main salt	100
4.2	Beryllium Control and Radiation Protection	101
4.2.1	General issues for beryllium and radiation safety.....	102
4.2.2	Building ventilation	102
4.2.3	CTAH tube and manifold leaks	103
4.2.4	Coolant activation and main salt pipe shielding	104
4.3	Coolant Chemistry, Particulates, and Inventory Control	104
4.3.1	Main salt cold traps and spray contacting.....	104
4.3.2	Main salt particulate filtering	105
4.3.3	Main salt inventory control, drain tanks, and batch cleanup	106
4.3.4	Option of adding ZrF ₄ to coolant salt.....	106
4.4	Structural Materials Degradation and In-Service Inspection	108
4.4.1	Mk1 structural materials in-service inspection	108
4.4.2	Mk1 structural material corrosion.....	109
4.4.3	Mk1 structural material thermal aging.....	111
4.4.4	Mk1 structural material long-term creep	113
4.5	Cover Gas Chemistry, Particulates, Salt Carry-Over, and Inventory Control.....	113
4.6	Pebble Handling and Storage System.....	113
4.6.1	Pebble Handling and Storage System Functions and Description.....	113
4.6.2	Pebble Handling and Storage System Operation	120
4.7	Plant Instrumentation and Control (I&C).....	127
4.7.1	Reactor protection system	127
4.7.2	Digital Control System	128
4.7.3	Online Monitoring and Plant Health Optimization.....	129
5	Mark-1 Power Conversion	131
5.1	Gas Turbine	131
5.2	Heat Recovery Steam Generator System	135
5.3	Natural Gas Supply and Safety Systems	135
5.3.1	Fuel gas skid and isolation valves.....	136
5.3.2	Fuel gas flow startup	137
5.3.3	Isolation of CTAHs during shutdown	137
5.3.4	Gas supply physical arrangement	137
5.4	Other Power Conversion System Design Topics	138
6	Lessons-Learned from the Mark-1 Design Project.....	139
6.1	PBMR Requests for Additional Information.....	139
6.2	FHR Tritium Control and Recovery	140
6.3	FHR Fuel and Materials Selection and Development	141
6.4	FHR Fuel Handling	141
6.5	FHR Safety.....	142

6.6	FHR Power Conversion	143
6.7	FHR Development and Licensing Strategy	144
6.8	Summary	144
7	References	145

List of Figures

Figure 1-1. Mk1 PB-FHR flow schematic.....	13
Figure 1-2. The Mk1 PB-FHR interface with its NACC power conversion system.	13
Figure 1-3. The Mk1 PB-FHR reactor vessel	16
Figure 1-4. The Mk1 PB-FHR reactor shield building adjacent to the power conversion system.	17
Figure 1-5. Plan view of Mk1 reactor building arrangement.....	18
Figure 1-6. Elevation view of Mk1 reactor building.	19
Figure 1-7. Google Maps satellite view of the 3700 MWe (peak) Turkey Point Generating Station in Florida, with the outline of the baseline 12-unit Mk1 site superimposed.	21
Figure 1-8. Mk1 site arrangement for a 12-unit, 180-acre PB-FHR plant, capable of producing 1200 MWe base load and 2900 MWe peak.	22
Figure 1-9 V.C. Summer Unit 2 AP1000 Reactor Cavity Module CA04 being installed Sept. 27, 2013.	24
Figure 1-10 The Mk1 PB-FHR uses 10 primary structural modules.....	24
Figure 1-11. A lift tower of similar size to that needed for Mk1 construction, being used to assemble a heat recovery steam generator.	25
Figure 1-12. Modular construction of a Mk1 unit uses a lift tower, with construction occurring outside the protected area (with a double fence system that runs between shield buildings and power conversion systems), adjacent to an existing unit.....	26
Figure 1-13. ASME Boiler and Pressure Vessel Code allowable stresses for candidate structural alloys.	30
Figure 1-14. Design of a PB-FHR pebble fuel test capsule (left) and thermal analysis of capsule using Comsol (right) by the 2010 UCB NE-170 senior design class.	33
Figure 2-1. A PB-FHR pebble fuel element.	36
Figure 2-2. Mk1 pebble core geometry showing fuel pebble (green) and graphite reflector pebble (yellow) regions.....	40
Figure 2-3. Comparison of the Mk-1 annular core design MCNP model (left) and SolidWorks model (right).....	41
Figure 2-4. Mk1 pebble injection channels schematic.....	42
Figure 2-5. UCB NE-92 class experiment using the XPREX facility with 1.27-cm-diameter polypropylene spheres to study heap geometry for reflector pebbles fed into a wide slot with a downward-moving piston. Note in this case the slot is tapered (left), and the x-ray image (right) shows instrumented pebbles and the bed geometry. ..	43
Figure 2-6. Replaceable Mk1 center graphite reflector	44
Figure 2-7. Radial reflector block retaining system used in the MSBR design.....	45
Figure 2-8. An upper ring of the Mk1 outer radial reflector, showing coolant suction holes and slots for radial retaining rings and vertical retaining ribs.....	46
Figure 2-9. Mk1 metallic core internals.....	48
Figure 2-10. Primary coolant flow paths under normal power and shutdown cooling operation.	50
Figure 2-11. Primary coolant flow paths under natural-circulation-driven decay heat removal. ..	51
Figure 2-12. Top (left) and side (right) views of the outlet collection plenum in the outer radial graphite reflector.	52

Figure 2-13. Buoyant control rod system, showing buoyant rod tested in scaled experiments at UCB (left) and schematic of fluidic snubbing channel to stop a buoyant rod (right).	56
Figure 2-14 Results of a study in MCNP5 indicate the combined worth of 1, 2, 4, and all 8 control rods.	56
Figure 2-15. Shutdown blade system, showing CAD figure of blade tested at UCB which had lowest insertion force (1 is blade, 2 is ribs, 4 is screws to hold ribs).	57
Figure 2-16 Results of a study in MCNP5 indicate the combined worth of 1, 2, 4, and all 8 shutdown blades.	58
Figure 2-17. COMSOL predictions for Mk1 bulk coolant temperature distribution (above) and fuel kernel temperature distribution (below) under power operation.	61
Figure 2-18. MSBR drain tank cooling system schematic (left) and fuel-salt drain tank with internal cooling coils to remove decay heat (right).	63
Figure 2-19. Schematic (left) and isometric view (right) of the Mk1 modular DRACS.	63
Figure 3-1. Isometric view showing major components of the Mk1 heat transport system.	79
Figure 3-2. Schematic diagram of hot well and main salt pumps.	82
Figure 3-3. Cold-leg stand pipe system with (top) upper maintenance access, isolation valve, and pressure control/relief system, and (bottom) lower chemistry-control cold-trap well and drain line.	83
Figure 3-4. MSBR “short-shaft” pump design.	86
Figure 3-5. CTAH sub-bundle design.	88
Figure 3-6. Mk1 CTAH vessel.	88
Figure 3-7. UCB CTAH test bundle (left) with close up of tube support bars (right).	92
Figure 3-8. Tube-to-tube-sheet joint for the CTAH manifolds (left) and diffusion bonding demonstration sample fabricated by UCB NE-170 senior design class [] (right)..	92
Figure 3-9. Hot duct liner system design used in the PBMR (left) and a commercial high-temperature butterfly valve (right).	94
Figure 4-1. Schematic figure of hot-salt manifold pipe showing inspection and maintenance flange and annular tritium and particulate filter cartridge.	99
Figure 4-2. Schematic showing cold traps located at the bottom of each cold-leg stand pipe. ..	105
Figure 4-3. Variation of the fracture strain with test temperature for Alloy N surveillance samples removed from the core of the MSRE after 22,533 hr at 650°C and exposure to a thermal fluence of 1.5×10^{21} neutrons/cm ² (from ORNL-4449, pg. 168).	109
Figure 4-4. Photos of (a) natural circulation LiF-BeF ₂ -ZrF ₄ -UF ₄ -ThF ₄ corrosion test loop fabricated from 304 SS that operated for 80,000 hr, cross sections of 0.64-mm-thick 304 SS coupons exposed at the maximum loop temperature of 688°C for (b) 5700 hr and (c) 45,724 hr (ORNL-4286, pg. 29-32).	110
Figure 4-5. Rate of formation of sigma phase.	112
Figure 4-6. Simplified material schematic for the Pebble Canister Transfer System.	116
Figure 4-7. Transfer canister decay heat load for transfer frequencies of 16, 32, and 64 days and the increase in decay time associated with one to four canisters.	118
Figure 4-8. Defueling devices used in THTR (left) and HTR-10 (right). The THTR design includes a mechanical screw that agitates the bed and sorts broken pebble fragments. The HTR-10 design uses alternating pulse gas to dislodge pebbles near the small diameter orifice.	119

Figure 4-9. HTR Module reactor burnup measurement system, showing pebble location (red dot) and germanium detector location outside the shielded pebble handling space ...	121
Figure 4-10. Simplified process flow diagram for PHSS under Phase 1 of Initial Core Loading. Radial zoning is established during this phase.	121
Figure 4-11. Simplified process flow diagram for PHSS under Phase 2 of Initial Core Loading. Fresh fuel is exchanged for the start-up fuel to prevent approaching criticality from an over-moderated core configuration with graphite pebbles.	122
Figure 4-12. Simplified process flow diagram for PHSS under Normal Operation.	123
Figure 4-13. Simplified process flow diagram for PHSS under Phase 1 of Full Core Unloading. Graphite pebbles are removed by the PCTS for disposal.	125
Figure 4-14. loading. Active fuel pebbles are removed, cleaned, and sorted based upon burnup levels before the they are reloaded into the core.	125
Figure 5-1. Cross section of the modified GE 7FB GT used for power conversion in the Mk1 PB-FHR.	133
Figure 5-2. Base-load 100-MWe Mk1 Thermoflex power conversion system flow diagram....	134
Figure 5-3. Peaking 242-MWe Mk1 Thermoflex power conversion system flow diagram.....	135
Figure 6-1. Scaled comparison of the UCB CIET integral effects test facility and the Mk1 PB-FHR, showing the heights of major heat sources/sinks.....	143

List of Tables

Table 1-1. Key Mk1 PB-FHR design parameters.....	14
Table 1-2. Mk1 reactor system stainless steel, graphite and salt inventories.	27
Table 1-3. Mk1 reactor building and air duct vault steel and concrete.....	28
Table 1-4. Comparison of estimated Mk1 material inputs to other power plant types.....	29
Table 1-5. Design stresses for Mk1 reactor vessel and CTAH tubes, with comparison to S-PRISM reactor vessel.	31
Table 1-6. Ranking of Mk1 PB-FHR structural alloys.	32
Table 1-7. Comparison of Mk1 design parameters with the large 2012 ORNL AHTR, a 4-loop Westinghouse PWR, the PBMR, and the S-PRISM.	34
Table 2-1. Mk1 PB-FHR fuel and core design.	38
Table 2-2. Flibe volumes by system and subsystem in the Mk1 PB-FHR.	49
Table 2-3. Temperature coefficients of reactivity for the Mk1 PB-FHR.	59
Table 2-4. DHX parameters, based on a straight shell and tube configuration.	64
Table 2-5. Detailed TCHX parameters.	66
Table 3-1. Comparison of Mk1 PB-FHR pumps with MSRE and MSBR pump designs.....	87
Table 3-2. Key Mk1 CTAH design parameters.	90
Table 4-1. Operating Parameters for Pebble Handling and Storage System.	115
Table 4-2. Characteristics of the Pebble Canister Transfer System.....	116
Table 5-1. Operational parameters for an unmodified GE 7FB GT.	131
Table 5-2. Mk1 NACC cycle operating parameters at ISO conditions.	134

Acronyms and Abbreviations

AGR – Advanced Gas Reactor
AHTR – Advanced High-Temperature Reactor
API – American Petroleum Institute
ASME – American Society of Mechanical Engineers
ATR – Advanced Test Reactor
ATWS – Anticipated transient without scram
BDBE – Beyond design basis event
BOP – Balance of plant
BUMS – Burnup measurement system
CAD – Computer Aided Design
CFRC – Carbon-fiber reinforced composite
CNC – Computer numerically controlled
CTAH – Coiled tube air heater
DHX – DRACS heat exchanger
DRACS – Direct reactor auxiliary cooling system
DST – DRACS storage tank
EFPD – Effective full power day
EFPY – Effective full power years
EPR – European Pressurized Reactor
FCCU – Fluid catalytic cracking unit
FHR – Fluoride-salt-cooled, high-temperature reactor
FL – Faulted level
FOAK – First-of-a-kind
GDC – General Design Criteria
GE – General Electric
GT – Gas turbine
GT-MHR – Gas Turbine Modular Helium Reactor
HP – High-pressure
HRSG – Heat recovery steam generator
HTGR – High-temperature gas-cooled reactor
HTR – High-Temperature Reactor
HVAC – Heating, ventilation and air conditioning
IAEA – International Atomic Energy Agency
I&C – Instrumentation and control
INL – Idaho National Laboratory
IRP – Integrated Research Project
LMR – Liquid metal reactor
LOFC – Loss of forced circulation
LOHS – Loss of heat sink
LP – Low-pressure
LWR – Light water reactor
LWR-SMR – Light-water small modular reactor
MIT – Massachusetts Institute of Technology
Mk1 – Mark-1

MSBR – Molten Salt Breeder Reactor
MSRE – Molten Salt Reactor Experiment
NACC – Nuclear air-Brayton combined cycle
NGCC – Natural gas combined cycle
NGNP – Next Generation Nuclear Plant
ORNL – Oak Ridge National Laboratory
PB-FHR – Pebble-bed fluoride-salt-cooled, high-temperature reactor
PBMR – Pebble Bed Modular Reactor
PCRV – Pre-stressed concrete reactor vessel
PEI – Post-Event Instrumentation
PWR – Pressurized water reactor
RAI – Request for additional information
RPS – Reactor protection system
RRCLS – Refractory reactor cavity liner system
SC – Steel-plate composite structure
SINAP – Shanghai Institute of Applied Physics
SFR – Sodium fast reactor
SmAHTR – Small Modular Advanced High-Temperature Reactor
S-PRISM – Super Power Reactor Innovative Small Module
SSCs – Systems, structures and components
SWU – Separative work unit
304 SS – 304 stainless steel
316 SS – 316 stainless steel
TCHX – Thermosyphon-cooled heat exchanger
TMSR-SF – Thorium Molten Salt Reactor – Solid Fuel
TRISO – Tristructural-isotropic
UCB – University of California, Berkeley
UCT – Underground common tunnel
USNRC – U.S. Nuclear Regulatory Commission
UW – University of Wisconsin
X-PREX – X-Ray Pebble Recirculation Experiment

1 Mark-1 PB-FHR Design Overview

Previous design studies for fluoride-salt-cooled, high-temperature reactors (FHRs) [1][2][3][4][5][6][7] have all suggested the potential to achieve attractive economic performance while meeting high standards for reactor safety and security. Based on this earlier work, the U.S. Department of Energy initiated a 3-year, \$7-million Integrated Research Project (IRP) in January 2012 with the Massachusetts Institute of Technology (MIT), University of California at Berkeley (UCB) and University of Wisconsin (UW) at Madison, to develop the technical basis to design, develop, and license commercially attractive FHRs. FHRs are differentiated from other reactor technologies because they use high temperature, coated particle fuels, cooled by the fluoride salt flibe (Li_2BeF_4). As a key deliverable for this IRP project, UCB has developed a new pre-conceptual design for a novel pebble-bed FHR (PB-FHR), which is described in this report. The design documented in this report is designated as the Mark-1 (Mk1) PB-FHR. Future PB-FHR designs will be designated with subsequent numbering.

Fluoride salt coolants have uniquely high volumetric heat capacity, low chemical reactivity with air and water, very low volatility at high temperature, effective natural circulation heat transfer, and high retention of most fission products. These characteristics, along with high solubility for uranium and thorium fluorides and reasonably low neutron capture probability, and good neutron moderation capability, explain the selection of fluoride salts as the primary coolant and fuel solvent for the original fluid-fueled Aircraft Nuclear Propulsion reactor in the 1950's [8]. The Mk1 PB-FHR design described here is the first integrated FHR design to propose driving a nuclear air-Brayton combined cycle (NACC) for base-load electricity generation.

The purpose of the Mk1 design is to provide efficient and highly flexible power output and grid support services, and therefore to enable a new value proposition for nuclear power. The 236-MWth Mk1 PB-FHR uses a General Electric (GE) 7FB gas turbine (GT), modified to introduce external heating and one stage of reheat, in a combined-cycle configuration to produce 100 MWe under base-load operation, and with natural-gas co-firing to rapidly boost the net power output to 242 MWe to provide peaking power. Figure 1-1 shows a flow diagram for the Mk1 reactor, main salt loop, and power conversion systems. Figure 1-2 provides an isometric view of the reactor and power conversion system, illustrating how the Mk1 reactor couples to its NACC power conversion system. Table 1-1 summarizes key Mk1 design parameters.

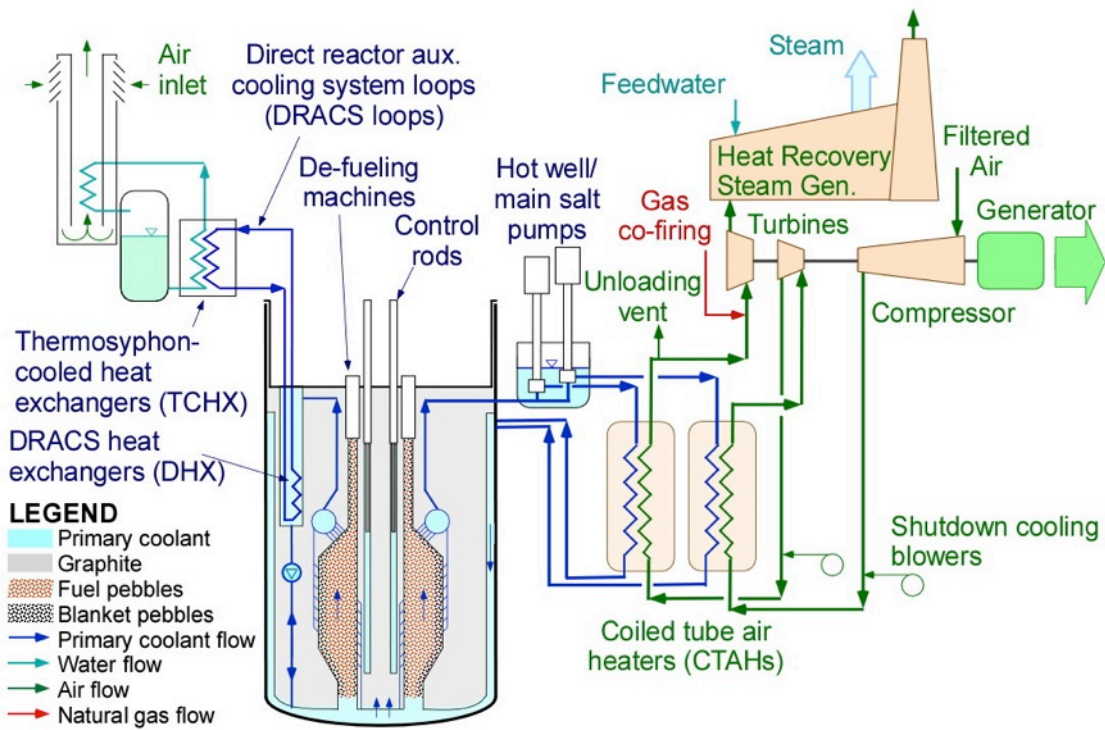


Figure 1-1. Mk1 PB-FHR flow schematic.

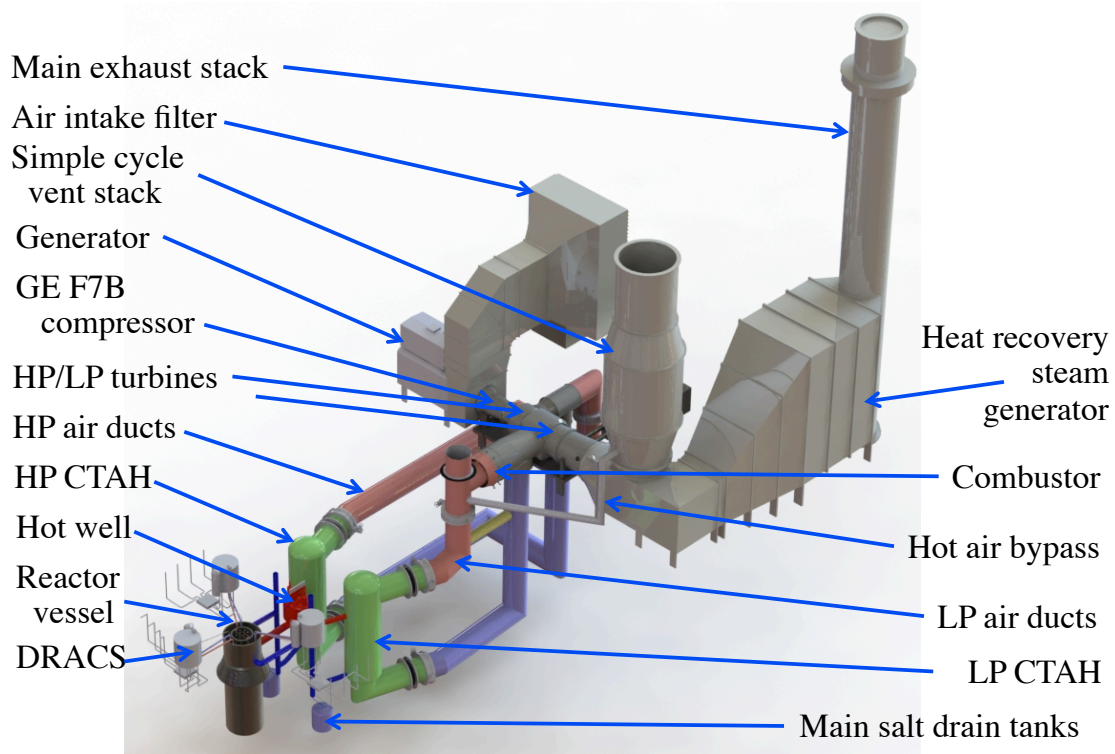


Figure 1-2. The Mk1 PB-FHR interface with its NACC power conversion system.

This chapter provides a high-level overview of the Mk1 PB-FHR reactor design, options for multi-unit site arrangements, and the basis for materials selection and fuel qualification. The subsequent chapters provide more detailed descriptions of key systems, subsystems, structures, and components in the Mk1 design. The intent of this report is to provide sufficiently detailed information about this design that transient and safety analysis, fuel cycle analysis, and economics analysis can be conducted. A number of systems in the Mk1 design have not been designed in detail, where basic functional requirements are specified instead. Several, such as the pebble defueling machine and pebble handling/assay/storage systems, are important and need near-term attention to further develop. Chapter 6 summarizes key gaps. This said, the current report does provide sufficient detail that many aspects of FHRs designed to drive NACC power conversion systems can be evaluated.

Table 1-1. Key Mk1 PB-FHR design parameters.

Reactor Design	
Thermal power	236 MWth
Core inlet temperature	600°C
Core bulk-average outlet temperature	700°C
Primary coolant mass flow rate (100%power)	976 kg/sec
Primary coolant volumetric flow rate (100% power)	0.54 m ³ /sec
Power Conversion	
GT model number	GE 7FB
Nominal ambient temperature	15°C
Elevation	Sea level
Compression ratio	18.52
Compressor outlet pressure	18.58 bar
Compressor outlet temperature	418.7°C
Compressor outlet mass flow (total flow is 440.4 kg/s; conventional GE-7FB design uses excess for turbine blade cooling)	418.5 kg/sec
Coiled tube air heater outlet temperature	670°C
Base-load net electrical power output	100 MWe
Base-load thermal efficiency	42.5 %
Co-firing turbine inlet temperature	1065°C
Co-firing net electrical power output	241.8 MWe
Co-firing efficiency (gas-to-peak-power)†	66.4 %

† The co-firing efficiency is the ratio of the increased power produced (total minus base load) during peaking, to the energy input from combustion of natural gas, and represents the efficiency with which the natural gas combustion energy is converted into electricity.

1.1 Mk1 Reactor Design Overview

As with earlier UCB designs, the Mk1 fuel pebbles are 3.0 cm in diameter, half the diameter of pebbles used in conventional helium-cooled pebble bed reactors. The very low circulating power for the coolant in salt-cooled reactors, compared to helium-cooled reactors, makes it practical to use these smaller pebbles. This small-pebble design, which also uses an annular fuel layer, doubles the pebble surface area per unit volume and halves the thermal diffusion length, enabling a substantial increase in power density while maintaining relatively low peak fuel particle temperature. Low fuel temperature reduces the thermal transient caused by hypothetical anticipated transient without scram (ATWS) accidents. The 3.0-cm-diameter pebble is also small enough to be irradiated in current U.S. test reactors for fuel qualification.

Analysis for the Mk1 design shows that the graphite fuel and reflector pebbles can act as effective sinks for tritium produced by neutron interactions with the Mk1 flibe coolant. Thus absorption into the graphite surfaces of blanket and fuel pebbles is selected as the tritium recovery method for the Mk1 design. Additional graphite surface area can be added, if required, using modular filter cartridges located in the coiled tube air heaters (CTAHs). The critical question for the Mk1 design, which requires further investigation, is whether the baseline tritium diffusion barrier system selected for the CTAH tubes, which are clad on the outside with an alumina-forming alloy, will reduce tritium releases sufficiently. Preliminary analysis, presented in Section 4.1 (“Tritium Control and Recovery”), suggests that the permeation barrier could be sufficiently effective, but further study is required.

Figure 1-3 shows a cross section of the Mk1 reactor vessel, internals, and core. The Mk1 design uses an annular pebble core geometry. Because Mk1 pebbles float in the flibe coolant, they are fed into the bottom of the core and move slowly upward, to be removed through an annular defueling slot at the top of the core by two defueling machines. Based upon results from a series of Pebble Recirculation Experiments (PREX) performed at UCB, the Mk1 core uses a simplified pebble core composed of a homogeneous mix of fuel pebbles adjacent to the center graphite reflector, with a layer of inert graphite reflector pebbles on the outside that reduces the fast-neutron fluence to the outer fixed radial graphite reflector sufficiently for it to last the life of the plant.

The center graphite reflector is much shorter and smaller than center reflectors that have been designed for helium-cooled pebble bed reactors, making it simpler to design for replacement and for seismic qualification. The center reflector provides 8 channels for insertion of buoyant control rods, and it also provides flow channels for radial injection of coolant into the pebble core, to provide a combined radial and axial flow distribution that increases the effectiveness of heat transfer from the fuel and results in lower average fuel temperature.

To enable near-term deployment, the Mk1 design uses a core barrel and other core internal structures fabricated from the same metallic material as the reactor vessel and main salt piping. The outer radial reflector blocks are aligned and held against the metallic core barrel using a system of axial alignment ribs and radial retaining rings quite similar to designs originally developed for the Molten Salt Breeder Reactor (MSBR) project. The use of metallic core internal structures, rather than advanced ceramic composites, simplifies fabrication and licensing for the Mk1 design.

Chapter 2 provides a detailed description of the design of the center and outer radial reflectors, the flow distribution through the core, and the systems for reactivity control and reserve shutdown.

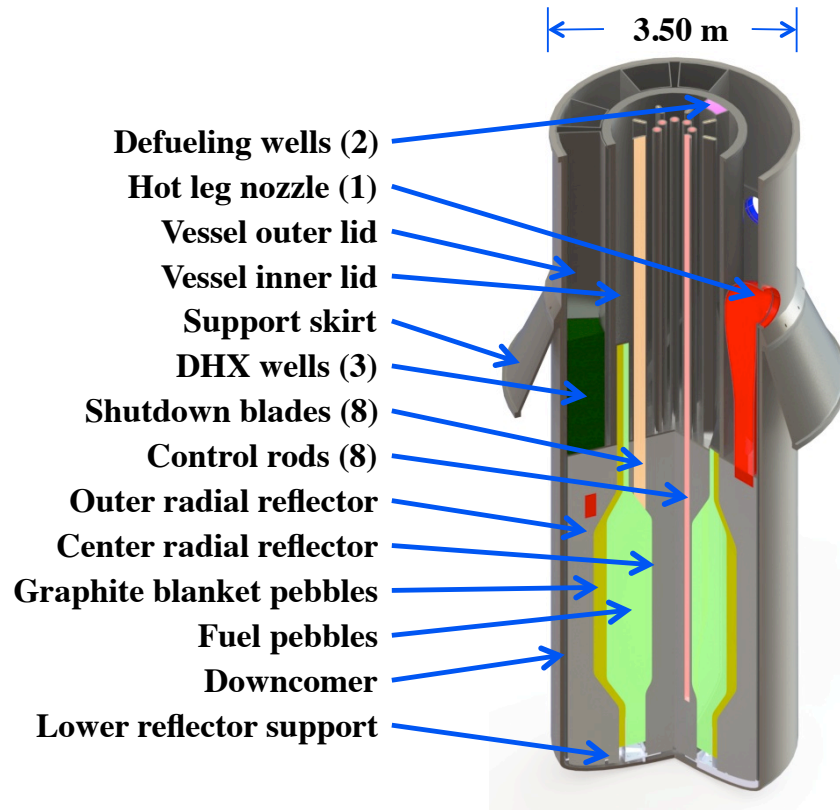


Figure 1-3. The Mk1 PB-FHR reactor vessel

1.2 Mk1 Reactor Building Arrangement

The 2014 UCB NE 170 senior design class developed the preconceptual design of the Mk1 PB-FHR and provided a detailed design report, including a description of its modular construction approach, in their design report [9]. The Mk1 reactor building and NACC system arrangements they designed supports a multi-module plant configuration, shown in Fig. 1-4, by allowing multiple Mk1 PB-FHR units to be lined up in a row with a clear boundary between the reactor and its vital areas, versus the balance of plant (BOP). The GT and associated equipment are configured to minimize the air pressure loss and circulating power in the air ducting, while maintaining a clear boundary between the reactors and the BOP. As discussed further in Section 1.3 on site arrangement, this configuration makes it easier to co-locate combined nuclear services on one side of a multi-module plant (training, fresh fuel handling/receipt, spent fuel dry storage, security, access control, multi-module control room, hot-rad/Be shops, etc.), and have BOP combined services on the other side (off-site transmission, process steam loads and/or steam bottoming turbines, cooling towers, etc.).

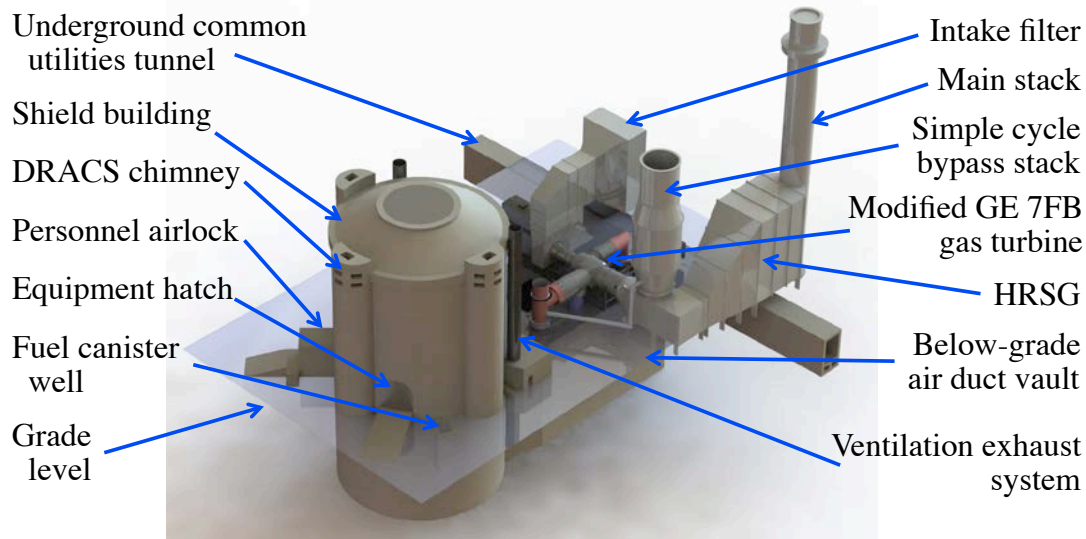


Figure 1-4. The Mk1 PB-FHR reactor shield building adjacent to the power conversion system.

The Mk1 reactor building is partially embedded below grade, with the reactor deck located slightly above grade, shortening the air duct lengths and the depth of the air-duct vault. The baseline Mk1 reactor building design uses a cylindrical shield building fabricated from steel-plate/concrete composite (SC) modules, quite similar to the Westinghouse AP1000 shield building. The overall height and diameter of the Mk1 shield building are 47.5 m and 24.5 m, respectively, compared to 83 m and 42 m for the 1150-MWe AP1000, so the Mk1 shield building volume is 2.2 times greater than the AP1000, per MWe baseload.

The cylindrical shield building geometry provides a stiffer, lighter structure than is possible with a rectangular building geometry. The low-leakage containment boundary is provided by the liner of the reactor cavity and its gas space. With the containment boundary located well inside of the reactor building external walls, the primary function of the cylindrical structure is to provide an external events shield. It also acts as an element of the secondary filtered confinement volume used for control of beryllium and radioactive contamination. Because the refueling deck area of the reactor building must be accessed periodically during power operation for fuel transfer work associated with on-line refueling, the refueling deck is designed to provide effective biological shielding.

The Mk1 PB-FHR uses two CTAHs to transfer heat from the main salt to pressurized air in the NACC power conversion system. Due to the compact size of the Mk1 reactor vessel and main salt system, these CTAHs are located only 13 m from the centerline of the reactor vessel. Even though significant thermal expansion occurs when the reactor and main salt system are heated from their installation temperature of approximately 20°C to their normal operating temperature of 600°C, the relatively short spacing between the reactor vessel and CTAHs allows this expansion—about 0.13 m—to be accommodated by placing the CTAHs on horizontal bearings and using bellows in the air ducts to accommodate thermal expansion, as illustrated in Figures 1-5 and 1-6. This is very similar to the approach taken to manage thermal expansion in the primary loop of conventional pressurized water reactors (PWRs), where the steam generators

are supported on vertical bearings and move horizontally in response to thermal expansion of the reactor hot and cold leg pipes.

For the Mk1 PB-FHR, implementing bellows in the CTAH air ducts is relatively easy, because the duct pressures are relatively low and with the internal insulation the bellows operate at low temperatures. However, the bellows cannot carry axial tensile loads, so appropriate restraints are required in the duct system. Snubbers are provided to restrain salt piping motion during seismic events. Using the air duct system to accommodate for thermal expansion in the main salt piping has beneficial implications for the main salt system configuration, allowing short, direct pipe routing to be used, minimizing reactive forces and associated creep ratcheting during thermal transients, and minimizing the volume of salt outside the reactor containment.

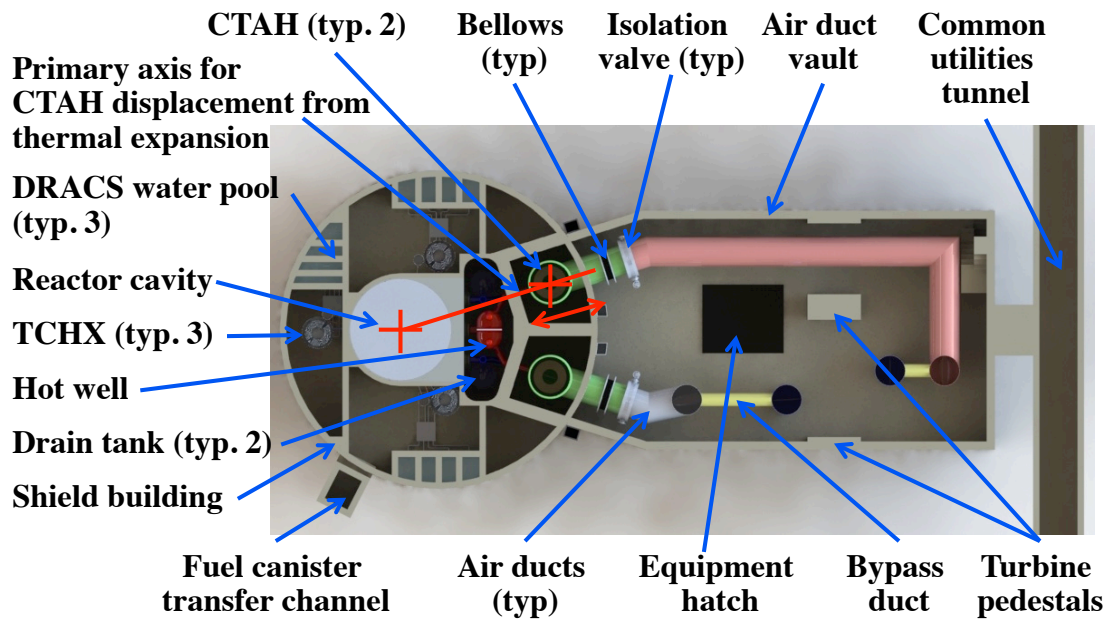


Figure 1-5. Plan view of Mk1 reactor building arrangement.

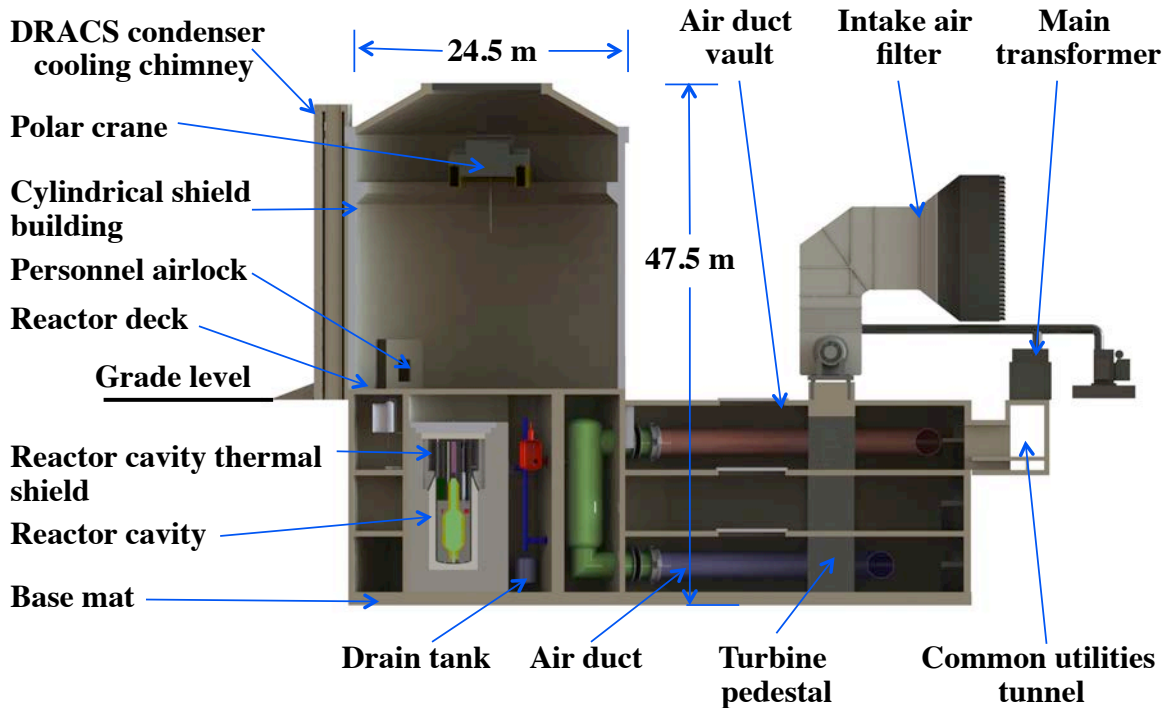


Figure 1-6. Elevation view of Mk1 reactor building.

The Mk1 design introduces another novel feature, a “gas gap” system, to make it physically impossible to transmit excessive pressures to the reactor vessel and reactor cavity/containment from potential tube or manifold pipe ruptures in the CTAH. The gas gap is created adjacent to the containment penetrations for the hot and cold legs. For the hot leg, the gas gap is formed by the free surface in a hot well, which also contains hot leg isolation valves and two main-salt pumps. In each cold leg, the gas gap is formed by a free surface in a stand pipe, which also contains a cold leg isolation valve.

As discussed in greater detail in Section 3.1 (“Primary Loop ‘Gas-Gap’ Subsystem”), with a gas gap and isolation valves to isolate the hot and cold leg penetrations into the reactor containment, leaks or breaks in the main salt piping and CTAH tubing cannot affect the pressure of the reactor vessel and containment, or the capability of the safety-related direct reactor auxiliary cooling system (DRACS) to remove decay heat. As noted in Section 4.2.2 (“CTAH tube and manifold leaks”), the principal safety concern for tube leaks involves beryllium control. For these reasons, as is the case with the turbine condensers in boiling water reactors, it is expected that the PB-FHR CTAHs do not need to be classified as safety related equipment, and instead can be classified to be non-safety-related, special-treatment components.

Another best practice in modern nuclear structure design is to provide a “tank-within-tank” configuration for spent fuel pools, which can be extended to the design of all safety-significant water pools (IAEA, 2011, pg. 111). In this concept, the primary water pool is located inside a secondary leakage detection and containment system, which can also limit inventory loss and allow the pool to continue to perform its safety function even if a leak occurs. For the Mk1 PB-FHR, water pools are used inside the shield building to provide water to thermosyphon-cooled heat exchangers (TCHXs) in the DRACS modules, as well as to the reactor cavity liner cooling

system. Because these water pools also provide a source of water for evaporative cooling under beyond-design-basis event (BDBE) conditions, they are provided with a similar secondary confinement.

1.3 Mk1 Reference 12-Unit Site Arrangement

The smaller size and power output of the Mk1 design, compared to large light water reactors (LWRs) like the AP1000, is more practical from the perspective of building a first-of-a-kind (FOAK) FHR station. No gigawatt-size FHR design would be credible to take on the FOAK risks, unless smaller plants had been built and operated successfully before.

The relatively small power output of the modular Mk1 PB-FHR, and the requirement to design to facilitate construction of new units adjacent to operating units, alters construction compared to that for large LWRs. An excellent, broad summary of modern construction technologies for advanced LWRs is provided in a 2011 International Atomic Energy Agency (IAEA) construction methods report [10]. This report emphasizes the importance of planning the site infrastructure and layout to facilitate smooth movement of personnel, material and equipment during construction and subsequent plant operation. The detailed design of the site arrangement requires input from engineers and planning personnel experienced with nuclear construction. Infrastructure to support offloading, assembly, and outfitting of modular components must be in place before the pouring of the first nuclear concrete, including sufficient area for storage, prefabrication, and pre-assembly of modules. Utilities, trenching, and excavations must be tabulated and designed so they can be completed early in the construction process.

The ability to add additional generation capacity, to address regional load growth, is also an important design feature. The Mk1 PB-FHR configuration is optimized so that additional units can be added with construction work occurring outside the nuclear protected area, to reduce construction costs, and then the protected area can be expanded to include the new module after construction is completed. Key questions for spacing between modules will involve temporary security measures needed to separate construction work from the neighboring operating reactor as well as measures to control construction impacts on operation and maintenance of modules that have entered service; these questions must be addressed during detailed design.

Experience with co-locating nuclear and gas plants already exists at the Turkey Point Generation Station in Florida, shown in Fig. 1-7, where two 885-MWe PWRs are sited adjacent to two 400-MWe gas/oil-fired steam plants and a short distance from a 1,150-MWe, 4-unit, GE-7FA natural gas combined-cycle (NGCC) unit. Due to the significant commonality between the Turkey Point station and the Mk1 site, dimensions for key Mk1 site facilities such as the main switchyard, cooling towers, and steam turbine generator buildings were selected to match those for Turkey Point.

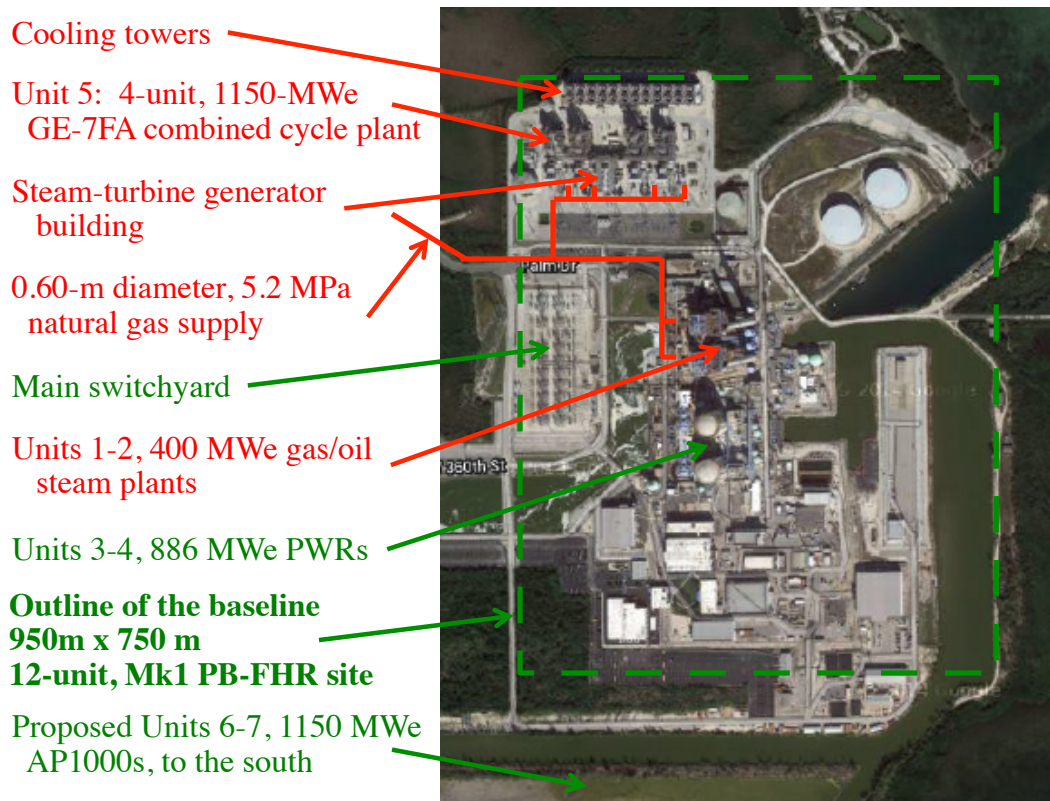


Figure 1-7. Google Maps satellite view of the 3700 MWe (peak) Turkey Point Generating Station in Florida, with the outline of the baseline 12-unit Mk1 site superimposed.

Figure 1-8 presents a notional 180-acre site arrangement for a 12-unit Mk1 PB-FHR power plant, capable of producing 1200 MWe base load and 2900 MWe peak power output. The much smaller cooling requirements of FHRs means that they do not need to be sited near bodies of water. Population centers tend to be located near bodies of water, which means that FHRs can be sited in areas where fewer people want to live. So rather than attempt to minimize the site footprint, the more important goal is likely to facilitate construction of modules adjacent to operating modules, and to optimize the degree to which some services are shared.

For the Mk1 design, it is assumed that some facilities will optimize to serve a subset of the reactor modules. For example, in the reference site arrangement each block of 4 PB-FHR units shares a common steam turbine generator building and cooling tower. This means that for the first module of a block of 4, these support facilities must be built, but the cost to construct the facilities for the next set of 4 PB-FHR units can be deferred until the 5th, and then the 9th units enter construction. Other facilities, such as the administration building and the training center, may need to be expanded after several initial Mk1 units are deployed. The optimal approach to sharing of facilities will be determined during detailed design.

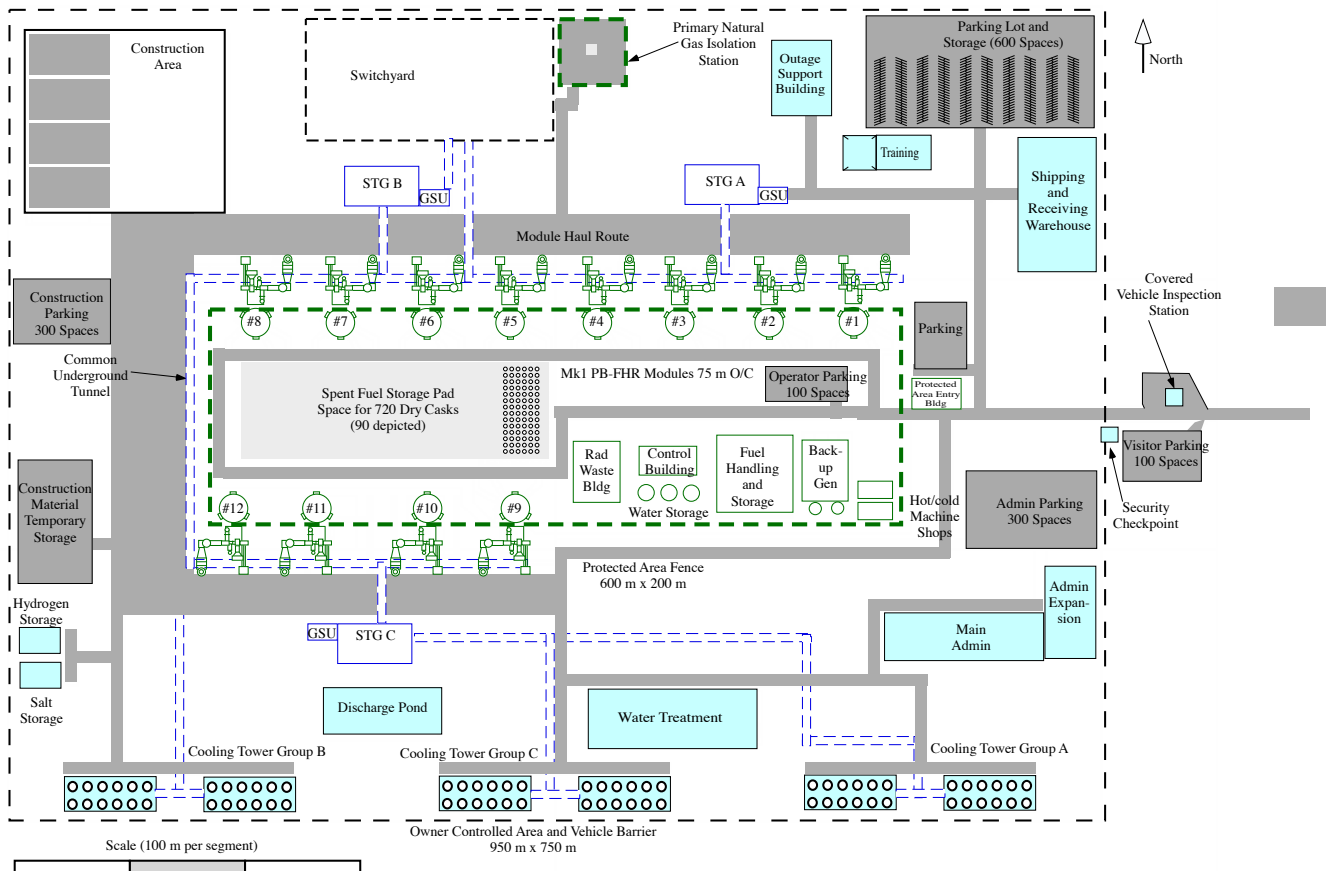


Figure 1-8. Mk1 site arrangement for a 12-unit, 180-acre PB-FHR plant, capable of producing 1200 MWe base load and 2900 MWe peak.

A best practice in modern nuclear site design is to provide underground common tunnels (UCTs) for BOP utilities, connecting the turbine buildings, which can eliminate the need for buried piping and for multiple excavations during construction [11]. The UCT has a rectangular cross section and multiple racks for process piping, fire protection piping, domestic water piping, raw water piping, steam piping, power cable trays, control cable trays, instrument cable trays, communication cable trays, and heating, ventilation and air conditioning (HVAC) ducts. Due to flammability, for the Mk1 site arrangement natural gas piping is buried separately from the UCTs. Section 5.3 provides a more detailed description of the natural gas distribution and safety systems. Permanent construction openings are provided to the UCTs to provide access to install equipment and perform subsequent maintenance. In the Mk1 site arrangement, the UCTs run adjacent to and under the power conversion systems.

The Vogtle Early Site Permit Application notes that the area requirements for the construction of two new Westinghouse AP1000 reactors, capable of producing 2234 MWe, includes 70 acres for switchyard expansion, 75 acres for the power block, 70 acres for cooling towers, and additional space for spent fuel storage and administrative facilities, totaling 310 acres [12]. The 7.2 MWe/acre footprint of the Vogtle AP1000 site can be compared to the 6.7 MWe/acre (base load), 16.1 MWe/acre (peak) footprint of the notional Mk1 site. As seen in Fig.

1-7, the reference Mk1 site is larger, per MWe, than the site for the combined nuclear and fossil generation at the Turkey Point station, but is still comparable.

1.4 Mk1 Modular Design and Construction

The Mk1 PB-FHR is designed so that all components—including the reactor vessel, GT, and building structural sub-modules—can be transported by rail, enabling modular construction. The design constraint of rail transport limits the width of components (laid down to be horizontal) to 3.6 m; this result constrains the Mk1 reactor vessel size and thermal power to a value that matches well to the largest rail-shippable GTs now commercially available. FHRs can be designed to implement passive safety even at gigawatt power levels; however it is a pragmatic choice for the Mk1 design to select a lower power level for the first commercial FHRs, comparable to the typical light-water small modular reactors (LWR-SMRs) now under development.

The modular construction methods used for the Mk1 plant closely follow technologies developed for the Westinghouse AP1000. In the AP1000 design, approximately two thirds of the 350 sub-modules used to construct the plant are mechanical and one third are structural. Modules for the Mk1 PB-FHRs can be fabricated in the same factories, or similar factories, as those now being fabricated to construct AP-1000 reactors, such as the Chicago Bridge and Iron Works module factory in Lake Charles, Louisiana, as well as facilities operated by Oregon Iron Works and by Newport News, in the United States.

Factory fabrication of sub-modules has the benefits of performing work with a skilled, stable workforce and training and quality control programs. Sub-module fabrication and delivery occur in parallel with module assembly and plant civil construction at the reactor site. Multiple types of structural sub-modules, fabricated using computer-controlled manufacturing, as well as mechanical modules reduce site fabrication and installation work. The SC structural submodules consist of steel plates and additional structural elements such as tie rods and stiffening elements, that are delivered to the site, assembled into larger, crane liftable modules, that are then installed and filled with concrete.

Figure 1-9 shows a SC AP1000 reactor cavity module, similar to the design that would be used for the Mk1 PB-FHR, being installed at the V.C. Summer plant. As shown in the figure, the AP1000 reactor cavity module is shaped as an octagon to simplify the fabrication of the liner assembly. The Mk1 cavity uses a dodecagon (12-sided) geometry, which with its 3x2x2 symmetry facilitates the connections of the hot and cold legs, DRACS modules, fuel pebble transfer lines, and pebble assay collimating tubes.

The 2014 UCB NE170 senior design class developed a detailed design for the Mk1 reactor building including modularizing the building and developing a “storyboard” to illustrate its assembly [13]. Figure 1-10 provides an exploded view of the 10 SC structural modules designed by the NE170 class to build a Mk1 PB-FHR unit. Section 1.7 gives additional information about these modules, including the mass of steel and concrete used for each module. Similar to the AP1000, these modules are assembled from submodules in a covered assembly facility and then moved to the crane pick-up area using a multi-wheeled, hydraulic transporter.



Figure 1-9 V.C. Summer Unit 2 AP1000 Reactor Cavity Module CA04 being installed Sept. 27, 2013 [14].

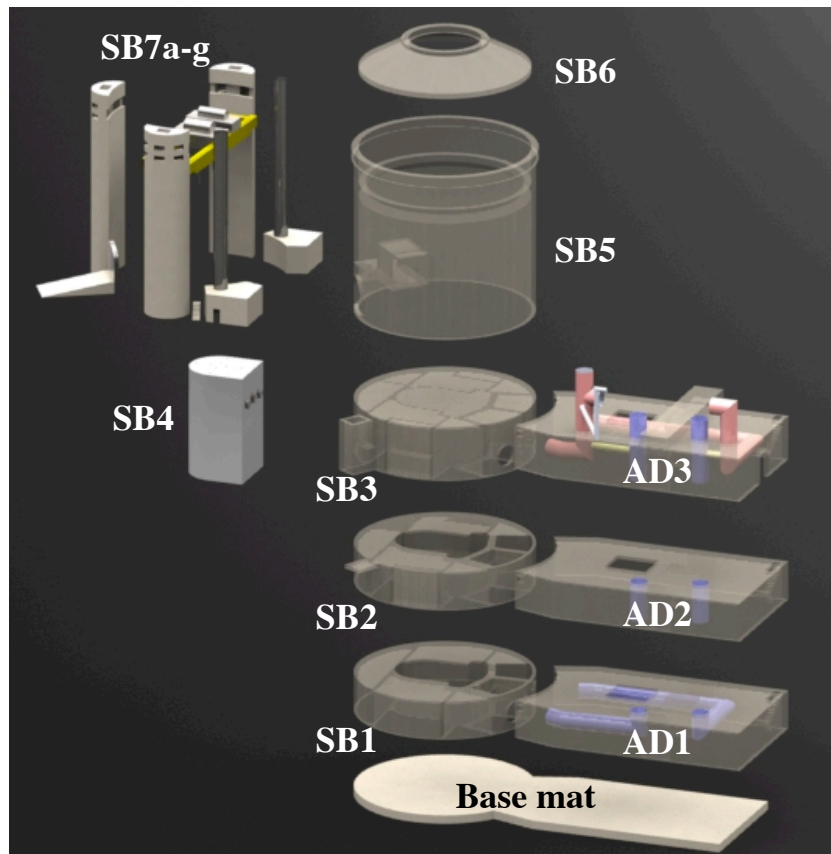


Figure 1-10 The Mk1 PB-FHR uses 10 primary structural modules [15].

The baseline Mk1 unit design is configured to use a lift tower, similar to the example shown in Fig. 1-11, to transfer modules from the heavy-haul transporter route adjacent to the unit, to the

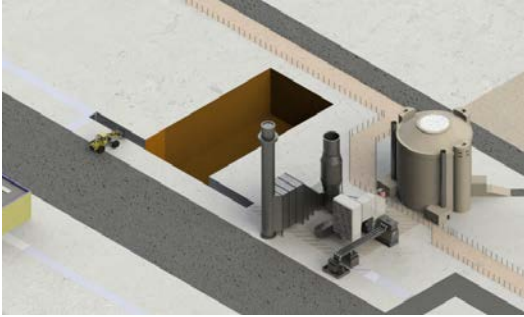
rectangular excavation where the base mat foundation is assembled and poured. Lift towers have advantages over conventional heavy-lift cranes for this type of construction because they have compact footprints, can be assembled and disassembled rapidly, do not require heavy counterweights, and are less susceptible to failure during high winds.

Figure 1-12 illustrates the construction sequence used to build a Mk1 unit. The excavation for the PB-FHR reactor building and air duct vaults is rectangular in shape (Fig. 1-12(A)), and may have a haul ramp on one side to facilitate the removal of excavated soil and rock. The Mk1 base mat (Fig. 12(B)) is 1.2 m thick and consists of a circular area with an adjacent rectangular extension under the air duct vault. The base mat is poured over a conventional water proofing membrane [16], and the below-grade external surfaces of the building also use a conventional waterproofing system.

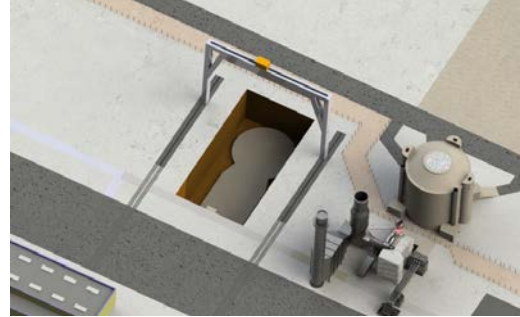
The design uses three below-grade SC structural modules to form the air duct vault, three SC structural modules for the below-grade portion of the shield building, and a reactor cavity module (Fig. 1-12(C)). The excavation is backfilled before the above-grade modules and equipment are installed (Fig. 1-12(D)). While the reactor vessel and the CTAHs are installed before the last below-grade shield-building module using the open top method, the 5-m-diameter equipment hatch is large enough for these vessels to be removed and replaced if required.



Figure 1-11. A lift tower [17] of similar size to that needed for Mk1 construction, being used to assemble a heat recovery steam generator.



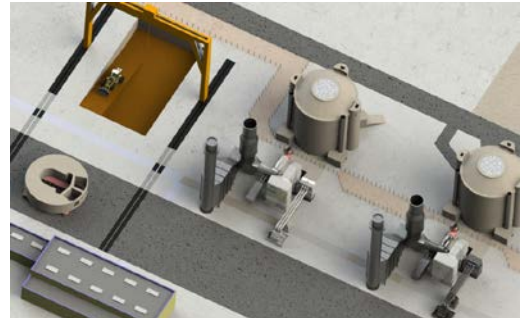
(A) Excavation occurs adjacent to an existing Mk1 unit, with protected area fence rerouted



(B) Basemat is poured after common tunnel and lift-tower have been installed



(C) Below-grade structures installed as six structural modules and reactor cavity module



(D) After above-grade modules are installed, fence is rerouted before loading fuel

Figure 1-12. Modular construction of a Mk1 unit uses a lift tower, with construction occurring outside the protected area (with a double fence system that runs between shield buildings and power conversion systems), adjacent to an existing unit [18].

Many of the most important modularity questions for multi-module PB-FHR plants are generic with LWR-SMRs, and will be resolved by the LWR-SMRs that are entering near-term deployment.

1.5 Mk1 Materials Quantities

For performing life-cycle assessments (LCA) and cost estimates, it is helpful to have estimates for total quantities of materials used in reactor designs. Table 1-2 presents the quantities of stainless steel, graphite, and salt used in the main components of the Mk1 reactor system, as calculated by the Solidworks computer aided design (CAD) program that was used to develop the system models [19].

Table 1-2. Mk1 reactor system stainless steel, graphite and salt inventories.

	Mass (kg)
316 Stainless Steel	408,420
Reactor vessel (6.0 cm wall below ring, 4.0 cm wall above)	57,150
Upper internals	49,160
Core barrel (3.0 cm wall)	13,290
Lower outer reflector support skirt	9,640
Lower center reflector support ring	133
Hot leg and cross-over leg piping (3.0 cm wall)	5,690
Hot well (5.0 cm wall)	18,990
Cold legs and stand pipes (3.0 cm wall)	11,624
Drain tanks (3.0 cm wall)	9,240
CTAH tube bundles (Table 3-2)	63,500
High-Alloy Steel	710 ,000
Combined cycle power conversion system†	568,000
All other uses in plant (assume 25% addition)	142,000
Graphite (density of 1,740 kg/m³)	49,250
Outer reflector	43,310
Center reflector	5,940
Flibe (Table 2-2, average flibe density of 1962.7 kg/m³)	91,900
Core, reactor internals and DHX wells (11.67 m ³)	22,900
Main salt piping, hot well and CTAHs (31.59 m ³)	62,010
DRACS (3.56 m ³)	6,990

† Quantity of high-alloy steel is taken from Table 1-4 value for a typical NGCC plant, and multiplied by a ratio of 280 MWe/100 MWe to correct for the lower baseload power output of a NACC compared to a conventional NGCC plant.

Table 1-3 presents the quantities of carbon steel (density of 7800 kg/m³) and concrete (density of 2400 kg/m³) used to construct the reactor shield building and air duct vaults, shown previously in Fig. 1-10, again using values derived from the Solidworks model. The steel masses were calculated assuming that the steel plate used in the modules is 1.25 cm thick everywhere except on the outside of the shield building and the inside of the CTAH cavities, where the steel plate is 2.50-cm thick. The total mass of steel calculated was increased by 10% to account for additional tie rods and other fixtures between the plates. The mass of steel used in the base mat, which uses conventional reinforcing bar, was assumed based upon the use of 18 gage rebar (20.3 kg/m) used in two layers in a square pattern with a spacing of 0.30 m.

Table 1-3. Mk1 reactor building and air duct vault steel and concrete.

	Carbon Steel (1000 kg)	Concrete (1000 kg)
Basemat	336.8	3601.5
Shield building level 1 (SB1) module	163.8	1638.1
Shield building level 2 (SB2) module	163.8	2293.0
Shield building level 3 (SB3) module	202.6	2994.0
Reactor cavity structural module (SB4)	111.9	1674.0
Shield building upper ring (SB5)	598.8	3498.7
Polar crane*	200	0
Shield building roof (SB6)	166.0	680.2
Shield building external structures SB7a-g (DRACS chimneys, etc.)	305.8	1954.1
Air duct vault level 1 (AD1) module ††	258.2	1713.3
Air duct vault level 1 (AD2) module ††	180.6	1713.3
Air duct vault level 1 (AD3) module ††	335.4	2267.4
NACC power conversion system †	56.0	6104.0
Vehicle barrier system (1.7m W x 1.2m H x 3400m L)/12 units	54.0	578.0
Support buildings (assume 25% of total)	783.4	7677.3
TOTALS	3917	38387

* Polar crane mass assumed to be 2 times its 100 t capacity

† Quantity of steel and concrete are taken from Table 1-4 value for a typical NGCC plant, and multiplied by a ratio of 280 MWe/100 MWe to correct for the lower base load power output of a NACC compared to a conventional NGCC plant. Concrete is multiplied by 0.5 to reflect the fact that the Mk1 air duct vault replaces the foundation needed for a conventional NGCC plant.

†† Includes steel mass of 2.5-cm-thick air duct pipes preinstalled in module.

It is useful to compare these Mk1 PB-FHR material inputs to those required for other types of power plants. Table 1-4 presents comparisons with a wide range of values found in the literature. It is important to emphasize that the Mk1 values are approximate. This said, it is noteworthy that the quantities of carbon steel and concrete needed to construct a 1200-MWe base load, 12-unit Mk1 station are comparable to the quantities needed to construct large LWRs with similar base-load power output.

Table 1-4. Comparison of estimated Mk1 material inputs to other power plant types.

	Carbon Steel (1000 kg/MWe)	High Alloy and Stainless Steel (1000 kg/MWe)	Concrete (1000 kg/MWe)
Mk1 PB-FHR (100 MWe) (Tables 1-2 and 1-3)	39.2	11.2	383.9
ORNL 1970's PWR (1000 MWe) *	36.1	2.1	179.5
CRS nuclear plant range **	26 to 72	§	198 to 685
ABWR (1380 MWe) †	46.0	§	332.7
GT-MHR †	26.9	§	183.1
NGCC plant (620 MWe) ††	0.20	2.2	47.8
CRS NGCC plant range **	34 to 56	§	53 to 108
Pulverized coal steam plant (1000 MWe) †††	62.2	§	178.3
CRS coal plant range **	24 to 56	§	175 to 354

* ORNL 1974 study [20].

** Congressional Research Service (CRS) 2007 study [21]. Carbon steel values cited in this study may be for a conventional natural gas steam plant, rather than a combined cycle plant.

† UC Berkeley 2005 study [22].

†† U. Wisc. 2002 study [23].

††† Pacca and Hovath, 2002 [24].

§ Information not available

1.6 Mk1 Structural Materials Selection

The selection of structural materials for the Mk1 PB-FHR involves important tradeoffs. Structural materials options were reviewed in detail at the 3rd FHR Workshop in August, 2012 [25]. A key conclusion was that to minimize corrosion potential, a single metallic material should be selected to be in contact with salt. It was also recommended to select an alloy that has appropriate corrosion resistance and structural performance, rather than using a corrosion-resistant cladding with a different structural material. The other major structural material used in the Mk1 PB-FHR is graphite. Ceramic composites also have limited use, with carbon-fiber reinforced composite (CFRC) tubes being used as liners for instrumentation and graphite-test-coupon holes in the center reflector, and CFRC or SiC/SiC composites as structural materials in control rods and shutdown blades.

To provide a basis for design calculations, for example to have specific values for thermal conductivity, thermal expansion coefficient, and density, the baseline structural alloy selected for the Mk1 PB-FHR is 316 stainless steel (SS). Alternative materials that can be used are 304 SS, Alloy N, and potential advanced alloys that might be developed and qualified. Detailed engineering analysis will be required to make a final selection among these candidate materials.

A key benefit of FHRs is that they deliver heat at significantly higher temperature than liquid metal reactors (LMRs). As shown in Fig. 1-13, FHRs operate at higher temperatures than LMRs so thermal aging and thermal creep phenomena is more severe. Because the capability to manage and mitigate the effects of thermal aging, thermal creep, and corrosion is important to the viability of FHR technology, this section reviews key issues related to materials performance, and the Mk1 PB-FHR design approach for managing materials degradation.

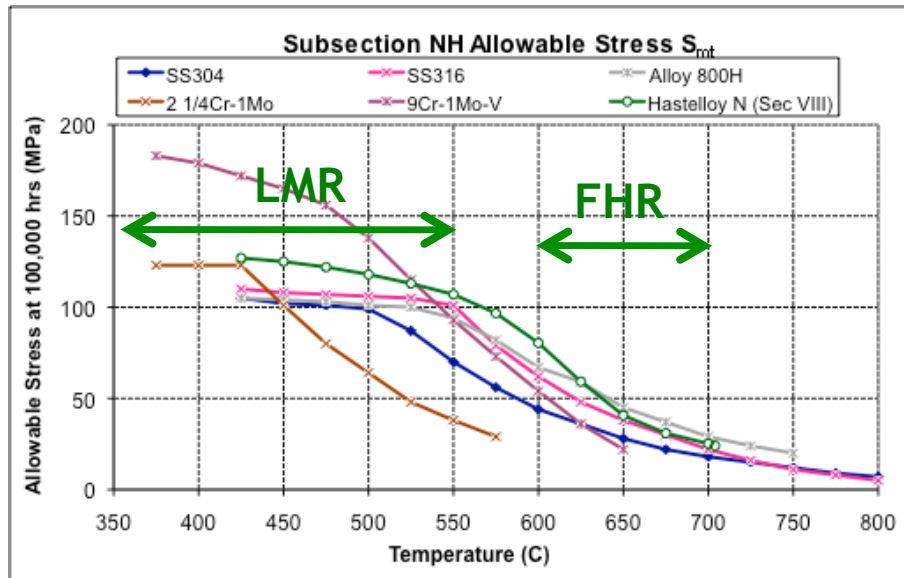


Figure 1-13. ASME Boiler and Pressure Vessel Code allowable stresses for candidate structural alloys.

1.6.1 Mk1 structural design approach

The Mk1 reactor vessel wall thickness is selected to keep vessel stresses within limits defined by the American Society of Mechanical Engineers (ASME) Boiler and Pressure Vessel Code, Section III, Division 5. The wall thickness will also be selected to limit stresses so that the maximum dimensional change to the vessel due to creep deformation in a 60-year service life would be 0.25%.

Likewise, the CTAH tube wall thickness will be designed to maintain stresses within limits sufficient to keep creep deformation below 0.25% during a 60-year service life. The stresses in these tubes are also maintained to be sufficiently low to allow salt freezing transients to be survived, including accounting for effects of low-temperature embrittlement due to long-term formation of sigma phase in the tubes.

While detailed engineering analysis will be needed to establish the reactor vessel and CTAH tube wall thicknesses, as well as required values for nozzles, heads, pipes, and other components, as a preliminary estimate wall thicknesses were computed based upon achieving von Mises stress level a factor of 4 or more lower than the ASME allowable stress for 100,000 hr of operation. Table 1-2 summarizes results of these calculations, and provides a comparison with the design and allowable stresses in the Super Power Reactor Innovative Small Module (S-PRISM) reactor vessel [26].

Table 1-5. Design stresses for Mk1 reactor vessel and CTAH tubes, with comparison to S-PRISM reactor vessel.

	Reactor vessel	HP CTAH tubes	LP CTAH tubes	S-PRISM reactor vessel†
Outside diameter (cm)	350.0	0.635	0.635	919.5
Wall thickness (cm)	6.0	0.0889	0.0889	5.0
Maximum pressure differential (bar)	2.50	16.72	2.95	1.41
Circumferential stress (MPa)	7.30	5.97	1.05	13.01
Axial stress (MPa)	3.71	3.47	0.61	6.54
Von Mises stress (MPa)	6.32	5.19	0.91	11.26
Von Mises stress (ksi)	0.92	0.75	0.13	1.63
Nominal operating temperature (°C)	600	700	700	355
ASME allowable stress for 316 SS for 100,000 hr (MPa)	60.0	23.00	23.00	110.00
Ratio of allowable to actual stress	9.49	4.43	25.19	9.77

† Pressure differential for S-PRISM based upon sodium hydrostatic head of 16.7 m

1.6.2 Mk1 structural material selection criteria

Section 4.4 reviews various degradation mechanisms that will affect the performance and service life of metallic components in the Mk1 PB-FHR system. This section also reviews the in-service inspection provisions of the Mk1 design, including the stand pipe locations where sample coupon baskets will be placed. Table 1-6 reviews the different selection issues/criteria for the Mk1 metallic structural material. Final selection of the structural material will occur during detailed design, but the Mk1 design considers the least favorable properties of all of these candidates (allowable stress, thermal expansion coefficient, and thermal conductivity), and can accommodate these properties.

Table 1-6. Ranking of Mk1 PB-FHR structural alloys.

Ranking Criteria	Better → Worse
Application experience at FHR temperatures	304 > 316 >> Alloy N
Cost	304 < 316 << Alloy N
Corrosion in flibe with redox control	Alloy N >> 304 ≈ 316
Allowable stress	Alloy N > 316 > 304
Sigma phase formation	Alloy N << 304 < 316
Neutron irradiation damage	304 > 316 >> Alloy N
ASME Section III code status	316 ≈ 304 >> Alloy N
Thermal conductivity	Alloy N > 316 ≈ 304
Thermal expansion coefficient	316 < 304 < Alloy N

1.7 Mk1 Fuel Development and Qualification

The United States, through its investments in the Next Generation Nuclear Plant (NGNP) program, has developed the complete set of capabilities required to manufacture, irradiate, and examine and characterize coated particle fuels. Testing at the Idaho National Laboratory (INL) of Advanced Gas Reactor (AGR) fuel compacts fabricated by Oak Ridge National Laboratory (ORNL) and irradiated over a 3-year period to 19.5% burn up in the Advanced Test Reactor (ATR) demonstrated that the new fuel manufacturing methods developed at ORNL provide impressively high quality fuel, that can retain fission products up to 1800°C [27].

Based upon the NGNP AGR irradiation capsule design (see [28], Fig. 29, pg. 94), the 2010 UCB NE-170 senior design class developed a fuel test capsule design of the same size, where the graphite holders for three stacks of cylindrical AGR fuel compacts are replaced by graphite spacers machined with hemispherical ends to hold 3.0-cm diameter PB-FHR fuel spheres. Their design, shown in Fig. 1-14, uses the same gas-gap system with a variable mixture of helium and neon to control the temperature of the fuel pebbles, and contains the same through tubes for thermocouples, flux wires, and gas lines. Their 2-D Comsol thermal model verified that conduction in the graphite spacers enables a remarkably symmetric temperature boundary condition around the pebbles, with minimal temperature differences between the poles and equators of the spheres.

Because the Mk1 fuel reaches full depletion in 1.4 years, it can be irradiated to full burn up in approximately 1/3 the 3-year time needed for the AGR irradiations. This is sufficiently rapid that fuel development and qualification is not expected to affect the critical path for design, licensing, and deployment of the Mk1 PB-FHR.

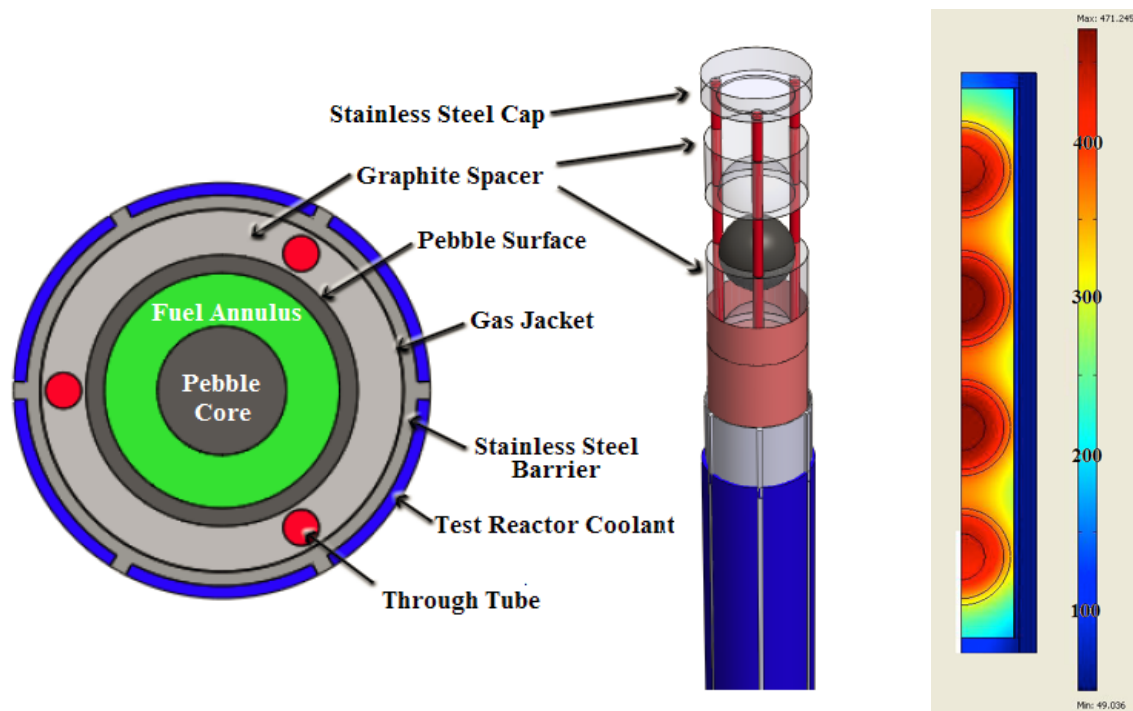


Figure 1-14. Design of a PB-FHR pebble fuel test capsule (left) and thermal analysis of capsule using Comsol (right) by the 2010 UCB NE-170 senior design class [29].

1.8 Comparison with Other Reactors

Table 1-7 compares several key design parameters for the 236-MWth Mk1 PB-FHR with values for four other reactor designs: the 3400-MWth 2012 ORNL Advanced High Temperature Reactor (AHTR) design, which is a large, fixed-fuel FHR coupled to a supercritical steam cycle [30]; a Generation II 4-loop Westinghouse PWR [31]; the helium-cooled Pebble Bed Modular Reactor (PBMR) [32]; and the sodium-cooled GE S-PRISM fast-spectrum reactor [33]. Several observations can be made based on this data.

First, the PB-FHR and ORNL AHTR both have remarkably small in-core inventories of Cs-137, approximately 1/3 the inventory in a typical PWR, per megawatt electric. Because Cs-137 has a 30-year half life and strong gamma emission, Cs-137 is the most important isotope responsible for creating requirements for long-term land-use restrictions following the major accidents at Chernobyl and Fukushima. While it is understood that FHRs have much larger thermal margins to fuel damage, and that cesium fluoride has low volatility and is strongly retained in fluoride salt coolants, the fact that FHRs have an intrinsically smaller Cs-137 inventory than LWRs is still noteworthy. This occurs in part due to the higher thermal efficiency of the FHRs, but primarily to the very short time required for FHR fuel to reach full depletion (1.0 yr for the ORNL AHTR and 1.4 yr for the PB-FHR) that also reduces the total inventory of fuel needed in the core.

Table 1-7. Comparison of Mk1 design parameters with the large 2012 ORNL AHTR, a 4-loop Westinghouse PWR, the PBMR, and the S-PRISM.

	Mk1 PB-FHR	ORNL 2012 AHTR	Westing- house 4-loop PWR	PBMR	S- PRISM
Coolant	flibe	flibe	water	helium	sodium
Core inlet/outlet temperatures (°C)	600-700	650-700	292/326	500/900	355/510
Reactor thermal power (MWt)	236	3400	3411	400	1000
Reactor electrical power (MWe)	100	1530	1092	175	380
Fuel enrichment †	19.90%	9.00%	4.50%	9.60%	8.93%
Fuel discharge burn up (MWt-d/kg)	180	71	48	92	106
Fuel full-power residence time in core (yr)	1.38	1.00	3.15	2.50	7.59
Power conversion efficiency	42.4%	45.0%	32.0%	43.8%	38.0%
Core power density (MWt/m ³)	22.7	12.9	105.2	4.8	321.1
Fuel average surface heat flux (MWt/m ²)	0.189	0.285	0.637	0.080	1.13
Fuel specific surface area (area/volume) (1/m)	120	45	165	60	285
Reactor vessel diameter (m)	3.5	10.5	6.0	6.2	9.2
Reactor vessel height (m)	12.0	19.1	13.6	24.0	19.6
Reactor vessel specific power (MWe/m ³)	0.866	0.925	2.839	0.242	0.292
Start-up fissile inventory (kg-U235/MWe) ††	0.79	0.62	2.02	1.30	6.15
EOC Cs-137 inventory in core (g/MWe) *	30.8	26.1	104.8	53.8	269.5
EOC Cs-137 inventory in core (Ci/MWe) *	2672	2260	9083	4667	23359
Spent fuel dry storage density (MWe-d/m ³)	4855	2120	15413	1922	-
Natural uranium (MWe-d/kg-NU) **	1.56	1.47	1.46	1.73	-
Separative work (MWe-d/kg-SWU) **	1.98	2.08	2.43	2.42	-

† For S-PRISM, effective enrichment is the Beginning of Cycle weight fraction of fissile Pu in fuel

†† Assume start-up U-235 enrichment is 60% of equilibrium enrichment; for S-PRISM startup uses fissile Pu

* End of Cycle (EOC) life value (fixed fuel) or equilibrium value (pebble fuel)

** Assumes a uranium tails assay of 0.003.

The short time for FHR fuel to reach full depletion also causes the ORNL AHTR and the Mk1 PB-FHR to require much smaller fissile inventory to start up, less than 1/3, compared to a typical PWR. This characteristic has the economic benefit of reducing the cost of the initial core load for reactor startup.

The Mk1 PB-FHR fuel has slightly better natural uranium utilization than the ORNL AHTR and typical PWRs, but requires slightly more separative work for enrichment. Overall the four low-enriched uranium designs achieve similar utilization of uranium resources. The Mk1 PB-FHR requires about 3.2 times more dry storage volume for its spent fuel compared to a PWR, but less than half the storage volume needed for the ORNL AHTR and the PBMR.

While the pebble bed core of the Mk1 PB-FHR operates with almost twice the power density of the fixed plate fuel ORNL AHTR, the heat flux from the fuel surface to the coolant is significantly lower in the Mk1 core due to the higher specific surface area provided by the pebble fuel, which is comparable to the specific surface area in a PWR. Because the average convective heat transfer coefficients are similar for the Mk1 and AHTR cores (4700 and 5000 W/m²°C

respectively), the Mk1 design operates with lower average fuel temperature than the AHTR, which reduces the thermal transient caused by ATWS BDBEs.

Because FHRs operate at low pressure and use pool-type reactor vessels, their capital costs can be compared most directly to sodium fast reactors (SFRs) such as S-PRISM that share these features. One key new characteristic of the Mk1 PB-FHR is that it eliminates the intermediate coolant loop used in all previous FHR designs and in all SFRs built to date. SFRs use intermediate loops because sodium reacts energetically when contacted with water in a steam generator (as well as with air and carbon dioxide). The fluoride-salt coolant used in FHRs has high chemical stability. ORNL performed experiments in 1955 that dumped 190 kg of molten flinak salt at 815°C into a 3.0-m-diameter pool of water over a period of 45 seconds, and observed that during this experiment, “Water adjacent to the tank bottom boiled briskly, but not violently enough to shake the steel tank visibly or cause any noise other than the burbling of boiling water.” [34].

The Mk1 primary system is more compact compared to conventional SFRs and PBMRs. For pool-type reactors the electrical power generated per unit of reactor vessel volume provides one metric for the primary system cost. The relationship is less direct in comparing FHRs with helium-cooled PBMRs, but is still useful. The Mk1 PB-FHR reactor vessel has a volumetric power density of 0.9 MWe/m³. This Mk1 PB-FHR value is nearly 3 times greater than that of the S-PRISM [35] and the PBMR. The Mk1 volumetric power density is comparable to that of the 100-MWe lead-bismuth-cooled “SVBR” fast reactor that is in advanced development phase in Russia [36]

1.9 Organization of Report

This report is structured to provide descriptions of the major systems used in the Mk1 PB-FHR design. Chapter 2 reviews the nuclear heat supply systems, including the reactor and its internals, reactivity control, emergency decay heat removal, and the reactor containment systems. Chapter 3 reviews the heat transport systems, including the main salt piping and pumps, CTAHs, air ducts, and normal shutdown cooling systems. Chapter 4 reviews main support systems, including tritium control, beryllium control and radiation protection, coolant chemistry and inventory, cover gas chemistry and inventory, fuel handling and storage, and instrumentation and control systems. Chapter 5 reviews the Mk1 NACC power conversion system, including results from modeling the system using the Thermoflex code. Chapter 6 describes key remaining gaps in the Mk1 design and outlines future research needs.

2 Mark-1 Nuclear Heat Supply

This chapter describes the major nuclear heat supply systems of the Mk1 PB-FHR, which include the reactor internals, reactivity control, DRACS, and reactor vessel and cavity/containment systems.

2.1 Reactor Internals System

This subsection reviews the design of the Mk1 PB-FHR reactor vessel internals, including the fuel and reflector pebbles, graphite structures, core barrel and upper core support structures, and primary coolant flow paths.

2.1.1 Fuel and reflector pebbles

As shown in Fig. 2-1, the Mk1 PB-FHR uses 3.0-cm-diameter, spherical pebble fuel elements with coated particles in an annular fuel zone, and a low-density center graphite core. PB-FHR pebbles are expected to operate at much lower average and peak temperatures than pebbles in previous helium-cooled pebble bed reactors, such as the German “AVR” reactor, which experienced significant releases of Cs-137 into its helium coolant. This is due to the lower outlet temperature of the PB-FHR (700°C vs. 950°C), the annular geometry of the PB-FHR fuel layer, and the mechanisms that increase cooling of hot spots in the PB-FHR core (salt viscosity drops, rather than increases, with increasing temperature; and buoyancy forces aid flow, rather than reduce it, for up-flow of coolant).

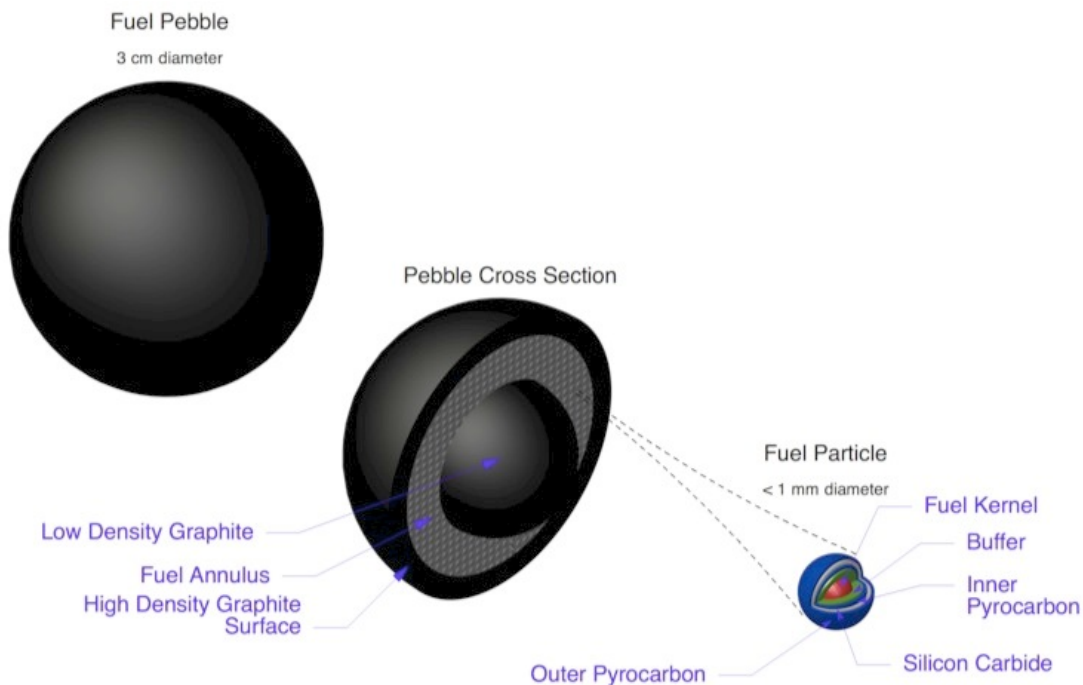


Figure 2-1. A PB-FHR pebble fuel element (Credit: D. Holcomb, ORNL).

Because the diffusion of metallic fission products like silver and cesium in pyrocarbon and graphite depends very strongly on temperature [37], with its lower temperature PB-FHR fuel is expected to provide significantly better retention than helium-cooled reactor fuels under normal operation and accident conditions, even if a significant number of defective fuel particles exist.

Likewise, important differences exist in the retention and transport of fission products released from PB-FHR fuel elements versus helium-cooled reactor fuel. In helium-cooled reactors, the cesium and other metallic fission products accumulate on various surfaces, including on graphite dust particles. It is difficult to predict both the inventory and how it might be mobilized by high-velocity helium flow during a loss-of-coolant accident. Conversely, fission products released from FHR fuel either form stable fluorides, like CsF, which distribute homogeneously in the salt coolant and can be monitored accurately, or precipitate on metal surfaces (e.g. silver) where they are immobilized, or are noble gases (e.g. krypton) and are released to the FHR cover-gas system. The Mk1 design has cold traps (Section 4.3.1), where noble metal fission products are expected to precipitate preferentially. Cesium fluoride will remain dissolved in the salt, but can be removed using off-line processing with reductive extraction to bismuth-lithium (Section 4.3.3).

The reduced fuel temperature also provides improved response to hypothetical ATWS accidents. The coolant of FHRs does not boil as is the case in ATWS transients in LWRs. The negative fuel temperature reactivity feedback in FHRs is significantly larger than the coolant temperature reactivity feedback, because the coolant does not boil, and larger than the graphite moderator temperature reactivity feedback. Under the beyond design basis ATWS accident where reactor scram does not occur upon loss of flow or loss of heat sink, the FHR coolant equilibrates to a temperature close to the original fuel temperature. Simplified analysis for the Mk1 design, discussed in Section 2.2.4, indicates that this equilibrium ATWS temperature will be below 800°C.

As shown in Table 2-1, each Mk1 pebble contains 1.5 g of 19.9% enriched uranium encapsulated inside 4730 coated particles with 400- μm uranium kernels. This can be compared to the AGR-1 fuel compacts that have undergone irradiation tests in the INL Advanced Test Reactor, which each contained 0.9 g of 19.8% enriched uranium in 4150 particles with 350- μm uranium kernels, inside cylindrical, 1.25-cm-diameter, 2.54-cm-long compacts [38]. Mk1 pebbles are sufficiently small that they can fit inside the same canisters used in the AGR-1 fuel testing.

One key issue for nuclear systems that use coated particle fuel is that the fabrication costs of tristructural-isotropic (TRISO) are highly speculative. Estimates for TRISO fuel fabrication costs range from 1,650 to 10,000 \$/kgU [39][40]. Assuming fabrication costs of 10,000 \$/kgU, fuel fabrication can account for 41% of the fuel costs, about 0.58 cents/kWhr-e. The NGNP/AGR program is scaling up TRISO fuel fabrication from the lab scale to a pilot line with Babcock and Wilcox, with a goal of reducing fabrication costs [41].

Table 2-1. Mk1 PB-FHR fuel and core design.

Fuel pebble design	
Pebble diameter	30.0 mm
Graphite coating thickness	1.0 mm
Inner graphite core diameter	25.0 mm
Uranium enrichment	19.9%
Pebble heavy metal loading	1.5 gHM
Carbon to heavy metal ratio	300
Number of coated particles per pebble	4730
Coated particle packing fraction in fuel layer	40%
Average pebble thermal power	500 W
Average pebble density	1745 kg/m ³
Average pebble discharge burnup*	180 MWd/kgHM
Average pebble full-power lifetime	1.40 yr
Fuel kernel design	
Fuel kernel diameter	400 μm
Fuel kernel density	10,500 kg/m ³
Fuel kernel composition	UC _{1.5} O _{0.5}
Buffer layer thickness	100 μm
PyC inner layer thickness	35 μm
SiC layer thickness	35 μm
PyC outer layer thickness	35 μm
Core design	
Thermal power	236 MWth
Electrical power	100 MWe
Average pebble bed void fraction	40.0%
Inner reflector radius	0.35 m
Outer radius of fuel pebble region	1.05 m
Outer radius of graphite pebble region	1.25 m
Average power density in active fuel region**	23.0 MW/m ³
Number of fuel pebbles in core and defueling chute	470,000
Number of graphite pebbles in core and defueling chute	218,000
Volume of active fuel region	10.4 m ³
Volume of graphite reflector pebble region	4.8 m ³
Volume of defueling chute***	1.03 m ³

* Estimated based on design studies for a 290MWth core, scaled to 236 MWth core

** Volume for fuel pebbles in entrance-, active- and converging regions

*** Volume for seed and inert graphite pebbles to reside in the defueling chute for 4 days; additional decay occurs in the low flux region at the top of the core

These costs are driven by small batch sizes for particle fabrication and arduously high quality destructive testing required to minimize off-site dose in high-temperature gas-cooled reactors (HTGRs). Testing of a large number of sample particles is required to obtain the statistics necessary to ensure the quality of the loaded fuel since 100% inspection is not possible as is performed today for LWR pellet fuel. Due to a combination of mild operating and severe accident conditions and fission product retention in the liquid salt coolant in FHRs, these reactors

could exhibit similar or enhanced safety with respect to HTGRs with less destructive testing of TRISO fuel, significantly reducing the fuel costs. However, fuel performance modeling for normal operation and accident transients is required to definitively confirm this assumption. Further innovations in fuel fabrication methods, such as continuous particle fabrication, could reduce costs further.

High fuel fabrication costs lead to fuel designs optimized for high burnup, utilizing uranium enriched above 5%. Most commercial enrichment facilities, such as new centrifuge facilities planned in Lee County, New Mexico [42], and Bonneville County, Idaho [43], are licensed to produce uranium enriched up to a maximum limit of 5%. While higher enrichment levels can be obtained by down blending excess highly enriched uranium, the existing Russian down-blending program is ending and the U.S. does not currently downblend highly enriched uranium for use in civilian applications. The Russian enrichment company Tenex can provide uranium enriched to higher levels, but the very small demand for separative work units (SWU) for enrichment above 5%, and the existence of a single existing supplier, makes it likely that SWU for FOAK FHRs will be more expensive than for LWRs. Conversely, while URENCO and other centrifuge enrichment facilities are technically capable of enriching to above 5%, the lack of current demand makes it unattractive for enrichment vendors to spend the funds needed to amend their licenses to allow enrichment to higher levels. This chicken-and-egg problem that limits the number of potential enrichment suppliers, and thus creates risks that at least early on SWU prices will be significantly higher for FHRs than LWRs, is a significant concern for the initial deployment of commercial FHR reactors.

There are two U.S. vendors that are currently pursuing licenses to construct enrichment facilities for enrichment levels exceeding 5%. The American Centrifuge Plant in Piketon, which will be licensed to produce uranium enriched up to a maximum of 10% [44]), and the Global Laser Enrichment facility in Wilmington, which will be licensed to produce fuel enriched up to 8% [45].

The Mk1 fuel design uses 19.9% enrichment. To increase the number of suppliers for enrichment services and reduce the cost of SWU for initial commercial FHRs, it is desirable in the future to identify potential fuel design using uranium enriched to 8% to 10%. The issue is that the relatively small core volume of the Mk1 reactor, the neutron leakage probability is high and the attainable fuel utilization is highly reduced at these enrichment levels. Determining the optimal enrichment and uranium loading will require improved understanding of fuel fabrication methods, fabrication costs, and separative work costs at different enrichment levels, as well as exploring approaches to increase the diameter of the reactor core, which can improve fuel utilization at lower enrichment levels.

2.1.2 Core design

The Mk1 PB-FHR uses an annular pebble-bed core geometry. As shown in Fig. 2-2, the Mk1 core consists of two radial layers, an inner, homogeneously mixed region of fuel pebbles, and a thinner, outer region of graphite reflector pebbles. The graphite reflector pebbles provide shielding to the fixed outer radial graphite reflector to increase its service life. While the center reactor internals need to be replaced periodically due to radiation damage, the shielding of the outer reflector is intended to allow it to be used for the full operating life of the plant.

Because FHR fuel has positive buoyancy in the coolant salt, the pebbles are introduced into the bottom of the bed, with fuel pebbles being introduced by four inner pebble injection channels and reflector pebbles introduced by four outer channels. The pebbles move upward through the core at a low speed, with an average residence time of 2.1 months. The pebbles are removed through an annular slot at the top of the core, that converges into two defueling machines.

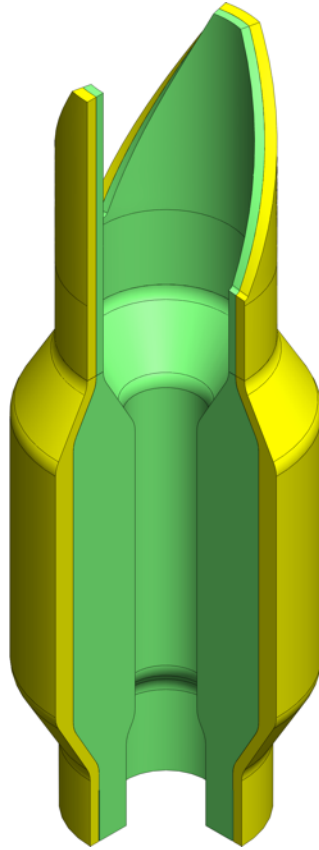


Figure 2-2. Mk1 pebble core geometry showing fuel pebble (green) and graphite reflector pebble (yellow) regions.

The 3-D Mk1 core has been modeled neutronically using MCNP, as shown in Fig. 2-3. Detailed results of the physics modeling can be found in the dissertation of A.T. Cisneros [46]. Table 2-1 summarizes key design parameters for the baseline low-enriched uranium fuel and core designs. Section 4.6 (“Fuel Handling and Storage”) describes the Mk1 fuel management concept in greater detail. The baseline concept for fuel handling in the Mk1 PB-FHR is that pebble handling, assay, and recirculation are performed inside the reactor vessel, and that fuel additions and removal from the reactor vessel are performed using canisters located outside of the reactor cavity.

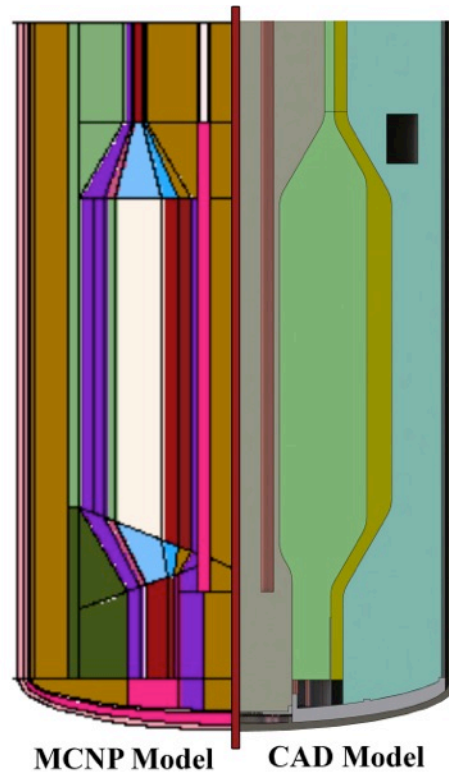


Figure 2-3. Comparison of the Mk-1 annular core design MCNP model (left) and SolidWorks model (right).

2.1.3 Pebble injection subsystem

The Mk1 PB-FHR design includes pebble injection channels integrated into the inner surface of the reactor core barrel, as shown in Fig. 2-4. These channels also serve as axial ribs to maintain alignment of the outer reflector graphite blocks, as described in later in this section. The square channels have a nominal 3.75 cm inside width and 4.75 cm outside dimension, with 0.50-cm-thick walls. The pebble injection channels follow the curvature of the bottom of the reactor vessel before discharging pebbles through the replaceable lower center reflector support structure.

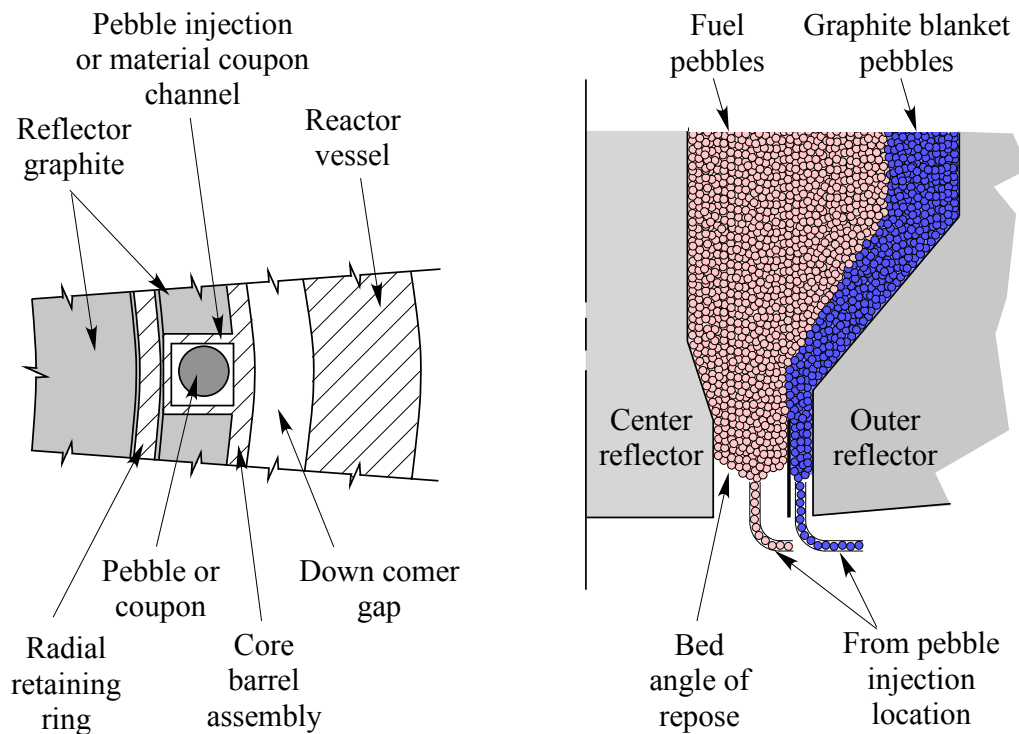


Figure 2-4. Mk1 pebble injection channels schematic.

As pebbles are defueled from the top of the core, the bed moves away from these tubes, and additional pebbles enter, maintaining an annular pebble heap above each injection tube based on the angle of repose. To obtain a sufficiently uniform geometry for the bottom of the pebble bed, fuel pebbles and graphite reflector pebbles are each injected at 4 locations around the circumference of the bed. The resulting heap height for the fuel pebble and graphite pebble regions will be 9.4 cm and 12.6 cm, respectively, based on a friction coefficient of 0.2. The pebble hopper divider plates in the lower reflector support structure extend 50 cm above the top of the pebble injection channels to ensure that distinct zoning is maintained as pebbles flow upward into the diverging region.

Fig. 2-5 shows experimental results using the UCB X-ray Pebble Recirculation Experiment (X-PREX) to study the slot-flow of the reflector pebbles, confirming that pebbles spread at an approximately constant shallow angle emerging from the injection tube when plug flow is simulated experimentally using a downward-moving piston. The injection channel in this system contains a column of pebbles that is not jammed and will flow readily to the top of the heap as pebbles are removed from the bottom of the container. The polypropylene pebbles show an angle of repose of 20 degrees, corresponding to a friction coefficient of 0.37. This is assumed to be higher than that of graphite lubricated in salt, but additional confirmation measurements will be required. These tests also demonstrate pebble flow without bridging, even in a slot representing a significantly deformed divider plate that converges to 2.4 pebble diameters at its end at an angle of 1.5 degrees. No mechanism for pebble jamming has been identified for slots that maintain a vertical geometry.

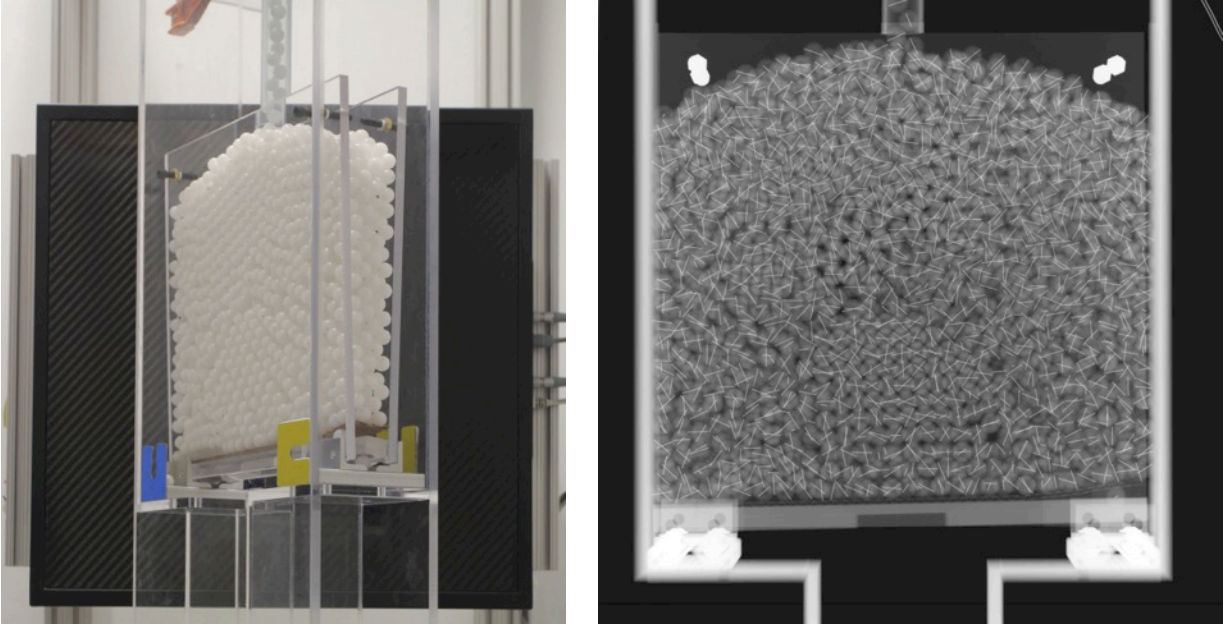


Figure 2-5. UCB NE-92 class experiment using the XPRES facility with 1.27-cm-diameter polypropylene spheres to study heap geometry for reflector pebbles fed into a wide slot with a downward-moving piston. Note in this case the slot is tapered (left), and the x-ray image (right) shows instrumented pebbles and the bed geometry.

In addition to the pebble injection tubes, additional vertical square tubes are integrated along the inside surface of the core barrel to hold 316 SS irradiation samples to monitor effects of neutron irradiation on the core barrel and reactor vessel material. These channels mirror the design of the pebble injection channels and can be sized later in the design process based on the material sample requirements. These channels will also serve as axial ribs to maintain the radial alignment of the outer reflector blocks.

2.1.4 Graphite structures

The two primary graphite structures in the PB-FHR are the center and outer radial reflectors, which confine the annular pebble-bed core. In addition, graphite is used in other parts of the reactor, primarily to displace the primary coolant and reduce the total coolant volume, and also to carry compressive stresses under BDBE conditions. This subsection describes the design of the center and outer radial reflectors.

All of the graphite structure blocks are designed so that they can be machined using a multi-axis computer numerically controlled (CNC) milling machine. The geometries of the center and outer reflector blocks all contain no reentrant features, and can be machined with a multi-axis CNC milling machine using only plunging motions. All of the features can be machined in two steps, the first where the graphite billet is placed in the machine and features on one side are completed, and the second where the billet is inverted, and features on the bottom side are machined.

2.1.4.1 Center reflector

The center graphite reflector, shown in Fig. 2-6, performs multiple functions. Because the center reflector receives high neutron dose, it is designed to be replaceable as a modular unit. It

is fabricated from 0.26-m-thick graphite billets, which are machined to a net thickness of 0.25 m to provide keys that maintain the vertical alignment of the reflector blocks. The maximum diameter of the blocks is 1.42 m at the top of the reflector structure, which is comparable in size to the 1.0-m-diameter, 0.9-m-thick graphite blocks that have been fabricated for use in the high temperature test reactor in Japan [47]. The South African PBMR project had established the capability to produce graphite blocks at SGL Carbon in Germany, which is also providing graphite for testing for the Shanghai Institute of Applied Physics (SINAP) Thorium Molten Salt Reactor-Solid Fuel (TMSR-SF) research reactor. In the center region, the diameter of the reflector drops to 0.70 m, and it expands back to 0.90 m at the bottom.

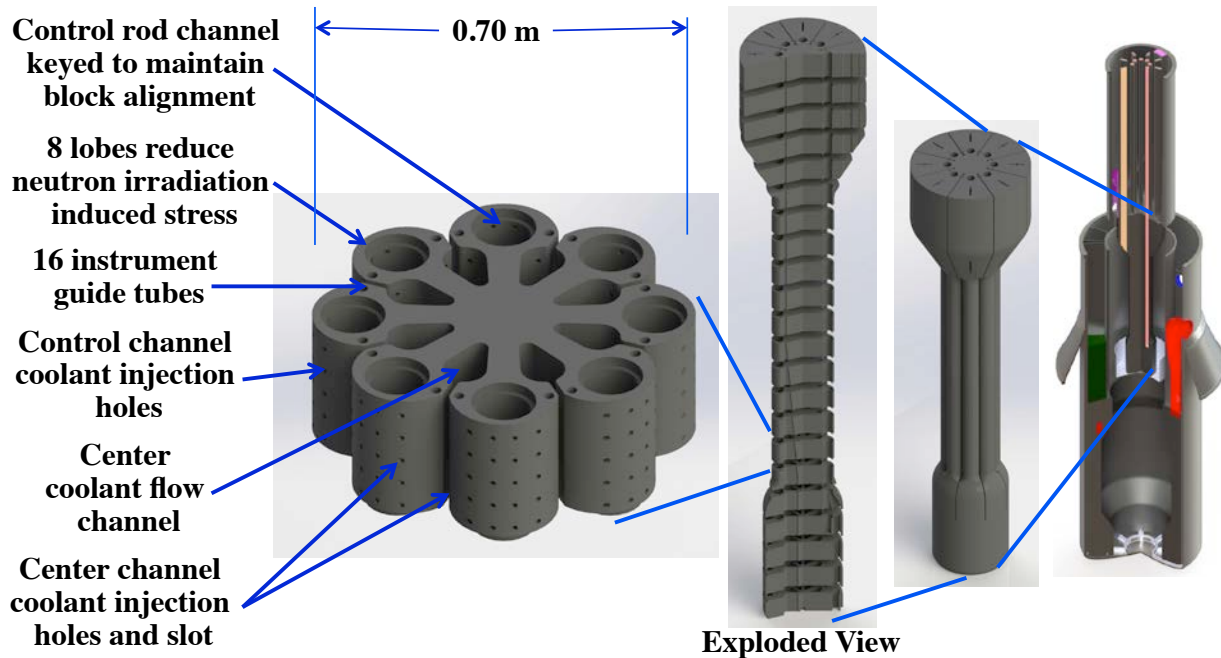


Figure 2-6. Replaceable Mk1 center graphite reflector

Because the nominal density of the graphite, 1740 kg/m^3 , is slightly lower than the density of the primary salt (1963 kg/m^3 at 650°C), these blocks are nearly neutrally buoyant, but float in the primary coolant. Thus the blocks float upward, and rest against the metallic center upper core support structure, which is keyed to maintain alignment so that shutdown blade and control rod elements can pass through channels machined into the reflector blocks.

Because the center reflector lifetime will be limited by neutron-irradiation-induced shrinkage and swelling, the geometry of the center reflector is selected to reduce the peak stresses caused by shrinkage. The center reflector design has 8 lobes around its circumference. Under neutron irradiation graphite initially shrinks, which creates tensile stresses. The lobe design reduces the resulting peak circumferential stress, by accommodating the shrinkage via bending of the web around the control rod hole and by changing the gap dimension between the lobes. Likewise, the axial stress is reduced by having the blocks have a relatively small individual height of 25 cm, which is comparable to the circumference of each lobe, $\pi(70\text{cm})/8 = 27.5 \text{ cm}$. Cisneros (2013, pg. 200) concluded that the Mk1 center reflector would take 10 effective full power years (EFPY) to reach a peak irradiation damage level of 22.1 displacements per atom (DPA).

A key design constraint for the center reflector is to prevent buckling of the block stack under seismic loads. Because the blocks are nearly neutrally buoyant in the coolant, actual horizontal loads imparted to the center column during seismic events are reduced significantly, and because the column diameter increases at the top, the column is stabilized against buckling. The outer lobes of the center reflector have 16 2.0-cm diameter instrumentation holes, that will have hollow CFRC tubes to provide access for neutron flux mapping, temperature mapping, and insertion of irradiation coupons. These tubes are also expected to carry tensile loads between blocks and assist in restraining buckling.

2.1.4.2 Outer radial reflector

The Mk1 outer radial reflector uses rings of 24 graphite blocks, with each ring being 0.50 m high. When the vessel is filled with salt, the blocks float upward against the upper, outer metallic core internals structure. Because the core-barrel structure is 316 SS, the reflector block alignment system must accommodate the differential thermal expansion between the blocks and the core barrel, when the system is heated from room temperature to its operating temperature.

The MSBR design used a system of vertical ribs and radial retaining rings, to maintain its reflector blocks positioned against the vessel wall, as shown in Fig. 2-7.

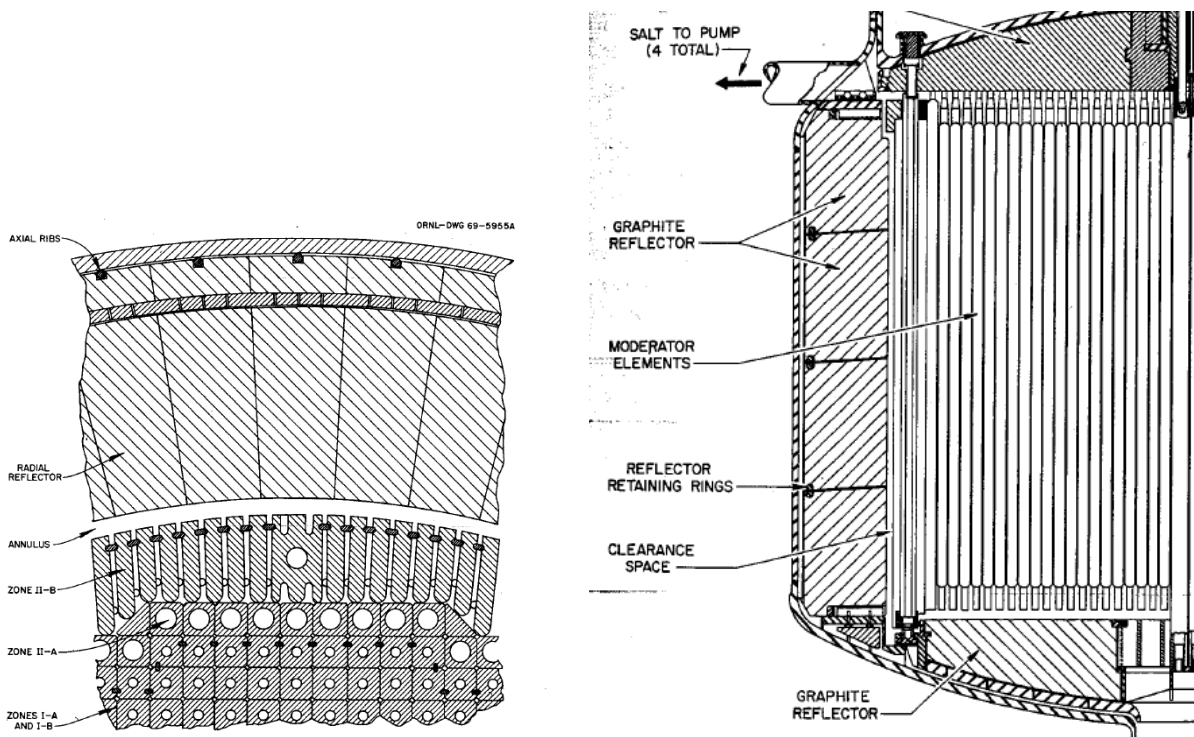


Figure 2-7. Radial reflector block retaining system used in the MSBR design [48].

The Mk1 reflector uses the same alignment design system originally developed for the MSBR radial reflector. As shown in Fig. 2-8, each column of blocks is positioned in the circumferential direction by a vertical rib welded to the inside of the core barrel, that engages a slot on the back of the block. Likewise, metallic radial retaining rings are placed in

circumferential slots machined in the top and bottom of each block. Because these retaining rings are heated to nearly the same temperature as the core barrel, they expand radially by a nearly equivalent amount, and thus push the graphite blocks out to nearly the same radial position, keeping the blocks positioned against the core barrel and engaged with the axial core barrel ribs.

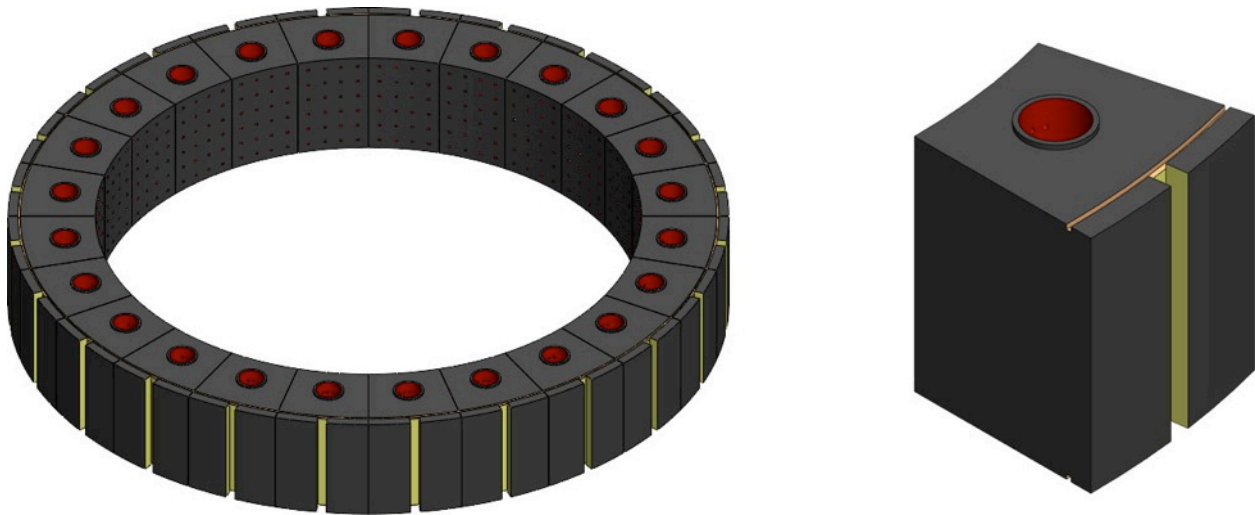


Figure 2-8. An upper ring of the Mk1 outer radial reflector, showing coolant suction holes and slots for radial retaining rings and vertical retaining ribs.

When heated from room temperature to 600°C, the retaining ring diameters increase by approximately 3.4 cm. The circumference of the rings increases by 10.7 cm, so the expansion opens the gaps between the 24 columns of blocks by 0.45 cm. While this gap is much smaller than the 3.0 cm diameter of the reflector pebbles and thus prevents pebbles from becoming lodged between the block, it still provides a bypass flow path. As a result, in the Mk1 design, the blocks in each row are staggered by 2 cm relative to the blocks below to restrict bypass flow up this gap. Likewise, triangular notches are machined into the upper and lower corners of the blocks where they contact the core barrel, to allow segments of braided carbon fiber tube to be inserted to suppress vertical bypass flow between the blocks and the core barrel.

Cisneros [49] concluded that the reflector pebbles are highly effective in protecting the Mk1 outer reflector from neutron damage, estimating the service life to be over 600 years. While the reflector pebble blanket and the outer radial reflector are effective in thermalizing fast neutrons, thermal neutrons react with nickel to form helium that embrittles the 316 SS core barrel and reactor vessel. Cisneros concluded that the helium generation in the 316 SS core barrel would limit its life to 10 EFPY unless it is shielded from thermal neutrons. The Mk1 reflector block design includes space to insert pins containing boron, to absorb neutrons and reduce this dose rate. The 2012 UCB senior design project studied the design of 316 SS clad pins with boron carbide pellets, for this purpose [50]. The 316 SS cladding helps isolate the boron carbide from the primary coolant, since having even small amounts of boron become dissolved in the coolant would cause problems with the core neutronics. As an alternative, boron carbide or boron oxide in the form of coated particles in cylindrical compacts may also be used.

It is not considered to be practical to transport the PB-FHR vessel with the core internals and reflector blocks installed. Instead, the outer radial reflector blocks are installed into the core internals at the reactor construction site, with the internals in the vertical orientation, and then the internals are lifted and installed into the reactor vessel with the blocks in place. If the outer radial reflector requires replacement, it is expected that the entire core internals support structure would be replaced as well.

The installation of the reflector blocks is performed in air, and thus the blocks are negatively buoyant. The bottom row of blocks is installed on alignment pins on a movable 316 SS lower support ring. Subsequent rows of blocks and retaining rings are then installed.

Under dry installation conditions, support for the outer reflector structures will be provided through the core barrel lower support structure. The bottom support ring has 8 vertical, radial support ribs that are located to match the axial ribs that are inside the core barrel. These radial support ribs are welded to a dished ring designed to fit just above the bottom of the reactor vessel that has vertical pins welded into it to maintain radial alignment of the bottom row of blocks. These blocks are slotted to fit over the radial ribs.

After the top row of blocks is installed, the lower support ring is lifted using hydraulic jacks, to lift the radial reflector blocks. Once lifted, the ribs of the lower support ring are welded to the slots in the core barrel, and the pebble injection tubes are installed on the outside of the core barrel. Once this assembly is complete, the core internals are lifted by crane and installed into the reactor vessel.

2.1.5 Core barrel and upper core support structures

The Mk1 PB-FHR uses a metallic core barrel, which is integral to the upper core support structures. The Mk1 upper core support structures adopt the design approach common to molten salt reactors like the MSBR [51], where the structures and reactor lid extend down inside the reactor vessel.

The reactor vessel has two cold legs and one hot leg penetration, located immediately above the conical vessel support skirt ring. The upper core support structure, shown in Fig. 2-9, rests on top of an internal flange inside the reactor vessel. This flange defines the top of the downcomer annulus in which cold salt flows from the cold legs to the bottom of the reactor vessel. This internal flange wraps around the majority of the vessel circumference above the top of the cold leg nozzles, but drops down to run at the skirt elevation locally next to the hot leg nozzle.

The internal flange has an o-ring seal to limit bypass flow from the downcomer to the annular space above the flange. Orifice holes in the flange, opposite the hot leg, provide a controlled bypass flow into this annular gap. Salt then flows around the gap, to the hot leg, where it is entrained into the hot leg flow.

The nominal gap between the core barrel and reactor vessel is set to give the desired average coolant flow velocity. For a nominal velocity of 2.0 m/s and volumetric flow of 0.54 m³/s, this ends up being 2.8 cm. As the coolant flow converges inward towards the center reflector, a nominal channel height of 8.8 cm is required at a radius of 45 cm to avoid excessive flow acceleration. This area will be accommodated by a combination of detailed design for the core

barrel lower support structure and the differential in vertical thermal expansion between the metallic core barrel assembly and the ceramic graphite reflector blocks. As the coolant is added to the conditioned reactor vessel, the reflector blocks will float upward due to buoyancy and loads will be transferred from the core barrel lower support structure to the upper core support structures.

The outer upper core support internals also house three DRACS heat exchanger (DHX) wells and equipment for pebble handling, assay, and recirculation. Detailed design of these systems was not performed for the Mk1 design, and will be developed later. The center upper core support internals are designed to be removed along with the center graphite reflector. The center upper core support internals house the two defueling machines and stand pipes for the 8 buoyant control rods, 8 reserve shutdown blades, and 16 center reflector instrument guide tubes.

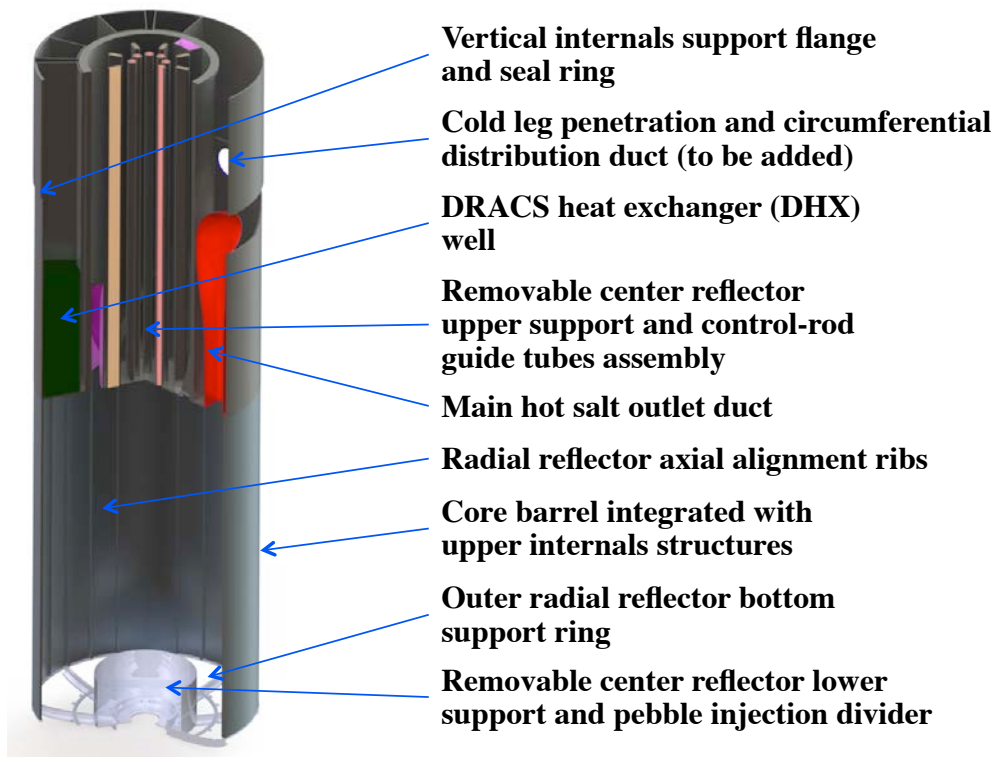


Figure 2-9. Mk1 metallic core internals.

2.1.6 Primary coolant flow path description

This section describes the primary coolant flow paths in the Mk1 reactor design, as well as the approaches used to minimize and predict pressure losses in the primary coolant loop. The Mk1 design is careful to minimize pressure losses, to simplify the implementation of the gas-gap isolation method. This description of the primary coolant flow path is also helpful for developing thermal hydraulic models for the Mk1 PB-FHR. The nominal coolant flow rate in the Mk1 design is 0.54 m³/sec (Table 1-1). To keep the dynamic head relatively low, nominal flow velocities around $u = 2.0$ m/sec (dynamic head $u^2/2g = 0.20$ m) are maintained.

Table 2-2 lists the volumes of flibe in the Mk1 reactor design by system and subsystem. The Mk1 design uses approximately 47 m³ (91,970 kg) of flibe as its main salt, or 0.92 kg per

kilowatt electrical power. This is approximately 5 times the volume of salt used in the 2008 UCB 900-MWth modular PB-AHTR design per kilowatt electric [52], and a factor of approximately 0.45 times less than the volume used in the 2012 ORNL AHTR design per kilowatt electric [53].

Table 2-2. Flibe volumes by system and subsystem in the Mk1 PB-FHR.

System/Subsystem	Flibe Volume (m ³)	Flibe Volume (%)
Core	7.20	15.4%
Active Core Region + Fueling Chute	6.52	13.9%
Defueling Chute	0.68	1.5%
Reactor Internals	3.38	7.3%
Coolant Injection Channels	0.14	0.3%
Control Rod Channels	0.36	0.8%
Pebble Injection Lines	0.25	0.5%
Free Space Below Pebble Bed	0.38	0.8%
Downcomer	2.50	5.3%
Cold Leg	6.91	14.8%
2x CTAH to Drain Tank	1.47	3.1%
2x Stand Pipe	3.45	7.4%
2x Stand Pipe to Reactor Vessel	1.99	4.3%
Hot Leg	11.13	23.8%
Hot Salt Collection Ring	1.00	2.1%
Hot Salt Extraction Pipe	0.95	2.0%
Reactor Vessel to Hot Salt Well	1.12	2.4%
Hot Salt Well	6.63	14.2%
2x Hot Salt Well to CTAH	1.44	3.1%
CTAH	13.55	28.9%
2x Hot Manifold Pipes	3.52	7.5%
2x Coiled Tube Inner Volume	8.65	18.5%
2x Cold Manifold Pipes	1.38	2.9%
DHX	0.83	1.8%
3x DHX Shell Side	0.83	1.8%
DRACS	3.56	7.6%
3x DHX Tube Side	0.69	1.5%
3x TCHX Tube Side	1.58	3.4%
3x DRACS Hot Leg	0.65	1.4%
3x DRACS Cold Leg	0.65	1.4%
Total	46.82	100.0%

The cost of the major constituents of the primary salt, beryllium and lithium, are approximately \$770/kg and \$63/kg respectively [54], or \$79/kg of flibe (2002\$). The cost to enrich lithium is uncertain. With the concentration of Li-7 in natural lithium being 92.41%, and for a tails assay of 85% (the tails can be sold for essentially the same price as the natural lithium is purchased for), the separative work to produce 99.995% enriched Li-7 is 0.97 SWU/kg of flibe. As a possible metric for cost, worldwide prices for uranium enrichment in 2010 ranged from \$40 to \$160/SWU [55]. Lithium is easier to enrich than uranium, but costs to develop infrastructure for this purpose must be incurred. If lithium enrichment were to cost \$100/SWU, then the total cost of flibe would contribute about \$200/kWe to the cost of the Mk1 PB-FHR.

The Mk1 design used a relatively simple design rule of maintaining flow areas to be sufficiently large for salt flow velocities to remain below 2.0 m/s. One of the objectives of detailed design, computational fluid dynamics modeling, and scaled fluid dynamics experiments, will be to reduce the salt inventory in the reactor, while keeping pressure losses in the system acceptably low.

Figures 2-10 and 2-11 show the primary coolant flow paths under normal power and shutdown cooling operation, and under natural-circulation-driven decay heat removal mode, respectively. Thicker lines indicate main flow paths. Bypass flows are not shown for simplicity, although these will need to be quantified as they can have a significant effect on the behavior of the primary coolant loop and structural materials.

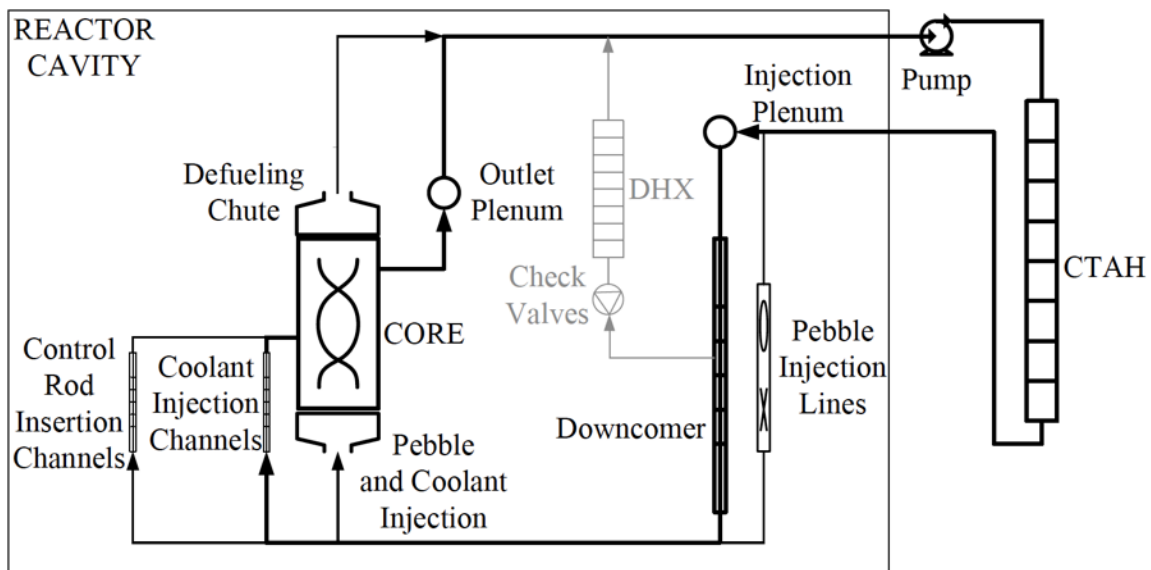


Figure 2-10. Primary coolant flow paths under normal power and shutdown cooling operation.

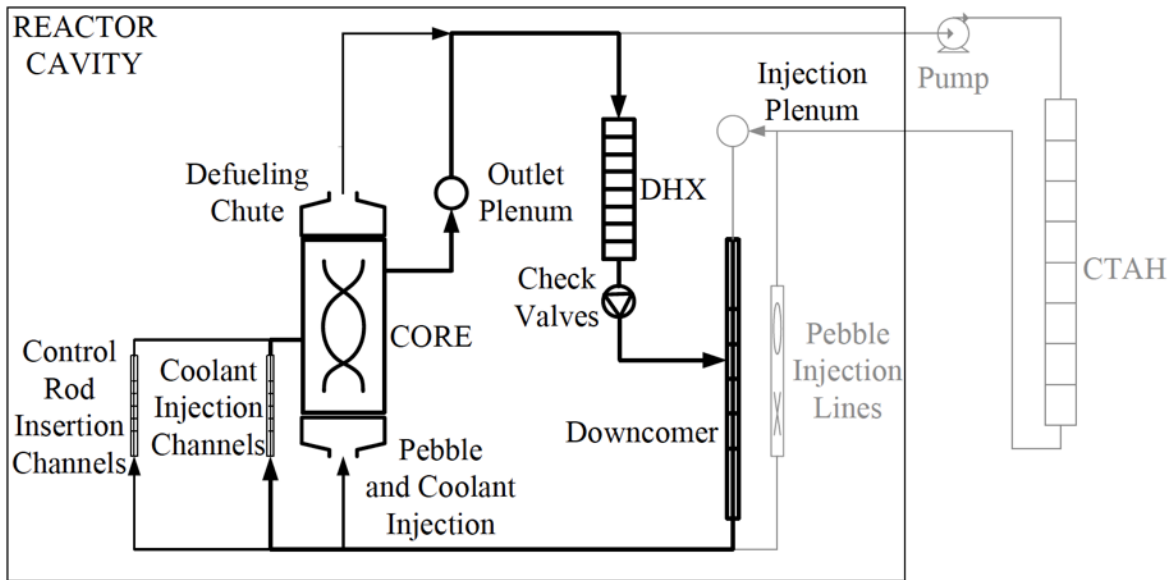


Figure 2-11. Primary coolant flow paths under natural-circulation-driven decay heat removal.

This section focuses on primary coolant flow paths inside the reactor cavity. Details about the primary loop “gas-gap” subsystem, the hot leg and cold leg subsystems outside of the reactor cavity, the main salt pump system and the CTAH system are given in Sections 3.1, 3.2, 3.3 and 3.4, respectively. Here, subsystems of the primary coolant loop are described in the order encountered by the salt as it flows inside the reactor cavity under normal operation.

2.1.6.1 Injection plenum

Cold salt enters the reactor cavity through two cold legs that cross horizontally over to the reactor vessel. The flow is then directed from the cold leg nozzles into a downcomer through a circular injection plenum integrated into the upper internal structures, which distributes the coolant circumferentially. As with all primary loop subsystems, one of the design goals is to keep pressure drop across this plenum as low as possible.

2.1.6.2 Downcomer

The coolant then flows downward in the 3-cm annular gap between the core barrel and the reactor vessel. Along the downcomer, fuel pebbles are injected through pebble injection lines with high flow resistance and minimal flow rates. From the downcomer, a fraction of the coolant (30% in the baseline Mk1 design) is directly injected into the bottom of the core and the remaining fraction is injected in the center reflector, where it is distributed between the coolant injection channels (74% of the center reflector flow rate) and the control rod insertion channels (26% of the center reflector flow rate).

2.1.6.3 Center reflector

The Mk1 center graphite reflector is shown in Fig. 2-6. The coolant is distributed between coolant injection channels and control rod insertion channels. From the coolant injection channels and control rod insertion channels, flow is distributed into the core through 1-cm-diameter injection holes. 9-mm-wide injection slots also allow flow from the coolant injection channels into the core. These structures are designed to allow for a major fraction of cross flow

in the annular core, thus reducing pressure drop across the core compared to fully axial flow, and therefore reducing total salt level swell when the main salt pumps are operating, as well as minimizing flow resistance from the core under natural-circulation-driven decay heat removal.

2.1.6.4 Pebble core

In the Mk1 baseline design, 30% of the flow is injected from the downcomer at the bottom of the core, resulting in mainly axial flow in the pebble core, while 70% of the flow is injected from the center reflector channels, resulting in mainly cross flow. The main design objectives are to limit pressure losses across the core, as well as providing efficient cooling of the fuel pebbles. To this effect, coolant injection from the center reflector directs cold salt to the hottest region of the core, thus increasing heat transfer efficiency, while the lower pressure drop reduces pumping power and associated electricity consumption.

2.1.6.5 Outlet plenum

Suction holes in the upper, outer reflector blocks provide a flow path for the coolant to emerge from the core and collect into a circular outlet plenum, shown in Fig. 2-12. Flow exits this outlet plenum to the hot leg, which then exits the reactor vessel and cavity. The purpose of the circular outlet plenum is to provide a uniform outlet pressure boundary condition around the circumference of the core, and thus to enable uniform flow distribution around the core.

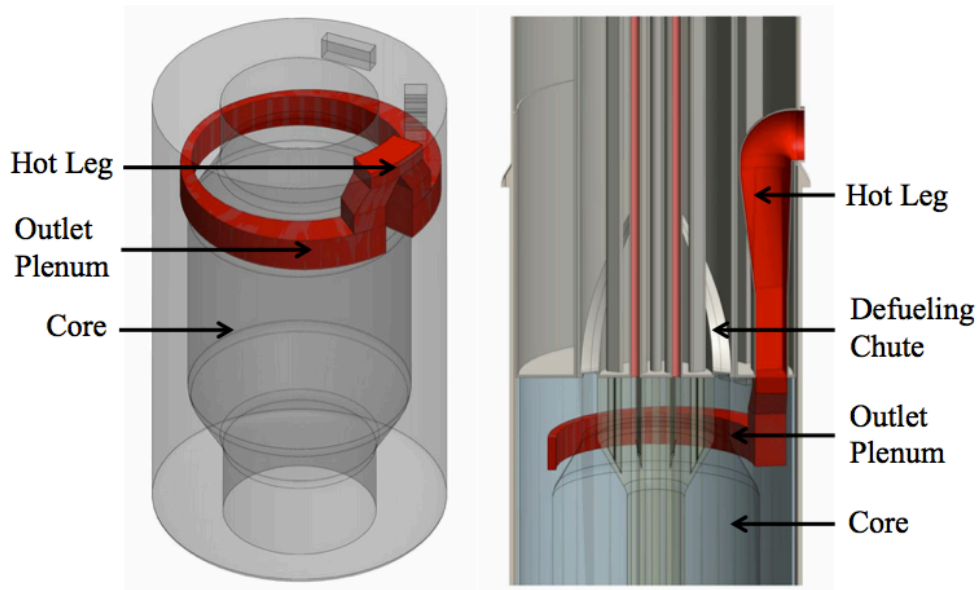


Figure 2-12. Top (left) and side (right) views of the outlet collection plenum in the outer radial graphite reflector.

2.1.6.6 Routing for defueling chute and DHX

One important challenge for the primary coolant flow paths is to limit heat losses from the primary loop under normal operation, while keeping upper core internal structures at an acceptable temperature level at any time and providing effective decay heat removal under natural circulation if the normal shutdown cooling system does not function. For this reason, flow routing in the defueling chute and DHX is a critical aspect of the Mk1 design. Details are provided in the following paragraphs.

Faulted salt levels

Design of the defueling chute and DHX flow routing depends on identification of faulted salt levels in the reactor. These are listed below:

- Faulted level (FL) 1: bottom of the hot and cold leg reactor vessel penetrations. This FL is due to loss or removal of coolant from the hot and cold legs.
- FL 2: 0.6 m below FL 1. This FL is due to a reactor vessel break and primary coolant filling the free space in the reactor cavity.
- FL B: 10 cm salt level drop. This FL, which adds to both FLs 1 and 2, is due to drop in coolant temperature from 900°C (accidental conditions) to 600°C and resulting volume shrinkage.

To maintain integrity of the DHX and its capability to provide a means for decay heat removal, the top of the DHX must be located below FL 2B. This way, the DHX will be covered at all times and remain functional, acting as a heat sink along with the reactor cavity.

Top of DHX to Hot Leg

The top of the DHX is connected to the elbow at the top of the hot leg. Routing of the flow between the hot leg elbow and the top of the three DHXs ensures symmetry of the flow going to each DHX. In each DHX, primary salt flows on the shell side of the heat exchanger.

DHX Inlet Manifold

In order to prevent sudden failure of the DHX should the salt level fault below the DHX inlet pipe, the top DHX coolant inlets can be designed such that as the level gradually drops, the flow rate also gradually drops. A manifold with most of the pipes at the top of the DHX and gradually fewer going down would implement this concept. This option must be further investigated, as this might be at the expense of some loss in the effective elevation of the natural circulation loop, or might be mediated by internal detailed design of the DHX shell and tubes.

Bottom of DHX to Downcomer

Flow is directed from the bottom of the DHX to the middle of the downcomer through penetrations in the core barrel, connecting to the bottom of the DHX shells. This penetration in the core barrel requires further design effort, as it provides a bypass way from the downcomer to the outer reflector graphite blocks.

Top of the Defueling Chute to DHX

A penetration in the outer wall of the vessel inner lid will connect the top of the DHX to the annulus formed by the inner and outer walls of the vessel inner lid. This annulus will then be connected to the top of the two defueling chutes. Flow routing from the annulus to the defueling chutes will depend on the axial distribution of the connecting coolant ports between the two walls of the vessel inner lid.

Flow through the defueling chute is upwards during both forced circulation and natural circulation. Allowing upwards flow through the defueling chute during natural circulation is important to prevent formation of stagnant hot pockets at the very top of the defueling chute.

Fluidic Diode Functionality

Previous designs of the FHR used a fluidic diode to prevent significant upwards bypass flow through the DHX under normal operation, while allowing free downwards flow of the coolant through the DHX during natural circulation. The fluidic diode function needs to be implemented immediately upstream of the DHX outlet manifold. In the Mk1 design, check valves are installed on the larger manifold lines, while smaller manifold lines are kept without check valves to ensure some amount of bypass flow.

The DHX bypass flow under forced circulation causes parasitic heat losses, which can be reduced by shutting louvers on the DRACS chimney, but must be sufficient to prevent overcooling of the DRACS loop, as detailed in Section 2.3.

2.1.6.7 Core bypass

A number of desired and undesired bypass flow paths must be identified, which may either protect some of the structural materials in the reactor, or bring penalties in terms of structural integrity of the plant components and overall economics. Two of these flow paths are detailed below.

Cold Leg Bypass

A deliberate fraction of bypass flow from the cold leg to a small annular slot in the upper core region will help keep the upper core structures at the same temperature as the downcomer. This small bypass will feed into the hot leg, and further analysis is required to limit temperature gradients in the upper core region that may lead to component failure. Other bypass of the cold leg will feed into the pebble injection lines, opposite of the hot leg.

Outer Reflector Blocks Bypass

Gaps between the outer radial reflector graphite blocks provide an undesired bypass route for coolant. To limit this bypass fraction, successive layers of blocks are staggered azimuthally so that when gaps open between blocks under thermal expansion, bypass flow through the cracks is blocked.

2.1.6.8 Level swell

An important issue related to primary coolant flow paths is the amount of level swelling resulting from salt thermal expansion and main salt pumps operation. To accommodate this effect, the reactor vessel extends at least 2 m above the hot leg level, and the primary coolant flow paths are designed to keep total head losses in the primary loop under 2 m.

Level change in the hot well due to thermal expansion and main salt pumps operation is another challenge. Section 3.1.1 discusses the hot well design and the different levels of the hot well salt free surface under various conditions. The goal is to keep the cross-over legs covered, while not overflowing the hot well. The cross-sectional area of the hot well is a design variable to this effect.

2.1.6.9 Pressure losses in primary loop

Minimizing pressure losses in the primary loop between the cold leg and the hot leg is an important design objective to limit level swelling from salt thermal expansion and primary pumps operation, limit required main pumps power, and reduce flow resistance for natural

circulation decay heat removal. Pressure losses in the external main salt piping and CTAHs are discussed in Section 3.2.3.

In the current Mk1 design, under normal operation, pressure drop in the downcomer is estimated to be approximately 3.34 kPa and, assuming that 70% of the total primary flow is directed through the central reflector, pressure drop across the center reflector is 2.03 kPa. This is a total of 5.4 kPa, or 0.28 m of head for 600°C flibe for the downcomer and center reflector.

The center reflector is the only location where there is little flexibility to increase flow area to reduce pressure losses. In all other parts of the primary coolant flow path, pressure losses can be reduced by assuring that the geometry of the flow path avoids significant form losses, except where absolutely necessary. The rest of the primary coolant is therefore designed to keep total head losses in the primary loop below 2 m.

2.2 Reactivity Control and Monitoring System

The Mk1 PB-FHR is designed to have negative fuel, moderator, and coolant temperature reactivity feedbacks. As discussed in Section 2.2.4, ATWS accidents are analyzed as BDBEs. The Mk1 PB-FHR design uses a buoyant control rod system for normal reactivity control, and the system also provides a passive shutdown function because the buoyant rods will insert if the reactor coolant temperature exceeds the buoyant stability limit. The design also uses shutdown blades that can insert directly into the pebble bed for reserve shut down. These systems are described in greater detail in the subsections below.

2.2.1 Buoyant control rod subsystem

The Mk1 PB-FHR uses 8 cylindrical buoyant control rods, as shown in Fig. 2-13, with a design derived from buoyant rods studied in scaled experiments at UCB [56]. The 8.0-cm diameter rods move vertically in 10.0-cm diameter cylindrical channels in the center reflector, and have a total stroke of 4.5 m from fully withdrawn to fully inserted. The rods are weighted to be neutrally buoyant in flibe at 615°C. The rods contain natural (unenriched) boron carbide and are clad with either 316 SS or CFRC.

Above each buoyant rod there is a 316 SS insertion rod. When fully inserted, the insertion rod extends to above the maximum salt level in the control rod stand pipe. A cable connects to the top of the insertion rod, and is used to withdraw it. Under forced circulation, bypass flow of inlet coolant maintains the salt in the channel at the core inlet temperature of 600°C, so the buoyant rod rises below the insertion rod. Any transient that raises the temperature of the coolant in the channel above the 615°C neutral buoyancy value causes the rod to insert passively.

Under reactor scram the magnetic latch in the control rod drive releases, and the insertion rod pushes the buoyant rod into the channel. Because the insertion rod is not physically connected to the buoyant rod, a snubbing cavity is used to absorb the buoyant rod kinetic energy and to arrest the motion of the buoyant rod as it reaches the bottom of the channel, as shown in Fig. 2-13.

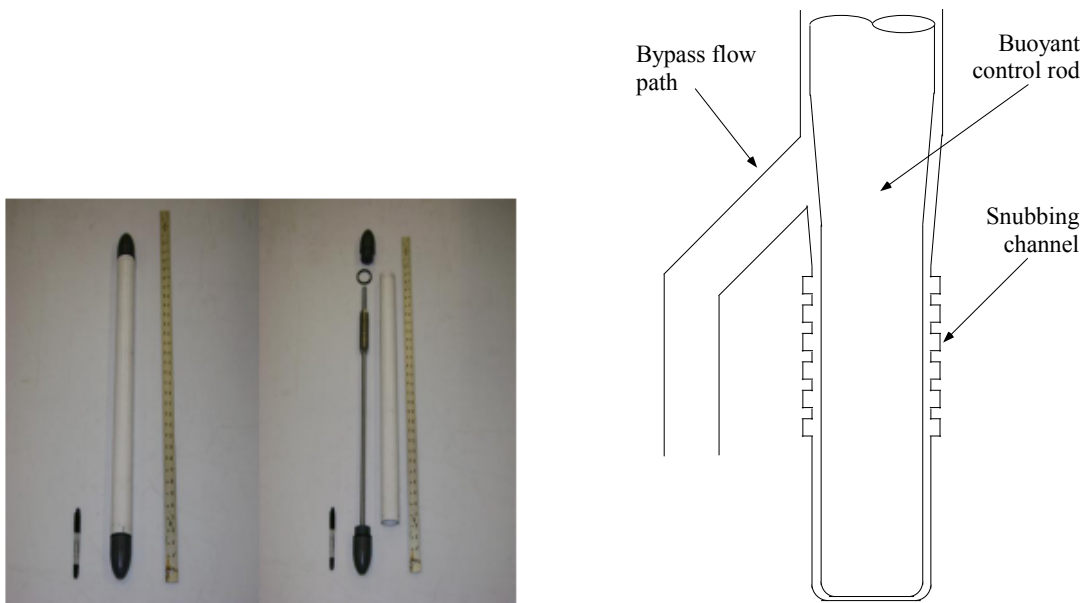


Figure 2-13. Buoyant control rod system, showing buoyant rod tested in scaled experiments at UCB (left) and schematic of fluidic snubbing channel to stop a buoyant rod (right).

In a change from the buoyant rod design studied earlier at UCB, the Mk1 rod channel is also used as a flow path for coolant injection into the center of the reactor core. This flow enters the shutdown-rod channel shortly above the snubbing cavity, and then flows through 1.0-cm diameter holes from the lower half of the channel into the pebble core.

Figure 2-14 shows MCNP5 results for the Mk1 cold zero power reactivity worth of insertion of various numbers of control rods into the center reflector. There is a reduction of the per-rod worth as more are inserted into the core and as the core multiplication factor is lowered to a subcritical level.

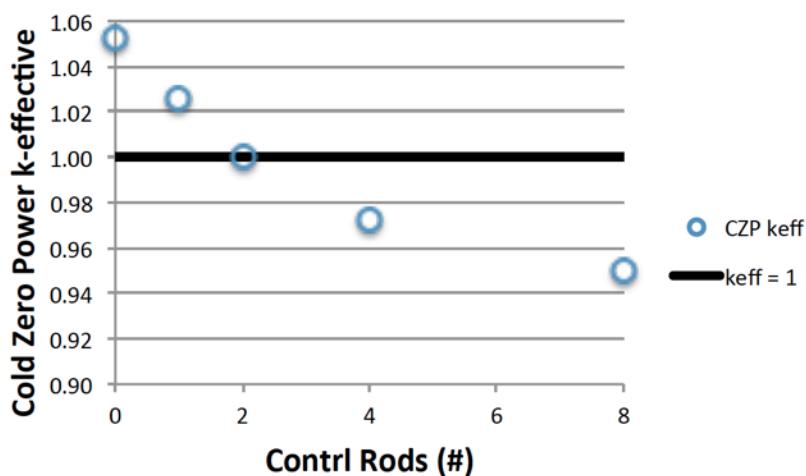


Figure 2-14 Results of a study in MCNP5 indicate the combined worth of 1, 2, 4, and all 8 control rods [57].

2.2.2 Shutdown blade subsystem

The Mk1 PB-FHR uses 8 shutdown blades that insert directly through the upper center graphite reflector into the pebble bed. The geometry of the blade, shown in Fig. 2-15, was developed and optimized by the 2012 UCB NE-170 senior design class [58]. The blade thickness is less than half of a pebble diameter, so that pebbles do not enter the cruciform channel that the blade emerges from. The blade tip geometry is designed to displace pebbles horizontally away from the blade as it enters the bed, rather than downward. Testing of a scaled blade showed that insertion forces are very low. The stiffening fins on the sides of the blades are only $\frac{1}{2}$ pebble diameter high, so they do not block pebble flow across the blade when defueling is performed with the blade inserted. As shown in Fig. 2-16, MCNP5 was also used to calculate the cold zero power reactivity worths of insertion of various numbers of shutdown blades.

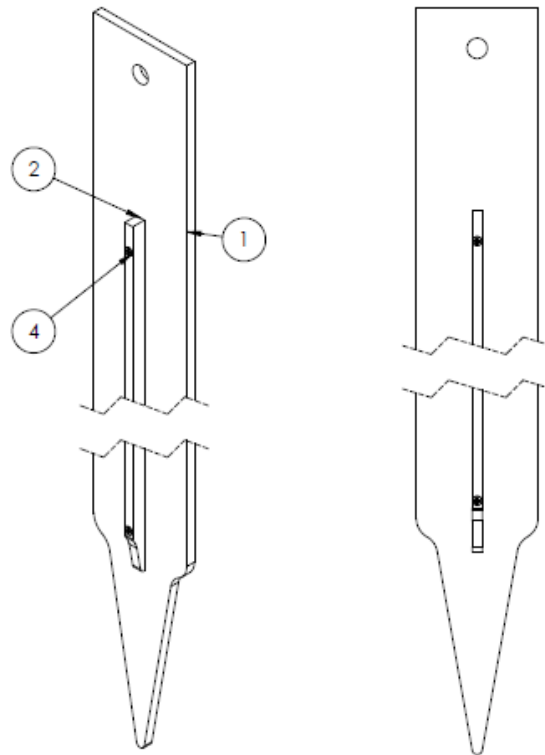


Figure 2-15. Shutdown blade system, showing CAD figure of blade tested at UCB which had lowest insertion force (1 is blade, 2 is ribs, 4 is screws to hold ribs).

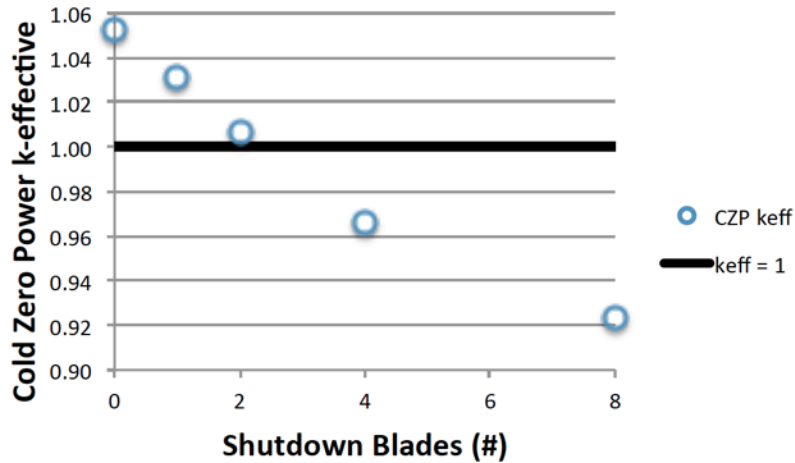


Figure 2-16 Results of a study in MCNP5 indicate the combined worth of 1, 2, 4, and all 8 shutdown blades [59].

2.2.3 Drive subsystem

The PB-FHR control rod and shutdown blade systems have options to use chain systems or cable drums to raise and lower the rods. Experience exists for similar control rods developed for the Molten Salt Reactor Experiment (MSRE) [60] [61]. The Molten Salt Breeder Experiment design also developed a control rod drive design [62]. Likewise, SINAP is currently developing and testing a similar control rod drive mechanism for its 2-MWth TMSR-SF1 research reactor. For the Mk1 PB-FHR, the control rod cable drive system design for the Gas Turbine Modular Helium Reactor (GT-MHR) has been adopted, as shown in Fig. 2-17, which also has operational experience in the Fort St. Vrain plant.

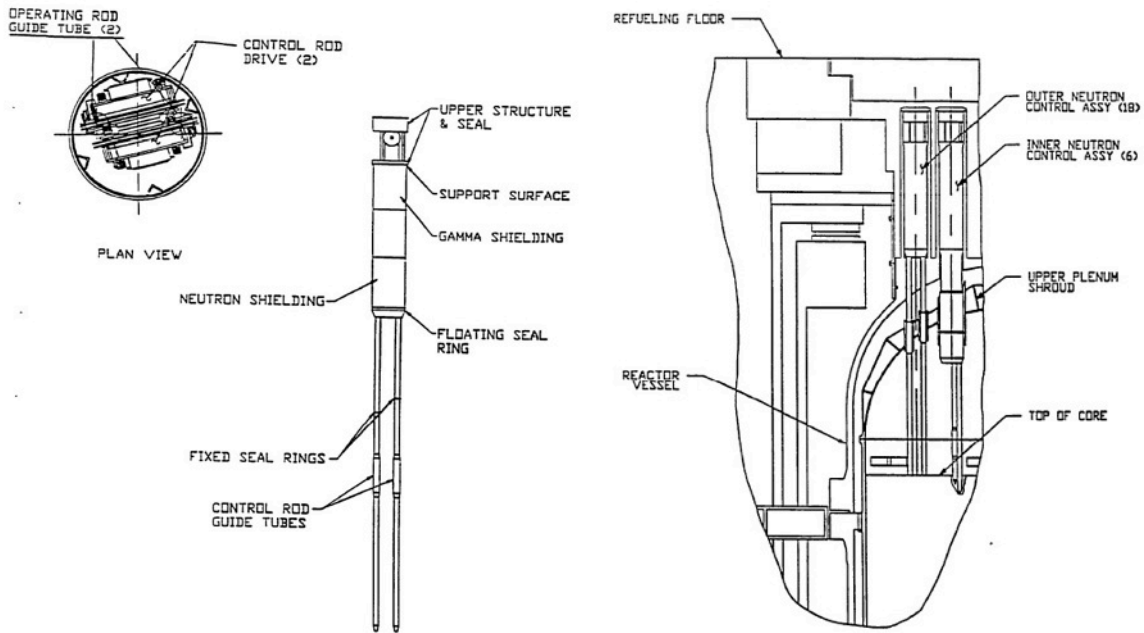


Figure 2-17. The GT-MHR control rod drive mechanism design, shown here [63], provides the basis for the Mk1 design.

As with the GT-MHR, the Mk1 drive equipment consists of a direct current torque motor, which uses a harmonic drive unit with 60:1 speed reduction to drive a cable storage drum. Small cable guide rollers below the drum locate the flexible, high nickel alloy cable in the correct position above the gamma shield penetration. The motor, speed reducer, and storage drum are mounted on a frame that pivots against a load cell, allowing the cable load to be monitored. Motor current instrumentation provides an independent measure of the cable load, and allows the detection of broken or stuck cable or control rod. Load resistors limit the rod velocity in the case that the power fails or the reactor trips (which interrupts power to the motor). The motor acts as a generator as the rod drops, and the resistors dissipate the resulting power.

Below the drive drum, the assembly has gamma shielding, neutron shielding, thermal insulation, and a control rod guide tube. The guide tubes extend downward to interface with channels in the upper core support structure. The cavity cover gas system is designed to supply cool, inert cover gas to the drive assemblies, and this gas flows down into the guide tubes and then into the reactor cavity to prevent BeF₂ vapor from entering the cool region of the drive assembly and condensing.

2.2.4 Anticipated Transient With Scram (ATWS)

Because both the buoyant control rod subsystem and the shutdown blade subsystem have high reliability, their combined failure to operate following loss of heat sink (LOHS) and loss of forced circulation (LOFC) events is considered to be a BDBE. However, due to the relatively low operating temperature of the Mk1 fuel, the response of the Mk1 core to ATWS is not expected to cause fuel or structural damage.

As shown in Table 2-3, the Mk1 fuel, coolant, and graphite moderator temperature reactivity coefficients are all negative, while the reflector temperature reactivity coefficients are small but positive. The fuel temperature reactivity coefficient is significantly larger than the coolant and graphite moderator coefficients.

Table 2-3. Temperature coefficients of reactivity for the Mk1 PB-FHR [64].

Component	Mk1 Temperature Reactivity Coefficient (pcm/K)
Fuel	-3.8
Coolant	-1.8
Inner graphite reflector	+0.9
Graphite moderator	-0.7
Outer graphite reflector	+0.9

During a hypothetical ATWS accident the fuel and coolant will eventually equilibrate to zero fission power at a temperature between the characteristic operating temperature of the fuel and the coolant. In a simplified model of ATWS accidents the fuel and coolant will equilibrate to produce a single characteristic core outlet temperature (noting that the temperature difference

between the fuel and the coolant needed to remove decay heat from the fuel to the coolant is small and can be neglected). In this simplified model the positive reactivity insertion from reducing the temperature of fuel kernels in the core is offset by negative reactivity insertion from increasing the coolant and graphite moderator temperatures to equilibrate locally with the fuel temperature.

The average ATWS hot shutdown temperature can be estimated algebraically with just the nominal characteristic temperatures of the fuel kernels and coolant along with the temperature reactivity coefficients for the fuel and the coolant. The limiting temperature for damage to metallic structures such as the DHX and reactor vessel is not this hot shutdown temperature, but the hot shutdown core outlet temperature. This limiting core outlet temperature can be estimated by assuming the temperature rise during passive cooling is 100°C and assuming that the hot shutdown temperature is approximately halfway between the inlet and outlet coolant temperature. This analysis predicts peak coolant outlet temperatures of under 750°C.

A fully coupled analysis of ATWS has not been conducted. However, a scoping study has been performed implementing a loose coupling between the COMSOL multiphysics software and MCNP5, using the same methodology as was applied to an earlier 900-MWth PB-ATHR core design [65]. The preliminary results of this scoping study suggest that under natural circulation alone, the maximum coolant temperature at the Mk1 outlet will reach approximately 722°C during ATWS.

Figure 2-18 shows the COMSOL simulations for flow distribution, coolant bulk temperature, and fuel temperature, in the Mk1 core under power operation. Again, average fuel temperatures are seen to be below 800°C, suggesting that ATWS events will not reach temperatures sufficient to cause damage to metallic structures in the PB-FHR primary system.

Future work will include a more tightly coupled analysis of ATWS response in the PB-FHR. Of particular interest will be the response to LOHS, LOFC, and reactivity insertion events.

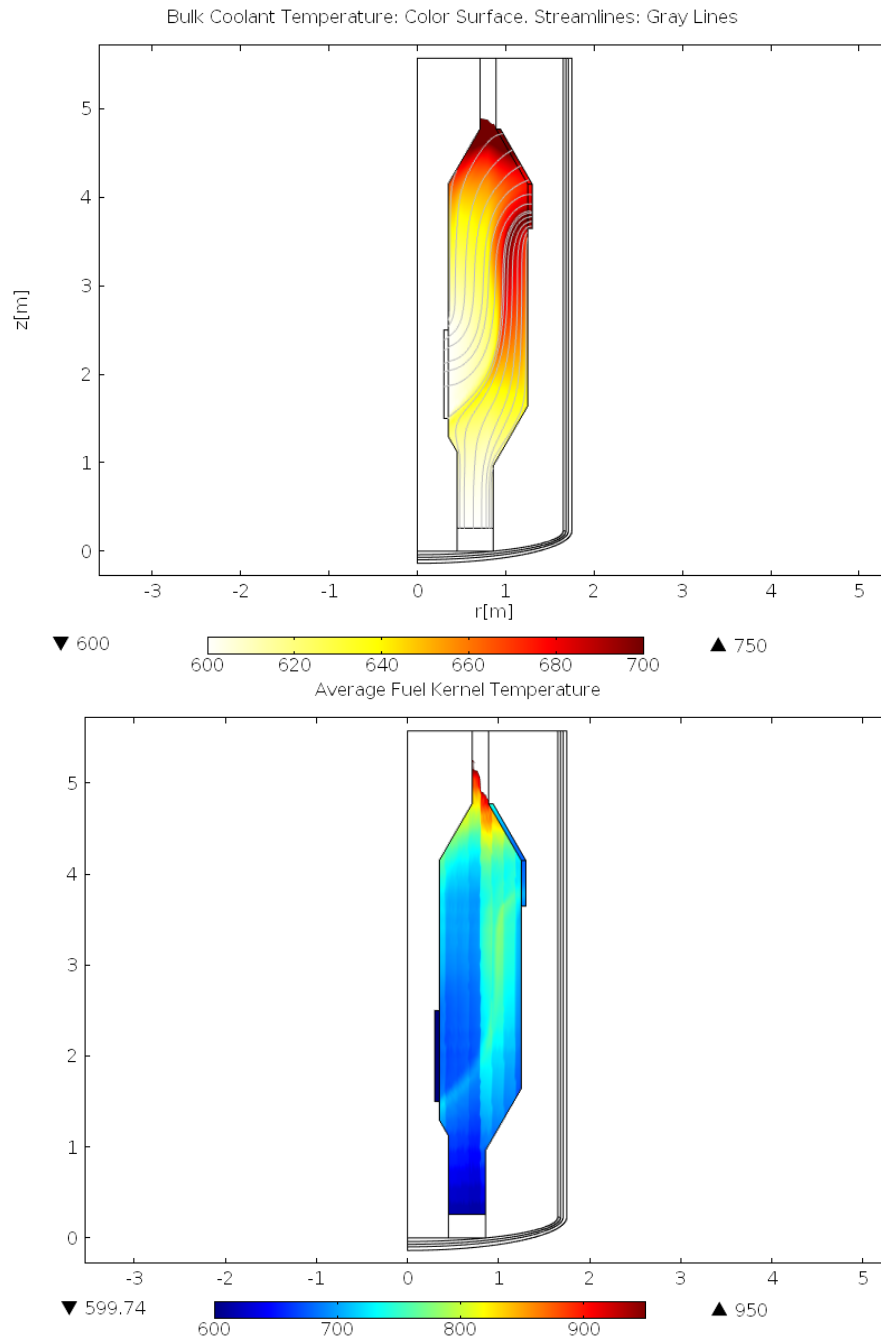


Figure 2-17. COMSOL predictions for Mk1 bulk coolant temperature distribution (above) and fuel kernel temperature distribution (below) under power operation.

2.2.5 Reactivity monitoring

The Mk1 PB-FHR has wells, located at quadrants around the reactor cavity liner, for ex-core neutron flux monitoring instruments. The number of wells will be established during detailed design, and will depend upon the specific neutron flux measuring instruments used (typical PWRs have 12 wells: 4 wide range, 4 linear power, 2 startup, and 2 control detectors). These

instruments provide the capability to monitor reactor power and the uniformity of power axially and circumferentially around the core, and provide inputs to the reactor protection system.

The option exists to locate the wells immediately adjacent to the reactor vessel, in between the electrical heating elements arrayed around the reactor vessel, where the wells operate at the same temperature as the reactor vessel (nominally 600°C), or embedded in the reactor cavity wall, where the wells operate at the reactor cavity liner temperature (nominally 30°C).

The neutron flux that will reach these sensors will be attenuated by the boron used to shield the core barrel. Detailed design will be needed to verify whether the flux will be sufficient to provide adequate power monitoring, particularly under source-range conditions.

The Mk1 center reflector has 16 instrument guide tubes, 4 of which have upper guide tubes designed to allow the insertion of core neutron flux mapping instruments. One of the guide tubes is designed to allow the insertion of a startup neutron source. The remaining guide tubes provide space to store graphite irradiation samples, or serve as spares.

2.3 Direct Reactor Auxiliary Cooling System

The Mk1 PB-FHR uses three modular 50% capacity DRACS loops to remove decay heat under emergency conditions, when the normal shutdown cooling system is not functional. Each DRACS loop is sized to be capable of removing 1% of nominal power (2.36 MW). The DRACS are passive and function by natural circulation. Their function is to maintain peak coolant temperatures below safety limits for the reactor's structural materials, and further design will require modeling of the Mk1 PB-FHR in thermal hydraulic codes such as RELAP5 to investigate safety and economics tradeoffs using two 100% capacity DRACS loops vs. three 50% capacity DRACS as retained in the Mk1 design. Each module consists of a DHX located inside the reactor vessel, a DRACS salt loop, a TCHX outside the reactor containment, which transfers heat from the DRACS salt loop to evaporate water, a water thermosyphon, an air-cooled condenser, a natural draft chimney to provide air flow to the condenser, and a water storage tank. Design of these subsystems is detailed below.

Because the Mk1 PB-FHR does not use an intermediate loop with a different salt, to further reduce the probability of the primary salt becoming contaminated with other salts due to heat exchanger leaks, the DRACS loops use the same enriched flibe salt as the primary loop. This also allows the DRACS loops to use the same or similar chemistry control methods as the primary system.

However, the use of flibe in the DRACS loops raises the issue of managing the high freezing temperature of flibe, 459°C. As shown in Fig. 2-19, the earlier MSBR design also used a natural circulation flibe salt loop to remove heat from the fuel salt drain tank, similar to the DRACS loop for the FHR. Heat was removed from this coolant salt by thermal radiation from the tubes of a TCHX to water-filled thermosyphon tubes, where water would boil and transport heat to a natural draft, air-cooled condenser. The intermediate water thermosyphon loop was adopted to avoid coolant freezing in the DRACS loop, even under conditions where the outside ambient air temperature is very low. The Mk1 DRACS design adopts this same approach.

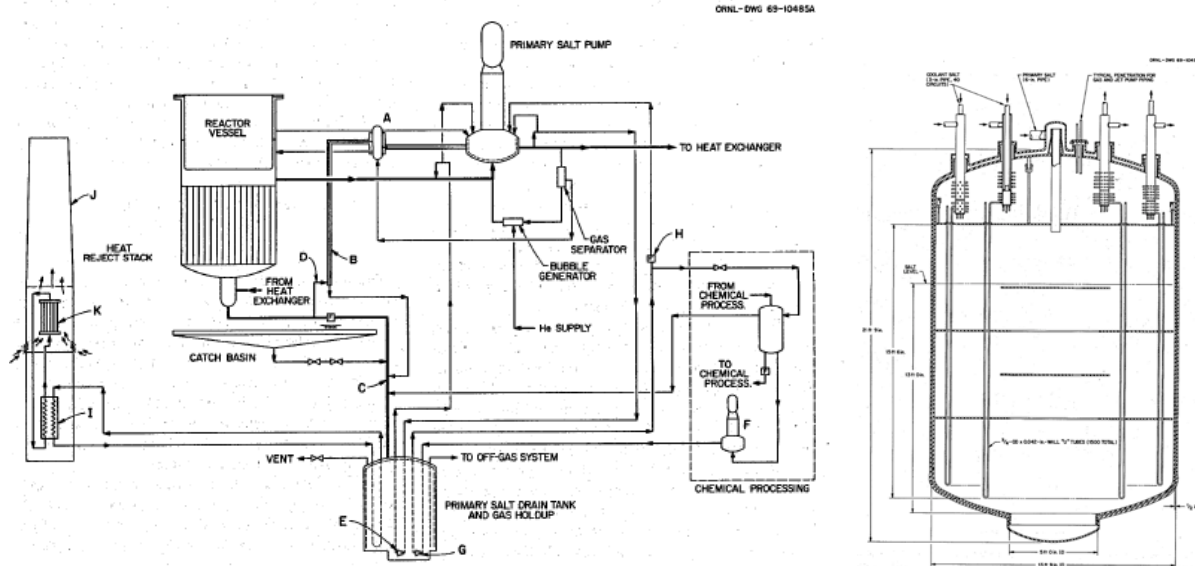


Figure 2-18. MSBR drain tank cooling system schematic (left) and fuel-salt drain tank with internal cooling coils to remove decay heat (right) [66].

Figure 2-20 presents both a detailed schematic view and an isometric view of a Mk1 DRACS loop. The loop has three major components: the DHX, the TCHX and the DRACS storage tank (DST), or fill tank.

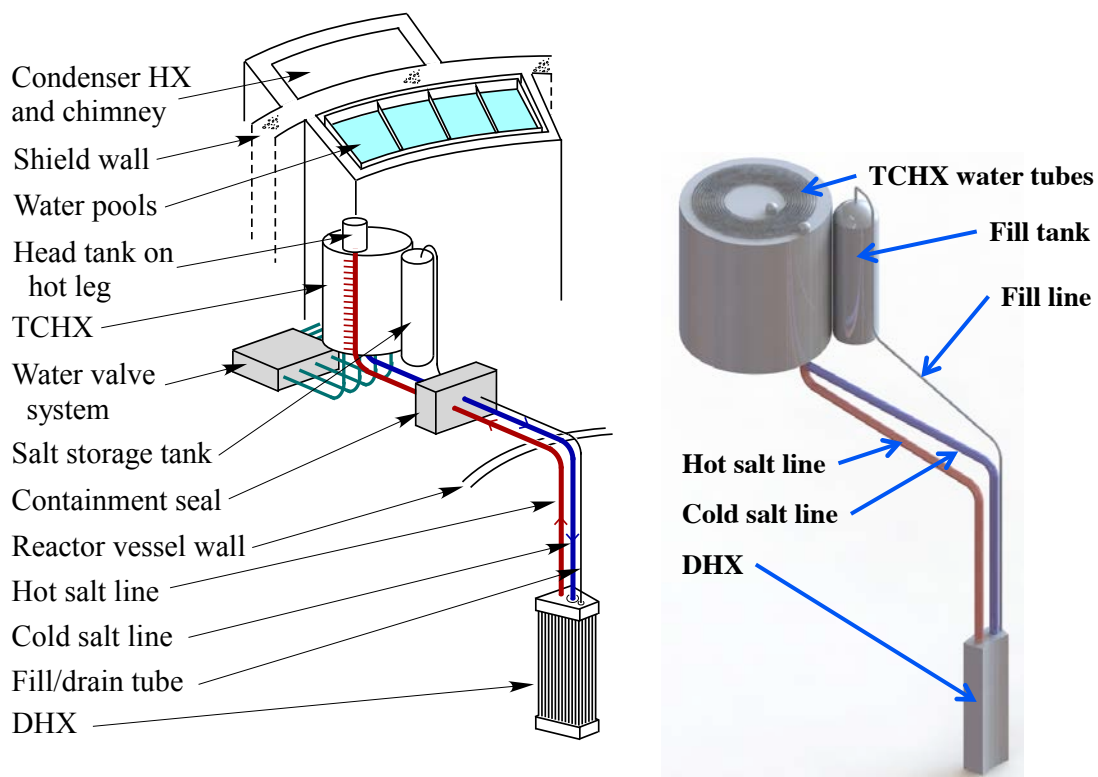


Figure 2-19. Schematic (left) and isometric view (right) of the Mk1 modular DRACS.

The DHX is a bayonet type of heat exchanger that uses a 2.5-m-tall bundle of twisted tubes, between a lower cold salt plenum and an upper hot salt plenum, to transfer heat from the primary loop to the DRACS loop. Detailed DHX parameters, based on a simpler, straight shell and tube heat exchanger, are provided in Table 2-4. The geometry of the DHX bundle is selected to fit into the three DHX wells in the reactor vessel upper internals structure. This well has a check valve at the bottom, which limits upflow of primary salt through the well under forced circulation operation, while opening to provide a low flow resistance for natural circulation downflow. A simple ball-type check valve, with a negatively-buoyant graphite and/or silicon carbide ball, is used in the check valve. A check valve is selected due to the capability to provide precise and predictable flow loss coefficients in both flow directions.

Table 2-4. DHX parameters, based on a straight shell and tube configuration.

Parameter	Value	Unit
<i>Shell side (primary salt)</i>		
Inlet temperature	700	°C
Outlet temperature	600	°C
Mass flow rate	9.77	kg/s
Velocity	0.045	m/s
Outside diameter	0.56	m
Inside diameter	0.548	m
<i>Tube side (DRACS salt)</i>		
Inlet temperature	526	°C
Outlet temperature	608	°C
Mass flow rate	11.91	kg/s
Velocity	0.065	m/s
Outside diameter	0.0127	m
Inside diameter	0.0109	m
Number of tubes	984	
<i>Heat exchanger</i>		
Heat load	2.36	MW
LMTD	82.7	°C
Overall U	291	W/m ² °C
Height	2.5	m
Heat transfer area	98	m ²

An important simplification for this check valve is that it does not need to provide a leak tight seal as conventional check valves do, and in fact needs to be designed to assure adequate bypass flow and parasitic heat losses to prevent overcooling of the DRACS loop during power operation. Thus the detailed seat design needs to be optimized to minimize the potential for clogging with debris. Temperature instrumentation in the DHX well is provided to detect insufficient bypass flow and DRACS loop overcooling during power operation. The cold leg

and the loop fill line pass through an opening in the upper hot salt plenum, so they can undergo thermal expansion independent of the DHX tubes.

The TCHX is located outside of the reactor containment and transfers heat from the DRACS salt loop to a water thermosyphon loop. It is designed with a coiled tube configuration similar to the CTAHSs, with hot salt entering from a stand pipe with a head tank, and the coiled tubes spiraling down into a cold salt manifold pipe. Because the pressure difference between the hot and cold stand pipes is small, the cold salt pipe is also open at the top to allow for inspection along the length of both the hot and cold pipes. These stand pipes also provide access for thermowells for monitoring the hot and cold salt temperatures, as well as level measurements that may provide a basis to monitor the salt flow rate through the TCHX. The coiled tubes are clad with the same alloy used for the CTAH tubes to generate an aluminum oxide layer to reduce tritium losses. The water-cooled thermosyphon pipes are then oriented vertically, and go up in between the salt tube coils. Heat transfer from the salt coils to the thermosyphons is dominantly by thermal radiation, with some natural convection. One TCHX tube bundle is shown in Fig. 2-21. Nine of these bundles are stacked vertically to form the TCHX, also shown in Fig. 2-21. Detailed TCHX parameters are provided in Table 2-5.

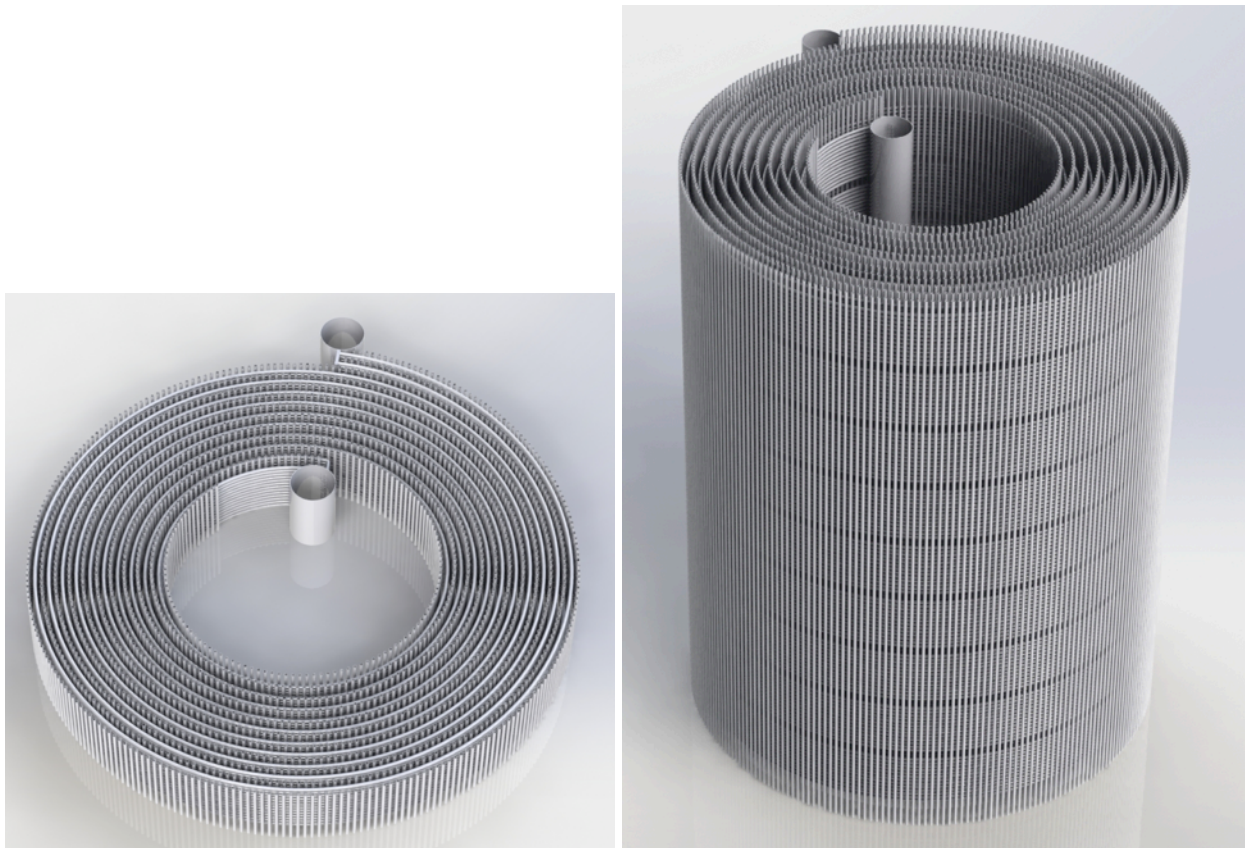


Figure 2-21. Isometric views of one TCHX bundle (left) and the full TCHX (right).

A DST or fill tank, shown in Fig. 2-20, is integrated into the loop and is used to fill and drain the loop. The loop has a small-diameter fill and drain line that runs from a dip tube in the DST to a dip tube at the bottom of the DHX cold plenum. This fill and drain line has a freeze valve.

The DRACS loop is filled by pressurizing the DST to transfer salt, until the head tank is partially full. One drains the loop back to the DST by pressurizing the head tank above the TCHX.

Table 2-5. Detailed TCHX parameters.

Parameter	Value	Unit
<i>Salt side</i>		
Inlet temperature	608	°C
Outlet temperature	526	°C
Mass flow rate	11.91	kg/s
Velocity	0.27	m/s
Outside diameter	0.0127	m
Inside diameter	0.0109	m
Number of tubes	234	
Tube length	24.0	m
<i>Water side</i>		
Temperature	100	°C
Mass flow rate	1.05	kg/s
Outside diameter	0.0127	m
Inside diameter	0.0109	m
Number of tubes	2050	
Tube length	2.5	m
<i>Heat exchanger</i>		
Heat load	2.36	MW
LMTD	465.8	°C
Overall U	22.6	W/m ² °C
Heat transfer area	224	m ²
Overall diameter	2.48	m

Each DRACS loop is fabricated and mounted into a frame that is crane liftable. A key issue for the detailed design of this modular structure is the containment penetration barrier needed for the horizontal legs going to and from the TCHX, and how to design the hatches above the frame to allow loop installation and removal. The DRACS loop is not accessed under normal operation, so these hatches are designed to act as effective, passive missile barriers.

The water pools, water supply valve system, steam return system, and air-cooled condensers are located at the same elevation, near the DRACS loops. The DRACS water pools are designed to have a sufficient reserve volume of water to accommodate early boil-off immediately after reactor shutdown when decay heat levels are high, and to provide gravity driven flow to the TCHXs. Because the water pools can reach temperatures of 100°C, the vessels are insulated. Following best practice for water pools, these insulated vessels are contained inside leak-tight pool enclosures which have the capability to limit water loss if the pool vessel leaks, and provide sumps to enable leak detection.

Future modifications to the design are expected to develop a complex manifold system to supply and collect water to/from the thermosyphon water tubes, so that they can be activated in banks. For now, the tubes are simply shown protruding from the top and bottom of the TCHX shell, as seen in Fig. 2-21. Future efforts will also involve detailed design of the air-cooled condenser and natural draft chimney. This will eventually require thermal hydraulic modeling in codes such as RELAP5 to confirm performance predictions and guide design enhancements.

2.4 Reactor Vessel and Cavity/Containment Systems

FHRs differ from most other reactor technologies because they use a coolant that is chemically stable and has a very high boiling temperature (the only comparable coolants are lead and lead/bismuth). The Mk1 FHR also has no source of water inside the reactor cavity. While the stainless steel reactor cavity liner plate is water cooled on the outside, a drain chase prevents any leakage into the reactor cavity. Absent coolant volatility/high-pressure and any source of chemical stored energy, FHRs have no physical mechanisms to generate significant pressure inside their containment structures except by the small pressure change caused by heating and cooling gases in the reactor cavity. The pressure change caused by heating is kept very small by having a cover gas handling system, which is included inside the low-leakage containment boundary, which has a much larger total volume than the volume of gas inside the reactor cavity.

U.S. regulations for LWRs require high-pressure, low-leakage containment structures. The fact that water is used to remove heat during accidents, and when converted to steam can transport radionuclides released from damaged fuel, is the principal reason why low-leakage is required at high containment pressure. Commonly, U.S. LWR Technical Specifications require that leakage rates be less than 1% of the containment inventory over a one-day period, and containment pressurization and leak testing is required ever 10 years to verify that leakage rates remain below this value.

One of the most important regulatory issues for FHRs involves how requirements for containment will be established and evaluated. The Mk1 containment design provides a low-pressure, low-leakage primary containment, as well as a secondary filtered confinement, which can be expected to provide overall performance equivalent to or greater than LWR containments. The MSRE containment design and experience, and MSBR design, provide valuable input for the Mk1 PB-FHR. The general design principle in the MSRE and MSBR used double metallic seals and welded containment membranes that encapsulated the reactor and drain tank cavities. In low pressure systems this can be effected with thin metal. When the MSRE drain tank cell was opened after 30 years, He-3 was found remaining from tritium decay [67]. It is difficult to contain He, indicating that these barriers have remained effective over a time span comparable to the operating life of a commercial reactor.

The Mk1 primary containment implements a refractory reactor cavity liner and insulation system, which eliminates the need for a guard vessel. Elimination of the guard vessel that is commonly used for pool-type reactor designs brings substantial benefits of simplification and cost reduction, and also eliminates BDBE scenarios where a common mechanism might cause rupture of both the reactor vessel and the guard vessel.

The refractory reactor cavity liner system also allows the reactor cavity gas volume to be minimized. Normal temperatures for cover gas and cavity gas in the Mk1 reactor cavity are approximately 600°C, and the normal pressure is close to atmospheric. If confined and not allowed to expand, under BDBE conditions where the cavity temperature might approach 900°C, the pressure of these gases would increase by a factor of $1173\text{K}/873\text{K} = 1.34$, so if confined, the pressure in the reactor cavity would increase by approximately 0.34 atm.

For this reason, the equipment for the cover gas and cavity gas control systems is located in a below-grade enclosure adjacent to the reactor cavity. This enclosure is designed to have low leakage, and all penetrations exiting this enclosure are designed to be isolated in accordance with LWR General Design Criteria (GDC) requirements. The volume of this enclosure is large compared to the volume of gas in the reactor cavity, and thus any increase in temperature of gas in the reactor cavity will not result in any significant change in the containment pressure. Therefore in the Mk1 containment the pressure differential available to drive leakage flows will be a small, of a magnitude where variability in barometric pressure must be considered in the detailed design.

The Mk1 design has primary salt piping, transfer, and equipment maintenance activities that occur outside of the primary containment. Due to the beryllium hazards associated with this flibe, all of these areas inside the secondary confinement and external event shield structures have highly effective ventilation and filtering systems, as well as isolation systems. The main filter banks, blowers and exhaust stacks are located in grade-level rooms immediately adjacent to the shield building, as shown in Fig. 1-4. One exhaust system filters exhaust from the shield building, while the second filters exhaust from the air-duct vault and CTAH enclosures. These filtered confinement systems, external to the primary containment, can be helpful in mitigating releases from the containment, and thus the Mk1 beryllium safety and reactor building filtered ventilation system provide defense-in-depth. Under beyond design basis external events involving external missiles (aircraft, tornados, etc.), the primary containment and reactor cavity structures also act as effective missile shields for any objects that might penetrate or spall from the external event shield.

The most important containment design decision that has been implemented in the Mk1 containment design is to not use internal isolation valves on the primary salt hot and cold legs. While it is technically possible to provide an internal isolation valve on these salt lines, as discussed in Section 3.1 describing the Mk1 gas-gap isolation system, because these lines are used for normal shutdown cooling, an internal isolation valve is expected to reduce overall safety. Here it is important to note that the inability to open the internal isolation valve for the Fukushima Unit 1 isolation condenser, because the operators closed it before the tsunami arrival to control the reactor cool down rate and were then unable to reopen it after the tsunami caused a loss of electrical power for the valve, was primary cause of overheating and fuel damage in that reactor (Units 2 and 3 did not have isolation condensers).

2.4.1 Thermal expansion and stress management

Because the Mk1 PB-FHR operates at high temperature, the primary system undergoes substantial dimensional changes due to thermal expansion when it is heated from its installation temperature to its normal operating temperature. The Mk1 CAD models presented in this report

all show the dimensions of equipment at their normal operating temperatures, not their cold installation temperatures.

The Mk1 reactor vessel and core barrel structures operate at the cold leg temperature. The cold leg temperature is maintained at 600°C under power operation, where the main salt pump speed and reactor power are controlled to maintain this temperature constant under changing power conversion loads. The normal shutdown cooling system, which uses one or both of the main salt pumps operated at low speed, and air circulated through one or both CTAHs to provide decay heat removal, is also controlled to keep the cold leg temperature constant at 600°C. The main salt pump speed and reactor power are controlled so that the hot leg temperature increases linearly from nearly 600°C at shutdown power to 700°C at 10% power, and then the hot leg temperature is controlled to be constant at 700°C up to 100% power.

Under emergency decay heat removal the hot and cold leg temperatures depart from these controlled values, resulting in additional thermal expansion and thermal creep. These effects will be considered in the detailed design.

Because the Mk1 PB-FHR has a compact design, thermal expansion of the reactor vessel and main salt piping is accommodated by allowing the hot salt well and CTAHs to move horizontally in response to this thermal expansion. The position of the reactor vessel is fixed by the vessel support skirt, which is located immediately below the hot and cold leg nozzles, so the vertical movement of these nozzles due to thermal expansion is small. The major components of the main salt system—the hot well, CTAHs, and cold leg stand pipes—are supported on vertical bearings at a similar elevation, so that vertical displacements due to thermal expansion approximately match those of the reactor vessel nozzles.

The vertical bearings allow slow horizontal motion to occur. Snubbers prevent relative motion from occurring during seismic events, similar to the snubbers used to restrain steam generators in PWRs during seismic events. The hot and cold leg penetrations through the reactor cavity/containment, and the cross-over and cold leg penetrations into the CTAH compartments have double-wall seal bellows. Bellow leakage can be detected by pressurizing the space between the bellows.

Because the 316 SS structural material expands by 1.06% when heated from the assembly temperature of 20°C to the operating temperature of 600°C, this requires that the CTAHs be capable of moving approximately 13 cm horizontally. This horizontal motion is accommodated by a bellows system in the warm and hot air ducts. The pressure boundary for these ducts is conventional carbon steel, with internal insulation, and operates at nearly room temperature, so design of the bellows system is simplified.

The main salt piping seal bellows, discussed in Section 2.4.5 are installed in a pre-stressed state, so that their reactive forces are minimized when the vessels and piping heat to their normal operating temperatures. By minimizing the reactive forces at normal operating temperature, long-term creep is also reduced.

2.4.2 Reactor vessel and support skirt

The PB-FHR reactor vessel, shown in Fig. 1-3, is fabricated from 316 SS (while 304 SS and Alloy N are alternative materials) and has an outside diameter of 3.50 m at its normal operating

temperature of 600°C, which contracts to 3.46 m at room temperature. The total height of the vessel is 11.02 m at its operating temperature of 600°C. The vessel has a 3.60-m-diameter (at the operating temperature) support ring located 8.12 m above the bottom of the vessel. This transfers the vessel gravity loads to a conical support skirt that has the same thickness as the vessel, which transfers gravity and seismic loads to the reactor cavity wall. The center of mass of the vessel and its internals is approximately 3.1 m below the support ring, so the vessel experiences a relatively small turning moment under seismic acceleration. The vessel extends 2.90 m above the support ring, and one hot leg and two cold leg penetrations are located immediately above this ring. The reactor vessel is designed to be replaceable, where the hot and cold leg pipes would be cut, and the vessel then pulled vertically upward into a storage cask.

The normal operating temperature for the vessel is 600°C. When heated from room temperature (20°C) to this normal operating temperature, the vessel dimensions change by 1.06%. The nominal vessel wall thickness is 6.0 cm (20% greater than the 5.0-cm S-PRISM vessel), which results in Von Mises stress that is a factor of 9.45 lower than the ASME allowable stress for 316 SS for 100,000 hr (Table 1-2).

The baseline design for the vessel uses seamless rolled cylindrical sections that are machined by lathe to final inner and outer diameters, to avoid the use of axial welds. Seamless rings with heights up to 1.5 m can be produced with currently available technologies [68][69]. For the baseline vessel design with 350.0-cm outside diameter and 5.0-cm wall thickness, the vessel weight is approximately 62 metric tons.

The vessel support skirt transfers horizontal and vertical seismic loads between the reactor vessel and the reactor cavity. The skirt is located approximately 3.1 m above the center of gravity of the reactor vessel and internals and thus horizontal seismic motion will transfer a rotational moment as well as horizontal thrust loads into the skirt. Detailed design of the skirt will consider these seismic loads, to assure that rotation of the vessel at the skirt is limited appropriately.

2.4.3 Reactor cavity insulation subsystem

The Mk1 reactor cavity system does not use a guard vessel. Instead, the volume between the reactor vessel and the reactor cavity liner plate is filled with refractory liner blocks. Figure 2-22 shows this refractory reactor cavity liner system (RRCLS). The RRCLS provides effective insulation during normal operation to reduce parasitic heat loss from the reactor vessel, while also providing effective heat removal during BDBEs. The reactor cavity liner plate, as well as the cavity cover and thermal shield liner plate, are fabricated from stainless steel backed by SC structures. These liner plates are cooled by water under normal operation, to maintain the structural materials behind the liner plates at acceptable operating temperatures.

This RRCLS takes advantage of the high freezing temperature of the primary coolant (459°C) to replace the coolant containment function provided by a guard vessel with coolant containment provided by the generation of a “cold crucible” of frozen salt near the reactor cavity wall, which remains at temperatures below the freezing temperature of the salt during any BDBEs that result in vessel failure. Because the majority of the volume of the cavity between the reactor vessel and the reactor cavity liner is filled with the refractory insulation blocks, the

volume of salt required to fill the remaining volume is reduced, and therefore the drop in coolant level if the reactor vessel leaks is also reduced.

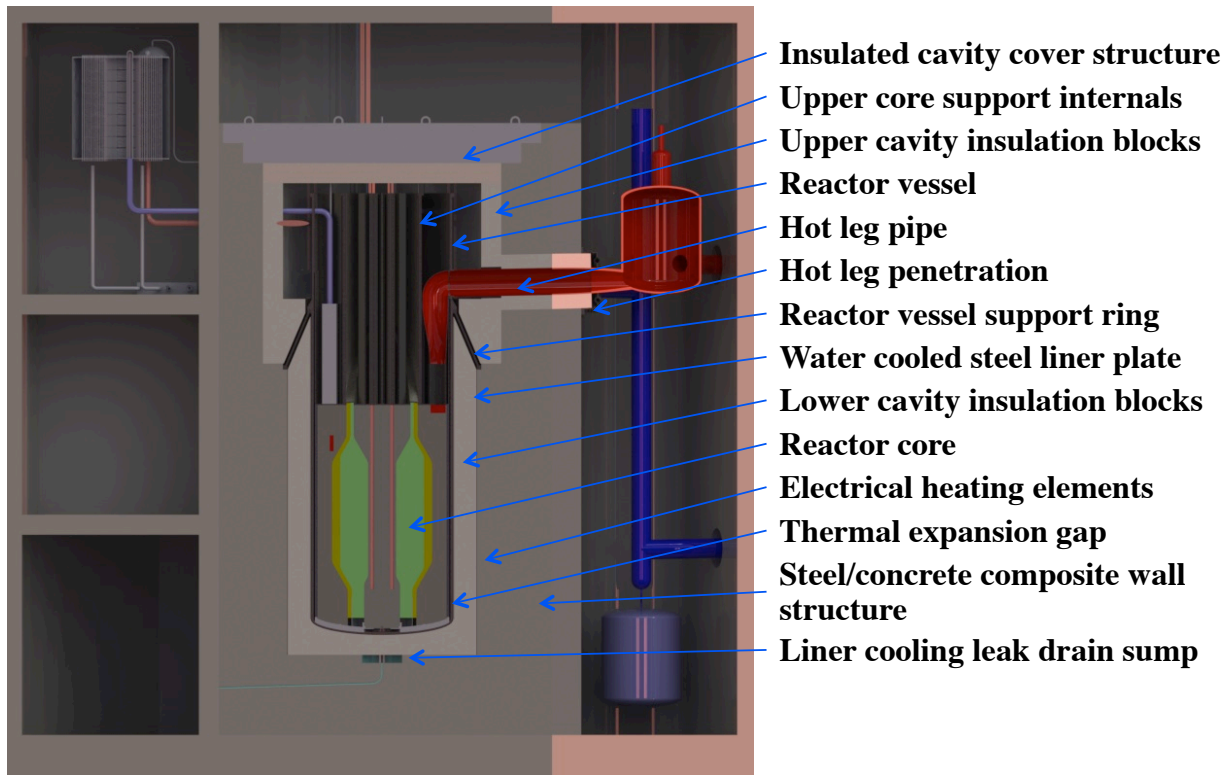


Figure 2-22. CAD model for the Mk1 PB-FHR reactor vessel and cavity, showing major elements of the RRCLS.

Under normal operation the refractory liner blocks provide insulation and limit parasitic heat loss. Conduction through the blocks, and natural circulation of the cavity gas in the spaces between the blocks, creates the primary mechanism for heat loss from the reactor vessel surface, which remains at temperatures around 600°C under normal operation. As described in the next section, the steel cavity liner plate is actively cooled by water flowing in pipes behind the plate to maintain the cavity liner plate at an acceptable temperature for the concrete behind the plate (nominally 30°C).

Under BDBE conditions where the reactor vessel or salt piping fails and coolant salt drains into the cavity, or when additional salt is injected deliberately into the cavity (options to be explored during detailed design include a frozen salt storage location located above the cavity, or an emergency salt injection system), the salt near the reactor vessel remains molten, because the reactor vessel surface temperature exceeds the salt melting temperature. Salt freezes at the cavity wall, because the temperature is below the salt freezing temperature. The fact that the salt freezes at a relatively high temperature allows leaks from the reactor cavity to be controlled—even if a crack occurs in the cavity liner, any salt that enters the crack would freeze and plug the leak path as long as the crack aperture is sufficiently small.

Initially the cavity wall and the cavity thermal shield are at their nominal temperature of approximately 30°C, but if active cooling is not maintained the temperature climbs over time. If

water is supplied to the cavity liner cooling system, even without active cooling the water will boil and maintain the liner at a maximum temperature near 100°C. Without water supply, the temperature of the liner and the concrete behind it will climb further, and heat removal occurs due to transient conduction into and heating of the SC structures of the reactor cavity and then into surrounding structures.

Because the reactor cavity can act as a heat sink under BDBE conditions, the Mk1 design provides external water injection connections outside the shield building so the cooling system water supply can be replenished using portable pumping equipment. The connection area also has connections for portable equipment to measure water inventories and system temperatures. The design of the injection connections will be based upon standardized U.S. FLEX equipment specifications.

An interface forms inside the cavity between frozen and molten salt, and the molten salt flows by buoyancy-driven natural circulation to transfer heat to this interface.

The Mk1 RRCLS uses a low density, insulating firebrick of the same type commonly used in high-temperature furnaces. The firebrick is composed of a mix of different oxides. When selected properly, these oxides will react slowly with fluoride salts. The fire bricks are porous and therefore require testing to determine if surface coatings or glazing is needed to prevent salt from imbibing into the porosity.

An alternative insulation material is baked carbon, which is formed by vibration molding of an isotropic pitch coke filler and coal tar pitch binder. It is baked at a temperature of 800°C to 1100°C, pitch impregnated, and baked a second time. Because the carbon is heated sufficiently to cause extensive graphitization, the thermal conductivity remains lower than graphite, but is higher than oxide ceramic insulation materials. Baked carbon is a second option that will have good compatibility with fluoride salts, but may oxidize in the presence of air, and has relatively high thermal conductivity around 3.6 W/m°C [70].

Key issues to be resolved in finalizing the selection include assessing the activation products produced in the alternative refractory materials, and gamma radiation heating and thermal stress effects. Also, the higher thermal conductivity of baked carbon may allow the reactor cavity liner cooling system to provide a useful decay heat removal path during BDBE conditions even if the reactor vessel does not rupture (alternatively, with low thermal conductivity fire brick, adding salt to the reactor cavity could enhance heat transfer and allow the cavity liner cooling system to provide useful decay heat removal). If oxide ceramics have acceptable performance from the perspectives of activation and thermal stress, then they may be preferred over baked carbon due to the lower rate of parasitic heat loss.

For the Mk1 blocks, firebrick from BNZ Materials has been selected as the baseline [71]. Type C22Z has relatively high strength, and a low thermal conductivity of 0.26 W/m°C at 538°C. The brick material can be machined to specific geometries.

The insulating bricks are nominally 0.50-m thick. The effective area of the insulated surface in the Mk1 cavity, including the sides, top and bottom, is

$$\pi((12.0\text{m})(3.50\text{m}+2(0.25\text{m})) + 2(3.50\text{m})^2/4) = 170 \text{ m}^2$$

The resulting heat loss depends significantly on the effective thermal conductivity of the liner blocks, and is nominally 50 kW for insulating fire brick (0.26 W/m°C) up to approximately 0.8 MW for baked carbon (3.6 W/m°C). This heat loss rate is low compared to the nominal reactor thermal power of 236 MWth. The final selection of the specific refractory material can be made based upon criteria in addition to heat loss, including chemical compatibility with fluoride salt, impermeability, mechanical strength, and cost.

It is desired that if the reactor vessel leaks, the maximum level drop in the vessel remains above the top of fuel located in the defueling chute, called FL here. The top of the defueling chute is nominally 7.0 m above the bottom of the reactor vessel. The total volume of the reactor cavity, below this elevation, is

$$V_{cf} = (7.0\text{m}) \pi ((3.5\text{m} + (0.5\text{m}))^2 - (3.5\text{m})^2)/4 + (0.5\text{m}) \pi (3.5\text{m} + (0.5\text{m}))^2/4 = 52 \text{ m}^3$$

The free volume in the cavity includes the volume in the gap between the reactor vessel and the blocks, and the volume of the gaps between blocks, other blocks, and the reactor cavity wall.

The gap between the reactor vessel and the refractory bricks is established to allow the vessel to undergo thermal expansion under BDBEs from its normal operating temperature of 600°C up to the temperature where the vessel material rate of thermal creep would become large. At this BDBE temperature, selected here to be 900°C, it is desired that the vessel begin to contact the refractory blocks, so that the blocks limit further expansion and creep of the vessel.

In heating from 600 to 900°C, the vessel diameter increases by 1.9 cm, and the bottom of the vessel drops 3.8 cm. The volume change of the vessel, due to this expansion in size, is 1.1 m³.

The volume of the gaps between refractory blocks is a design parameter that depends upon the geometry of the blocks and the precision of their manufacture. Here it is assumed that the nominal blocks are 0.5m x 0.5 m x 0.5 m. While this exceeds the maximum dimensions of commercial insulating fire brick, here it is assumed that these larger blocks would be fabricated by cementing together assemblies of smaller blocks. If the porosity of the blocks is found to be an issue for absorbing salt, it is also assumed that the blocks will be coated with a glazing material to reduce permeability of the surface.

It is assumed that gaps between blocks will vary between 0.5 and 1.0 cm, with an average gap width of 0.7 cm. In this case, the fraction of the total cavity volume occupied by gaps between the blocks and the cavity wall, and blocks with neighboring blocks, will be $(1+0.5(4))(0.7\text{cm})/(50\text{cm}) = 0.042$, or 4.2% of the cavity volume. In this case, the total void volume in the cavity will be

$$V_v = 0.042(52\text{m}^3) + 1.1\text{m}^3 = 3.3 \text{ m}^3$$

If salt occupies approximately 50% of the cross section of the reactor internals immediately below the vessel skirt, the drain down height to provide this 3.3 m³ is only 0.7 m.

2.4.4 Reactor cavity cooling subsystem

The stainless steel liner for the reactor cavity has a water cooling system behind the liner to remove heat and maintain the liner and concrete behind it at an acceptable temperature. This cooling system has two redundant sets of cooling tubes, each sized to provide 100% heat

removal capacity. The tubes are located in cavities behind the liner, that are designed to collect and direct any water leaks to sumps below the cavity to aid in the detection and control of water leaks. Figure 2-23 shows the interface of the liner cooling system with the reactor cavity thermal shield.

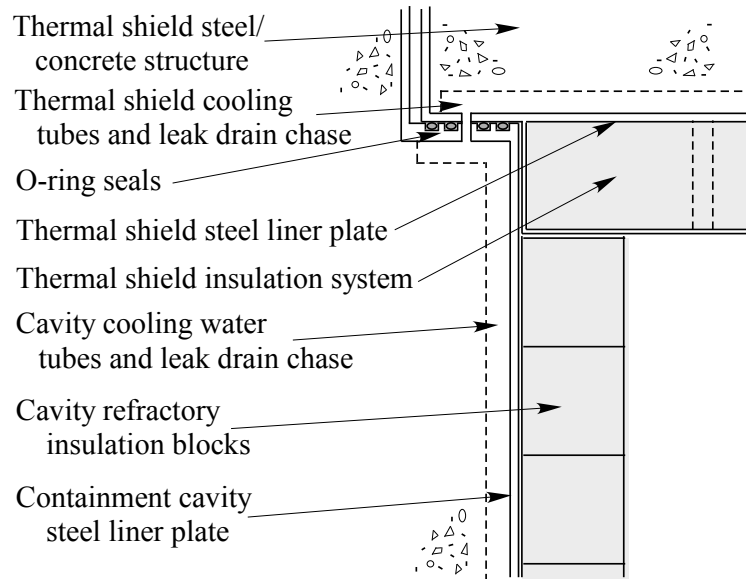


Figure 2-23. Schematic view showing the configuration of the reactor cavity cover liner and water cooling system.

Because the SC structures of the Mk1 cavity wall and thermal shield may be heated to temperatures above the normal 65°C limit for concrete, it is expected that the concrete used in these structures will be selected and qualified for high temperature service. ORNL performed an extensive review for the U.S. Nuclear Regulatory Commission (USNRC) of temperature response of different types of concrete, and of the design of high-temperature concretes, which provides background information on these topics [72]. The most directly relevant experience exists with concretes that were studied in the 1970's and 1980's for use in pre-stressed concrete reactor vessels (PCRVs) for HTGRs. The Fort St. Vrain reactor in the U.S. used a PCRV. The ASME code for PCRVs limits the temperature of concrete to 65°C at the liner interface and in the bulk concrete, while between cooling tubes (near the liner), 93°C is the maximum allowable [73]. More recent experience that is relevant, discussed in the ORNL review, involves the development of elevated-temperature cements for oil well casings that are based upon polymer silicates. Upon curing, these cements are reported to have the ability to withstand service temperatures up to 538°C (and up to 1093°C for some formulations) without alternation of mechanical or physical properties [74]. The American Concrete Institute Committee 349, "Concrete Nuclear Structures," has considered issues for concrete designs for higher temperatures, particularly as may occur during abnormal conditions and accidents [75].

2.4.5 Reactor containment penetration subsystem

The MSBR reactor cell design is described in [76]. A later MSBR report notes that all pipe penetrations coming from the cell are provided with double bellow seals to maintain containment and to provide a method for testing the integrity of the seals (by pressurizing the space between them) [77].

Figure 2-24 shows the bellows seal design adopted for the Mk1 PB-FHR salt-line penetrations. As with the MSBR, a double bellows system is envisioned to increase reliability and to enable simple leak testing. Because the Mk1 PB-FHR has a compact configuration, it is designed so that the salt piping is stiff and thermal expansion is accommodated by movement of major components (salt hot well, CTAHs) rather than by bending of salt piping. While this design approach greatly reduces reaction forces and stresses imposed in the piping, it requires that the bellows used to seal salt-line penetrations have the capability to accommodate relatively large axial displacements (5 to 20 cm).

All salt pipe penetrations, both for the reactor containment and for the CTAH enclosures, are oriented so that the displacements caused by thermal expansion are primarily axial along the length of the pipes. Therefore the bellows seals must accommodate substantial axial displacements, as well as moderate transverse displacements. The containment cold leg penetrations are expected to have the largest transverse displacements, while the transverse displacements for the hot-leg containment penetration and the CTAH enclosure penetrations will be smaller.

Because PB-FHRs are expected to spend the majority of their lifetimes at high temperature, the bellows are designed to be installed in a pre-stressed state, so that at normal operating temperatures the reactive forces imposed by the bellows, and the stresses in the bellows, are minimized. Detailed design of these seal bellows will need to consider a variety of issues, including the integration with the piping insulation system, cooling of the external portion of the seal, and replacement approach. Replacement of a bellow seal will likely require cutting the main salt pipe, and thus would be performed during a major outage where the reactor would be defueled (e.g., during a center reflector replacement outage).

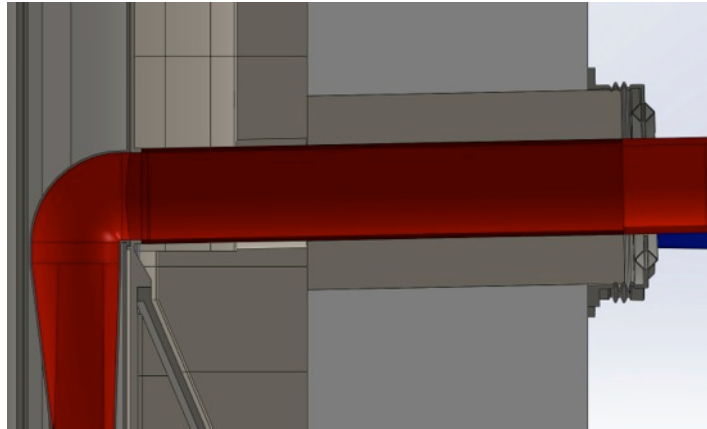


Figure 2-24. Mk1 hot and cold leg containment penetration bellow seal and thermal insulation system.

2.4.6 Electrical heating subsystem

The MSBR design provided auxiliary heating of the reactor cavity using electrically heated rods inserted into thimble tubes [78]. The Mk1 design uses the same approach, as shown in Fig. 2-25, with three banks of electrically heated rods integrated into thimble tubes slots in the refractory cavity liner system insulation blocks. The thimble tubes and rods are designed with an adiabatic section that extends through the thermal shield above the reactor cavity, where electrical power connections are made, and the rods can be replaced through openings in the refueling deck above the thermal shield.

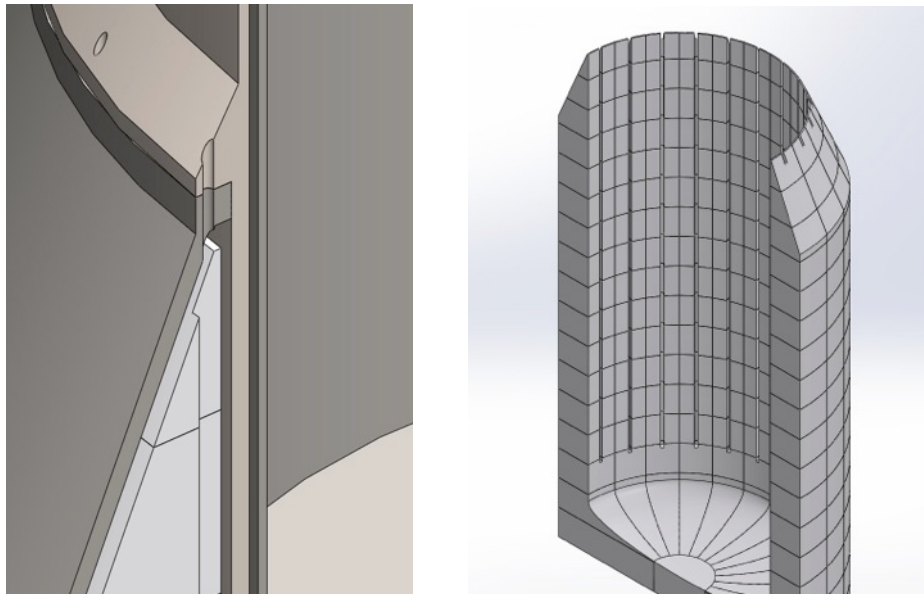


Figure 2-25. Reactor cavity electrical heating subsystem.

2.4.7 Steel-plate composite walls

The SC structures that have been used in the AP1000 reactor are game changers for new nuclear construction. The individual, rail transportable modules from which the buildings are assembled are fabricated in factories like the CBI Lake Charles facility using computer aided manufacturing. This means that the buildings are, in essence, 3-D printed using processes quite similar to those used in modern ship building. Module factories now used to manufacture AP1000 reactor buildings can readily produce modules for new FHR buildings as well.

In general, the design features of the Mk1 reactor building involve similar design principals to the AP1000. Novel features for the Mk1 reactor building relate to its reactor cavity, which uses SS lining like the AP1000 cavity but also requires a cooling system preinstalled in the cavity liner modules. The baseline PB-FHR shield building and air-duct vault structural designs are scaled to approximately match AP1000 design parameters and thus to have similar performance for external hazards such as commercial aircraft crash [79]. The baseline Mk1 design uses 1.25-cm- (1/2-inch-) thick steel plate for all SC walls, except for faceplates that must resist penetration during impact events (e.g., the above-grade, exterior surface of the shield building and the walls of the CTAH enclosures) which are 2.50-cm (1-inch) thick.

Detailed design of the PB-FHR will include structural engineering and analysis to adapt the SC method to the PB-FHR application. The American Institute of Steel Construction has recently issued a draft standard for the design of safety-related SC structures for nuclear applications [80], which would be used in detailed design. This draft standard includes guidance on the evaluation of impulsive loads, which can be used in assessing the response of the shield building to natural gas detonations. Likewise, detailed design of the shield building to resist commercial aircraft impact will use the Nuclear Energy Institute 07-13 methodology [81].

2.4.8 Considerations for reactor vessel replacement and plant decommissioning

The Mk1 design has not developed a detailed concept of operations for reactor vessel replacement and for decommissioning. The general process is expected to start with defueling of the core, followed by removal of the center reflector, which is a standard operation for center reflector replacement. The main salt pipes would then be drained and the salt removed to storage, and then the primary salt would be pumped from the vessel using a submersible pump. At this time the electrical heating of the vessel and main-salt piping would be ceased, and the vessel and internals allowed to cool to near room temperature.

The IAEA has developed a useful summary of experience with processing and disposal of graphite components, which includes a review of methods used in the decommissioning of graphite-moderated reactors [82]. They cite experience in the decommissioning of the Fort St. Vrain HTGR [83], where the reactor vessel was flooded with water to improve radiation protection during disassembly and removal of the core internals and graphite. The circulation of this water through filters and ion exchange columns was found to be effective in removing particulates and radioactive contamination (except tritium).

Because flibe is soluble in water, flooding the Mk1 vessel with water provides a method to remove beryllium contamination, and to perform work to cut apart and package core internals for storage and disposal while preventing the formation of airborne particles.

In principle the Mk1 reactor vessel can be pulled from the reactor cavity into a transfer cask for removal and replacement, after the hot and cold leg nozzles have been cut, but in practice it may be preferable to cut the vessel into smaller segments while keeping the reactor cavity flooded with water.

Following any BDBE that causes vessel rupture and coolant leakage into the reactor cavity, thermal shock and corrosion may cause damage to the cavity liner. While the high freezing temperature of flibe will prevent it from leaking from the cavity even if the liner fails, this leakage could be an important factor affecting the flooding of the cavity with water to enable decommissioning after the BDBE. However, as with other water storage in the Mk1 reactor building, the containment liner cooling system is designed with a secondary containment to enable leak detection, which also provides the ability to flood the reactor cavity even if the liner is not intact.

3 Mark-1 Heat Transport

This chapter describes the Mk1 PB-FHR heat transport system. As shown in Fig. 3-1, the major components of the heat transport system consist of the primary loop “gas-gap” system, main salt piping systems, main salt pumps system, salt drain tanks system, CTAHs system, warm and hot air ducts system, and the normal shutdown cooling and maintenance heat removal system.

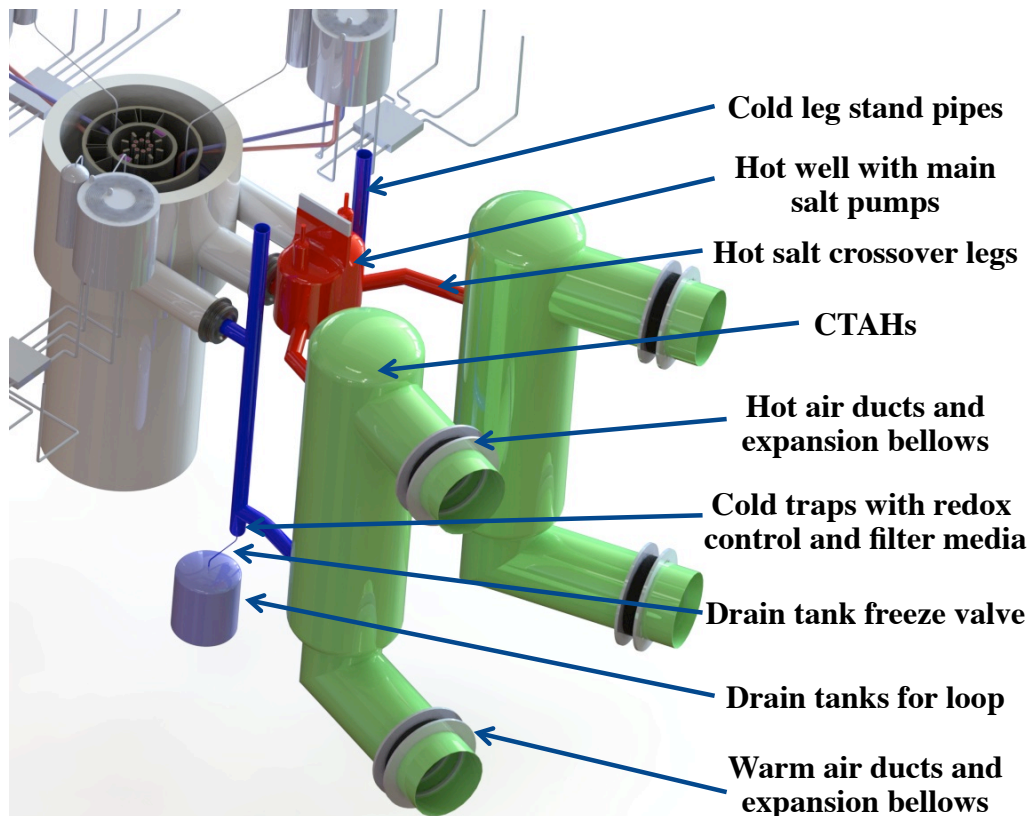


Figure 3-1. Isometric view showing major components of the Mk1 heat transport system.

The Mk1 heat transport system including the CTAHs is decoupled from the reactor by a “gas-gap” system, described in the next section.

3.1 Primary Loop “Gas-Gap” Subsystem

The Mk1 PB-FHR uses the primary coolant to directly heat air for the NACC power cycle. Compared to previous AHTR designs, as well as the long-term conventional practice for SFRs, the elimination of an intermediate loop in the Mk1 PB-FHR has major implications for simplification, cost reduction, and overall plant safety.

Besides the elimination of intermediate heat exchangers and associated intermediate loop equipment, one of the most important implications of direct air heating is the elimination of the potential for intermediate heat exchanger tube leaks to cause mixing of an intermediate salt into

the primary salt. The FHR coolant uses the fluoride salt combination with the lowest possible parasitic neutron capture (BeF_2 and ${}^7\text{LiF}$). Because low neutron capture is important to achieving negative coolant void reactivity feedback, contamination of the primary salt with other fluoride salt species would result in a much longer outage to clean/replace primary coolant than would result from air-ingress into the primary salt. The Mk1 PB-FHR also selects flibe as its coolant for the DRACS loops, as seen in Section 2.3, so a leak in a DHX would not cause similar problems.

The reason that intermediate loops have been conventional for SFRs has been the requirement to mitigate the potential over pressure, water hammer, and shock loading that would occur if sodium and water were to interact following tube failure in a steam generator. Because fluoride salt coolants are chemically stable, no significant chemical reactions will occur under a tube failure in a CTAH (or a steam generator). However, it is possible that a tube failure could cause temporary pressure increase and generate water hammer in the salt piping subsystem.

The Mk1 PB-FHR design introduces the concept of using “gas gaps” in the hot and cold salt piping system to decouple the reactor vessel and reactor cavity/containment from the external salt piping system and CTAHs. Immediately adjacent to the containment penetration, both the hot and cold salt legs have free surfaces communicating with the salt cover gas system, which make it deterministically impossible to transmit high pressure into the reactor vessel and containment.

For the hot leg, the free surface exists in a hot well, which has two cavities with gate-type isolation valves, inside which two cantilevered, sump-type main salt pumps take suction. For each cold leg, a free surface is provided in a stand pipe, which also contains an isolation valve.

The isolation of the hot and cold legs is further enhanced by a gate valve, which has an activation stem that extends up through the liquid free surface. The gate valves use a carbon fiber reinforced seat material on the valve wedge to prevent self-welding when closed.

Critical flow of air will occur at the CTAH break location if the ratio of the absolute salt pressure p_s to the absolute air pressure p_o is less than the ratio,

$$\frac{p^*}{p_o} = \left(\frac{2}{\gamma + 1} \right)^{\frac{\gamma}{\gamma - 1}} = 0.537$$

where p^* is the critical pressure for choked flow and $\gamma = 1.35$ is evaluated at the average air temperature of 545°C . Under power operation, the air pressure in the high-pressure (HP) CTAH is 18.8 bar absolute (Table 3-2), giving a choked flow pressure of 10.1 bar absolute, and for the low-pressure (LP) CTAH the air pressure is 5.0 bar absolute giving a choked flow pressure of 2.7 bar absolute. Under power operation the salt pressures in the CTAHs range from an inlet pressure of approximately 3.3 bar absolute to an outlet pressure of 1.5 bar absolute. So the air in-leakage rate will be limited by choked flow for the HP CTAH break, and will be the choked flow value or lower for the LP CTAH depending upon the local salt pressure.

CTAH air leaks will result in several detectable system responses, including level increase in the hot well, power reduction due to negative void reactivity feedback, and oxygen

contamination in the main salt cover gas system. The response to CTAH leaks is to trip the GT, isolate the CTAH air duct lines, and scram the reactor, maintaining positive pressure in the CTAH and reducing salt flow to a minimal value. The main salt system is designed to vent gas bubbles to high elevation points under zero flow, but under low flow gas from leaking tubes will accumulate in the top of the CTAH cool salt manifold pipe where the gas accumulation can be detected by electric resistivity probes. After the leak location has been determined, the leaking CTAH is isolated and drained for repair, and on-line chemical cleanup of the remaining primary salt is initiated.

3.1.1 Hot well “gas-gap” subsystem

The hot well is located immediately adjacent to the reactor cavity to minimize the length of the hot leg, as shown in Fig. 3-2. The hot well is supported by vertical bearings that allow horizontal movement to accommodate thermal expansion of the hot leg. Snubbers restrain the hot well from rapid motion during seismic events. The water-cooled reactor cavity liner extends through the wall, with internal insulation, and the containment boundary is formed by a bellow seal between the hot leg and the containment liner. After the bellow seal, all salt piping and the hot well use an external insulation system with internal trace heating.

The primary monitoring of salt inventory for protective functions uses level instrumentation located in the hot well. The hot well is designed to have a sufficiently large salt surface area that level swell due to thermal expansion of the coolant and due to level changes at other free surfaces in the primary system result in acceptable level changes in the hot well. Under normal power operation, the salt level in the hot well is above the partition boundary between the two pump cavities, and cross flow between the cavities keeps the level constant in the hot well. Two gate valves in the hot well allow the hot leg to be isolated.

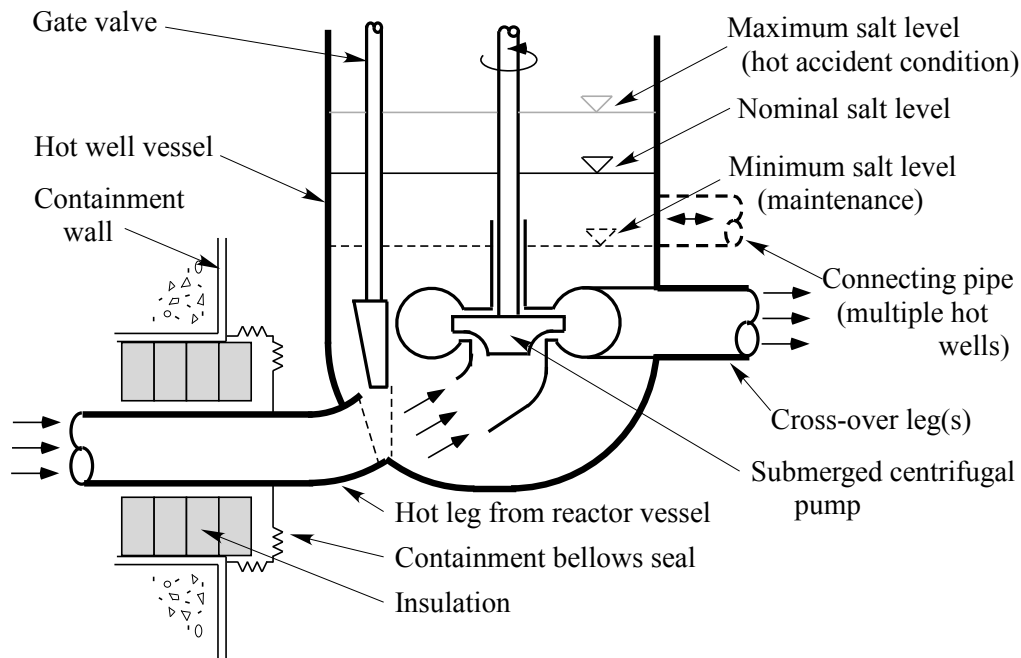


Figure 3-2. Schematic diagram of hot well and main salt pumps.

The hot well cover gas system maintains a constant gas pressure over the hot well surface. When a loop is drained for maintenance, the cover gas system supplies the gas that fills the loop as the cross-over leg drains toward the CTAH. For CTAH tube rupture events, the cover gas system has over-pressure control that can direct gas, air, and entrained salt to a knock-out drum and filter system.

3.1.2 Cold-leg stand pipe “gas-gap” subsystem

Because the Mk1 PB-FHR primary coolant, flibe, has a very high volumetric heat capacity, and because the design temperature drop across the core is relatively large (100°C), the total volumetric flow of primary coolant to transport 236 MWth is only 0.54 m³/sec (Table 1-1). This makes it possible to design the reactor to operate with a relatively small pressure drop between the cold and hot legs, with the Mk1 PB-FHR design goal being a total pressure drop between 2 and 3 meters of head.

Each of the Mk1 PB-FHR cold legs has a vertical stand pipe, as shown in Fig. 3-3, located adjacent to the reactor cavity/containment wall. Because each stand pipe communicates with the salt cover gas system, they provide a “gas gap” to prevent overpressure of the reactor vessel and containment.

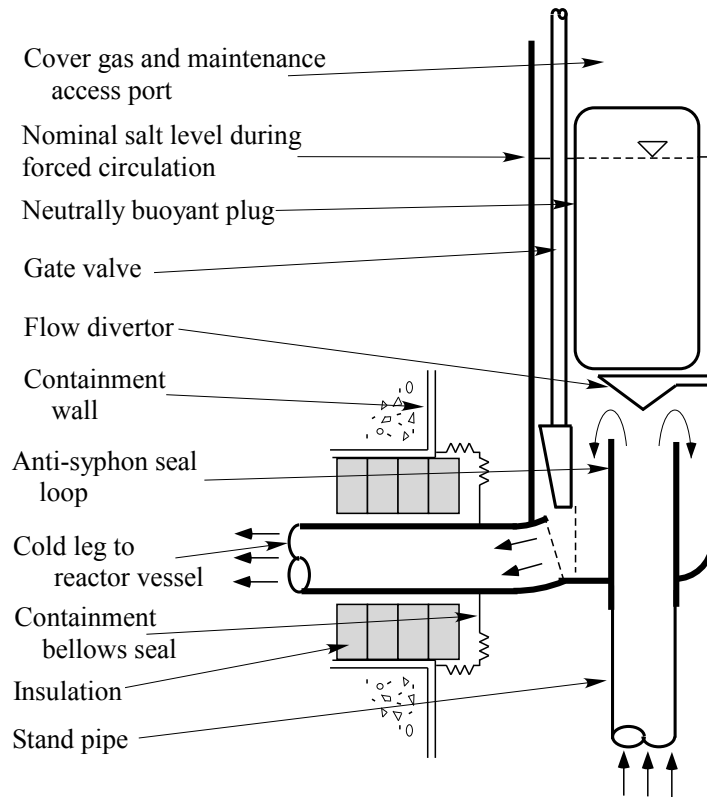


Figure 3-3. Cold-leg stand pipe system with (top) upper maintenance access, isolation valve, and pressure control/relief system, and (bottom) lower chemistry-control cold-trap well and drain line.

Cooled salt exiting the bottom of each CTAH flows in a downward sloping pipe over to the stand pipe, up the stand pipe, and then horizontally through a containment wall penetration into the reactor vessel. The stand pipe serves several functions. It transports the coolant vertically back up to the elevation of the cold leg penetrations, provides access to replace redox control and filter cartridges in the cold trap at the bottom of the stand pipe, provides a path for pressure relief for the gas-gap system, and provides a coolant free surface for the isolation valve stem so that no seal is required.

The top of each stand pipe extends above the upper horizontal cold leg, to accommodate the level swell that occurs under main salt pump operation due to the pressure difference across the reactor vessel. An overflow pipe is provided above the normal maximum free surface elevation, which will drain salt back to the hot well if the pressure drop across the reactor exceeds its normal design value or if the cold leg is over pressurized.

Each cold leg has a seal loop, which allows the stand pipe to be drained for maintenance without draining the upper horizontal cold leg section. A gate valve in each standpipe provides additional capability to isolate each upper horizontal cold leg.

Each upper stand pipe has a nearly neutrally buoyant plug, designed to displace most of the salt volume above the upper horizontal cold leg to minimize the level drop that occurs in the hot

well when the primary pumps operate and the salt level increases in the cold-leg stand pipes. The plug is designed to move freely in the vertical direction, to prevent overpressure of the reactor vessel from occurring during CTAH tube rupture events. The bottom of the plug may also incorporate a burst diaphragm or compressible cavity to mitigate transmission of hypothetical water hammer shocks into the upper horizontal cold leg.

3.1.3 Additional regulatory considerations

For LWRs which have high pressure containments, the U.S. NRC 10CFR50 Appendix A GDC number 55 requires that all primary-loop lines that penetrate containment have isolation valves inside and outside containment. For the low pressure containment of the PB-FHR, the PB-FHR designers argue that the combination of the seal loop formed by the hot leg well (and a similar seal loop integrated into the cold-leg isolation system), with a single isolation valve, is likely to provide equivalent or better containment leakage prevention, and that the reliability penalties of placing additional isolation valves inside containment would degrade the overall system safety.

Detailed probabilistic risk assessment analysis is needed to verify whether internal isolation valves should be used in the PB-FHR hot and cold salt legs. Here it is important to note that the root cause of the early fuel melting in the Fukushima Daiichi Unit 1 reactor was the inability to reopen the internal containment isolation valve for the isolation condenser, which was closed to control overcooling of the reactor vessel, and became impossible to reopen after the tsunami occurred and the AC power needed to open the valve was lost.

Because the gas-gap system provides intrinsic protection of the reactor vessel and containment from overpressure, the Mk1 PB-FHR designers also recommend that all equipment external to the gas-gap, including the main salt pumps and CTAHs, be classified as non-safety-related, with special treatment. The safety-related portions of the hot and cold legs are fabricated from piping with a larger wall thickness than the non-safety-related portions, so that deflections, stresses, and thermal creep associated with piping thermal expansion are concentrated in the non-safety-related portions.

3.2 Main Salt Piping System

The main salt piping system transfers salt from the reactor to the main salt pumps, the CTAHs, and back to the reactor. The main salt piping system also includes drain and fill lines. The major elements of the main salt piping system are described in the following subsections.

3.2.1 Hot leg and cross-over legs subsystems

Under shutdown conditions, normal shutdown cooling is accomplished by running one or both primary pumps at low speed to circulate salt through the CTAHs. Bypass valves in the CTAH air supply provide sufficient air flow to match decay heat removal and maintain the reactor system nearly isothermal at its normal shutdown temperature of 600°C. The primary pump motors can be operated at low speed using AC power with the motor variable frequency drives, but for reliability also have small direct current pony motors that can be operated with non-safety battery power.

To perform maintenance, a single CTAH loop can be drained and cooled, while the other loop continues operation to maintain normal shutdown cooling. The cross-over leg slopes down toward the CTAH. When the drain valve is opened to a loop's drain tank, the other loop drains down to the level of the cross-over partition. The drained loop drains down to the level of the inlet suction of the main salt pump. Because the main salt pump suction ports are above the top of the hot leg, a seal is formed that keeps the hot leg filled with salt.

3.2.2 Cold legs subsystem

The bottom of each cold-leg stand pipe has a cold trap, described in more detail in Section 4.3, where salt chemistry-control media is located, and a freeze valve with a line extending to a maintenance drain tank.

3.2.3 Drain tank subsystem

Each main salt loop has a drain tank, connected to the bottom of the cold-leg stand pipe by a small-diameter line with a freeze valve. The drain tank is equipped with insulation, electrical heating, and additional transfer lines to allow salt to be added or removed using portable transfer containers. If determined to be beneficial during detailed design, the drain tanks may also be lined with nickel so that the salt they contain can be purified by HF/H₂ sparging. Cover gas for the drain tanks is supplied by the cover gas inventory control system.

3.3 Main Salt Pump System

The Mk1 main salt pumps use a cantilevered shaft design, with pump bowls located in a common hot well that provides a salt free surface and also acts as a seal bowl. The Mk1 pumps have smaller size but similar requirements to the vertical-shaft, single-stage centrifugal pump designs that were developed in the early 1970's for the MSBR. Figure 3-4 illustrates a MSBR pump. As shown in Table 3-1, the Mk1 operates with pump flow rates intermediate between the MSRE and MSBR, but requires lower pump head, power and shaft torque. The higher specific speed of the AHTR-MI primary pump, compared to the MSBR, is comparable to that typical of PWR primary pumps (for example the European Pressurized Reactor – EPR – primary pumps have a specific speed of 4160 rpm (l/s)^{1/2}m^{-3/4}). The higher specific speed results in the use of a mixed-flow impellor design, which can be more readily designed using current fluid dynamics modeling tools than was possible at the time of the MSBR project.

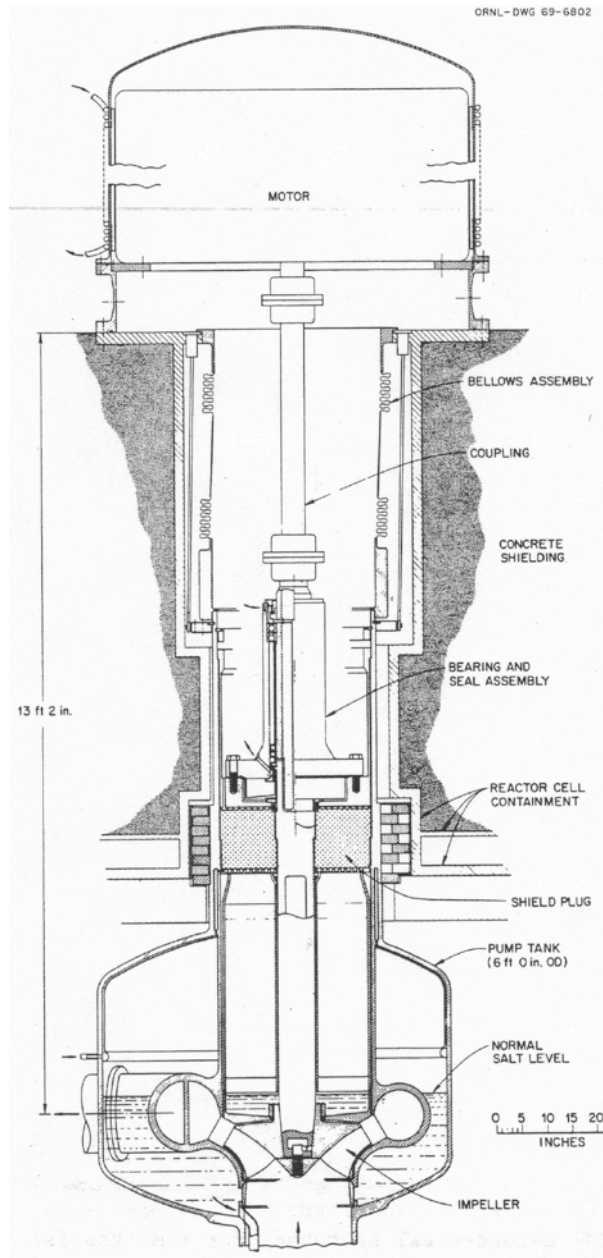


Figure 3-4. MSBR “short-shaft” pump design [84].

Table 3-1. Comparison of Mk1 PB-FHR pumps with MSRE and MSBR pump designs [85].

	MSRE	MSBR	Mk1 PB-FHR
Number of salt loops	1	3-4	2
Design temperature (°C)	700	700	700
Pump capacity (m ³ /hr)	272	4,770 – 3,630	972
Head (m)	15.2	45.7	15.4
Speed (rpm)	1150	1190	1800
Specific speed N_s (rpm(l/s) ^{1/2} m ^{-3/4})	1300	1840 - 1607	3800
Net positive suction head required (m)	3.0	6.4 - 5.5	
Impellor input power (kW)	35.8	2160 - 1640	130

The Mk1 pumps use variable frequency drives to enable flow rate control. Because there are some shutdown conditions where only a single main salt pump operates, the main salt pumps have anti-reverse-rotation devices to prevent reverse rotation if they are shut down and experience reverse flow.

3.4 Coiled Tube Air Heater System

The baseline PB-FHR design has two CTAHs, which transfer heat from the primary salt flibe to compressed air from the GT system. The CTAHs are located below grade in the filtered confinement volume, immediately adjacent to the PB-FHR reactor cavity. The CTAHs use an annular tube bundle formed by coiled tubes, with air flow radially outward over the tubes, as shown in Fig. 3-5. These CTAH's are similar to the heat exchanger design patented by Gilli et al. in 1973 [86].

The coiled tube assembly of each CTAH is located in a vertical, cylindrical pressure vessel that is insulated on the inside to allow the vessel to operate at near room temperature. Figure 3-6 shows a cut-away view of a CTAH vessel. The air temperatures in the CTAHs are comparable to air temperatures inside modern heat recovery steam generators (HRSGs) for NGCC plants, so the design of the insulation system can draw upon this experience base.

CTAHs share substantial commonality with conventional PWR steam generators, so CTAHs can be inspected and repaired using the USNRC NUREG-0800 Standard Review Plan requirements for steam generator programs with modest modifications [87]. A key difference between CTAHs and most PWR steam generators (except the NuScale steam generator) is that CTAHs have a higher pressure on the shell side than on the tube side, so the tubes operate in compression rather than tension. This largely eliminates tube rupture as a failure mode for CTAHs, but requires that the tubes be designed and evaluated for buckling.

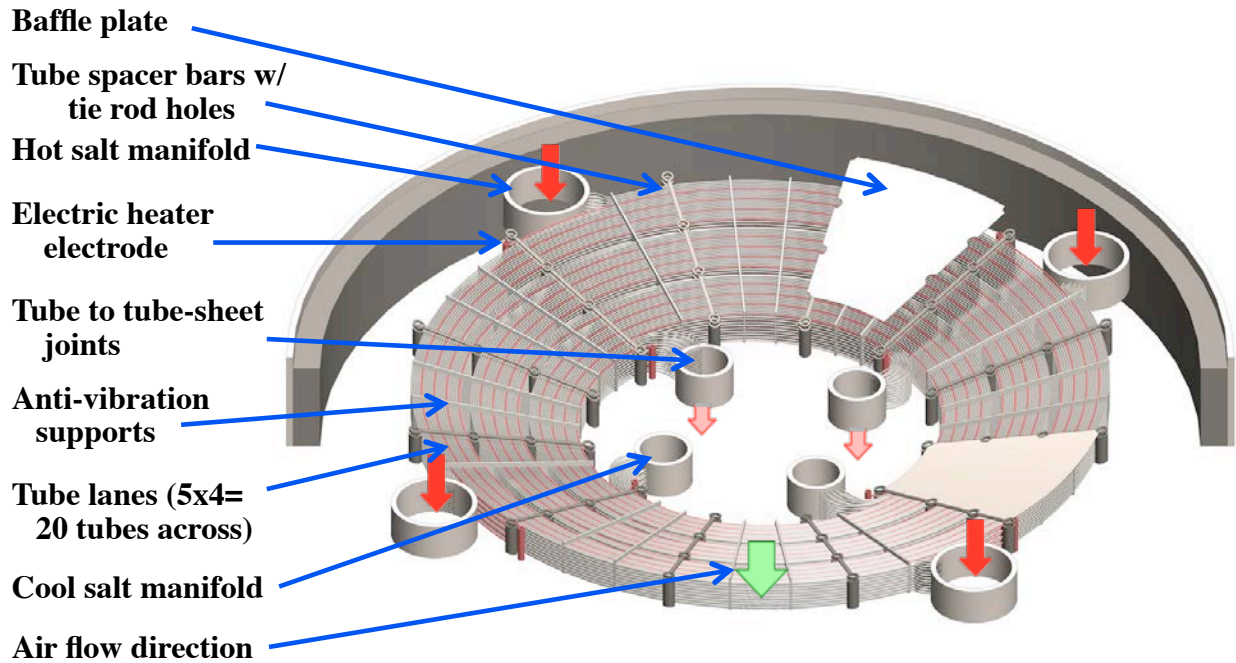


Figure 3-5. CTAH sub-bundle design.

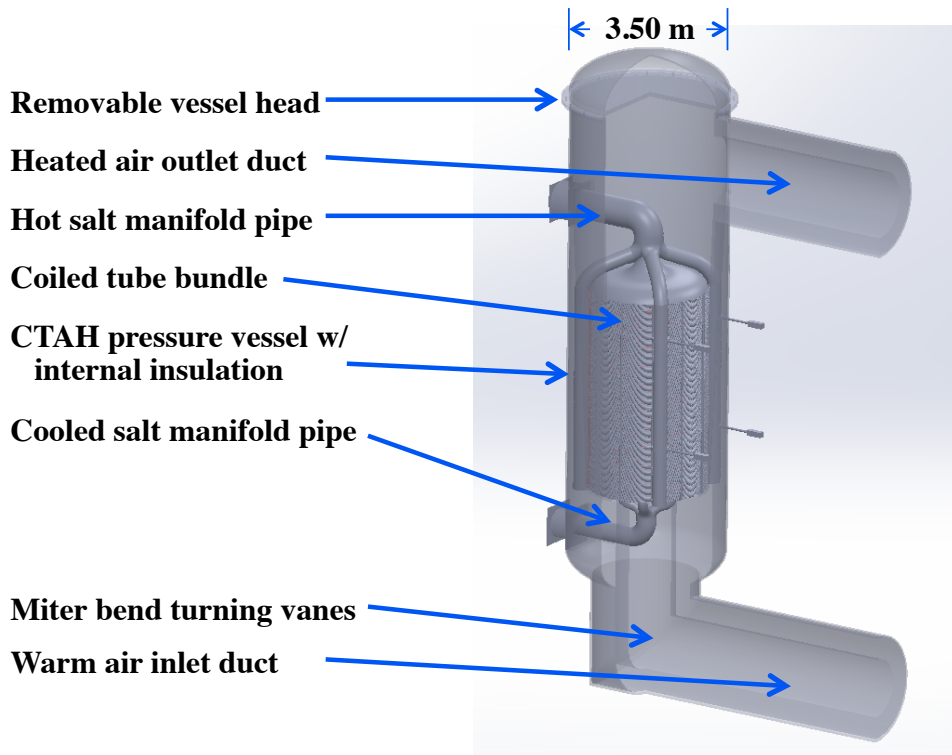


Figure 3-6. Mk1 CTAH vessel.

High-pressure air from the power conversion system enters the bottom of each vessel at a nominal temperature of 420°C, depending upon operating conditions, flows into the center of the

coiled tube bundle, flows radially outward in cross flow across the coiled tubes, and then exits upward from the vessel having been heated to the gas outlet temperature (nominally 670°C).

The baseline tubes have a relatively small diameter, 6.35 mm (0.25 in) outside diameter with 0.889-mm- (0.035-in-) thick walls, which is a standard English tubing size that is readily available in the U.S., arranged with a triangular lattice with a pitch-to-diameter ratio of 1.45. The baseline material for construction is 316 SS (the alternative material for construction is Alloy N). As described further in Section 4.1 (Tritium Control), these tubes have an aluminized cladding or coating on their outside surface. The aluminized tube surface is intended to form a self-healing aluminum oxide coating, which is known to have favorable properties as a tritium diffusion barrier. The specific aluminized coating method will be selected during detailed engineering design. Localized removal of this coating must be included in the process to generate welded tube-to-tube-sheet joints.

With the small tube diameter, the liquid flowing inside the tubes is in laminar flow, with a Nusselt number of approximately 3.66. The power density achieved in the Mk1 CTAH tube bundle is 5.2 MWth/m³; this can be compared to 4.0 MWth/m³ in the EPR steam generators [88]. Table 3-2 summarizes key design parameters for the CTAH tube bundles.

Each CTAH uses an inlet and outlet manifold system that distributes the liquid flow into the coiled tubes. This manifold system consists of four vertical hot liquid manifold pipes that enter from the top of the vessel and extend downward along the outside of the coiled tubes. The Mk1 hot manifold pipes are 0.320 m in outside diameter with 0.020-m-thick walls, and the cold manifold pipes are 0.215 m in diameter with 0.020-m-thick walls. At each tube row elevation in the coiled tube bank, hot liquid is supplied into multiple tubes that then wrap around the coiled bundle, forming a single “lane” of tubes at that elevation that wraps around the tube bank one or more times. Likewise, at the center of the tube bundle there are three vertical cool liquid manifold pipes that receive the flow from the tubes, and direct it downward and out of the heater vessel.

Each vertical manifold pipe in the CTAH has an access flange at the top. After the CTAH is drained and cooled, the CTAH vessel cover can be removed to provide access to inspect the tube bundle. The flanges allow access for inspection and plugging of the tube inlets and outlets. In the hot manifold pipes, the access flange is also used to enable removal of an annular carbon filter cartridge, used to trap tritium generated in the reactor core, as discussed in greater detail in Section 4.1 (Tritium Control). Because flanges are challenging to maintain leak-tight in fluoride salt service, detailed engineering for these manifold flanges should consider a variety of potential designs, as well as providing a secondary containment around the flange to contain leaks if they occur.

The air flowing radially outward from the bundle first flows over lanes of tubes which have relatively cool liquid, before flowing over lanes of tubes that have hotter liquid, so the flow approaches true counter-flow, even though the actual flow configuration over the tubes is cross-flow. Here the resulting heat exchanger effectiveness is assumed to be $\eta = 0.90$, however, future detailed calculations should include a multi-dimensional analysis of flow through the coiled tube bundle to determine the actual effectiveness.

Table 3-2. Key Mk1 CTAH design parameters.

CTAH Design Summary Results	Heater 1	Heater 2
Thermal power (MWt)	116.00	116.00
Air mass flow (kg/s)	418.5	418.5
Air pressure (bar absolute)	18.76	4.99
Air heater inlet temp (°C)	418.59	418.59
Air heater outlet temp (°C)	670.00	670.00
Salt mass flow rate (kg/s)	480.2	480.2
Salt volume flow rate (m ³ /s)	0.245	0.245
Salt inlet temp (°C)	700.0	700.0
Salt outlet temp (°C)	600.0	600.0
Heater LMTD (°C)	84.14	84.14
Air heat transfer coefficient (W/m ² °C)	637.9	637.9
Salt heat transfer coefficient (W/m ² °C)	831.2	831.2
Overall heat transfer coef. U (W/m ² °C)	301.5	301.5
Effectiveness	0.90	0.90
Tube outside diameter (mm)	6.350	6.350
Tube wall thickness (mm)	0.889	0.889
Tube transverse (vertical) pitch ST/D	1.450	1.450
Tube longitudinal (radial) pitch SL/D	1.256	1.256
Diameter to middle of tube bank (m)	1.96	1.96
Width of tube bank (m)	0.64	0.64
Height of tube bank (m)	5.92	5.92
Number of vertical manifold pipes	4	4
Outside diameter of hot manifold pipes (m)	0.320	0.320
Wall thickness of hot manifold pipes (m)	0.020	0.020
Outside diameter of cold manifold pipes (m)	0.215	0.215
Wall thickness of cold manifold pipes (m)	0.020	0.020
Average cross-sectional area of bank (m ²)	35.4	35.4
Total tube surface area (m ²)	5041	5041
Total tube length (m)	252697	252697
Number of loops per tube	3	3
Tube length (m)	18.47	18.47
Total number of tubes	13680	13680
Total number of electric heater tubes	720	720
Slope of tubes (for drainage)	0.010	0.010
Salt velocity in tubes (m/s)	1.09	1.08
Salt pressure drop (bar)	2.09	2.07
Tube bundle power density (MWt/m ³)	5.15	5.15
Total tube mass (kg)	31749	31749
Air velocity between tubes (m/s)	4.83	18.18
Air Reynolds number	7348	7348
Air pressure drop across bundle (bar)	0.041	0.115
Air circulating power across bundle (MW)	0.218	2.299

The Mk1 CTAH tube bundle is divided vertically into 36 sub-bundles, each 20 tube rows high (the total number of tube rows in the vertical direction is 720). Each sub-bundle is separated by a conical sheet metal divider plate, which should help to increase uniformity of the air flow through the bundle.

The tubes have a spiral slope of 1.0%, and thus over their 18.5-m length around the bundle drop a distance of 18.5 cm from the outside to the inside of the bundle. This allows liquid to be drained from the tubes to the outlet manifold pipes which exit from the bottom of the vessel, to prevent freezing under shutdown conditions and to facilitate room-temperature inspection and maintenance. Access ports are provided in the vessel to allow access for inspection on the shell side of the tube coil, and access for inspection of the tube side of the coil can be obtained from the inside of either the hot or the cold manifold pipes. Similar to PWR steam generators, CTAH tubes can also be stabilized and plugged if necessary.

In each row vertically, there are 5 tube-to-manifold connections for each manifold pipe, except for one of the pipes where one tube is replaced with an electrical resistance heater element. The heater elements consist of a metal sheath around an insulator and an internal electrical resistance heating wire, and connect to electrodes that run parallel to each manifold pipe. The resistance heater element connections rotate by one manifold pipe at each vertical level, so that the heaters are distributed uniformly through the tube bundle volume. Like the tubes, the heater elements spiral 3 times around the bundle. Electrical power is supplied to these heaters by the electrodes located at the inside and outside of the bundle.

There are 12 spacer bars located circumferentially around the bundle, 3 between each manifold pipe. Each spacer bar has half-round slots milled into each side, offset to orient and space tubes correctly in their downward, inward radial spiral. Rings at the two ends of the bar, and two rings equally spaced in the middle, are provided for four 3.0-cm-diameter tie bars. There are 20 tube slots between each tie-bar ring. Additional anti-vibration supports are located between the spacer bars to prevent flow-induced vibration.

Figure 3-7 shows photos of a spacer bar design used at UCB to fabricate a CTAH test bundle. The spacing between the bars allows a gap between each lane of tubes, which simplifies the assembly of the coiled bundle.

Because CTAHs operate with a higher pressure outside the tubes than inside, the tube-to-tube-sheet joints operate in compression, with fluid pressure pushing the tubes into the tubesheet holes, rather than pulling them out. Figure 3-8 shows the proposed tube-to-tube-sheet joint design for the CTAH manifold pipes, as well as a test diffusion-welded joint fabricated by the UCB 2014 NE-170 senior design class [89]. To facilitate diffusion welding, the tube ends are machined to remove the aluminized coating and to provide a small taper, enabling a compression fit into the tube-sheet hole machined into the side of the manifold pipe. The use of this type of tapered tube-sheet joint is unconventional, but is practical because the CTAHs operate in compression.



Figure 3-7. UCB CTAH test bundle (left) with close up of tube support bars (right).

The MSRE used welded tube-to-tube-sheet joints in its primary heat exchanger, with the tubes then being brazed to the tube-sheet on the shell side [90]. Given the large number of tubes in the Mk1 CTAHs, automated assembly and welding will be required to maintain high quality levels for these joints. Orbital welding of small diameter tubing is performed routinely, particularly for applications in the semiconductor industry [91], but further development will be needed if the technology is applied to seal CTAH tube-to-tube-sheet joints. Because high-quality diffusion-bonded welds appear feasible, seal welds may not be required.

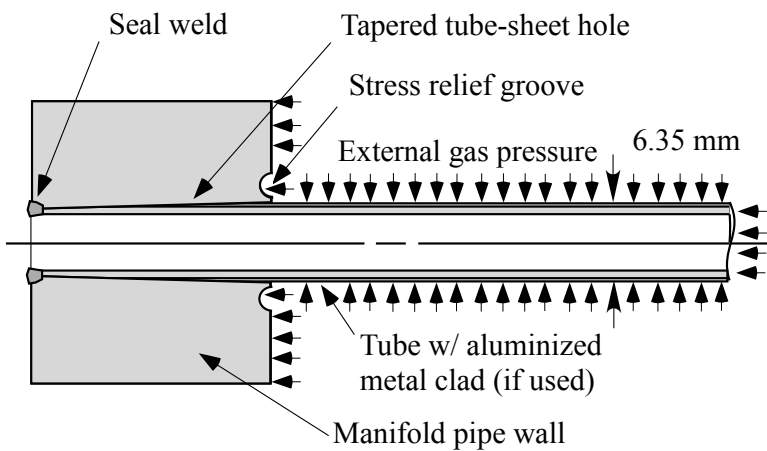


Figure 3-8. Tube-to-tube-sheet joint for the CTAH manifolds (left) and diffusion bonding demonstration sample fabricated by UCB NE-170 senior design class [92] (right).

As shown in Fig. 3-6, conical ducts are provided inside and outside of the annular tube bundle to guide and uniformly distribute the air flow through the bundle. The conical duct at the center of the coiled bundle guides and distributes the air flow entering the inside of the bundle, and the tapered annular duct outside the bundle collects and directs the air flow upward to the

outlet duct. The volume between this outside duct and the vessel wall can be filled with insulation to reduce heat losses.

The viscosity of the salt increases as its temperature drops. To prevent freezing, the tubes that are exposed to colder air in the front rows of a lane may have slightly shorter lengths than the tubes in the back rows, to compensate for the higher average viscosity of the salt flowing in these tubes.

3.5 Main salt freeze protection and recovery

Overcooling of the main salt loops, particularly the CTAHs, is a concern due to the high melting temperature of the coolant salt and potential for freezing and thawing to cause damage. This section reviews topics related to freeze protection and recovery for the Mk1 design.

3.5.1 Prior experience with freeze protection and recovery

The 8-MWth MSRE provides useful experience, since it was also air-cooled with flibe. The MSRE experienced two major incidents of freezing in its air-cooled radiator, the first involving 30 of the 120 tubes; in both cases the radiator was then thawed without damage [93]. Both events involved reactor scrams where the coolant circulation pump also stopped. Changes to the control logic to assure that the pump continued to operate prevented further freezing events.

Operating experience with test loops, such as the MSR-FCL-2 forced-circulation materials test loop that operated with LiF-BeF₂-ThF₄-UF₄ fuel salt (71.7-16-12-0.3 mole %) [94], found that freezing could occur in coolers after the loop heating and forced circulation was shut down, because of heat transfer to structures around the cooler that were maintained at low temperature by the air flow. Again, this loop could also be thawed without damage, as long as during reheating melted salt was not trapped between frozen plugs. Procedures developed for the MSR-FCL-2 test loop to maintain reduced-speed pump circulation for a period of time after the trip of the heaters were found to be effective in preventing freezing, and serve as an important knowledge basis for FHR freezing control.

A key benefit of the Mk1 coolant, flibe, is its very low volume change upon freezing, estimated to be 2.07%. Thoma et al. commented that flibe is “unique among the complex fluorides which have significance in molten-salt reactor technology, in that it undergoes the least volume change associated with the melting-freezing transition of any of the compounds encountered” [95]. They attribute this small volume change upon freezing to the formation of an uncommon void structure in the frozen flibe crystal. The observed freezing and thawing behaviors of flibe are also interesting, because between the “freezing” temperature and about 480°C a slurry of LiF crystals remains suspended in the melt.

3.5.2 Main salt piping insulation and trace heating subsystem

All salt piping external to the reactor cavity is insulated and heat traced. The insulation is designed to assure that insulation surfaces remain below 60°C for personnel safety, and is designed to be removable to facilitate in-service inspection of pipe surfaces. A baseline approach to heat tracing has not been determined. One option is to use electrical trace heating. Because electrical resistance heating delivers power largely independent of the local temperature, relatively complex control is required to avoid localized over or under heating, which may result

in reliability problems. A second option is to use a heated gas circulation system that would force the circulation of a heated gas through annular openings between insulation and pipes. The gas circulation system would have better intrinsic capability to prevent localized over and under heating, and to maintain uniform temperature in the heated system, but requires further design effort to confirm workability and practicality. The 2011 IAEA construction technologies report provides a review of practical issues for insulation systems [96].

3.5.3 Freeze protection and recovery in Mk1 heat exchangers

The CTAHs design includes electrical heating elements that replace selected tubes and spiral through the bundle, similar to the heating elements used in the MSRE air radiator, to provide supplemental heating to prevent freezing. As shown in the sub-bundle view in Fig. 3-5, there are 4 separate banks of heating elements, each with individual electrical power supplies, to provide redundancy.

The TCHXs are also designed to use the same trace heating system as the salt piping, to prevent freezing during overcooling transient. If this system uses heated gas circulation, the gas system will be designed to also circulate gas through the space between the salt and the thermosyphon tubes.

3.6 Warm and Hot Air Duct System

The CTAH air ducts use a hot duct liner system, which is designed similar to the duct liner developed for the PBMR, shown in Fig. 3-9. The liner system includes sliding elements, similar to snake scales, to accommodate differential thermal expansion. It is designed with consideration of foreign material exclusion, for example, to trap foreign objects that may slide along the bottom of a duct, and to prevent the potential for generation of debris from the hot duct itself. The insulation system is also designed to provide a controlled temperature environment to prevent air in the insulation system from dropping below its dew-point temperature. If needed, the outside of ducts and the CTAH vessels have insulation to maintain the surface temperature below 50°C for personnel protection.

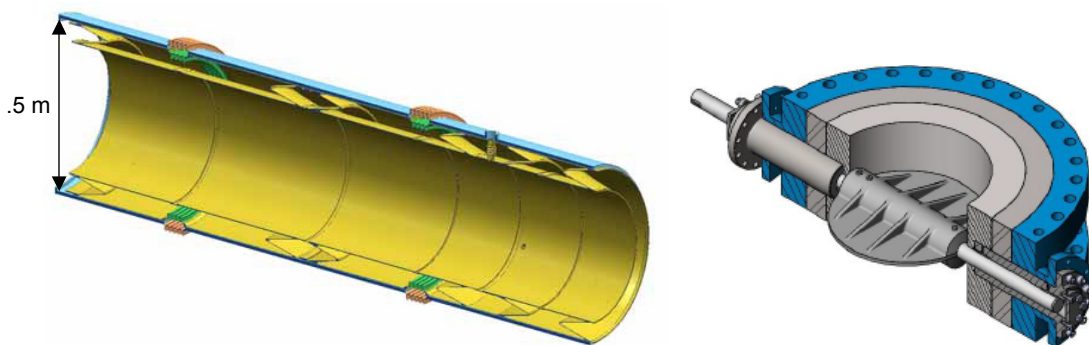


Figure 3-9. Hot duct liner system design used in the PBMR [97] (left) and a commercial high-temperature butterfly valve [98] (right).

The Mk1 GE 7FB GT is located at grade level immediately adjacent to the reactor building, at the same elevation as the refueling deck, with the LP take-off duct and combustor oriented toward the reactor to minimize the length of the LP duct. The air ducts and CTAHs are located

in a vault, below grade, with the CTAHs recessed into enclosures under the reactor building so that CTAH inspection and maintenance can be performed using the reactor building crane system, and so that the CTAH enclosures can use the same HVAC system as the reactor building to provide beryllium filtering and control.

The air ducts come out of each CTAH at an angle that is parallel to the axis between the reactor vessel and the CTAH, which is the principal axis for thermal expansion of the main salt piping. A short distance along the duct, there is a bellow system capable of accommodating up to 0.20 m of displacement of the CTAH along this axis to respond to main salt pipe thermal expansion. The bellow section is approximately 0.50-m long.

Immediately after the expansion joint, the air ducts have a low-angle miter joint so the ducts turn to run perpendicularly away from the reactor building. Immediately after these miter bends, there are small-diameter tees for the 0.80-m-diameter shutdown-cooling air lines, followed by a butterfly isolation valve. Figure 3-9 shows a typical high-temperature butterfly valve, manufactured by Leeds Valve Company in the United Kingdom. For service in the temperature range of 600°C to 800°C, these valves use a carbon steel body, stainless steel disk and shaft, ceramic bearing, and refractory internal insulation designed to match that used in the remainder of the high-temperature piping system.

Following the CTAH isolation valves, the air ducts then run over toward the GT. Each hot and warm air duct has a bypass line between the ducts, which are 70% of the diameter of the main ducts. The bypass lines have a butterfly valve to control the bypass air flow rate. These bypass lines are used to prevent overcooling of the CTAHs during startup of the GT. The GT is started up by motoring the generator to spin the turbine up to its normal operating speed of 3600 rpm, as is done with conventional GTs. This startup is performed with the CTAH isolation valves closed and the bypass valve open. Power is then increased by slowly opening the CTAH isolation valves, so a fraction of the air flow goes through the CTAH and is heated to a nominal temperature of 670°C. The turbine inlet temperature is controlled by mixing this heated air with bypass air, to control the turbine power at part load. Andreades et al. describes the NACC startup procedure in greater detail [99].

The horizontal ducts then turn upward using 90° miter bends with internal turning vanes. The LP hot air duct has a back-flow damper in this vertical leg, consisting of two half disks that are lifted when air flow occurs, and which drop and close when air flow ceases. A blowdown air bypass line is also connected in this vertical leg, and provides the capability to bypass hot air directly to the bypass stack. Each vertical and horizontal duct length also has at least one expansion bellow.

Compressor and turbine blade failures can occur in GTs. Generally these events cause extensive damage to the turbine and its casing, but air flow stops rapidly and carry-over of shrapnel is relatively small. The fact that blades are not ejected through the turbine casing is different than for the much larger blades in LP steam turbines, so the PB-FHR GT can be oriented parallel to the reactor containment structure, whereas steam turbines must be oriented perpendicular. Both the CTAHs and their supply ducts are designed to minimize the risk of damage to tubes and salt leakage in the event of blade failure. The air supply duct system is designed to slow down and stop blade shrapnel. The miter-bend turning elbows and turning vanes act as filters to stop shrapnel from reaching the CTAHs. Thus the baseline design replaces

the first 2 to 4 rows of tubes in the air heater (which will have about 70 to 100 rows total) with solid rods or electrically heated rods that would protect the interior tubes from damage.

3.7 Normal Shutdown Cooling and Maintenance Heat Removal System

The Mk1 PB-FHR uses the CTAHs for normal shutdown cooling and maintenance heat removal. For shutdown cooling, one or both main pumps are operated at low speed to circulate salt. A variable-speed blower system circulates ambient air through one or both of the CTAHs. The air flow rate is controlled to match the CTAH heat removal to the decay heat generation rate, and the salt flow rate is controlled to keep the salt cold leg temperature constant at 600°C to minimize thermal stresses to the reactor vessel and core internals.

Because the CTAHs can be drained independently, for maintenance a single CTAH is drained while the other CTAH continues to provide shutdown cooling.

4 Mark-1 Main Support Systems

Main support systems in the Mk1 PB-FHR include tritium control; beryllium control and radiation protection; coolant chemistry, particulate, and inventory control; cover gas control; fuel handling and storage; and plant instrumentation and control. This chapter provides descriptions of these support systems for the Mk1 design.

4.1 Tritium Control and Recovery

FHRs produce on the order of 1000 to over 10,000 times more tritium than do PWRs, per unit of electrical power produced. PWRs emit this tritium in gaseous and liquid discharges. At equilibrium, the Mk1 core produces 0.023 mol per effective full power day (EFPD) of tritium [100], or 0.069 g/EFPD = 670 Ci/EFPD. This is 3500 times more tritium, per MWe, than the 700 Ci/year of a typical 1000-MWe PWR, and the rate of production will be several times higher when the coolant is new, depending upon the lithium enrichment of the coolant. The goal of the Mk1 PB-FHR design is to maintain total tritium emission rates close to those for PWRs, which requires that at least 99.9% of tritium be recovered.

The phenomena associated with tritium transport and recovery in FHRs are complex, and a variety of different potential methods exist to achieve control [101]. The Mk1 PB-FHR design uses an aluminized coating which forms an aluminum-oxide tritium diffusion barrier on the CTAH tubes and on coolant piping to control the release of tritium, and uses tritium transport to carbon surfaces to recover and remove tritium. Carbon surfaces are expected to have a high capacity to absorb tritium, so that essentially all tritium that diffuses through the salt to a carbon surface can be effectively immobilized.

4.1.1 Tritium absorption by graphite

The fuel and reflector pebbles in the Mk1 design provide a large carbon surface area to absorb tritium. The Mk1 CTAH vertical hot salt manifold pipes are designed to contain annular cartridges packed with small (2.0-mm-diameter) carbon spheres to aid the recovery of tritium. Hot salt flows down the center of these cartridges, then radially outward through the packed spheres, into the annular volume around the cartridge, and then into the hot-salt tubes. Small graphite spheres in the size range from 0.05 to 5.0 mm can be manufactured using the same processes and materials used to produce over-coated TRISO fuel particles [102].

Experience with the MSRE has suggested that graphite can provide an effective sink for tritium. In reviewing studies on chemisorption of tritium on graphite, ORNL researchers stated,

“The MSRE data suggested that the bonding of tritium [on graphite] was tenacious, even at the high temperatures of the reactor and that the kinetics of sorption were fast in comparison with the fuel salt circulation time.” [103]

In modeling tritium transport in the MSBR, Briggs states,

“On reaching graphite surfaces in the reactor core, tritium and tritium fluoride diffuse into the pores and are sorbed on surfaces. Because the amount found on graphite removed from

the MSRE was so large, we base our calculations on retention by the graphite of all the tritium and tritium fluoride that reaches the surfaces.” [104],

To further increase tritium capture into graphite surfaces, the Mk1 PB-FHR design also contacts 100% of the hot-salt flow with a carbon-particle bed before the flow enters the CTAH tubes, in a replaceable, annular cartridge shown in Fig. 4.1.

Each vertical manifold pipe in the CTAH has an access flange at the top, as shown in Fig. 4-1. After the CTAH is drained and cooled, the CTAH vessel cover can be removed to provide access to inspect the tube bundle. The flanges allow access for inspection and plugging of the tube inlets and outlets. In the hot manifold pipes, the access flange is also used to enable removal of an annular carbon filter cartridge, used to trap tritium generated in the reactor core. Locating the filter cartridge inside the manifold pipe enables the use of relatively small, fine carbon particles with large surface area to enhance tritium recovery, while maintaining a geometry that can be readily drained.

The carbon filter cartridges provide an additional carbon surface area of 2300 m². By approximately doubling the available carbon surface area in the Mk1 main salt system, they can halve the tritium loss to air in the CTAHs. Even in this case, the total mass transfer through the CTAH tubes must be reduced by a factor of 100, by the tritium permeation barrier to achieve acceptable emissions.

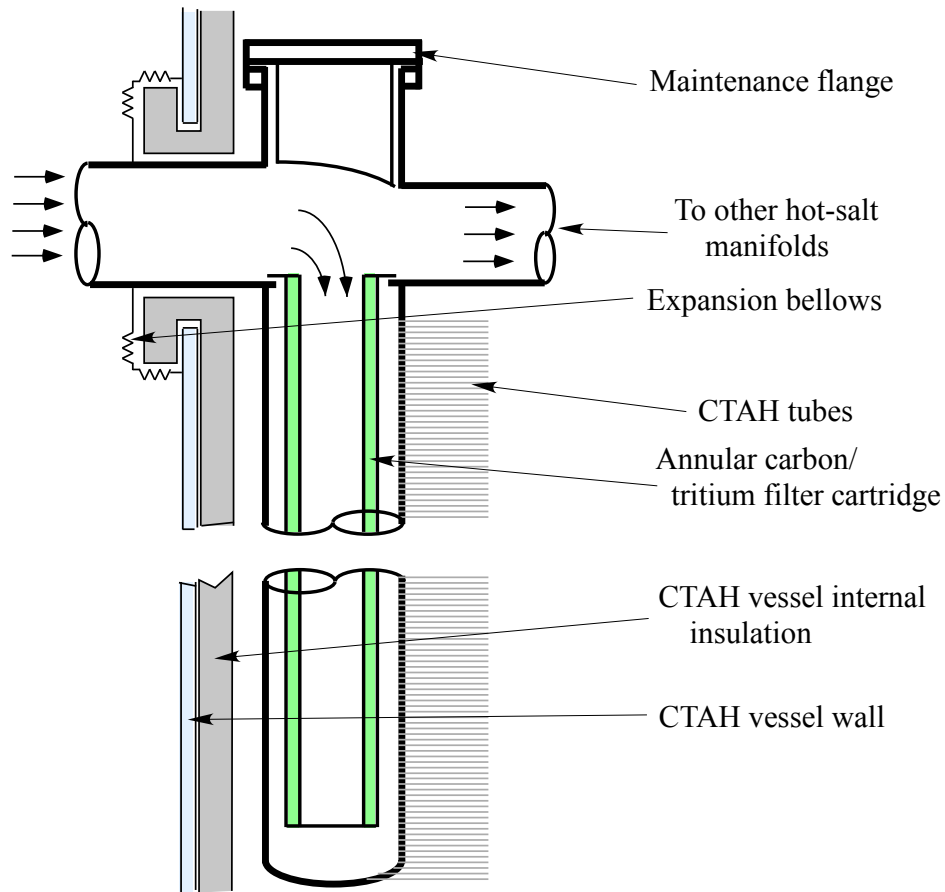


Figure 4-1. Schematic figure of hot-salt manifold pipe showing inspection and maintenance flange and annular tritium and particulate filter cartridge.

4.1.2 Tritium permeation barrier

The MSRE shares an important similarity with the Mk1 PB-FHR, because it used air as its heat sink. Briggs notes that measurements of tritium in the cooling air of the MSRE indicated a release of approximately 4 Ci/day, around 8% of the total ~54 Ci/day generated, but that these measurements were difficult due to the extremely low tritium concentration in the cooling air. Tritium release measurements made by placing a jacket around a 0.6-m-long section of radiator pipe, and extrapolating the measured release to the total area of the radiator, indicated a release rate of only 0.2 to 0.4 Ci/day [105]. After shutdown, samples taken from the radiator were found to have an oxide coating about 50 μm (2 mils) thick [106].

ORNL researchers attributed the relatively small fraction of tritium released to the MSRE cooling air to the permeation reduction caused by this oxide coating. Subsequent research in the fusion community has identified approaches to further reduce tritium permeation through high-temperature structural metals using a variety of ceramic coatings. Coatings of aluminum oxide, Al_2O_3 , have been demonstrated to be particularly effective, providing permeation reduction factor values of 10 to above 10,000 (107). The baseline design of the Mk1 CTAHs uses an aluminized coating on the tubes and manifold pipes to reduce tritium permeation. While

permeation barriers have had limited success when tested in high radiation environments in reactors (108), when used on the air side of CTAH tubes the coatings are in an ideal oxidizing environment for self-healing of the coatings.

An aluminized coating consists of an aluminum-based intermetallic coating generated by controlled diffusion of aluminum into the substrate metal. A variety of methods have been studied to generate aluminized coatings on austenitic stainless steels, such as dipping in molten aluminum, precipitation from liquid metals, flame spraying, vacuum plasma spraying, ion implantation, chemical vapor deposition, sputter deposition, and packed-bed cementation (109).

Given the simple geometry of the CTAH tubes, another option is to co-extrude the tubes with a thin (0.10- to 0.05-mm-thick) cladding layer of an alumina-forming alloy on the outside surface. Candidate alumina forming alloys for use for co-extrusion include alloys developed by Kanthal, such as Kanthal AF [110] and Alkrothal 14 [111]. Co-extrusion may be attractive for CTAH tubing, since it generates a well controlled aluminized alloy composition on the tube surface and can be performed at relatively low cost for production in the quantities of tubing needed for the CTAH application.

The mass diffusivity of tritium in Al_2O_3 has been measured to be extremely small, $10^{-19} \text{ m}^2/\text{s}$ [112], many orders of magnitude smaller than the diffusivities in flibe and in 300-series stainless steels as well as in air ($2.0 \times 10^{-5} \text{ m}^2/\text{s}$). So the effectiveness of the tritium diffusion barrier depends primarily on the quality of and defects in the oxide layer.

The high temperature air environment in the CTAHs should provide favorable conditions to form and heal oxide layers on the CTAH tubes. Bell, Redman and Bittner [113] found similar self-healing behavior with oxide formation on Alloy 800 tubes in steam environments, where tritium diffusion dropped by a factor of 214 over 158 days when the tube was exposed to 0.70 atm steam at 660°C . They also found that the oxide layers survive slow thermal transients, but observed that thermal shock due to rapid cooling from 660°C to 550°C over a period of 5 minutes increased tritium permeation through the tube by a factor of 10. Self-healing of the layer was also observed, with the tritium permeation rate dropping to the original value within 5 days of exposure to steam at 660°C .

The specific aluminized coating method for CTAH tubes and PB-FHR piping and vessels will be selected during detailed engineering design of the PB-FHR. Several issues must be considered in selecting among coating and cladding options. Pure aluminum melts at 660°C , so it is necessary that the aluminum be alloyed. Spray methods may result in coatings that are not fully dense. A key issue is the potential for higher aluminum concentrations to make the surface alloy brittle. This combined with the effects of the different thermal expansion coefficients of the base alloy, the surface alloy, and the Al_2O_3 oxide layer, may lead to cracking which can substantially reduce the permeation reduction provided by the oxide layer.

4.1.3 Tritium mass transfer in main salt

Because heat generation in FHRs occurs in solid fuel, rather than in the primary salt, FHRs have much larger graphite surface areas than the MSRE and MSR in general. To understand how the graphite surfaces of the fuel and reflector pebbles can compete with the CTAHs for tritium mass transfer, an approximate analysis of tritium is presented here. One tritium loss

pathway in the PB-FHR is the CTAHs, where the Mk1 design has a total tube surface area of $A_{CTAH}=11,800 \text{ m}^2$, and the average salt heat transfer coefficient is $h_{CTAH}=830 \text{ W/m}^2\text{C}$.

Heat and mass transfer to the graphite pebbles in the core can be predicted using the Wakao correlation for the heat transfer coefficient, h_G ,

$$Nu_G = \frac{h_G d_p}{k_F} = (2 + 1.1 Re^{0.62} Pr^{0.33}) \quad (4.1)$$

where Nu is the Nusselt number, k_F the thermal conductivity of the salt, d_p is the diameter of the pebbles, and $Pr = 15.8$ the salt Prandtl number. The total core volume of the Mk1 PB-FHR is 16 m^3 , which at a pebble packing fraction of 0.60 contains a total of 470,000 fuel and 218,000 graphite reflector pebbles (Table 2-1) with a total surface area of $A_G=1940 \text{ m}^2$, an average Reynolds number of $Re=500$ and thus a heat transfer coefficient of $h_G=4700 \text{ W/m}^2\text{C}$. The graphite reflector pebbles may be manufactured with surfaces specifically optimized to provide high tritium absorption and retention capacity.

The diffusivity of tritium in flibe is relatively low, and has been estimated to be approximately $3 \times 10^{-9} \text{ m}^2/\text{s}$ at 650°C [114]. The heat and mass transfer analogy can be used to estimate the relative mass transfer resistance to the CTAH tubes, versus to the fuel and reflector pebbles. In applying the analogy, the Schmidt number ($Sc = 870$) is substituted for the Prandtl number in the heat transfer correlations. Because the heat and mass transfer for laminar flow in the CTAH tubes are not a function of Pr or Sc , the relative thermal resistance for mass transfer of tritium to the CTAH tubes, versus to the fuel and reflector pebbles, is

$$(h_G A_G)(Sc/Pr)^{0.33} / (h_{CTAH} A_{CTAH}) = 3.8 \quad (4.2)$$

If the CTAH tube surfaces acted as perfect sinks for tritium, then for every 3.8 Ci of tritium absorbed by graphite, 1.0 Ci would diffuse through the CTAH tubes (e.g., 21%).

To achieve the FHR tritium recovery goal of 99.9%, the permeation barrier system in the CTAHs must reduce tritium releases through the CTAH tubes by a factor of 200, or a factor of 100 considering additional graphite surface area provided in the CTAH hot manifold pipe annular cartridges. Experimental studies and additional analysis to determine whether the necessary mass transfer resistance can be achieved are needed, to select a specific coating method and to determine whether the Mk1 PB-FHR tritium control system is capable of achieving its tritium control target. Further work to study this question will be important to perform as the PB-FHR design is refined.

4.2 Beryllium Control and Radiation Protection

The beryllium used in the PB-FHR primary coolant provides the most important chemical hazard that must be managed in FHRs. Because the primary hazard associated with beryllium involves the risk of inhaling aerosol particles that contain beryllium, in FHRs beryllium protection and controls are closely integrated with systems for radiation protection and control, particularly those systems associated with monitoring for, controlling, and decontaminating radioactive materials in air and on surfaces. For example, in FHRs careful attention is paid to selecting coatings for surfaces to aid monitoring and decontamination.

4.2.1 General issues for beryllium and radiation safety

Previous UCB design projects have addressed issues for beryllium and radiation control for FHRs. In particular, the 2008 UCB senior design project report devotes a chapter to beryllium and radiation safety, including discussing medical surveillance, radiotracers for beryllium detection, mixed waste management and disposal issues, and design of building ventilation systems and access control [115].

Likewise, as an element of their research program to perform corrosion studies with flibe, UW has developed the following process to clean up flibe spills, which to date has been used by UW to clean up flibe in the form of dust and chunks [116]:

- Create detailed plan of operation to be performed, including necessary tools, trash bags, and rags.
- Inform Environmental Health and Safety Department of nature of work.
- Receive swipes and airborne monitor.
- Don full personal protective equipment including respirator and disposable coverall garment.
- Enter room, turn on airborne monitor.
- Assess if flibe is stuck to the surface, or if it is easily peeled off. If not easily removable, cover with a rag and chip with a hammer or other object until it becomes dislodged. Use a heavy duty putty knife for this.
- Place large chunks of flibe in trash bag.
- Vigorously wipe the surface with a wet rag, repeating several times with a new rag each time. Perform until surface is visibly clean.
- Spray surface with Formula 409, or similar cleaner. Clean two more times.
- Wet swipe test and sample approximately 10X10 cm.
- Preserve swipe test.
- Double bag any trash produced and leave in the area until chemical safety pickup arrives.
- Analyze swipe tests. If below 3 micrograms/100cm² operation is complete.
- If greater than 3 micrograms/100cm² return and re-perform cleaning.

This procedure is similar to what would be required if there were the potential for airborne radioactive contamination from any source. The maintenance approach for Be or Be + radioactively contaminated equipment needs further study and elaboration. The reference Mk1 site has a hot-shop facility for decontamination and maintenance of such components. The maintenance at the reactor will be designed to limit areas that would be routinely contaminated by using enclosures, bagout processes, or bagless transfer operations derived from current practices at hot-cell facilities.

4.2.2 Building ventilation

The Mk1 PB-FHR reactor building ventilation system is zoned so that air flow through the building goes from areas of low beryllium and radioactive contamination to areas of higher contamination.

4.2.3 CTAH tube and manifold leaks

The novel beryllium safety issues for the Mk1 PB-FHR design arise from its direct heating of air for the NACC power conversion, which creates a potential pathway for tube or manifold leaks in a CTAH to release beryllium into the environment.

During GT operation, the maximum salt pressure in the CTAHs is under 3.0 bar, which is lower than the pressure of the air in the HP (18.8 bar) and LP (5.0 bar) CTAHs (Table 3-2). The air pressure exceeds the salt pressure both under power operation and under normal GT startup and shutdown, so any leakage would result in air ingress into the main salt loop, rather than salt ingress into the CTAH air. For startup, the CTAHs air ducts are isolated and air flow occurs through bypass valves. As with conventional GTs, the compressor is motored using the generator to spin it up to its normal operating speed of 3600 rpm and normal air mass flow rates and pressures. The bypass valves are left open, the CTAH air inlet isolation is opened to pressurize the CTAH, and the air outlet valve is then gradually opened, so that heated air flowing through the CTAHs mixes with bypass air to gradually increase the turbine inlet temperature and power. Under normal shutdown this process is reversed to ramp down the power conversion system power and normal shutdown cooling is then established using one or two of the CTAHs.

When a tube or manifold leak occurs during GT operation, the leak may be detected by a variety of methods, including reduction in reactor power (due to negative coolant void reactivity feedback), coolant level swell in the hot well, and coolant and cover gas chemistry change. In detailed design, a method to determine which CTAH has the leak will be developed.

The response to detection of a leak in a CTAH when the GT is operating is to open the air bypass valves, then to close the CTAH air-duct isolation outlet valve followed by the inlet valve. If the CTAH that is leaking is known, normal shutdown cooling is initiated with the other CTAH; otherwise, the DRACS is relied upon to remove decay heat. The CTAH with the tube leak is then drained, cooled, inspected, and repaired.

When an abrupt GT trip occurs, the air mass flow and pressure will drop rapidly. Under this event the air bypass valves are opened, the isolation valves closed, and normal shutdown cooling is established using one or both of the CTAHs. Reactor trips generate a turbine trip, which results in the same response of the isolation valve system. The main salt circulating pumps continue to operate, to prevent freezing of salt during the thermal transient. If this transient causes a tube failure or manifold leak, leak detection and isolation use the same methods for leaks occurring when the reactor is in normal shutdown cooling mode.

When the GT is not operating, as is the case under normal shutdown cooling, the CTAH air duct isolation valves are closed and the salt pressure exceeds the air pressure inside the CTAH. The CTAH tube bundles and manifold pipes have drip trays that collect salt that leaks. Leak detection occurs in the collection sumps using electrical conductivity probes. Also, the normal shutdown cooling air flow is monitored, along with other building exhaust flows, for radiation and beryllium, so any entrained salt is detected by this system.

The Mk1 design uses the CTAHs for normal shutdown cooling. Air mass flow rates for normal shutdown cooling are far smaller than under power operation, both due to the much lower reactor thermal power under shutdown conditions and due to the much larger increase that occurs in the air temperature. A functional requirement for detailed design of the CTAHs is to assure

that normally no salt will be entrained in the air flow if a salt leak occurs in a CTAH being used for normal shutdown cooling. If this functional requirement cannot be met, then an independent normal shutdown cooling system should be required.

4.2.4 Coolant activation and main salt pipe shielding

Neutron reactions with fluorine in the primary coolant salt produce O-19 (26.9 s half life) and N-16 (7.1 s half life), as has been observed in gas sampling during irradiation of FHR corrosion samples in the MIT research reactor [117]. Because the circulation time for the PB-FHR coolant salt, given by the ratio of the coolant salt volume to the volumetric flow rate, is approximately 80 s, a significant fraction of the decay reactions occur in the hot well, main salt piping, and CTAHs. For O-19, 50% of decays produce a 1.4 MeV gamma, while for N-16, 67% of decay reactions produce a 6.1 MeV gamma. However, the most important short-lived isotope is F-20 (11.0-s half life), formed by thermal neutron capture in F-19. For F-20, 100% of the decays result in a 1.633 MeV gamma ray, and 0.0082% of the decays produce a 3.333 MeV gamma.

The complete design of the shielding for external piping of the PB-FHR will need to consider gamma dose under power operation, where F-20 decay will dominate, and gamma dose after shutdown, when decay of flibe impurities, corrosion products, and fission products released from defective fuel particles will be most important. Corrosion products can be expected to precipitate preferentially into the cold traps, but may also precipitate in cold parts of the CTAHs. Many of the reactions that will form these activated species will involve fast neutrons (n-2n, n-p) where cross sections may not be well known.

4.3 Coolant Chemistry, Particulates, and Inventory Control

The Mk1 PB-FHR will use active control of the coolant chemistry to control and minimize corrosion of metallic and graphite structures by the main coolant salt. The primary concern for corrosion of metallic structures involves thermally-driven transport of chromium from hot to cold parts of the loop. Following recommendations provided in the 3rd FHR Workshop, the Mk1 design uses a single metallic structural material in contact with the salt. The baseline material used in the structural analysis is 316 SS, but the final selection between the candidate materials (316 SS, 304 SS, and Alloy N) will be made during detailed design. Graphite is also known to play an important role in corrosion, and the potential for graphite to act as a sink for chromium or other more reactive metals, by forming metal carbides on graphite surfaces, and to cause localized carburization of the metallic structures, must also be managed.

The specific methods used to control coolant chemistry, particulates and inventory will be decided during detailed design. However, the Mk1 main salt system design includes key capabilities—particulate filters; cold traps; droplet/gas spray contacting; drain and chemistry treatment tanks, corrosion sample holders, and salt-contacting component in-service inspection, repair, and replacement. Also, detailed design of the PB-FHR will include evaluation of potential benefits for chemistry control provided by the addition of 1 to 5 mole percent ZrF₄ to the main salt. This section reviews these topics.

4.3.1 Main salt cold traps and spray contacting

The Mk1 main salt system includes two cold traps, at the bottoms of the cold-leg stand pipes, which also serve as low-point drain locations for the two Mk1 main salt drain tanks. PB-FHR

coolant chemistry control is performed by contacting a side-stream of flibe salt with a solid redox control agent in these cold traps, as shown in Fig. 4-2. Three potential redox control agents are considered for use in the cold traps: (1) a mixture of zirconium carbide (ZrC) and graphite particles, (2) a mixture of cerium carbide (CeC_2) and graphite particles, and (3) a mixture of beryllium carbide (Be_2C) and graphite particles. These cartridges are designed to be readily removable and replaceable through the cold leg stand pipes. Besides providing a source of active metal to remove free fluorine produced by transmutation in the reactor core, it is expected that salt contaminants will precipitate in the cold traps and can be removed on a periodic basis when the redox control cartridges are replaced. As discussed below, because ZrO_2 has particularly low solubility in the main salt, if ZrF_4 is used as an additive in the salt the cold traps may also provide a sink for precipitation of oxygen contamination in the main salt.

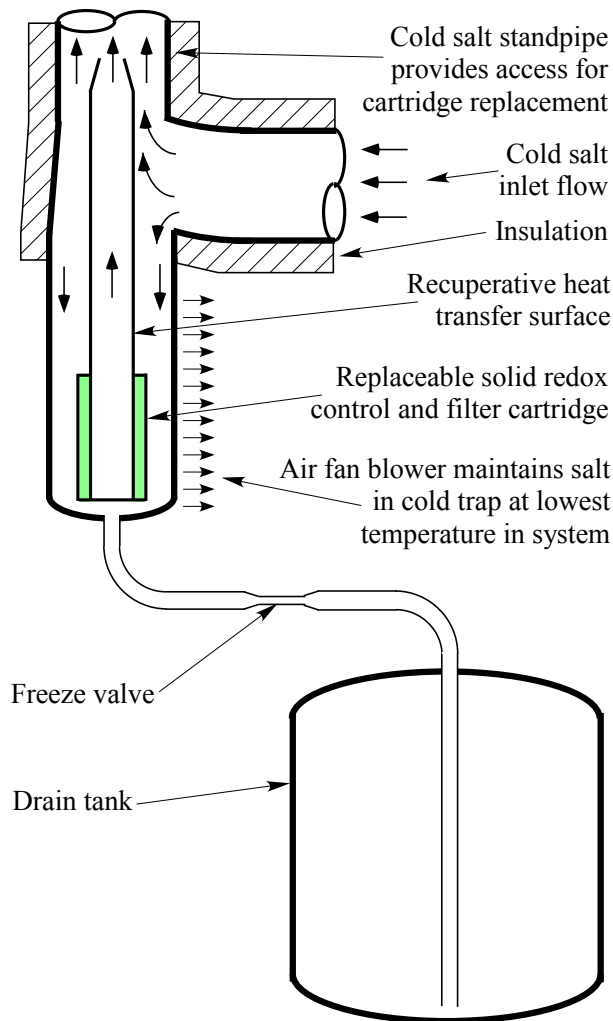


Figure 4-2. Schematic showing cold traps located at the bottom of each cold-leg stand pipe.

4.3.2 Main salt particulate filtering

Particulates can originate from a variety of sources, including dust formed by erosion of graphite surfaces due to pebble motion, crushed pebbles, and releases of graphite and other

particles from chemistry control and tritium capture cartridges, and precipitation of corrosion products. Likewise, particulates may be introduced as foreign material during manufacturing, installation, and maintenance of equipment. Small graphite dust particulate is expected to accumulate at the salt free surfaces, particularly around the defueling machine and the hot well, where it can be skimmed. The defueling machines are designed to recover and remove broken pebble fragments. Other particulates are expected to be filtered primarily by the tritium removal cartridges in the CTAH vertical manifold pipes, and in the redox control cartridges of the cold traps. Finally, when the center reflector is replaced, inspection will be performed of the bottom of the reactor vessel for foreign materials.

4.3.3 Main salt inventory control, drain tanks, and batch cleanup

The drain tanks are lined with either nickel or copper, with the intention that it be possible to chemically treat salt in the drain tanks to increase purity (for example by sparging with HF and H₂). Copper-lined tanks were developed and used in the MSBR program to process carrier salt [118]. A nickel vessel, contained inside a stainless steel vessel, has been used at UW Madison for processing flibe. The UW vessel uses 0.625-cm-thick rolled nickel, supported inside a bed of high-temperature insulation inside the stainless steel vessel. Key issues identified by UW [119] for designing a lined drain tank include accommodating the differential thermal expansion of the tank and the liner, preventing oxygen from contacting the liner when in use (particularly copper), and designing the tank to accept the pressure differential needed to use gas pressure to transfer salt through a dip tube into the main salt loops. If these design constraints cannot be met in the detailed drain tank design, then a separate tank would be provided to perform batch salt purification.

The drain tanks are used for long-term salt additions and removal. During defueling, salt drained from one of the main salt loops may be transferred into the reactor vessel to maintain inventory. The drain tanks are designed to have the capability to transfer salt to either the bottom of the cold leg where the salt is drained, or to the main salt cold leg, for transfer through the cold leg directly into the reactor vessel. As is conventional with molten salts, transfers from the drain tank are performed by pressurizing the drain tank with cover gas, which forces salt into a dip tube to perform the transfer.

Transfer of the salt to a separate batch cleanup system will be required to remove CsF and other stable-fluoride fission products that may be released from defective fuel particles. This can be accomplished using reductive extraction to bismuth-lithium alloy [120, 121, 122]. Because inadvertent addition of bismuth to the primary system would cause severe corrosive damage, in the Mk1 design this process would be performed off-line with salt removed from the drain tanks.

Short-term coolant inventory control is performed primarily by the hot well, which can accommodate coolant volume changes due to temperature changes, as well as volume changes due to level swell at other free surfaces in the loop as pump speeds are changed. The drain tank system is designed to allow salt to be added and removed from the loop, when larger adjustments in salt inventory are needed.

4.3.4 Option of adding ZrF₄ to coolant salt

There may be benefits to adding 1 to 5% ZrF₄ as an additive to flibe for FHR applications. The MSRE fuel salt used a “carrier” salt composition of LiF-BeF₂-ZrF₄ (66-29-5 mole %) as a

solvent for UF_4 [123]. When frozen in a container, the surface of an ingot of carrier salt [124] shows a nearly flat surface, indicating that the volume change upon freezing is small.

ZrF_4 was added to the MSRE fuel salt due to its very high affinity for oxygen and very low solubility of ZrO_2 in flibe. Early work at ORNL [125] had measured the stability and solubility of different oxides in fluoride salt mixtures, and found that zirconium, uranium and hafnium precipitate as dioxides (e.g., ZrO_2) and have very low solubility in the salts, below the detection limits of the radiochemical methods used to measure their concentration, while BeO is slightly more soluble, and oxides of barium, strontium, calcium, potassium, sodium and lithium have the highest solubilities. At the time the solubility of oxides were being studied for their potential use for chemical separations, but shortly afterwards it was discovered that precipitation of UO_2 occurs easily from $\text{LiF-BeF}_2\text{-UF}_4$ salts contacted with graphite (which can be a source of oxygen), while similar precipitation does not occur for NaF-ZrF_4 solvents.

Because it was known that ZrO_2 is more stable than UO_2 in fluoride salts, the study of using ZrF_4 as an additive to flibe to prevent precipitation of UO_2 was initiated [126]. These studies confirmed that adding 5 mole percent ZrF_4 into flibe, for 1 mole percent UF_4 , was effective in preventing precipitation of UO_2 , and instead precipitation of solid ZrO_2 was observed when the salt was contacted with graphite containing residual oxygen [127]. This work also studied whether different fluoride salts might be used as cleaning agents to remove oxygen contamination from graphite; $\text{LiF-BeF}_2\text{-UF}_4$ and $\text{LiF-BeF}_2\text{-ThF}_4\text{-UF}_4$ were found to be ineffective, while the zirconium-bearing salt $\text{NaF-ZrF}_4\text{-UF}_4$ (50-46-4 mole %) was found to be the most effective purging salt.

Also, zirconium may be effective in preventing the formation of chromium carbides on graphite surfaces, as is observed in some corrosion experiments. Zirconium carbide has been noted to have substantially greater stability than chromium carbide [128]. Zirconium metal was used, along with hydrogen purge, to adjust the fluorine potential of the MSRE carrier salt after it had been fluorinated to remove uranium, prior to adding $^{233}\text{UF}_4$. In this treatment, corrosion products that precipitated due to the reduction by zirconium metal were filtered from the salt [129]. However, in systems with graphite the addition of zirconium metal has been observed to cause damage to the graphite due to the formation of zirconium carbides [130]. This suggests that ZrC may act as an appropriate redox control agent, but demonstration in corrosion experiments remains to be performed.

The density of the MSRE carrier salt ($\text{LiF-BeF}_2\text{-ZrF}_4$, 64.7-30.1-5.2 mole %) was measured, and can be predicted from the formula ρ (kg/m^3) = $2538.7 - 0.5769 T$ ($^\circ\text{C}$) [131]. Estimates for other properties of the MSRE fuel salt ($\text{LiF-BeF}_2\text{-ZrF}_4\text{-UF}_4$, 65-29.1-5-0.9 %) at 600°C were also developed by Cantor [132], as being $c_p = 1.97$ $\text{kJ/kg}^\circ\text{C}$ (0.47 $\text{cal/g}^\circ\text{C}$), viscosity 9×10^{-3} Pa-s (9 cP), and thermal conductivity 1.4 $\text{W/m}^\circ\text{C}$. This predicted thermal conductivity is 40% higher than that of pure flibe, which if correct could result in notable improvement to heat transfer.

Cantor assessed the vapor pressure of carrier salt to be “negligible,” even with the relatively high volatility of ZrF_4 , and the freezing temperature to be 434°C . From the Cantor (1973) measurements, the density at 600°C is 2193 kg/m^3 . Then the kinematic viscosity is $\nu = (9 \times 10^{-3} \text{ Pa-s}) / (2193 \text{ kg/m}^3) = 4.1 \times 10^{-6}$ m^2/s , and $\rho c_p = 4320$ $\text{kJ/m}^3^\circ\text{C}$.

Further study is warranted to measure key properties and assess the potential use of ZrF_4 as a constituent in the PB-FHR main salt, and the optimal concentration for this application.

4.4 Structural Materials Degradation and In-Service Inspection

This section discusses degradation issues for the candidate Mk1 metallic structural materials, and the in-service monitoring that would be applied to monitor this degradation.

4.4.1 Mk1 structural materials in-service inspection

PB-FHR metallic and graphite structures will experience significant material property changes during their lifetime. Predicting these property changes due to thermal aging, neutron irradiation, creep, and corrosion accurately in advance is challenging. While FHR structures will be designed to have conservatively low stresses and will be evaluated using 3-D finite element modeling, as reviewed in the 2nd FHR Workshop [133], the uncertainties in long-term property changes are large enough that it will be necessary to design the PB-FHR to hold materials samples in several locations where the samples will be exposed to the same environmental conditions as the PB-FHR metallic structures. Candidate metallic sample geometries include tensile test specimens, Charpy V-notch specimens, and gas-pressurized tube creep specimens. These specimens will also serve the dual purpose of monitoring local corrosion rates.

The Mk1 design provides sample coupons in several locations, including the reactor core barrel and center reflector, the CTAH hot and cold manifold pipes, and the DRACS TCHX tube sheet manifold pipes. The low-pressure operation of FHRs makes it practical to locate most of these samples in stand pipes where access to recover samples is relatively easy. The sample holders will be similar in design to those in the MSRE, which used perforated baskets to hold and irradiate samples of Alloy N and graphite [134]. The MSRE samples included tensile test samples taken from the heat used to fabricate the cylindrical portion of the reactor vessel, and additional samples from the heat used to fabricate the top and bottom heads. The MSRE samples were removed after 22,500 hours at 650°C and exposed to a thermal fluence of 1.5×10^{21} neutrons/cm². As shown in Fig. 4-3, the reduction in fracture strain compared to unirradiated samples, a measure of the loss of ductility, is significantly larger in the high-temperature strain tests.

The center reflector in the Mk1 PB-FHR will experience substantial neutron-irradiation-induced damage, sufficient to require its replacement periodically. Neutron irradiation causes dimensional changes that induce stresses. The 2014 NE 170 senior design class studied how the geometry of the center reflector can be optimized to reduce these stresses [135]. Extensive experience also exists with inspection of graphite structures in CO₂-cooled AGRs in the United Kingdom. The inspection methods used there for the coolant channels in graphite structures include: (1) the use of specialized cameras to inspect channels for degradation and other issues affecting their structural integrity such as defects; (2) the use of feeler gages and other types of probes to measure the ovality of channels in the graphite, as well as the diameter of the channels; and (3) the removal of small graphite samples for analysis [136].

The uncertainty associated with FHR materials aging must ultimately be managed by having limits on acceptable materials properties and conditions established during detailed design, and through the materials surveillance program verify that PB-FHR materials remain within their

licensed limits. Because materials may age or corrode more rapidly than originally predicted, for investment protection all major salt-contacting components in the Mk1 PB-FHR are designed to be replaceable, including the reactor vessel.

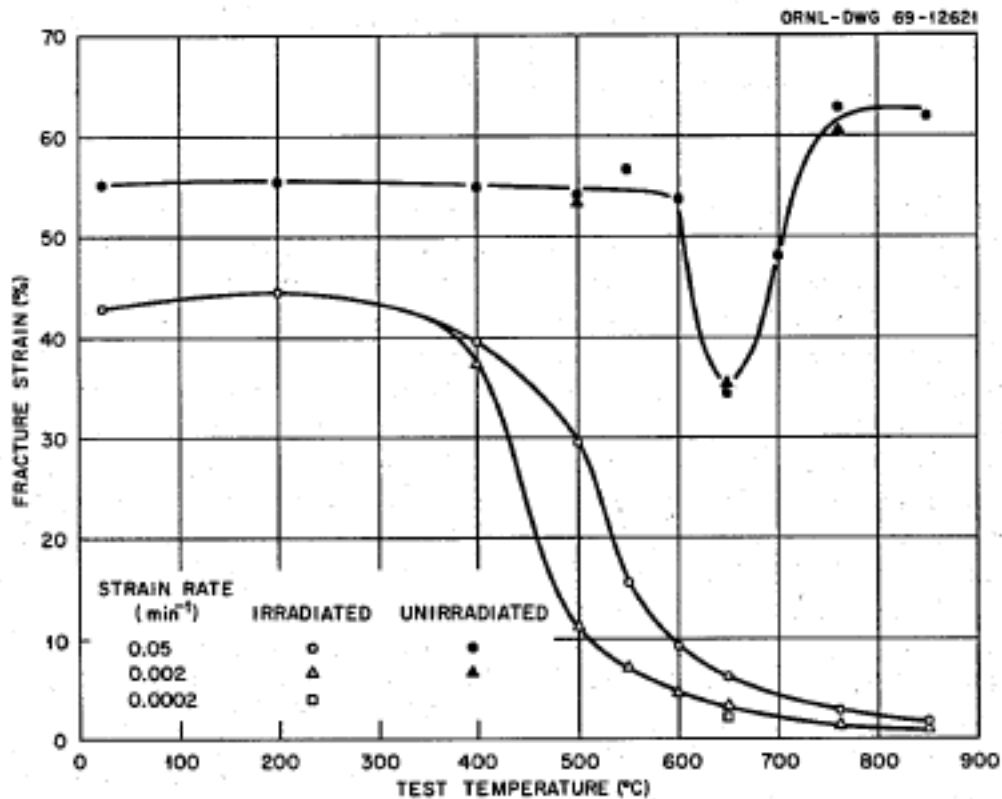


Figure 4-3. Variation of the fracture strain with test temperature for Alloy N surveillance samples removed from the core of the MSRE after 22,533 hr at 650°C and exposure to a thermal fluence of 1.5×10^{21} neutrons/cm² (from ORNL-4449, pg. 168).

4.4.2 Mk1 structural material corrosion

While the specific metallic structural material used in the PB-FHR will be selected during detailed design, the use of 316 or 304 SS is of significant interest due to the large base of experience that exists with these materials, including in non-nuclear applications at PB-FHR-relevant temperatures, and their relatively low costs compared to Alloy N.

During the MSBR program, in addition to operating a number of natural circulation loops to study corrosion of Alloy N, ORNL also operated a 304 SS and a 316 SS loop [137]. The 304 loop operated with a LiF-BeF₂-ZrF₄-UF₄-ThF₄ (70-23-5-1-1) salt mixture for 80,000 hr (9.1 yr). ORNL referred to flibe with ZrF₄ addition as “carrier salt”. Figure 4-4 shows this loop, as well as 304 SS test coupons exposed for 5700 hr (0.65 yr) and 49,700 hr (5.7 yr) in the salt. For 304

SS coupons exposed for 49,000 hr (5.6 yr), the maximum weight loss for the coupons corresponded to a uniform corrosion rate of 22 $\mu\text{m}/\text{yr}$ (0.86 mil/yr).

Of significant interest, after 62,400 hr of operation, the thermocouple and heater systems in the 304 SS loop began to experience increasingly frequent failures. The report states that “the loop was successfully thawed and loop operation continued” (ORNL-4286, pg. 33). The lack of damage to the loop can be attributed, at least in part, to the fact that this carrier salt composition exhibits a very small volume change upon freezing [138]. This suggests that the use of ZrF_4 as an additive to flibe merits exploration, including its effects on freezing volume change.

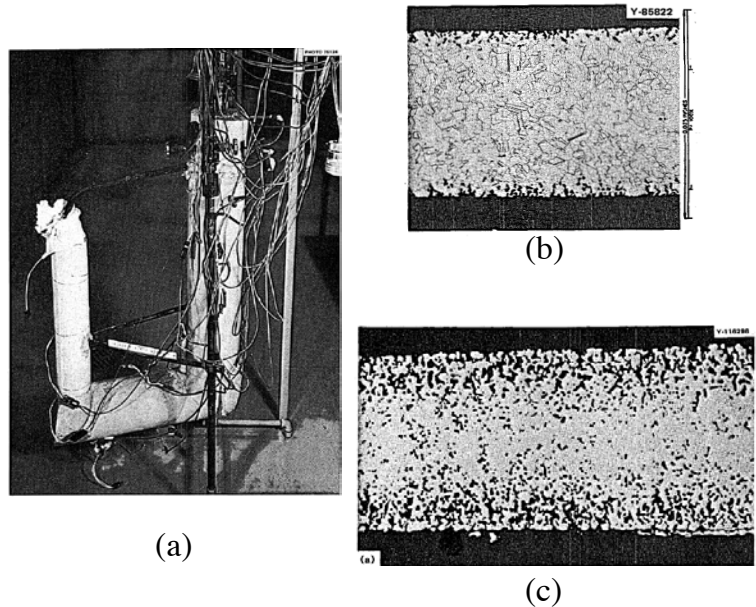


Figure 4-4. Photos of (a) natural circulation $\text{LiF}\text{-BeF}_2\text{-ZrF}_4\text{-UF}_4\text{-ThF}_4$ corrosion test loop fabricated from 304 SS that operated for 80,000 hr, cross sections of 0.64-mm-thick 304 SS coupons exposed at the maximum loop temperature of 688°C for (b) 5700 hr and (c) 45,724 hr (ORNL-4286, pg. 29-32).

The 316 SS loop described in ORNL-4286 was operated for 4491 hr with $\text{LiF}\text{-BeF}_2\text{-ZrF}_4\text{-UF}_4\text{-ThF}_4$. After 2842 hr (0.32 yr) of operation, the coupon at the hottest part of the loop (650°C) experienced a weight loss of 24 $\mu\text{m}/\text{yr}$ (0.96 mil/yr). In the next 645-hr period, the weight loss rate dropped to 21 $\mu\text{m}/\text{yr}$ (0.83 mil/yr), but then in the final 811-hr period increased to somewhat over 25 $\mu\text{m}/\text{yr}$ (>1 mil/yr). This is comparable to or slightly greater than the mass loss rate observed for 304 SS.

A key question for FHRs is whether further reduction in corrosion rate is possible for flibe, without UF_4 , when active redox control is used. Experiments described by Keiser et al. [139] demonstrated that corrosion rates for 316 SS can be reduced to very low levels if flibe is contacted with beryllium metal to maintain a low fluorine potential. However, reactive metals like beryllium and zirconium cannot be used in excess in the PB-FHR, due to their capability to cause damage to graphite structures by generating carbides. The baseline Mk1 corrosion control system, described in Section 4.3 (“Coolant Chemistry, Particulates and Inventory Control”), uses solid redox control agents (mixtures of graphite and zirconium, beryllium or cerium carbides)

located in cold traps to control redox potential. In addition, the Mk1 design provides the capability for gas-phase chemistry control by contacting a spray flow in the main salt hot well with gas containing hydrogen.

4.4.3 Mk1 structural material thermal aging

A very large base of experience exists with austenitic stainless steels, particularly 304 SS, in the service temperature range of 565°C to 750°C in refinery applications, particularly equipment used in fluid catalytic cracking units (FCCUs). This experience is summarized in an excellent draft report written by the American Petroleum Institute (API) Subcommittee on Corrosion and Materials [140]. The major issues summarized in the report, that must be considered in the design of structural components that operate in the 600°C to 700°C service temperature range of FHRs, include sigma-phase embrittlement, stress relaxation cracking, and carburization. Sigma phase formation would not be expected to occur in Alloy N, but other aging mechanisms must still be considered. While the service in these refinery applications generally involves more frequent and severe thermal transients than occur in FHRs, this extensive experience base is valuable in assessing issues for the structural design of FHR metallic components using 304 or 316 SS.

Sigma phase formation occurs in high-temperature applications of austenitic alloys, where over time a hard, brittle, non-magnetic intermetallic compound of iron and chromium forms. Sigma forms most easily in ferrite phases, particularly in welds, but can also form in austenite over sufficiently long time periods. Higher sigma phase concentrations are found in areas that have been cold-worked.

Hau and Seijas [141] provide a detailed review of experience with sigma-phase formation and embrittlement in austenitic stainless steel. They note that the formation of sigma phase slows with time, stating that

“In general, in several examinations that have been performed in different refineries, there has been no clear tendency of increasing sigma phase formation measured in subsequent turnarounds. Measurements have been repeated with a frequency of 2 to 6 years and the amount of sigma phase appeared unchanged.” (pg. 5)

“Although undoubtedly more data would be required to draw valid conclusions, the indication is that precipitation of sigma phase becomes so slow after some time that it appears as if an equilibrium amount of sigma phase is reached in a few years of service” (pg. 9)

These observations are consistent with data reported by Minami et al. [142], showing that the rate of formation of sigma phase is lowest for 304 SS, as shown in Fig. 4-5.

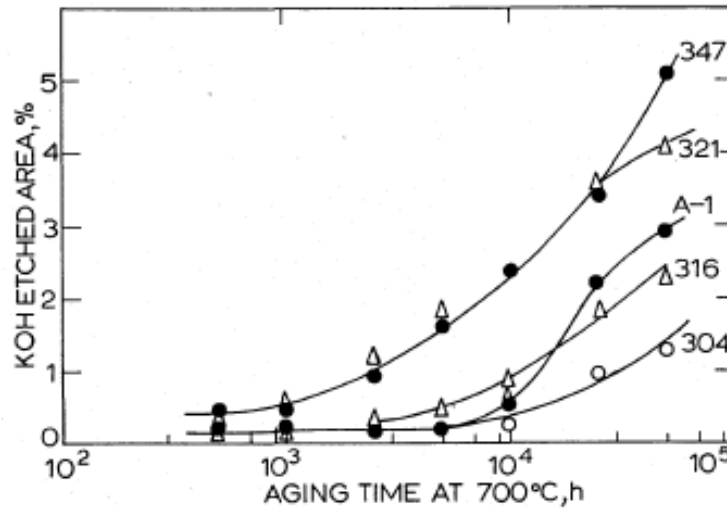


Figure 4-5. Rate of formation of sigma phase [143].

Tests to assess the effects of sigma-phase formation on ductility include Charpy V-notch tests and tensile strain tests. Generally, the loss of ductility due to sigma-phase formation is larger at low temperatures than at service temperatures. Thus cracking caused by sigma phase is most commonly observed when components are cooled down for maintenance, which as the components approach room temperature results in reduced ductility under conditions of higher stress due to transient cooling. For this reason, detailed design analysis will be required to assess stresses during cooldown of CTAHs for maintenance and to establish allowable cooling rates. It also requires assuring that excessive cooldown is not possible during power operation, where the 418°C nominal CTAH air inlet temperature is helpful in limiting the potential for overcooling that could occur more readily in a heat exchanger cooled by room-temperature air (as was experienced in the MSRE radiator as described in Section 3.5.1).

The formation of sigma phase can also make austenitic alloys unweldable. The normal solution in maintenance involves high-temperature, localized annealing in the area where the weld will be performed. Such annealing may be required when CTAH tube bundles are replaced and new welds must be made in the cross-over legs.

Carburization can occur, normally at low rates, in regenerators used to burn coke from FCCU components. It is not clear whether similar issues may exist for FHRs, but studies of coupled metal and graphite samples under prototypical salt chemical conditions are warranted. Direct contact of metal structures with graphite will only occur for reactor internals, such as the core barrel, and not for the pressure boundary structures, but assessment for whether carburization could occur over longer time periods for pressure boundary structures is also warranted.

Long-term creep cracking is sometimes observed in FCCU regenerator internal support structures. Sigma-phase formation, especially in welds, can reduce creep life. When observed stress relaxation cracking can be associated with fabrication heat treatments or short-term thermal in-service failures due to low creep ductility, but is uncommon in FCCU applications. It is reported in the API study to be particularly unlikely with type 304H SS.

4.4.4 Mk1 structural material long-term creep

The principal strategy for managing long-term creep effects in the Mk1 design is to design high-temperature structures to operate at stress levels well below the ASME allowable values (Table 1-5). However, creep effects remain important and must be considered during detailed design.

4.5 Cover Gas Chemistry, Particulates, Salt Carry-Over, and Inventory Control

The Mk1 PB-FHR uses argon as its cover gas for all locations where gas contacts salt or fuel. Argon has the benefit of being relatively inexpensive. It has lower thermal conductivity than helium, and thus is more effective in insulating salt surfaces to reduce heat loss. However, when pebbles are removed from the PB-FHR in canisters, the lower thermal conductivity of argon, compared to helium, may be an issue. The selection of the blanket gas for fuel transfers requires more study, and will be considered during detailed design of the fuel handling system.

4.6 Pebble Handling and Storage System

The Mk1 PB-FHR includes a notional system design for the Pebble Handling and Storage System (PHSS) that will function to ensure the sustained fission reaction in the core through the addition and removal of fuel and graphite pebbles. While the Mk1 PB-FHR design includes detailed designs for the pebble injection channels at the bottom of the annular core and the defueling slot above the core, the design effort did not develop detailed designs for other key pebble handling equipment in the PHSS. The description of the PHSS nominal system parameters, operating modes, and functional requirements are described in the section that follows. Space has been allocated in the upper core internals and in the reactor building for key PHSS subsystems and components including the core unloading devices, pebble burnup measurement system, and pebble canister transfer system, but detailed design has been deferred to the Mark-2 PB-FHR.

4.6.1 Pebble Handling and Storage System Functions and Description

This section includes the key functional requirements for the Pebble Handling and Storage System, the system operating parameters, and descriptions of some of the key subsystems and components that merit attention in future PB-FHR development.

The PHSS in the Mk1 PB-FHR in many ways achieves the same set of functions as the fuel handling systems in pebble bed HTGR [144]. Therefore the system shares many of the basic functional requirements. Some of the key functional requirements for the PHSS are:

- Sustain the fission reaction in the core through the addition of fresh fuel pebbles and the removal of spent fuel pebbles above a maximum burn-up threshold.
- Circulate pebbles through the core by inserting them at the bottom through pebble injection channels and removing them at the top of the defueling chute.
- Ensure that the pebble bed core remains fully packed under normal operation.

- Perform initial pebble loading to safely approach criticality from an under-moderated core configuration.
- Monitor and track pebble inventories.
- Ensure sub-critical margins are maintained for all locations where fuel pebbles are present outside of the core.
- Manage damaged pebbles and pebble fragments so that they do not inhibit the operation of the reactor.
- Manage pebble surface contamination with gas, moisture and/or salt.
- Facilitate remote operation and maintenance and ensure acceptable doses to plant staff.
- Provide redundancy so that subsystem failures can be addressed during scheduled plant outages.
- Minimize pebble wear and graphite dust generation.

Table 4-1 gives the key preliminary system parameters for the Mk1 PB-FHR PHSS that can be used as the basis for system operating requirements in the detailed design. Under normal power operation, the core contains 440,000 active fuel pebbles and 204,000 inert graphite pebbles located in a radially-zoned outer pebble reflector. The graphite pebbles shield the outer radial reflector from fast neutrons, reducing damage rates so that the reflector blocks can survive for the life of the plant. Fuel pebbles pass through the core approximately eight times with an average total residence time of 1.40 years at full power operation. The average residence time for a fuel pebble on each pass is 60 days in the active core followed by four days of cooling time in the defueling chute. These values are based on the relative volumes of these regions of the core. The pebble consumption rate for the Mk1 PB-FHR is 920 pebbles / full power day (FPD).

The pebble circulation rate for the PHSS at full power operation is 450 pebbles per hour (8 seconds per pebble). Pebble injection into the core is achieved through eight pebble injection channels: four for the active fuel pebble region and four for the inert graphite pebble outer reflector region. Two Core Unloading Devices (CUDs) remove pebbles from the top of the defueling chute operating under normal conditions. In preparation for defueled maintenance operations, the PHSS for the Mk1 PB-FHR will perform a faster core unloading process at the nominal rate of 3,600 pebbles per hour (1 second per pebble). At this unloading rate, the core can be defueled in eight days.

Table 4-1. Operating Parameters for Pebble Handling and Storage System.

Parameter	Value	Unit
Total Pebbles in Core and Defueling Chute	688,000	Pebbles
Total Pebbles in Core	644,000	Pebbles
Core Sphere Composition	68.3%	Fuel
	31.7%	Graphite
Fuel Spheres in Active Core Region	440,000	Pebbles
Graphite Spheres in Active Core Region	204,000	Pebbles
Fuel Pebble Residence Time (Nominal)	1.40	Years
Number of Passes Through Core (Nominal)	8	--
Active Core Residence Time (Nominal)	60	Days
Defueling Chute Residence Time (Nominal)	4	Days
Fuel Pebble Consumption (Full Power)	920	Pebbles/FPD
Pebble Circulation Rate (Normal)	10,800	Pebbles/Day
	450	Pebbles/Hour
	0.125	Hz
Fuel Pebble Injection Channels	4	--
Graphite Pebble Injection Channels	4	--
Core Unloading Devices	2	--
Pebble Circulation Rate (Max)	3,600	Pebbles/Hour
Time to Unload Full Core	8	Days

4.6.1.1 Pebble Canister Transfer System

The Mk1 PHSS includes a notional design for a Pebble Canister Transfer System (PCTS) that allows for batch handling of pebbles transferred into and out of the primary coolant. The design concept includes multiple transfer canisters in each Mk1 PB-FHR unit that can be used to add and remove pebbles from recirculation in the primary coolant. The type of pebble being transferred depends on the operating mode of the reactor and is described later in Section 4.6.2. Figure 4-6 shows the simplified process flow schematic for the pebble canister transfer concept implemented in the Mk1 PB-FHR and includes one complete train for pebble recirculation and transfer. Significant redundancy is desirable in the PHSS due to its continuous operation and the desire to avoid the need for unplanned outages to repair subsystems or components due to any failures. Therefore a second train is included in this early conceptualization of the PHSS. Table 4-2 gives the preliminary specifications for the PCTS in the Mk1 PB-FHR.

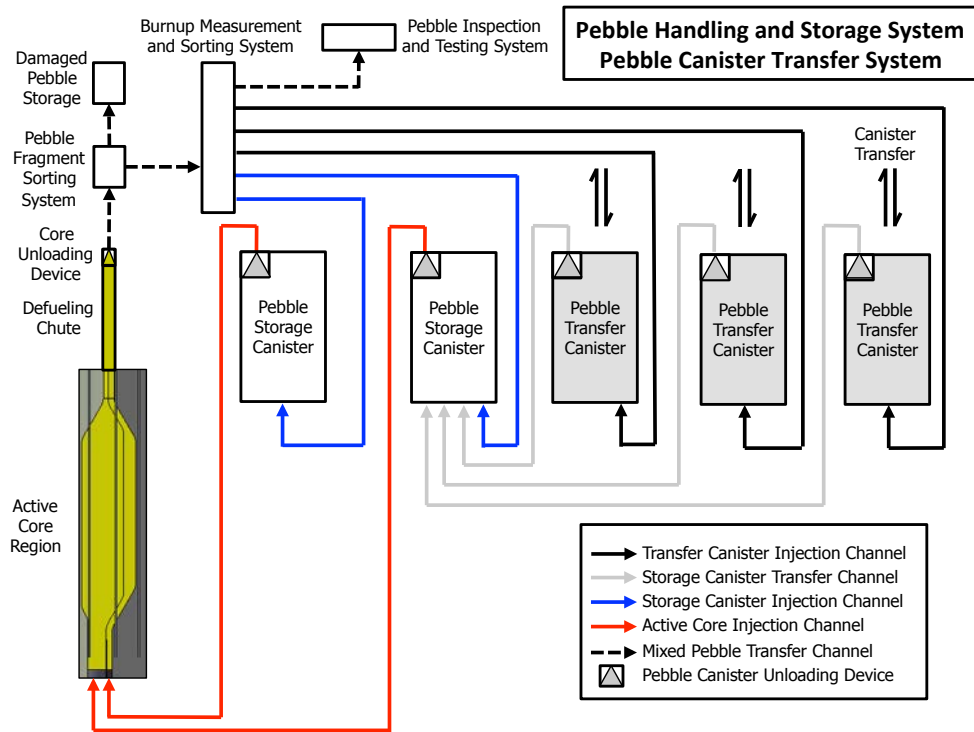


Figure 4-6. Simplified material schematic for the Pebble Canister Transfer System.

Table 4-2. Characteristics of the Pebble Canister Transfer System

Parameter	Value	Unit
Active Fuel Pebble Storage Canisters	2	--
Graphite Pebble Storage Canisters	2	--
Fresh Fuel Transfer Canisters	2	--
Spent Fuel Transfer Canisters	4	--
Spent Fuel Burnup	180	MWd/kgHM
Transfer Canister Capacity (Nominal)	29,440	Pebbles
	32	FPD
Spent Fuel Canister Heat Load (Normal)	25	kW
Spent Fuel Canister Heat Load (Max)	41	kW
Transfer Canister Volume	0.7	m ³
Transfer Canister Height	1.75	m
Transfer Canister Area	0.40	m ²
Square Transfer Canister Side	0.63	m
Round Transfer Canister Diameter	0.71	m

The primary motivation to use batch handling is that it allows for a centralized pebble handling facility on a multi-unit site that serves to distribute fresh fuel canisters to multiple units and can receive used fuel canisters from each unit. The centralized pebble handling reduces the long-term pebble storage requirements in each Mk1 PB-FHR unit reactor building before used fuel can be transferred to passive dry cask storage in the protected area.

The PCTS should also simplify the implementation of pebble accounting and IAEA safeguards monitoring in the Mk1 PB-FHR because it will reduce the number of locations where small numbers of pebbles can be diverted from the normal material flow. Monitoring requirements for material flow in the Mk1 PB-FHR will primarily track used fuel pebble canisters that are transferred from each unit on the site to the central fuel handling facility. Smaller material streams will exist in each unit for damaged pebbles and the Pebble Inspection and Testing System (PITS) that will also require IAEA safeguards monitoring for material diversion.

In the material flow schematic for the PCTS, Fig. 4-6, mixed pebbles exit the core before pebble of different types are dispersed by the Burnup Measurement and Sorting (BUMS) System to the pebble storage and transfer canisters. The pebble canisters are located in a hot pebble-handling chamber adjacent to the reactor cavity. This chamber is located within the reactor containment and should be insulated to minimize heat loss and to maintain the primary coolant above the freezing temperature limit.

Two types of pebble canisters are included in the pebble-handling chamber: fixed pebble storage canisters that circulate fuel into the reactor core and transfer canisters that can be exchanged under power operation. The fixed pebble storage canisters ensure that the geometry of the pebble injection lines to the core remains intact at all times while transfer canisters are exchanged and is not vulnerable to misalignments or operator errors in the canister insertion process.

The pebble transfer canisters are exchanged by vertical motion into a gas-lock system. The gas-lock system is located above the pebble-handling chamber and allow for the transfer of canisters into and out of the primary coolant in an inert gas to minimize the potential contamination of the salt. Canisters can be transferred to and from the gas-lock from an air atmosphere either internal or external to the reactor building. Additional consideration will need to be taken in the detailed design effort to ensure that a robust containment boundary is maintained as canisters are transferred to and from the gas-lock.

Under normal operation, fresh fuel canisters are transferred into the PHSS to maintain an adequate inventory of fissile material in the core while spent fuel canisters are removed and transferred to the centralized fuel handling facility on the reactor site. Fresh fuel will need to have acceptable levels of surface impurities and it may prove beneficial for these canisters to be sealed in the central pebble handling facility and opened by remote operation within the pebble handling chamber. Upon removal from the primary coolant, the spent fuel will require cleaning to remove residual salt and cooling to maintain acceptable fuel temperatures in the gas environment. Future design effort and analysis will be required to ensure that these functions can be adequately performed.

The nominal dimensions for the transfer canisters in Table 4-2 are based on the competing motivations to reduce both the frequency of pebble canister transfers and the decay heat removal requirements for cooling the transfer canisters in a gas environment. The frequency of pebble canister transfers is based on the pebble consumption rate of 920 pebbles per full power day and decreases with larger canister volumes. The cooling requirements for the spent fuel canisters can be decreased by a combination of smaller canister volumes with fewer pebbles or with a greater number of canisters that allows for some decay time in the primary coolant salt before the canister is removed. Figure 4-7 shows the decay heat removal requirements for transfer frequencies of 16, 32, and 64 days with one to four canisters. The preliminary design specifications for the Mk1 PB-FHR are four transfer canisters with total capacity of 29,440 pebbles and transfer frequency of 32 full power days that has a decay heat load of 25 kW per canister under normal operation. However, the peak canister decay heat load will occur during the relatively fast core unloading required for defueled maintenance outages, which is described in Section 4.6.2. Without the additional month of decay time, the peak decay heat load for the transfer canister increases to 41 kW in this defueling operation. Future design efforts should confirm that adequate cooling could be supplied to fuel pebbles in both canister transfer scenarios. Alternative design options, such as pebble storage in primary salt, could be desirable for the core unloading in place of the canister transfers.

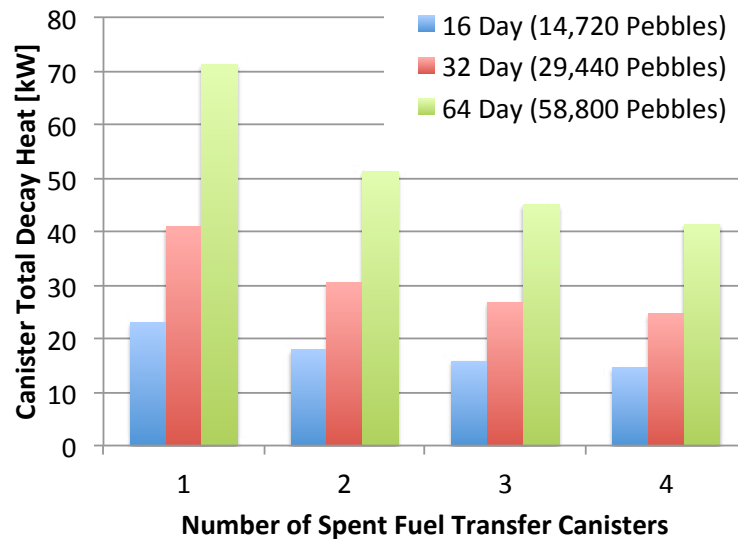


Figure 4-7. Transfer canister decay heat load for transfer frequencies of 16, 32, and 64 days and the increase in decay time associated with one to four canisters.

4.6.1.2 Core and Pebble Canister Unloading Devices

The PHSS includes two Core Unloading Devices (CUDs) and ten Pebble Canister Unloading Devices (PCUDs) that function to transfer pebbles from large diameter volumes containing packed beds to small diameter piping that is used to hydraulically transfer pebbles in the Mk1 PB-FHR. The relatively large number of unloading devices in the Mk1 PB-FHR, compared to HTGRs, will require a highly reliable design as well as integrated redundancy so that reactor operation can continue if one or more devices become inoperable. While the detailed design of

the CUDs and PCUDs remains a gap for future PB-FHR development efforts, some relevant design considerations are reviewed here to provide a basis for this work.

The primary functional requirement, stated above, of the CUDs and PCUDs is to extract pebbles from large diameter volumes to small diameter piping. This function requires the agitation of a small region of the packed bed with minimal pebble loading in order to prevent jamming that would inhibit this requirement. Previous HTGR experience suggests there are two strategies to agitate the bed and perform this function. The first method is to use mechanical agitation through some kind of repetitive rotational motion, such as a screw, which was employed in THTR [145]. The second method is to use pneumatic or hydraulic jets to agitate pebbles near the small diameter orifice, which was employed in HTR-10 [146]. Figure 4-8 shows the schematic diagrams for the CUDs in THTR (left) and HTR-10 (right). The comparison of these two designs shows the significant increase in complexity associated with the mechanical agitation approach and the relative simplicity of the fluid-based strategy. The Mk1 PB-FHR operates at low pressure and will not be able to use high pressure salt jets, but the high density of the primary coolant in the Mk1 PB-FHR allows for larger pebble drag forces with relatively less coolant flow than with helium. The use of simple hydraulic agitation in the CUD could also allow for redundancy in each device with two pebble extraction channels. Future design studies should be performed to adapt the unloading strategy in the HTR-10 for the PB-FHR concept.

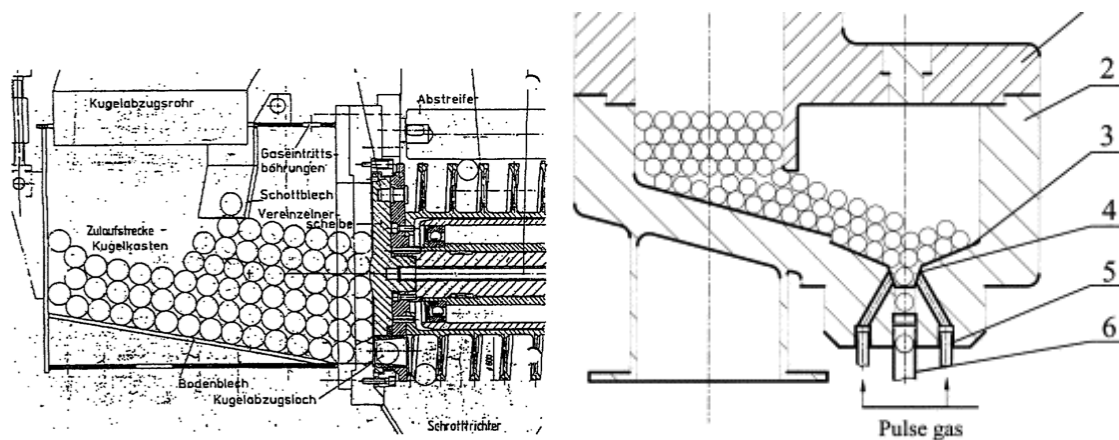


Figure 4-8. Defueling devices used in THTR (left) and HTR-10 (right), as reproduced in [147] and [148], respectively. The THTR design includes a mechanical screw that agitates the bed and sorts broken pebble fragments. The HTR-10 design uses alternating pulse gas to dislodge pebbles near the small diameter orifice.

4.6.1.3 Pebble Burnup Measurement and Sorting System

A recent IAEA coordinated research program developed a comprehensive review of methods that have been developed and used to measure pebble burn up in earlier PBMRs [149]. The PB-FHR pebble burnup measurement system (BUMS) uses the most successful method developed during these earlier efforts, which involves using a high-purity germanium detector to perform gamma spectroscopy to measure the ^{137}Cs inventory in each pebble. Because the fission yields for ^{137}Cs for ^{235}U (6.3%) and ^{239}Pu (6.5%) are very nearly equal, and because it has a 30-year half life, ^{137}Cs undergoes very little decay during the pebble lifetime; and because it has a negligibly

small cross section for thermal neutron capture, the inventory of ^{137}Cs provides an excellent basis to assess the relative burnup of pebbles.

A key issue for the design of the BUMS is to have a sufficiently long time period for the short-lived isotopes with gamma peaks neighboring the 661.6 keV ^{137}Cs peak (^{97}Np , ^{143}Ce , ^{132}I) to decay sufficiently. In addition, Compton scattering of high-energy 1-2.5 MeV gammas from other short-lived fission products creates an additional, broad Compton background which determines the measurement accuracy of the ^{137}Cs peak.

As described in the IAEA review, the 200-MW High-Temperature Reactor (HTR) Module reactor burnup measurement system used a 55-hr decay time and measured pebbles at a rate of one every 10 sec. The higher power density of the PB-FHR core will imply a higher inventory of short-lived fission products than existed in the HTR Module pebbles, however, current high-purity germanium detectors have better capability to resolve ^{137}Cs gammas from ^{97}Np , ^{143}Ce and ^{132}I gammas.

The HTR Module burnup measurement system, shown in Fig. 4-9, used a beam collimation tube passing through the shielding wall of the pebble handling room, so the germanium detector could be located in an accessible environment. Likewise, for the PB-FHR the BUMS will use a system to shuttle individual pebbles into a shielded cavity adjacent to a collimation tube, with the detector located outside and adjacent to the reactor cavity.

4.6.2 Pebble Handling and Storage System Operation

The PHSS operating modes are as follows:

Core Loading During Commissioning and Start-Up

During initial commissioning phase and testing of the reactor systems before criticality, the PHSS in the Mk1 PB-FHR will test the operation of all subsystems and components by loading the core and recirculating graphite pebbles. Under this mode of operation, canisters of clean graphite pebbles are transferred from outside the reactor building into the gas-lock chamber then subsequently loaded into the primary coolant in each of the six canister transfer wells in the pebble handling chamber. The graphite pebbles are moved to each of the four fixed pebble storage canisters before they are transferred in small diameter piping into the reactor vessel and into the core through the pebble injection lines. The CUD is used to extract graphite pebbles and any damaged pebble fragments are removed. The Burnup Measurement and Sorting System (BUMS) serves no sorting function in this operation mode and serves only to count graphite pebbles and dispatch them to the appropriate storage or transfer canister.

Upon completion of the commissioning phase, the PHSS is used to prepare the core with Phase 1 of the initial core loading before approaching criticality. The most important requirement for the PHSS in this phase is to load the core with a mixture of graphite pebbles and start-up fuel so that criticality will not be approached from an over-moderated state when the fresh fuel pebbles are loaded into the core. The specifications of the start-up fuel will be defined in future design efforts, but this initial loading phase is similar to that proposed for PBMR, which includes a transition from graphite pebbles to different ratios of graphite and fuel pebbles [150]. Figure 4-10 shows the simplified process flow schematic for the PHSS during Phase 1 of the initial core loading.

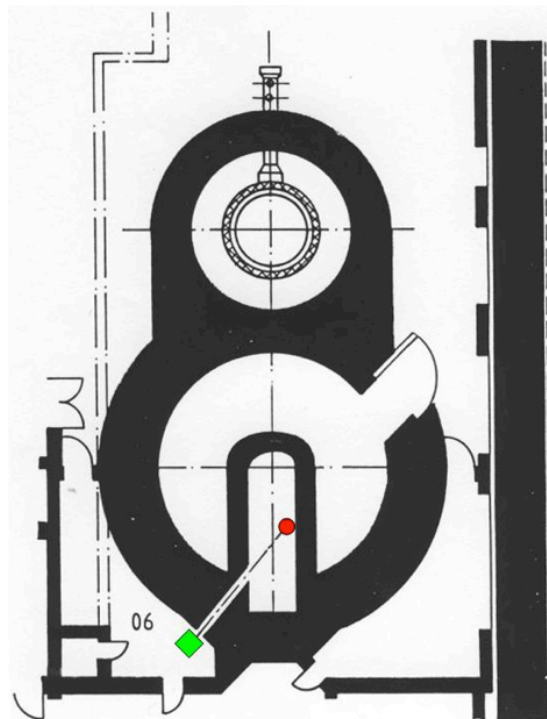


Figure 4-9. HTR Module reactor burnup measurement system, showing pebble location (red dot) and germanium detector location outside the shielded pebble handling space [151].

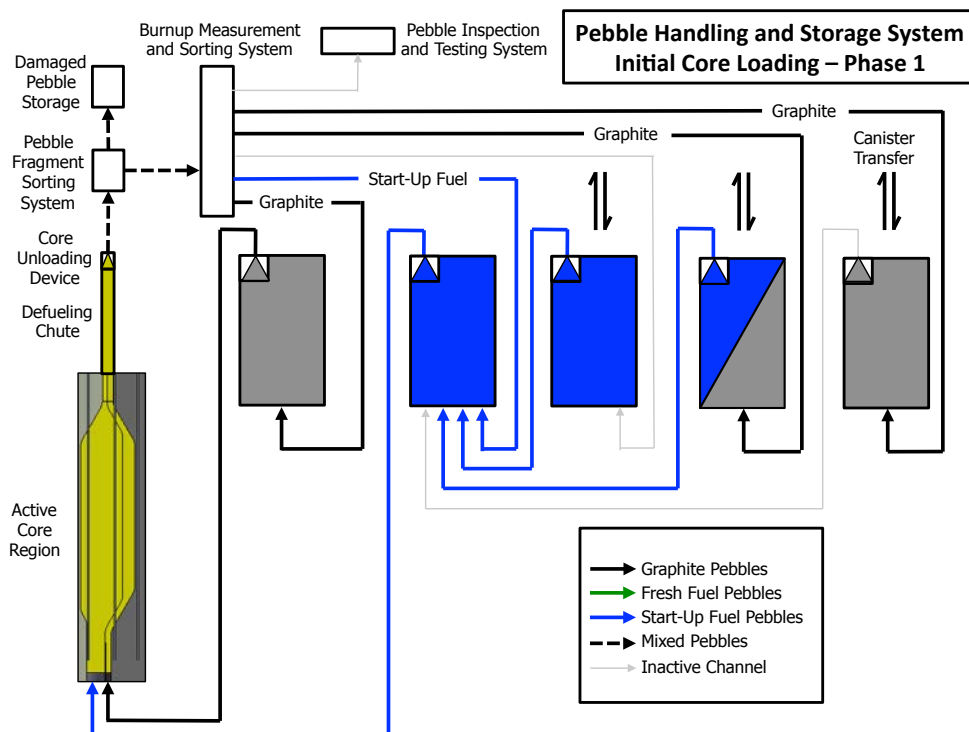


Figure 4-10. Simplified process flow diagram for PHSS under Phase 1 of Initial Core Loading. Radial zoning is established during this phase.

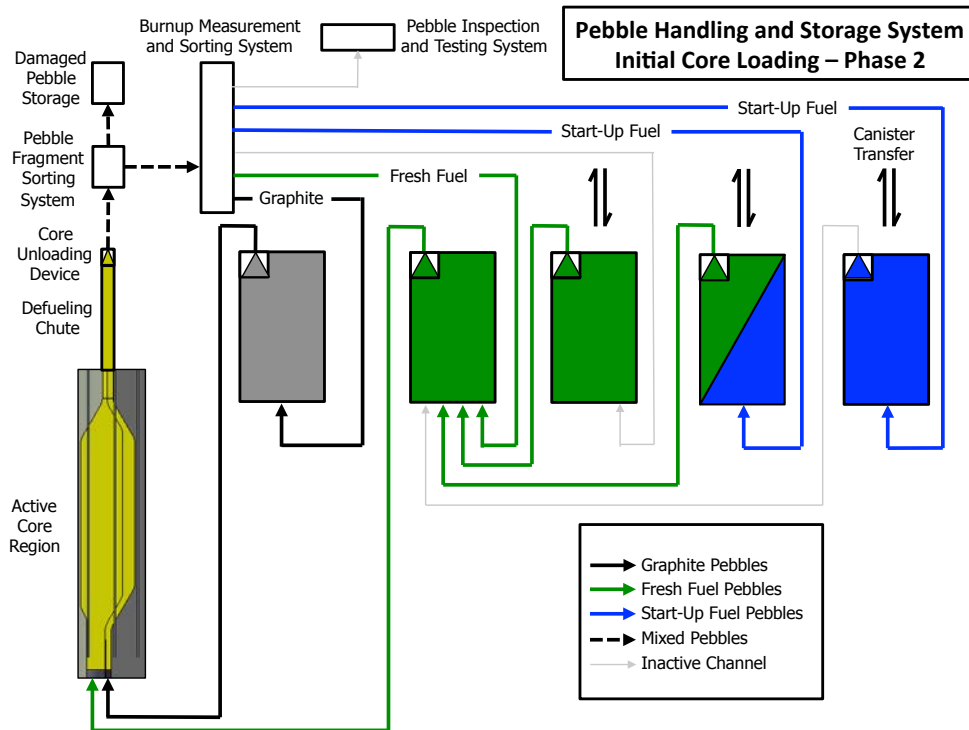


Figure 4-11. Simplified process flow diagram for PHSS under Phase 2 of Initial Core Loading. Fresh fuel is exchanged for the start-up fuel to prevent approaching criticality from an over-moderated core configuration with graphite pebbles.

4.6.2.1 Normal Operation Sphere Circulation

During normal operation, the PHSS circulates fuel and graphite pebbles through the reactor core and exchanges fresh fuel pebbles for spent fuel pebbles by batch transfers in the PCTS. The pebbles are transported through the PHSS by a combination of buoyancy and fluid drag forces in the primary coolant. Figure 4-12 shows the simplified process flow schematic for the PHSS during Normal Operation that represents one half of the system. The nominal operating conditions for the PHSS are matched to the core inlet at 600 °C and near atmospheric pressure.

Fuel and graphite pebbles are removed from the core by two CUDs, which are discussed above, and function to extract individual pebbles from packed bed configurations for transport in small diameter channels. The CUD should have the capability to extract damaged pebble fragments to prevent operational failure due to jamming near the small channel orifice that could occur with heterogeneous granular particles. Redundancy in each CUD could be included in the detailed design to allow for two pebble extraction channels so that an in-place alternative exists should one channel become jammed during operation. It is important to note that the probability of pebble damage in the Mk1 PB-FHR core should be significantly less than that in HTGR cores due to the greatly reduced body forces on the near-neutrally buoyant pebbles.

From the CUD, pebbles and pebble fragments are sorted in the Pebble Fragment Sorting System. Pebble fragments are extracted in a material stream and stored as high-level waste. This system, located at the top of the pebble bed core, would only be capable of extracting pebble fragments that have densities less than the primary coolant. Fragments with higher densities that might sink to the bottom of the active core would need to be removed from the

system by alternative means. One option could be a system to remove the dense fragments at the bottom of the reactor vessel during defueled maintenance for replacement of the central reflector column. Small numbers of these fragments would not be expected to cause major problems for normal reactor operation, but larger quantities of debris could block some coolant flow paths in the bottom of the core or in the central reflector. These effects would be highly localized due to the effective flow redistribution in the pebble bed core.

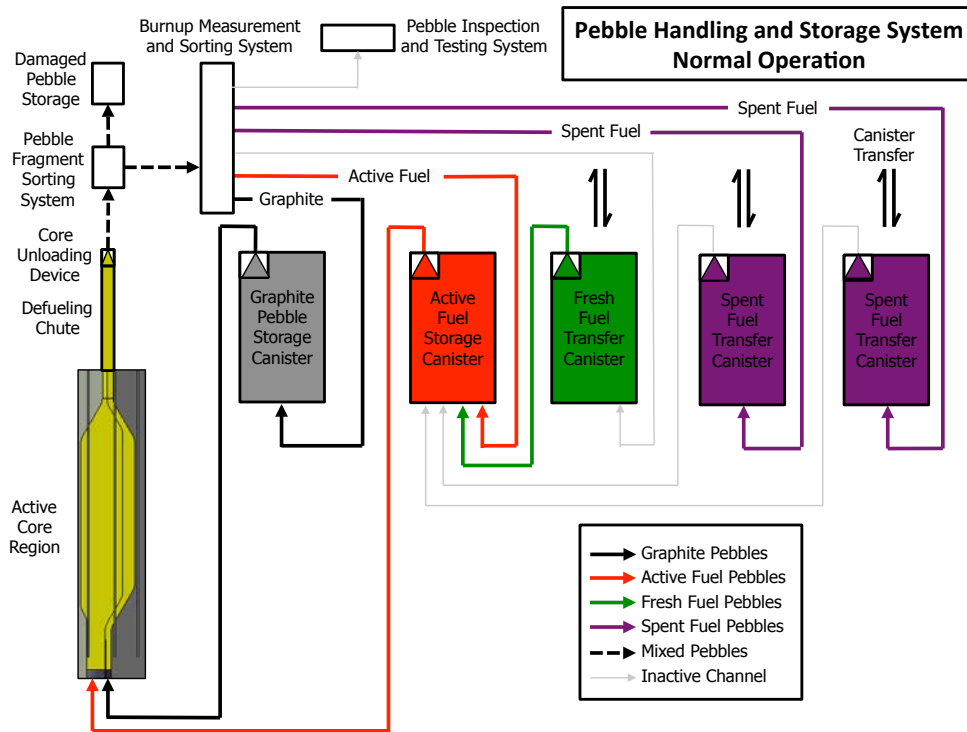


Figure 4-12. Simplified process flow diagram for PHSS under Normal Operation.

After damaged pebble fragments are removed, the fuel and graphite pebbles are subsequently distributed in the BUMS. The primary identification of graphite pebbles can be performed by means such as measurements of small mass differences in pebbles that should be relatively fast while the secondary burnup assessment is expected to take longer to complete. The normal sphere recirculation rate for the Mk1 PB-FHR is 450 pebbles per hour, based on full time operation of the PHSS. Confirmation will be required that the BUMS System can be designed to accommodate this frequency. Graphite pebbles and fuel pebbles below the permissible burnup limit are directed to their respective fixed pebble storage canisters before they are recirculated back into the two core pebble zones. Fuel pebbles that exceed the permissible burnup limit are directed to the four pebble spent fuel transfer canisters. The BUMS also allows for fuel and graphite pebbles to be extracted by the Pebble Inspection and Testing System for post-irradiation examination. This capability is important to monitor the condition of the graphite pebbles in the outer reflector blanket to ensure that they have adequate structural integrity.

Under normal operation, the fuel supply for the reactor is maintained at power through the batch transfer of pebbles with the PCTS. The Mk1 PB-FHR includes two fresh fuel canister wells and four spent fuel canister wells. This ratio allows for the short term cooling of one spent fuel canister before it needs to be pulled while the second spent fuel canister is loaded with

pebbles. Fresh fuel canisters are not subject to the same cooling requirements and therefore can be exchanged more frequently. Fresh fuel is extracted from the transfer canister by PCUDs and is transported from the transfer canister to the active fuel storage canister through small diameter channels. The fresh fuel is mixed with the active fuel pebbles recirculated from the core in the fuel storage canister before being injected into the core to ensure that a heterogeneous mixture of pebble burnup levels is maintained in the active core region.

4.6.2.2 Core Defueling and Refueling

Full core defueling and refueling may be performed by the PHSS in the event of a scheduled or unscheduled maintenance outage that requires fuel to be removed from the reactor core. Normal fuel removal under maintenance conditions is not expected for the Mk1 PB-FHR except for outages to replace the graphite central reflector due to damage from neutron irradiation. At the completion of all defueled maintenance operations, used fuel pebbles are to be loaded into the core in the fuel radial zone region in accordance with a loading to criticality procedure.

During defueling operation of the PHSS, pebble recirculation occurs at an increased rate in order to decrease the total time required to unload pebbles from the reactor core. At the nominal max rate of 3,600 pebbles per hour (1 Hz) from the two CUDs would take eight days to unload the entire core. A total of 24 pebble transfer canisters will be required to complete the full core unloading, including eight for graphite pebbles and sixteen for active fuel pebbles. During this fast pebble removal mode, simple sorting of fuel and graphite pebbles, without burnup evaluations, will accelerate the capabilities of the BUMS System and reduce the time to unload the core. Damaged pebble fragments may be removed from the system by an integrated or separate sorting system and stored as high-level waste.

The total time required to remove all pebbles from the core may also be reduced by two phases of core unloading. In Phase 1 of the Full Core Unloading process, active fuel pebbles are sorted to the four fixed pebble storage canisters and recirculated into the core while graphite pebbles are sorted to the six pebble transfer canisters and removed from the primary coolant by the PCTS. Figure 4-13 shows the simplified process flow schematic for the PHSS during Phase 1 of the Full Core Unloading. All pebbles should be cleaned to reduce the amount of entrained flibe that is removed from the system. In this defueling phase, the reactivity control system will need to provide sufficient shut down worth to maintain subcritical conditions in the core for a single zone of active fuel pebbles. Evaluation of the radiation damage to the graphite pebbles may be completed to determine if they should be replaced, but it may prove to be simpler to replace all graphite blanket pebbles in this maintenance condition to avoid the risk of introducing additional contamination into the primary coolant.

In Phase 2 of the Full Core Unloading process, the active fuel pebbles are sorted to the pebble transfer canisters. In the current concept of the PHSS, the fuel pebbles are removed from the primary coolant and may be stored and cooled in the transfer canisters in the reactor building or in the central fuel handling facility. Figure 4-14 shows the simplified process flow schematic for the PHSS during Phase 1 of the Full Core Unloading. All pebbles removed must be cleaned in stored in an inert atmosphere to reduce the risk of introducing contaminants into the primary coolant during the subsequent refueling operations. The decay heat load for the transfer canisters in this operational mode will be the highest for all normal operational modes. Adequate cooling capabilities must be maintained during this operation to keep peak fuel temperatures within

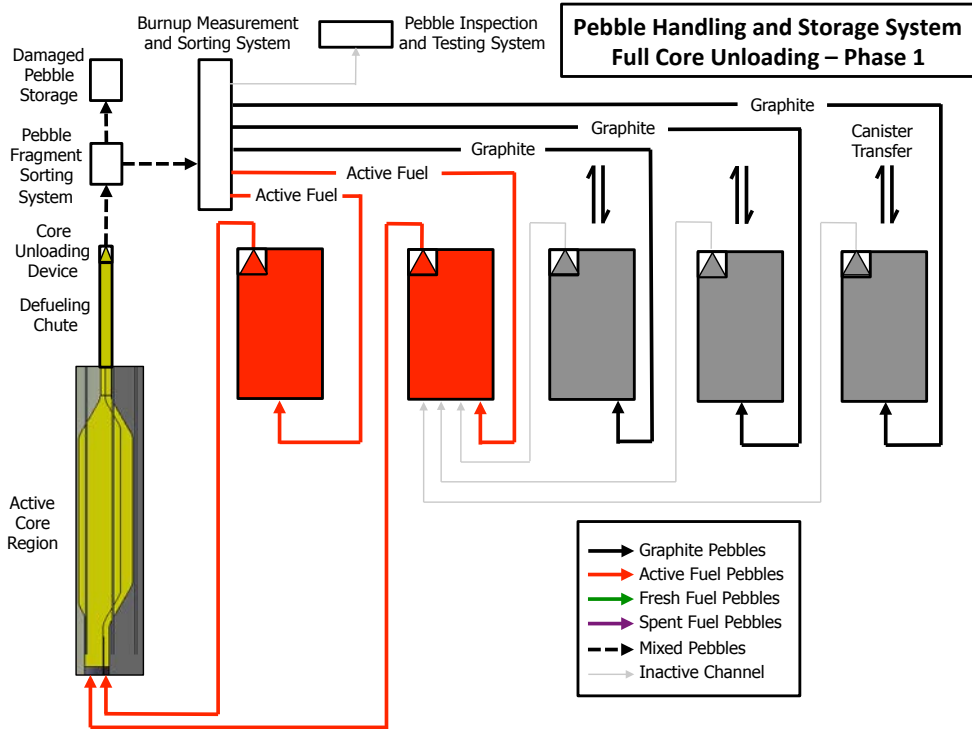


Figure 4-13. Simplified process flow diagram for PHSS under Phase 1 of Full Core Unloading. Graphite pebbles are removed by the PCTS for disposal.

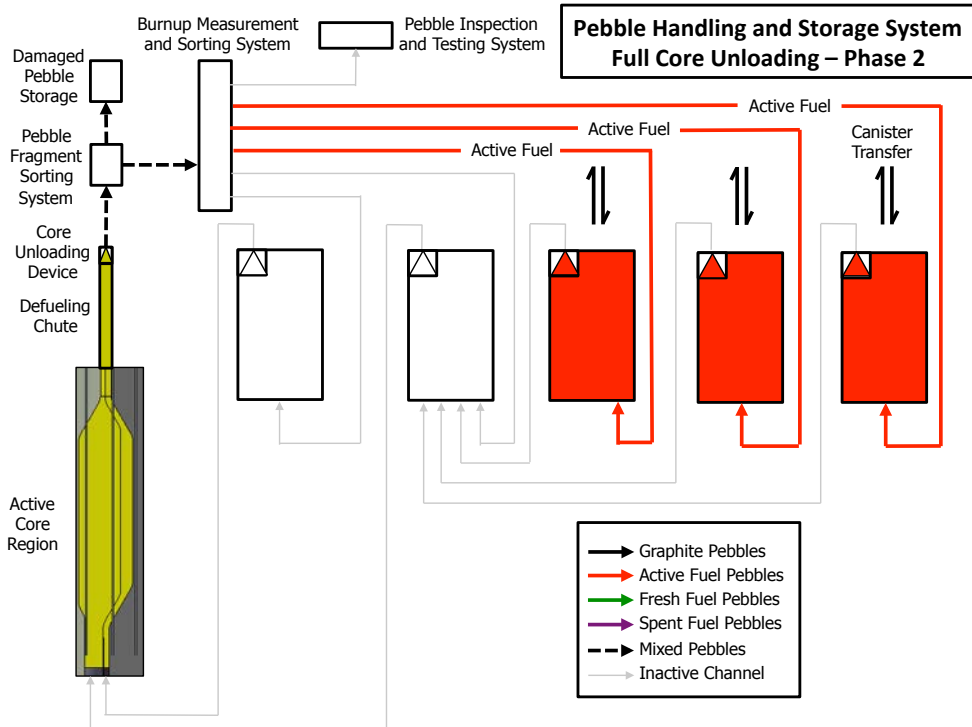


Figure 4-14. loading. Active fuel pebbles are removed, cleaned, and sorted based upon burnup levels before the they are reloaded into the core.

acceptable limits. Future design work will be required to determine how best to achieve this cooling in balance with the desire to limit the volume for pebble storage in primary coolant due to its high cost.

At the end of the life of the Mk1 PB-FHR, the PHSS will function to remove all pebbles from the reactor building through a similar core unloading process that is used during maintenance outages. However, under these conditions, sufficient cooling time in the primary coolant can be achieved to reduce the cooling requirements on the pebble transfer canisters so that they may be transferred to the centralized pebble handling facilities on a multi-unit site. Active fuel pebbles that may be reused in other units, such as for start-up fuel, should be cleaned and kept in an inert atmosphere to reduce the risk of salt contamination.

4.6.2.3 *Off-Normal Conditions and Accidents*

The PHSS will need to be designed for a range of possible off-normal reactor conditions or accident scenarios, which may be designated as anticipated operational occurrences, design basis events, or beyond design basis events depending on the anticipated frequency. Two categories of accident scenarios are discussed here briefly. A more detailed evaluation of the safety considerations of the PHSS will be required for future PB-FHR development.

Component Operational Failures. This class of events includes the inoperability of any subsystem of components in the PHSS that inhibits the capability to circulate pebbles under any of the normal reactor operating modes. These failures would result in a reduced operational capacity factor for the reactor, but would not lead to any significant risk of fuel failure in the PHSS because of the subcritical nature of the system, large fuel temperature margins, and ample cooling provided to pebbles under salt. These failures include flow blockages due to salt freezing within the pebble handling chamber.

Two particular scenarios that would merit evaluation include the loss of normal forced circulation in the PHSS that would result in a reduced capacity for decay heat cooling and the mechanical failure of the PCTS while a pebble canister is being transferred out of the primary coolant. The latter case may be one of the more significant accident scenarios for the Mk1 PB-FHR in terms of peak fuel temperatures if normal cooling systems are not functional or in the case of air ingress to the pebble transfer canister. However, these scenarios would impact a small fraction of the total fuel inventory and would not be expected to lead to containment failures in the event of any fission product release. The detailed design of the PCTS should consider methods to reduce the frequency and consequences of these accident scenarios within acceptable limits from both regulatory, reliability, and investment protection perspectives.

PHSS Loss of Coolant Accident. The failure of pipes or vessels in the PHSS may result in a loss of primary coolant from pebble storage and transfer canisters and a reduced capacity to cool the decay heat from these pebbles. An evaluation of pipe break scenarios should be included in the PHSS detailed design to ensure that pebbles remain covered under salt and that the peak fuel pebble temperatures remain within acceptable limits. Design modifications may be possible to reduce the risk of such loss of coolant scenarios and should be evaluated on a risk-cost basis. The loss of coolant from any part of the PHSS would not result in any significant risk to the active core region due to the lack of penetrations in the reactor vessel below the minimum elevation required to remove decay heat through the DRACS.

Reactor Accident Scenarios. This class of events includes any reactor accidents scenarios that must be evaluated in the licensing process for the Mk1 PB-FHR. The PHSS is not expected to play any significant role in the response to these accidents and is not expected to be relied upon in any design basis accidents.

Under beyond design basis ATWS scenarios, the PHSS could provide additional defense-in-depth for long-term accident management through the removal of fuel pebbles in the core. This operation would help to prevent re-criticality as the primary system cools after the initial shutdown due to negative temperature feedback. The PHSS could therefore help to reduce the total time at temperature of metallic structural components in the Mk1 PB-FHR in the event that cooling capabilities remain inhibited. Analysis of core criticality should be performed under configurations with a reduced number of pebbles to determine what capacity in the pebble storage and transfer canisters would be required to perform this function under ATWS scenarios.

4.7 Plant Instrumentation and Control (I&C)

As a Generation IV reactor, the Mk1 PB-FHR uses passive mechanisms to achieve key safety functions such as reactivity control, decay heat removal, and coolant inventory control. The emphasis on passive safety affects the Mk1 approach to I&C, which will use digital systems similar to those being used in new advanced LWRs and planned for LWR-SMRs. In the longer term, the UCB Compact Integral Effects Test facility will provide a test bed to study the design of control systems and logic to control PB-FHRs during startup, shutdown, and a variety of other transients.

4.7.1 Reactor protection system

Mk1 PB-FHR reactor protection functions are performed by a combination of passive mechanisms, control signals and actuators from the safety-grade digital reactor protection system (RPS), and from manual operator actions. Digital RPS are now normally used for new reactors, with an example of these new technologies being the Advanced Logic System platform developed by Westinghouse, which uses field-programmable gate-array technology and has recently been licensed by the USNRC [152].

For reactivity control, normal shutdown occurs when electrical power is interrupted to the motors of the cable drums in the drive mechanisms of the control rods and the shutdown blades. The insertion of the shutdown blades provides a reserve shutdown function. In addition, besides having negative coolant and fuel temperature reactivity coefficients, the PB-FHR has buoyant activation of rod system, where rod insertion occurs due to buoyancy forces when the temperature of the fluid in the control-rod channel exceeds 615°C [153].

In the PB-FHR core, the emergency heat removal safety function is also controlled by passive mechanisms. The PB-FHR uses a passive check valve to activate natural-circulation-driven heat transport to a set of three DRACS TCHX heat exchangers upon LOFC. Heat removal from the TCHXs is regulated by fail-open valves that supply water to the thermosyphons integrated into these heat exchangers. The valves are held closed during normal operation, and can also be closed to control over-cooling during prolonged reactor shutdown. In addition to the passive emergency decay heat removal provided by the DRACS, the PB-FHR power conversion

system and the normal shutdown cooling system provide heat removal capability and defense in depth in assuring adequate core heat removal.

The PB-FHR reactor coolant and DRACS coolant has a high freezing temperature (459°C). Due to the fact that overcooling transients have the potential to cause localized freezing blockage in the DRACS loop, thereby disabling core heat removal, the control of overcooling transients is also a safety-related function performed by the RPS.

Compared to the original MSBR design of the 1970's, under normal operation the potential for freezing in the main salt loop of the PB-FHR is reduced by the use of NACC power conversion where heat removal can be adjusted rapidly by bypassing air flow around the CTAHs, rather than the steam Rankine cycle of the MSBR design which contains a large inventory of water. However, under design basis events in the PB-FHR, the potential for overcooling exists due to the redundancy and diversity of decay heat removal systems.

The PB-FHR has substantial thermal inertia so overcooling transients evolve slowly. For the PB-FHR, overcooling control actions may be implemented automatically by the RPS or manually by the reactor operators. Operators may also activate main salt loop trace heating systems to mitigate overcooling transients.

The PB-FHR Post-Event Instrumentation (PEI) system will monitor primary system temperatures, as well as other safety related parameters, after design basis events. Data provided by the PEI allows operators to assess the evolving plant state and take appropriate long-term control actions, including assuring that overcooling does not occur.

Finally, coolant inventory control is provided by fully passive mechanisms that require no RPS or manual operator actions. The primary salt fulfills dual roles during design basis events, by providing natural-circulation heat removal and preventing chemical attack to fuel pebbles from exposure to air. The PB-FHR utilizes a pool-type reactor configuration, similar to the design adapted for many sodium fast reactors. For BDBEs where the vessel leaks or ruptures, the Mk1 refractory cavity liner insulation system controls the level change in the vessel and prevents uncover of fuel.

4.7.2 Digital Control System

The PB-FHR digital control system is designed so that neither its actions nor its failure to act would have any deleterious impact on the ability of the PB-FHR to respond safely to design basis events. The quality requirements for the control system then arise from the economic incentives to maximize system performance and to preserve the invested capital, and high-quality commercial-grade equipment is anticipated to be used for the PB-FHR digital control system.

Except during startup and low-power conditions, the PB-FHR operates with constant core inlet and outlet temperatures. Like the PBMR, the PB-FHR has load-following capability, and uses air bypass flow to respond to rapid load-change transients and turbine inlet temperature control (by bypassing air around the CTAHs) for slower transients. Pump speed control is then used to control the core temperature difference, and control rod position is used to control average temperature. The control system adjusts the pebble loading and unloading schedule to maintain sufficient excess reactivity to accommodate a xenon transient equivalent to a rapid power reduction from 100% to 40%.

Even with its relatively high-power-density core, all of the design basis events for the PB-FHR progress slowly. Additionally, the fuel damage threshold for coated particle fuel is several hundred degrees above the design operating temperature. Due to the high degree of plant passive safety resulting from the combination of liquid fluoride salt coolant and the coated particle fuel, the design purpose for the reactor trip functions is to control the maximum coolant temperature to prevent damage to metallic primary loop structures.

The PB-FHR control system is designed to allow the reactor to withstand grid transients, including loss-of-load, by venting hot air downstream of the LP CTAH, followed by a controlled reactor power run-back and activation of the shutdown cooling system to remove decay heat.

The reactor control portion of the PB-FHR plant control system will have common sensor elements to the RPS. All communications from the RPS to the control system will be via buffered one-way communication links (i.e., IEEE 7.4.3.2-2003 Annex E type links). The common sensing elements between the reactor safety and control system will include power range neutron flux, primary coolant temperature, primary coolant level and inventory, and primary coolant flow rate.

4.7.3 Online Monitoring and Plant Health Optimization

The cost effectiveness of any nuclear power plant is determined primarily by its capacity factor and operating lifespan. The PB-FHR introduces a number of structures, systems and components (SSCs) that previously have not commonly been employed in the nuclear power industry. Effective component health and performance monitoring to permit maintenance prior to catastrophic degradation is thus highly important to successful commercial deployment. To this end, the PB-FHR pilot scale plant, and FOAK reactor will all be heavily instrumented to provide extensive SSC health and performance information.

Wireless data networking is central to providing ubiquitous information on plant SSC health and performance information. Wireless data transmission has been applied at the Comanche Peak station in the U.S., to collect sensor data for safety-related pumps and associated equipment to satisfy ASME surveillance testing requirements, and for routinely operated pumps to collect equipment health data. The Comanche Peak wireless system also provides communications and networking capabilities. Arkansas Nuclear One in the U.S., and the José Cabrera Nuclear Power Station in Spain, also have implemented wireless data collection inside their reactor containments [154].

The flexibility afforded by wireless networking arises because it eliminates the need to design and install instrumentation cabling to sensors. Besides reducing construction costs, the elimination of the need to design and install new cabling is particularly useful during the program developmental phases where changing the sensing and communications architecture is an expected result of learning during the development process and implementing monitoring changes identified by the plant's corrective action program. While modern, wired communication bandwidths significantly reduce the need for a wireless network for a plant with an installed high-density data network, plant I&C architectures evolve and cables degrade over time providing a strong incentive for adaptable in-plant networking. Another benefit to wireless networking is its comparative ease of upgrading over the lifetime of the reactor. Digital electronics have much shorter lifecycles than reactor structures and considering the capability to

adapt as technology for online monitoring evolves would be significantly beneficial to long-term operation. Embedded cables have proven to be a significant liability in LWR plant life extensions. Finally, wireless technologies have become the norm for site mapping and communications during construction, so plant wireless systems should be compatible with and not interfere with wireless technologies used during construction of additional modular reactor units.

Reliable plant operation is greatly enhanced by effective maintenance. The prevalence of significantly different components in the PB-FHR makes effective training of operating and maintenance staff essential to ascending the learning curve for reliable plant operation. Some aspects of this training can be carried out at a pilot scale plant. However, training and maintenance planning would be greatly enhanced through augmented and virtual reality plant SSC simulations.

Sensors will be a key area where the PB-FHR I&C differs from other modern reactors. While the PBMR adds the additional sensor performance requirement of high temperature tolerance, the PB-FHR adds both a salt compatibility requirement and a high (albeit somewhat lower than the PBMR) operating temperature requirement. Some of the classical measurement technologies will function for the PB-FHR with only minor modifications (thermocouples with salt-compatible sheaths) while others will require significant modification such as in-core flux monitoring.

5 Mark-1 Power Conversion

The Mk1 PB-FHR uses NACC for power conversion with a modified GE 7FB GT. The GE 7FB was selected because it operates at 3600 rpm and thus generates 60-Hz electricity appropriate for the U.S. power grid, and it is the largest rail-shippable GT manufactured by GE. Two other vendors provide GTs of very similar size, the Siemens SGT6-5000F, and the Mitsubishi M501G1. So multiple vendors are available who would have the ability to supply GT equipment for the Mk1 PB-FHR.

The Mk1 NACC power conversion system is described in much greater detail elsewhere [155, 156]. The earlier modular SmaHTR FHR design considered both steam and supercritical CO₂ as power conversion fluids, which are predicted to give thermal efficiencies of approximately 45% and 48% respectively [157]. This is greater than the 42.4% base-load efficiency predicted for the Mk1 power conversion system, but the capability of the NACC system to also generate large amounts of peak power using cofiring generates additional revenues that would greatly exceed those from larger base-load thermal efficiencies.

5.1 Gas Turbine

The standard natural gas configuration of the GE 7FB has the parameters shown in Table 5-1.

Table 5-1. Operational parameters for an unmodified GE 7FB GT.

Pressure Ratio		18.5
Mass flow	kg/s	445
η_c	%	88.7
η_t	%	91.5
Turbine Inlet Temperature	°C	1371
Turbine Exit Temperature	°C	626
Power (simple cycle)	MWe	183.7
Power (combined cycle, STAG 107FB)	MWe	280.0

To implement nuclear heating the following configuration is used:

i) Air intake occurs through a filter bank, and the air is compressed to a pressure ratio of 18.5. For a nominal 15°C, 1.01 bar ambient condition the air exits the compressor at a temperature of 418°C.

ii) After the compressor outlet, the air passes through a HP CTAH and is heated up to a turbine inlet temperature of 670°C.

iii) The air is then expanded to approximately the same temperature as the compressor outlet temperature, 418°C. This criterion determines the expansion ratio of the first expansion stage at nominal design conditions.

iv) The air is then reheated back up to 670°C by passing through a second, LP CTAH. It is important to design this LP external heating system to have minimum pressure drop in order to achieve acceptable circulating power loss and cycle efficiency.

v) After the LP CTAH, the air is above the auto-ignition temperature of natural gas. To provide power peaking, a fuel such as natural gas can be injected and burned to increase the turbine inlet temperature and the power output.

vi) The heated air is then expanded down to nearly atmospheric pressure and 395-700°C, depending on the peak power level, by passing through the set of LP turbine blades, before entering the HRSG. The HRSG must be designed to accommodate a relatively wide range of air inlet temperatures due to the large change that occurs between low-carbon base-load operation and peak power operation with natural gas injection.

Figure 5-1 shows a three dimensional CAD model of the modified GT. Reheat and external firing are both proven technologies and are commercially available on large industrial GTs (e.g. Alstom GT11N2 and Alstom GT24).

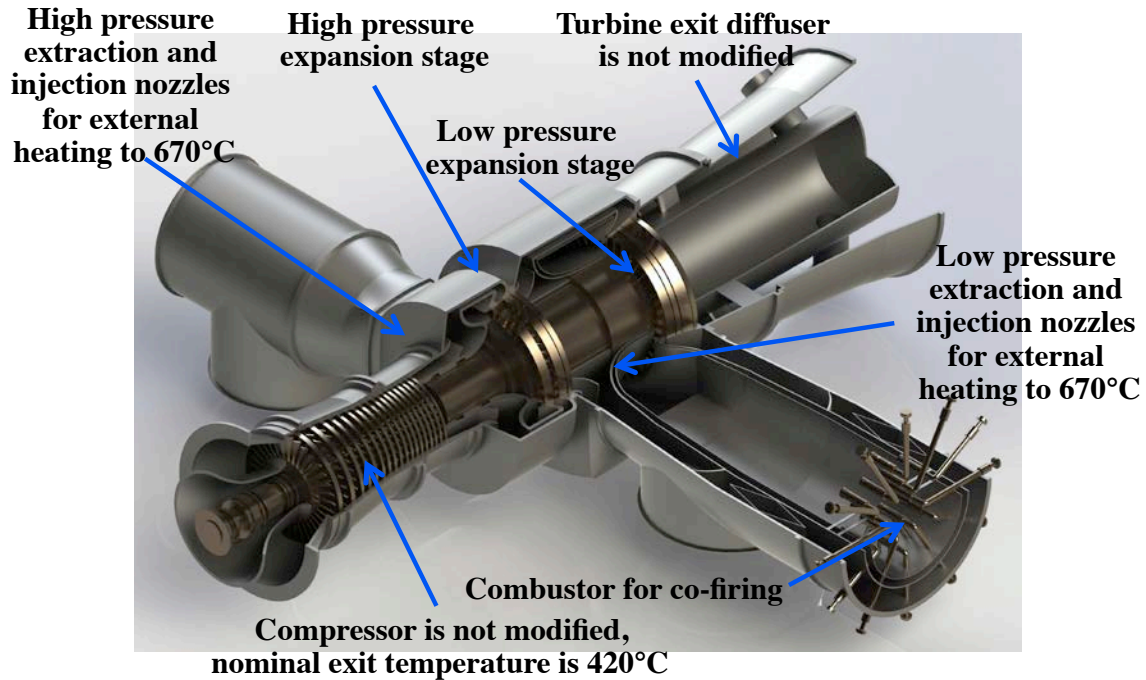


Figure 5-1. Cross section of the modified GE 7FB GT used for power conversion in the Mk1 PB-FHR.

The modifications needed to accommodate nuclear heat for the GE 7FB include an extended shaft to accommodate reheat, a redesigned GT casing, addition of a 4th row of turbine blades, removal of the can-annular combustors and replacement by fuel nozzle injectors in an external silo-type combustor within the air ducts. Additionally, options under consideration include removal of air cooling of the first expansion stage and lower strength metals due to the low temperatures they encounter.

Expected cycle operating parameters at ISO conditions are shown in Table 5-2. Schematic flow diagrams of the power conversion system are shown in Figs. 5-2 and 5-3.

Table 5-2. Mk1 NACC cycle operating parameters at ISO conditions.

$P_{\text{base-load}}$	MWe	100
P_{cofired}	MWe	241
$P_{\text{thermal, nuclear}}$	MW	236
$P_{\text{thermal, w/ cofiring}}$	MW	448
$P_{\text{condenser, nuclear}}$	MW	85
$\eta_{\text{base-load}}$	%	42.4
$\eta_{\text{cofired (net)}}$	%	53.8
$\eta_{\text{cofired (gas only)}}$	%	66.0

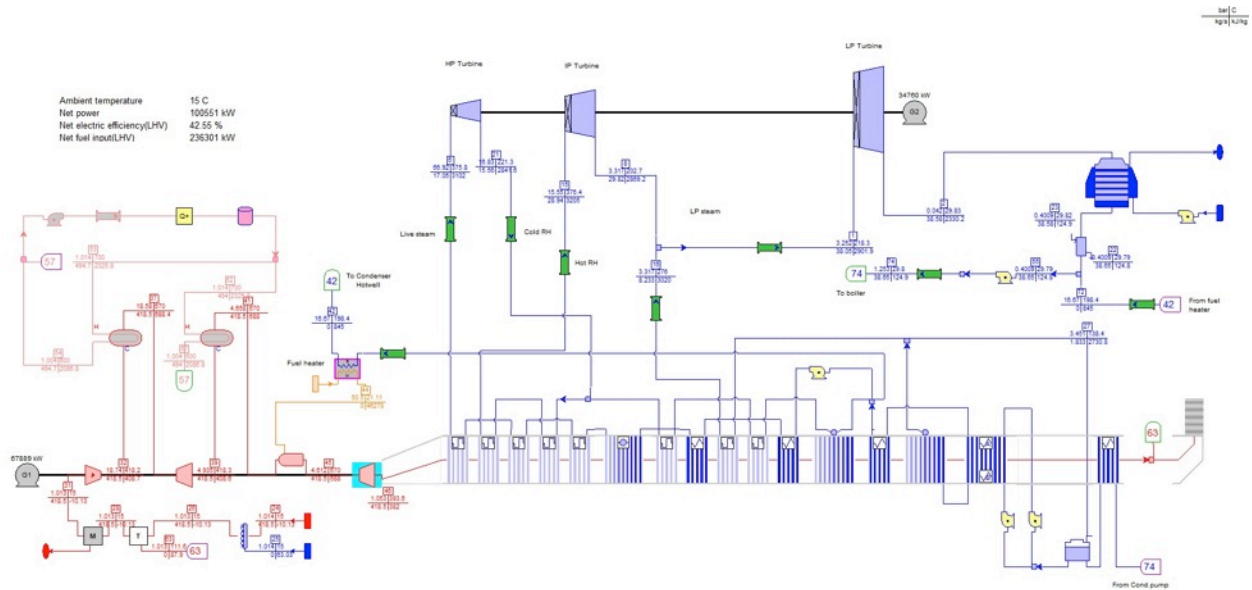


Figure 5-2. Base-load 100-MWe Mk1 Thermoflex power conversion system flow diagram.

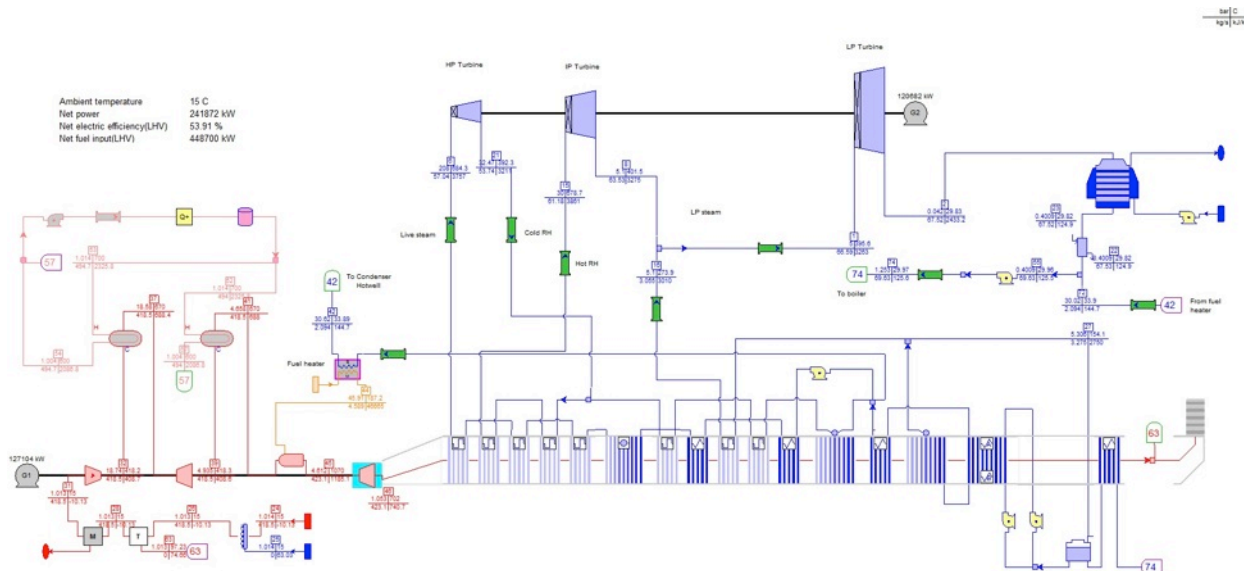


Figure 5-3. Peaking 242-MWe Mk1 Thermoflex power conversion system flow diagram.

5.2 Heat Recovery Steam Generator System

The HRSG and steam condenser need to be sized for full power operation at cofired conditions. The extreme HRSG inlet temperature variation between baseload and cofired operation modes introduces certain caveats to the steam cycle design. The decrease in pressure due to the drop in HRSG inlet temperature in baseload operation needs to be limited by steam turbine inlet valves. The valves introduce parasitic losses to the cycle but manage to maintain a reasonable pressure without starving steam flow to the steam cycle.

Power ramping for the GT is expected to be a frequent occurrence with the cofiring capability. The dissimilar ramping rates of the GT and the steam turbines/HRSG mean that they have to be decoupled from each other. The GT can react much quicker, while the steam turbine needs considerably more time to build up steam and pressure as temperatures are increased. In order to accommodate the dissimilar ramp rates of the two power cycles, turbine exhaust gas can be partially vented from the bypass stack of the HRSG as the steam cycle ramps up to full power. Additionally, an attemperation water spray can be provided to the inlet of the HRSG. Out of the additional 140 MWe generated in the cofiring mode of operation, the Brayton cycle generates 60 MWe.

5.3 Natural Gas Supply and Safety Systems

The natural gas used to generate peaking power in the Mk1 PB-FHR provides a source of stored energy that must be considered in safety and security design of the plant. The Turkey Point Generation Station in Florida provides a useful example for co-location of nuclear reactors immediately adjacent (within 100 m) to two 400-MW gas/oil-fired steam plants and 360 m from a 1,150-MW NGCC unit, as shown in Fig. 1-8. Natural gas supply to these gas-fired plants is provided by a 0.60-m- (24-in-) diameter, 5.2-MPa- (772-psig) pipeline buried 1.07 m (42 in)

deep. A more detailed description of the gas supply and potential hazards is available in Chapter 2.2 of the combined construction and operation license application from the proposed Units 6 and 7 at the site [158].

Natural gas is normally distributed at pressures between 1.4 to 10 MPa (200 to 1,500 psi), and thus requires no compression to be injected into the Mk1 combustor that operates at 0.5 MPa. Detailed engineering design will be required to fully develop the natural gas safety and security systems, however, this section discusses design features and issues associated with the Mk1 natural gas supply system.

Natural gas safety is an issue common to any gas-fueled plant. Natural gas installations are subject to hazardous area regulations, where any potential source of a gas leak requires a designated isolation zone and known ventilation requirements.

Due to the extensive experience available from conventional natural gas power plants, the Mk1 gas supply system uses a combination of standard safety features, as well as additional systems to further increase safety and security. This includes the fact that the Mk1 reactor and safety-related systems are located inside a reinforced shield building designed to withstand impact of a commercial aircraft, and that enclosed spaces such as the air duct vault where gas could conceivably accumulate are designed with blow-out panels to relieve pressure if gas did collect and ignite.

In addition, the Mk1 site natural gas supply system has a master isolation system located near the boundary of the owner controlled area. While the majority of the natural gas supply system is not classified as safety related, the master isolation system is for the Mk1 design, and thus is located in below-grade vaults, described in Section 5.3.4, enclosed in a small protected area. Gas is distributed from the isolation system to the individual units in buried pipes separate from the UCT system, and these lines can be purged prior to maintenance on individual units. Following conventional practice, the buried natural gas lines do not pass through the switchyard area, since all types of buried conductive pipeline become a conductive path if there are multiple switchyard failures that allow the voltage of the pipeline rise above its surrounding and become a current path to some other place. Likewise, the pipelines do not pass through the protected area, but instead are routed around its perimeter.

5.3.1 Fuel gas skid and isolation valves

The standard method to prevent gas from entering equipment in an uncontrolled fashion is to employ a double block and bleed. These are often employed twice. For example the gas supply to a GT fuel gas skid will have two block valves with a bleed or vent valve in between, all three valves having position feedback to the control system and a designated fail position. The block valves fail closed, the vent valve fails open. In addition to this, on the fuel gas skid itself there will normally be a block valve immediately upstream of the fuel gas regulating valve and a vent valve and then between the gas regulating valve and the machine there will be another block valve. Having two block and bleed valve trains one after the other with designated fail positions and position feedback is a common and robust means of keeping high pressure natural gas out of the GT.

The application of conventional hazardous area regulations helps ensure that there is no opportunity for a gas leak to create an explosive mixture in the presence of any possible ignition

source. These regulations have been in use over a very long period of time and are generally very effective and well structured. The high pressure gas pipe has low hazard so long as it has no flanges or fitting on it. The problematic areas are fittings, flanges, gaskets and impulse lines, so the detailed design of the Mk1 natural gas supply system focuses on minimizing these.

The stack gases leaving the HRSG are monitored to detect any unburned natural gas, as this is not only a safety hazard but also an equipment wear issue, as combustion of natural gas downstream of combustors can overheat and damage parts of the turbine. Gas flow through the vent lines is also monitored as an early warning that a block valve has failed or is not sealing correctly.

5.3.2 Fuel gas flow startup

The PB-FHR differs from conventional natural gas power plants because it starts and operates in base-load mode using nuclear heat, rather than fuel gas. Because peaking power is only generated when the power conversion system is already operating in base-load mode and is hot and spinning, the gas supply control system verifies that the power conversion system is at full base-load power before supplying gas. Additionally, passive and intrinsic methods to verify base-load operation are used where possible, for example compressed air to open the fail-close gas supply valves is supplied from the GT compressor outlet and thus is only available if the GT is running and has air flow. Likewise analog temperature measurement, such as a bimetallic switch, may be used to prevent supply valves from opening unless the combustor air inlet temperature is above the auto-ignition threshold.

The fact that during startup the GT will operate initially with nuclear heat for a significant period of time allows forced ventilation and purging of the turbine combustion chamber and HRSG to ensure that no combustible gas could be in the system prior to any injection of natural gas into the combustor.

5.3.3 Isolation of CTAHs during shutdown

The LP air duct has a back-flow damper between the LP CTAH and the combustor, which closes on low flow. After any normal trip the GT takes some time to spin down and while that is happening any remnants of natural gas are being displaced from the hottest parts of the system and will be either pushed out of the stack or wind up in areas at low temperature and free from any ignition sources. In addition to that, the effective dilution will ensure that any remaining gas will be too lean to support combustion or explosion. Depending on the nature of the trip event, the GT will normally go through a cool-down period where the generator is motored to keep the turbine spinning, with the air flow bypassing the CTAHs, which will fully purge the GT and the HRSG. Once the motoring is stopped and the turbine spins down, air flow ceases and the back-flow damper closes. The back-flow damper then prevents any back-flow of natural gas should the supply system fail, and protects the LP CTAH from overpressure if an explosion does occur in the LP turbine or HRSG.

5.3.4 Gas supply physical arrangement

The gas supply skid is located in two below-grade vaults with an independent ventilation system and an access control system to detect and prevent unauthorized entry. Each vault contains one of the block and bleed valve sets. All electrical and control equipment is located in locked cabinets and valves are locked to prevent inadvertent or deliberate mispositioning.

The HP gas line that supplies gas to the supply skid is buried to provide physical protection, and extends to a master isolation valve system located below-grade vaults a significant distance from the plant, typically near the fence that delineates the boundary of the owner controlled area. The master gas isolation system is considered to be safety-related, and thus is located inside a small protected area near the boundary of the owner-controlled area. The vaults are designed with hatches to provide long delay times for unauthorized access and with fences and intrusion detection systems similar to those used for independent spent fuel storage facilities. The isolation provided by the master valves is further augmented by nitrogen blanketing the gas line during periods when the plant is offline or in maintenance.

Natural gas is lighter than air, so leaks outside will form upward-flowing buoyant plumes and disperse. The Mk1 NACC design has the GT located outdoors, but the sound and insulation enclosure around the turbine and combustor is actively ventilated to prevent any accumulation of gas.

While the reliability of the natural gas supply system is very high, the potential for gas to leak into the LP CTAH air ducts, or the below-grade air duct vault, must be considered. If warranted by detailed design analysis, gas concentration monitoring, backup fans and sparking elements to prevent gas from accumulating to explosive concentrations may be provided. Both the air ducts and the vault are designed to relieve overpressure. The LP air duct has a large-diameter rupture disk located immediately before the inlet to the combustor, that vents upward, and the air-duct vault has blow-out panels on both sides of the GT to relieve overpressure.

5.4 Other Power Conversion System Design Topics

The system is sensitive to ambient conditions (temperature, altitude, relative humidity) because of the open nature of the power conversion cycle. However, a stable operating condition can be achieved by implementing standard GT technology. For colder ambient conditions, where air is denser, power levels can be maintained constant by recirculating warm air from three different points in the power cycle. During base-load operation (no flue gases) warm air can be recirculated either from the turbine exhaust or from the HRSG exhaust. During cofired applications warm air can be recirculated from the compressor discharge, a standard practice in current GTs. During high temperatures, where power decreases, the air flow can be cooled by injecting demineralized mist into the inlet or using a standard inlet chilling system. These systems are well known and extensively used.

Maintenance and operation issues for the GT affect the availability of the GT. The more frequent power ramps relative to the lower turbine inlet temperatures compared to conventional GTs on the service intervals and component life need to be examined. Typical replacement intervals for GT parts are in the range of 48,000 hours of operation.

6 Lessons-Learned from the Mark-1 Design Project

On May 8, 2014, UCB held a final design review meeting for the Mk1 PB-FHR. Two members from the IRP Advisory Panel, Dr. James Rushton and Dr. Douglas Chapin, as well as IRP co-Principal-Investigator Dr. Charles Forsberg, and visiting professor Dr. Wei Ji from Rensselaer Polytechnic Institute attended along with several UCBNE faculty. This design review meeting followed a review of NE 170 senior design project presentations, related to the Mk1 design, the previous day.

The review of the Mk1 design complemented its progress, and noted that the design effort continues to support the conclusion that FHRs can achieve very high levels of intrinsic safety, and by delivering heat at low pressure and high temperature, achieve high efficiency in generating electricity and producing process heat.

Moreover, the reviewers noted that the level of detail of the Mk1 design is helpful because it enables remaining gaps to be identified in significantly greater detail. Rushton noted that “[g]iven the stage of the design, there are hundreds of remaining tasks or gaps.” [159] He then advises that the experience from the design effort be summarized in the form of “key” gaps. “NASA’s development spirals would be a good model. Each spiral adds to the knowledge base and level of detail. Each spiral typically requires a higher level of investment. What should be the focus of the next spiral for PB-FHRs?”

This is an important conclusion, because now FHR research needs to be focused toward increasingly detailed technical questions. To give a flavor of the “hundreds” of design issues that must be resolved to bring an advanced reactor to the level of design completion needed for licensing and construction, it is useful to review a series of Requests for Additional Information (RAI’s) that were developed by the USNRC in during its preapplication review of the PBMR. The breadth of RAI’s is large, an illustrates the types of detailed issues that must be addressed in design. The next section reviews these PBMR RAI’s, and is followed by additional sections that briefly summarizes some of the key areas where gaps have been identified during the Mk1 design process and design review, that will merit attention during the next “spiral” of FHR studies.

6.1 PBMR Requests for Additional Information

Starting in 2001, the USNRC conducted a series of public meetings with the Exelon Generation Company and the U.S. Department of Energy where they received presentations on technical and programmatic topics supporting the PBMR pre-application review. Exelon submitted multiple white papers to the USNRC, and asked for feedback on technical, safety, and policy issues.

The letters that the USNRC sent to Exelon, listing Requests for Additional Information (RAIs), provide interesting insights into the types of information needed to develop a complete license application for a novel reactor design. These include RAI’s related to Exelon’s proposed approach to license the PBMR [160]; the modeling approach and supporting high-temperature irradiation data for graphite structures, approach to control chemical attack of

graphite during air or steam ingress, and design codes and standards to be applied including requirements for in-service inspection, design of core support structures, design of the containment building, and quality group designations [161]; analytical codes for prediction of fuel performance and validation with fuel irradiation test data, analytical codes for prediction of the dynamic response of structures, core design, reactivity control, and cooling with associated modeling modeling, and identification of operating modes [162]; and fuel fabrication, quality control, and performance monitoring with associated fuel qualification testing [163].

6.2 FHR Tritium Control and Recovery

The control and recovery of tritium is considered to be a key viability issue for FHRs, due to the much larger production than in LWRs as well as operation at higher temperatures which increase the rate of tritium diffusion through metallic structures including heat exchangers.

The control of tritium requires limiting its rate of release into the environment to be a small fraction, less than 0.1%, of its rate of production. The primary challenge for control involves the high diffusivity of tritium through hot metals, including primary piping and most importantly power-conversion heat exchangers. One solution that can greatly simplify the control of tritium is to use a closed gas Brayton cycle, such as a supercritical CO₂ or multiple-reheat helium Brayton cycle, for power conversion, because the tritium can be contained in and recovered from the power conversion system. However, closed gas Brayton power conversion technology is not commercially available, and its development and commercial deployment involves important technical and logistical challenges.

For both steam Rankine and air Brayton power cycles, tritium that diffuses through steam generators or air heaters into the power conversion fluid cannot be practicably recovered, and thus must be discharged into the environment. The key technical challenge for steam and air cycles, then, is to control tritium transport through heat exchangers into these power conversion fluids. Rushton states, “Given prior MSRE development and testing experience, the tritium issue is a potential technical show stopper to the NACC. Development efforts should address more than one solution just as multiple options are proposed for the redox control system.”

The baseline tritium control approach for the Mk1 PB-FHR, described in Section 4.1, is to clad the exterior surface of CTAH tubes with an alumina-forming alloy, which in the high temperature, oxidizing air environment of the heater, is expected to form a self-healing coating of aluminum oxide, which has a high permeation resistance to tritium. Further work is needed to study methods to apply cladding or coatings, and to study the effectiveness of tritium control under prototypical CTAH systems, as well as to study alternative options for tritium control (double wall heat exchangers, and intermediate loops with sodium fluoroborate molten salts that have high capacity to absorb tritium).

The baseline Mk1 approach to recover tritium is to absorb it onto the graphite surfaces of fuel and reflector pebbles, and if needed, to additional graphite media placed in annular filter cartridges in the CTAHs (Section 4.1). Further work is needed to study tritium uptake into representative pebble materials under prototypical conditions, as well as to study alternative recovery options (droplet spray towers, bubble disengagement, etc.)

6.3 FHR Fuel and Materials Selection and Development

The pebble fuel selected for the Mk1 PB-FHR has low technical risk, since the fuel geometry has been used before, operates at lower peak fuel temperatures than experienced in HTGRs, and with its 3.0-cm diameter size, can be tested in either ATR or HIFR, as described in Section 1.7. The key areas of technical risk involve operation at higher particle powers than is experienced in HTGRs, and fabrication of pebbles with two annular layers rather than the single layer used in existing pebble bed reactors. An alternative approach is to use fixed fuel forms, either with cylindrical compacts in prismatic blocks, where extensive experience exists, or in the form of plates. Plate fuel forms may be challenging to irradiate given their larger size, and require evaluation for potential risks of fuel layer delamination under thermal and irradiation induced stress (which may subject the layers to shear stresses).

Future work for Mk1 fuel and reflector pebbles is needed to demonstrate fabrication methods, to irradiate the fuel, and to perform post irradiation examination. Also, studies are needed to assess potential approaches to lower the fuel enrichment level to under 10%.

While the Mk1 fuel has low technical risk, as discussed in Section 1.6, insufficient information is available today to make a selection between candidate structural materials. Rushton notes, “Selection and qualification of a material system and coupled corrosion control system is another core issue. Excellent options are in hand; tests and demonstrations are required to make a final selection.”

The Mk1 design includes a number of features to aid in coolant chemistry and corrosion control, including provisions to contact the salt with cover gas, to contact the salt with redox control materials in cold traps, to filter the salt, and to drain the salt to allow batch cleanup processes, as described in Sections 4.3 and 4.5. Likewise, provisions to perform in-service inspection are included in the design (Section 4.4). Further work is required, however, to select specific approaches for salt chemistry control and cleanup, including experimental studies in flow loops to verify their effectiveness.

6.4 FHR Fuel Handling

The design of fuel handling systems for FHRs is complex, both for systems to perform online pebble fuel circulation (the Mk1 baseline), batch pebble refueling (the TMSR-SF1), and periodic refueling of fixed assemblies (the 2012 ORNL AHTR baseline). Pebble fuel handling has been developed successfully for helium-cooled pebble bed reactors, and in some respects handling of pebbles hydraulically in salt can be expected to be easier than pneumatically at high pressure with helium (such as reduced difficulties with graphite dust generation), but many engineering issues remain to be addressed.

The Mk1 baseline design (Section 4.6) includes specification of the method and locations for injecting fuel and reflector pebbles into the bottom of the core, as well as the design of defueling chutes and the location for two defueling machines. Likewise, the location of the hot-cell outside of the reactor cavity, where pebble handling occurs, and of a cask transfer system for moving fuel canisters into and out of the reactor building, are identified.

Further work is required to address the remaining engineering challenges, and to assure these challenges are systematically identified, tracked and addressed. During the review meeting several challenges were identified:

- Define and implement design for initial loading capability/start up of core; also address unloading partial and complete
- Define and assure implementation of handling damaged and broken pebbles, including pebbles getting stuck. Want to establish undesirable conditions are both acceptably unlikely, and if occurs, can be effectively resolved.
- Define and address handling undamaged pebbles stuck in tubes, and how resolve.
- Determine volume of salt in fuel handling system.
- Define approach for insulation and heating/cooling of external piping, and method to address freezing if it occurs in salt lines with pebbles.
- Define and address canister transfer operations and systems, including cooling methods.
- Define and address defueling device requirements and develop designs.
- Study power distribution and coolant flow, and identify potential for hot spots in defueling channel.

This listing of fuel handling system challenges provides a starting point for future RD&D.

6.5 FHR Safety

FHRs have unique safety characteristics, which include extraordinarily large thermal margins between peak accident fuel temperatures and fuel damage temperatures, high solubility for key fission products (particularly cesium) in their coolant, and intrinsically low operating pressure. Further work is required to perform more detailed assessment of the safety of the Mk1 PB-FHR design. Key activities include systematic identification of licensing basis events, as discussed during the first IRP FHR workshop [164], and the application of the Code Scaling, Applicability, and Uncertainty methodology to determine the applicability of safety modeling tools and the experimental data needed to validate them, as discussed during the second IRP FHR workshop [165]. FHR experiments should generally comply with NQA-1 standards for work, so safety analysis can meet USNRC requirements.

Further work is needed for the detailed design for the Mk1 decay heat removal system, both for normal shutdown cooling and for the DRACS used for emergency decay heat removal. This work includes evaluating and setting the number and capacity of DRACS modules, and addressing BDBA requirements for decay heat removal, including assessing coping time under various conditions. Detailed design of the DRACS should include assessments of the consequences of salt freezing and recovery from salt freezing.

Further work is needed to establish experimental programs needed to validate safety models, including strategy for using simulant fluids (Dowtherm) to perform separate effect test and integral effect test experiments. For example, validation of integral models for the coupled heat transfer from the Mk1 primary system to the DRACS system can be validated in scaled experiments performed in the UCB Compact Integral Effects Test (CIET) facility, as shown in Fig. 6-1.

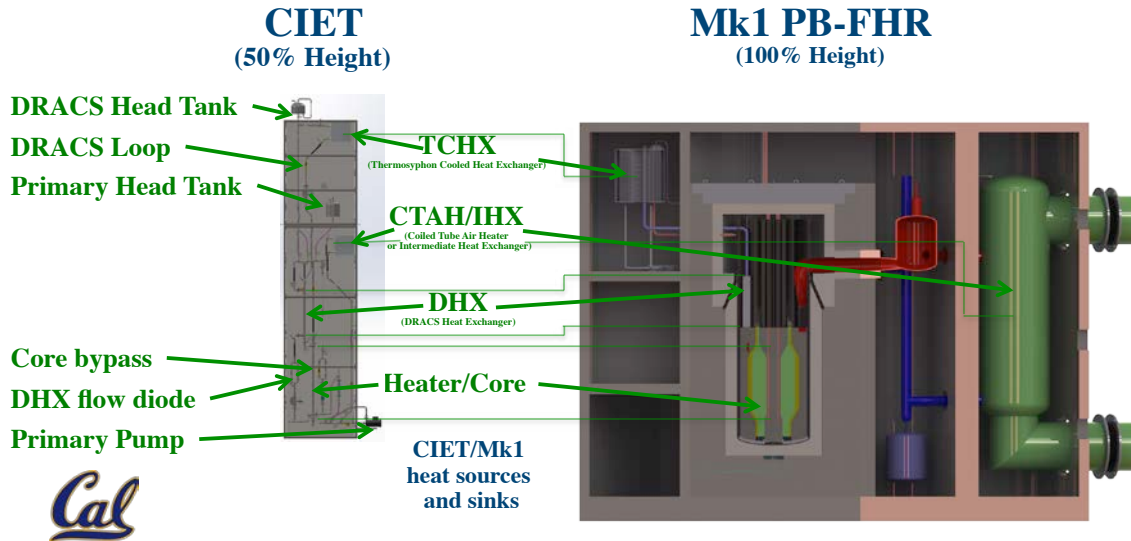


Figure 6-1. Scaled comparison of the UCB CIET integral effects test facility and the Mk1 PB-FHR, showing the heights of major heat sources/sinks.

For reactor physics, further studies and development to predict control rod and shutdown blade worth is needed. Reactivity accidents, both ATWS and reactivity insertion, needed to be defined and improved models, with coupled thermal hydraulics and neutronics, developed and validated. These models will feed back to potential decisions to modify key design parameters, such as core power density, to assure sufficiently low fuel temperatures to provide appropriate transient response during these accidents.

Further work is needed to study other safety design issues, particularly beryllium safety, including needed systems and hardware. For the cover gas, further work is needed to compare argon and helium from perspectives of cost, activation, and heat and mass transfer.

6.6 FHR Power Conversion

For NACC, further work is needed to develop heat exchangers for transferring heat from salt to air, while meeting a variety of performance requirements as discussed in Section 3.4. Key issues include methods to fabricate tube to tube-sheet joints and approaches to respond to tube leaks.

6.7 FHR Development and Licensing Strategy

Further work is needed to define and design all needed systems for use in all modes in a Mk1 unit. This includes establishing the need for, capabilities and size of plant staff: operations, maintenance, security, etc.

Further work is needed to define instrumentation requirements and develop specialized instruments as needed, e.g., thermocouples and other temperature measurements, pressure, level, nuclear power, pressure, flow rate, etc.

Further work is needed to assure access is established, defined and maintained to nuclear systems and equipment for operations and maintenance, and to address shielding, special cranes, tools, etc. James Rushton notes, “Accessing, testing, inspecting and removal and replacement of components and modules will determine whether the size of the reactor building is reasonably scoped now or if it must grow to accommodate efficient maintenance and investment protection.”

Reliability of FHR systems will be a key question in assessing the reliability and availability of future FHR commercial reactors. James Rushton notes, “Operating availability of this reactor type is highly uncertain at this time because of the novelty of the concept and lack of credible demonstrations capabilities in the near term. The Chinese Academy of Sciences experience with the TMSR-SF1 test reactor will offer the first sizeable test since the MSRE.” Component testing in flow loops, as well as the TMSR-SF1 test reactor experience, is needed to understand and assure operational reliability.

Further work is needed to review and understand options for licensing strategies, both for licensing commercial prototypes in the U.S. as well as China and internationally.

6.8 Summary

The Mk1 PB-FHR provides a pre-conceptual point design for a modular, commercial FHR, that can provide a starting point for future studies. The further work identified in this chapter is an incomplete subset of the total work that would be required to advance the Mk1 design to the level of completion required for licensing and construction of a prototype reactor. But the Mk1 design does provide a starting point for subsequent studies of various aspects of FHR design, and thus provides a foundation for building further the understanding of FHR technology, its safety, and its potential to provide attractive production of nuclear power.

7 References

- 1 Forsberg, C., P. F. Peterson, and P. S. Pickard. 2003. "Molten-Salt-Cooled Advanced High-Temperature Reactor for Production of Hydrogen and Electricity." *Nuclear Technology* 144 (3): 289–302.
- 2 Ingersoll, D. T., C. W. Forsberg, and P. E. MacDonald. 2007. *Trade Studies for the Liquid-Salt-Cooled Very High-Temperature Reactor: Fiscal Year 2006 Progress Report*. Oak Ridge: Oak Ridge National Laboratory.
- 3 Peterson, P. F., and H. Zhao. 2006. "A Flexible Base-Line Design for the Advanced High-Temperature Reactor Utilizing Metallic Reactor Internals (AHTR-MI)." In , 8–9. Reno, NV: Proceedings of the International Conference on Advances in Nuclear Power Plants (ICAPP 06).
- 4 Fei, T., D. Ogata, K. Pham, M. Solom, C. Zhao, C. Xu, A. Cheng, et al. 2008. *A Modular Pebble-Bed Advanced High Temperature Reactor*. Berkeley: University of California, Berkeley.
- 5 S. R. Greene, et al., "Pre-Conceptual Design of a Fluoride- Salt-Cooled Small Modular Advanced High-Temperature Reactor (SmaHTR), Oak Ridge National Laboratory, ORNL/TM-2010/199, Fig. 8-1, p. 8-2, December 2010.
- 6 D. E. Holcomb, F. J. Peretz, and A. L. Qualls, Advanced High Temperature Reactor Systems and Economics Analysis, ORNL/TM-2011/364, ORNL, Oak Ridge, TN, September 2011.
- 7 V. K. Varma, D. E. Holcomb, F. J. Peretz, E. C. Bradley, D. Ilas, A. L. Qualls, and N. M. Zaharia, AHTR Mechanical, Structural, and Neutronic Preconceptual Design, ORNL/TM-2012/320, ORNL, Oak Ridge, TN, September 2012.
- 8 H. G. MacPherson, "The Molten Salt Reactor Adventure," *Nuclear Science and Engineering*, Vol. 90, pp. 374-380 (1985).
- 9 Sea Hong, Diasuke Kazama, Huu Duy Nguyen, and Jaben Root, "NE-170 Physical arrangement and structural design for the Mk1 PB-FHR reactor building," Department of Nuclear Engineering, U.C. Berkeley, Report UCBTH-14-003, 2014.
- 10 IAEA, "Construction Technologies for Nuclear Power Plants," International Atomic Energy Agency, Nuclear Energy Series No. NP-T-2.5, Vienna, 2011.
- 11 IAEA, 2011, *ibid*, pg. 17.
- 12 Southern Nuclear Operating Company, "Early Site Permit Application: Part 3 – Environmental Report," Chapter 3, U.S. Nuclear Regulatory Commission Assension Number ML062290302, Table 3.0-1.
- 13 S. Hong, D. Kazama, H. D. Nguyen, and J. Root, "NE-170 Physical arrangement and structural design for the Mk1 PB-FHR reactor building," Department of Nuclear Engineering, U.C. Berkeley, Report UCBTH-14-003, 2014.
- 14 <http://www.flickr.com/photos/scegnews/sets/72157629244341909/>, accessed Oct. 13, 2013.
- 15 S. Hong, et al., 2014, *ibid*.
- 16 IAEA, 2011, *ibid*, pg. 45,
- 17 IAEA, 2011, *ibid*, pg. 147.
- 18 Hong et al., 2014, *ibid*.
- 19 Hong et al., 2014, *ibid*.

-
- 20 R.H. Bryan and I.T. Dudley, "Estimated Quantities of Materials Contained in a 1000-MW(e) PWR Power Plant," Oak Ridge National Laboratory, ORNL-TM-4515, 1974.
 - 21 S. Kaplan, Memorandum to Senator John McCain, "Concrete and Steel Requirements for Power Plants," Congressional Research Service, Table 1, Nov. 27, 2007.
 - 22 Per F. Peterson, Haihua Zhao, and Robert Petroski, "Metal And Concrete Inputs For Several Nuclear Power Plants," Report UCBTH-05-001, UC Berkeley, February 4, 2005.
 - 23 P.J. Meier, "Life-Cycle Assessment of Electricity Generation Systems and Applications for Climate Change Policy Analysis," U. WisconsinReport UWFD-1181, August, 2002.
 - 24 S. Pacca and A. Horvath, *Environ. Sci. Technol.*, 36, 3194-3200 (2002).
 - 25 G. Cao, et al., "Fluoride-Salt-Cooled High Temperature Reactor (FHR) Materials, Fuels and Components White Paper," Department of Nuclear Engineering, U.C. Berkeley, Report UCBTH-12-003, July, 2013.
 - 26 C.E. Boardman, et al., "A Description of the S-PRISM Plant," Proceedings of ICONE 8, 8th International Conference on Nuclear Engineering, Baltimore, MD, Fig. 5, April 2-6, 2000.
 - 27 World Nuclear News, "Triso fuel triumphs at extreme temperatures," Sept. 26, 2013. http://www.world-nuclear-news.org/ENF-Triso_fuel_triumphs_at_extreme_temperatures-2609137.html
 - 28 "NGNP Fuel Qualification White Paper," Idaho National Laboratory, INL/EXT-10-17686, Rev. 0, July 2010.
 - 29 J. Gomez, M. Hay, J. Lee, B. Tam, "Design of Fuel Testing and Qualification Capsules for the Pebble Bed Advanced High Temperature Reactor," Department of Nuclear Engineering, U.C. Berkeley, Report UCBTH-10-002, May 14, 2010.
 - 30 V. K. Varma, D. E. Holcomb, F. J. Peretz, E. C. Bradley, D. Ilas, A. L. Qualls, and N. M. Zaharia, AHTR Mechanical, Structural, and Neutronic Preconceptual Design, ORNL/TM-2012/320, ORNL, Oak Ridge, TN, September 2012.
 - 31 "The Westinghouse Pressurized Water Reactor Nuclear Power Plant," Westinghouse Electric Corporation, Water Reactor Divisions, 1984. (http://www4.ncsu.edu/~doster/NE405/Manuals/PWR_Manual.pdf)
 - 32 "Technical Description of the PBMR Demonstration Power Plant, Document Number 016956, Rev. 4, 2006.
 - 33 E. A. Hoffman, W.S. Yang, and R.N. Hill, "Preliminary Core Design Studies for the Advanced Burner Reactor over a Wide Range of Conversion Ratio," Argonne National Laboratory, ANL-AFCI-177, Tables 4.1, 4.3, and 4.4, 2006.
 - 34 L.A. Mann, "ART Accident Analysis Hazards Tests (U)," Oak Ridge National Laboratory, ORNL Central Files Number 55-2-100, February 11, 1955. (File: "LiquidSalt-WaterInteractions.pdf")
 - 35 C.E. Boardman, et al., "A Description of the S-PRISM Plant," Proceedings of ICONE 8, 8th International Conference on Nuclear Engineering, Baltimore, MD, April 2-6, 2000.
 - 36 G. Toshinsky and V. Petrochenko, "Modular Lead-Bismuth Reactors in Nuclear Power," *Sustainability*, 2012, 4, 2293-2316
 - 37 R.N. Morris, D.A. Petti, D.A. Powers, B.E. Boyack, and M.B. Rubin, "TRISO-Coated Particle Fuel Phenomenon Identification and Ranking Tables (PIRTs) for Fission Product Transport Due to Manufacturing, Operations, and Accidents," U.S. Nuclear Regulatory Commission, NUREG/CR-6844, Vol. 1, Fig. 3-9, pg. 3-21, July 2004.

-
- 38 AGR-1 Irradiation Test Final As-Run Report, Idaho National Laboratory, INL/EXT-10-18097, Revision 1, pg. 57, June 2012.
 - 39 H. Choi, “Advanced fuel cycle scenarios for High Temperature Gas Reactors” *Annals of Nuclear Energy* 38 (2011).
 - 40 D. E. Shropshire, “Advanced Fuel Cycle Cost Basis” INL/EXT-07-12107 (2007)
 - 41 D. Petti, “Status of NGNP/AGR Fuel Development” VHTR R&D FY12 Technical Review Meeting May 22-24 Salt Lake City, Utah (2012)
https://secure.inl.gov/VHTRRDTR12/pres/Opening/03_Petti_StatusofNGNPAGRFuel.pdf
 - 42 Safety Evaluation Report for the National Enrichment Facility in Lea County, New Mexico, Louisiana Energy Services,” U.S. Nuclear Regulatory Commission, NUREG-1827, June 2005.
 - 43 “Safety Evaluation Report for the Eagle Rock Enrichment Facility in Bonneville County, Idaho,” U.S. Nuclear Regulatory Commission, NUREG-1951, September 2010.
 - 44 USEC, Inc., “Safety Evaluation Report for the American Centrifuge Plant in Piketon, Ohio,” U.S. Nuclear Regulatory Commission, NUREG-1851, Docket No. 70-7004, pg. iii, September 2006.
 - 45 Safety Evaluation Report for the General Electric-Hitachi Global Laser Enrichment LLC Laser- Based Uranium Enrichment Plant in Wilmington, North Carolina,” U.S. Nuclear Regulatory Commission, NUREG-2120, February 2012.
 - 46 A. T. Cisneros, “Development of Depletion Analysis Methods and Design Optimization Methods for Pebble Bed Reactors Applied to the Design of the Pebble Bed Fluoride Salt Cooled High Temperature Reactor (PB-FHR),” Ph.D. dissertation, University of California Berkeley, Berkeley, CA, 2013.
 - 47 T. Iyokua, J. Smitaa, M. Ishiharab, and S. Uetaa, "R&D on core seismic design," *Nuclear Engineering and Design*, vol. 233, pp. 225–234, (2004).
 - 48 R.C. Robertson, “Conceptual Design of a Single-Fluid Molten Salt Breeder Reactor,” ORNL-4541, p.11-18 (1971).
 - 49 Cisneros, 2013, *ibid*, pg. 201.
 - 50 A. Monterrosa, A. Iyengar, A. Huynh, C. Madaan, “Boron Use and Control in PWRs and FHRs” Department of Nuclear Engineering, U.C. Berkeley, Report UCBTH-12-007, May, 2012
 - 51 R.C. Robertson, “Conceptual Design of a Single-Fluid Molten Salt Breeder Reactor,” ORNL-4541, p.11-18 (1971).
 - 52 P. Bardet, E. Blandford, M. Fratoni, A. Niquille, E. Greenspan, and P.F. Peterson, “Design, Analysis and Development of the Modular PB-AHTR,” 2008 International Congress on Advances in Nuclear Power Plants (ICAPP '08), Anaheim, CA, June 8-12, 2008.
 - 53 V. K. Varma, D. E. Holcomb, F. J. Peretz, E. C. Bradley, D. Ilas, A. L. Qualls, and N. M. Zaharia, AHTR Mechanical, Structural, and Neutronic Preconceptual Design, ORNL/TM-2012/320, ORNL, Oak Ridge, TN, pg. 37, September 2012.
 - 54 D. F. Williams, L. M. Toth, K. T. Clarno, "Assessment of Candidate Molten Salt Coolants for the Advanced High-Temperature Reactor (AHTR)," Oak Ridge National Laboratory, ORNL/TM-2006/12, March 2006.
 - 55 G. Rothwell, “Market Power in Uranium Enrichment,” *Science & Global Security*, Vol. 17 pp. 132–154, 2009.

-
- 56 E. Blandford and P.F. Peterson, "A Buoyantly-driven Shutdown Rod Concept for Passive Reactivity Control of High Temperature Fluoride Salt-Cooled Reactors," *Nuclear Engineering and Design*, vol. 262, pp. 600-610 (2013).
- 57 Cisneros, 2013, *ibid*.
- 58 S. Chang, A. Gonzalez, J. Kong, and N. Satterlee, "PB-FHR Reserve Shutdown System," University of California, Berkeley, Department of Nuclear Engineering, Report UCBTH-12-008, May 4, 2012.
- 59 Cisneros, 2013, *ibid*.
- 60 S.E. Beall et al., "MSRE Design and Operations Report, Part. V, Reactor Safety Analysis Report," ORNL-TM-732, pp. 47-55, Aug. 11, 1964.
- 61 M.W. Rosenthal, et al., Molten Salt Reactor Program Semiannual Progress Report for the Period Ending August 31, 1969, ORNL-4449, p.16 (1970).
- 62 J.R. McWherter, "Molten Salt Breeder Experiment Design Bases," ORNL-TM-3177, pg. 15, November 1970.
- 63 General Atomics, "Gas Turbine-Modular Helium Reactor (GT-MHR) Conceptual Design Description Report, Report 910720, GA PROJECT NO. 7658, pg. 4-30, July 1996.
- 64 Cisneros, 2013, *ibid*.
- 65 R. O. Scarlat, "Design of Complex Systems to Achieve Passive Safety: Natural Circulation Cooling of Liquid Salt Pebble Bed Reactors," Ph.D. Dissertation, University of California Berkeley, Berkeley, CA, 2012.
- 66 M.W. Rosenthal, et al., Molten Salt Reactor Program Semiannual Progress Report for the Period Ending August 31, 1969 ORNL-4449, p.52-56 (1970).
- 67 Personal communication, James Rushton, Oct. 3, 2013.
- 68 <http://www.specialsteel-forgings.com/steel-products/steel-forgings/rings/seamless-rolled-rings.html> (accessed Oct. 4, 2013)
- 69 http://www.machined-castings.com/rolled_ring.html (accessed Oct. 4, 2013)
- 70 George O. Hayner, "NGNP Conceptual Design, Study: Composites R&D, Technical Issues," INL/EXT-09-16542, pg. 100, October 2008.
- 71 <http://www.bnzmaterials.com/pdf/IFB.pdf>,
- 72 D. J. Naus, "The Effect of Elevated Temperature on Concrete Materials and Structures— A Literature Review," Oak Ridge National Laboratory, NUREG/CR-6900, ORNL/TM-2005/553 (2006).
- 73 D. J. Naus, 2006, *ibid*, pg. 101.
- 74 D. J. Naus, 2006, *ibid*, pg. 98.
- 75 D. J. Naus, 2006, *ibid*, pg. 104.
- 76 M.W. Rosenthal, et al., Molten Salt Reactor Program Semiannual Progress Report for the Period Ending February 28, 1969 ORNL-4396, p. 52 (1969).
- 77 M.W. Rosenthal, et al., Molten Salt Reactor Program Semiannual Progress Report for the Period Ending August 31, 1967 ORNL-4191, p. 65-71 (1967).
- 78 M.W. Rosenthal, et al., Molten Salt Reactor Program Semiannual Progress Report for the Period Ending August 31, 1967 ORNL-4191, Fig. 5-7, p. 70 (1967).
- 79 S. Hong, D. Kazama, H. D. Nguyen, and J. Root, "NE-170 Physical arrangement and structural design for the Mk1 PB-FHR reactor building," Department of Nuclear Engineering, U.C. Berkeley, Report UCBTH-14-003, 2014.

-
- 80 AISC Specification for Safety-Related Steel Structures for Nuclear Facilities, ANSI/AISC N690-12, draft issued for public comment, 2014.
- 81 Nuclear Energy Institute, Methodology for Performing Aircraft Impact Assessments for New Plant Designs, NEI 07-13 REV. 07 Public Version, May 2009.
- 82 “Characterization, Treatment and Conditioning of Radioactive Graphite from Decommissioning of Nuclear Reactors,” International Atomic Energy Agency, IAEA-TECDOC-1521, pg. 40, September 2006.
- 83 M. Fisher, “Fort St. Vrain Decommissioning Project”, Technologies for Gas-Cooled Reactor Decommissioning, Fuel Storage and Waste Disposal’, (Proceedings of an IAEA Technical Committee Meeting Julich, Germany, September 1997), IAEATECDOC-1043, IAEA, Vienna (1998).
- 84 D. T. Ingersoll, et al., “Status of Physics and Safety Analyses for the Liquid-Salt-Cooled Very High-Temperature Reactor (LS-VHTR),” Oak Ridge National Laboratory, ORNL/TM-2005/218 (Draft), pg. 227, September 2005.
- 85 M.W. Rosenthal, P.N Haubenreich, and R.B. Briggs, “The Development Status of Molten-Salt Breeder Reactors,” ORNL Report 4812, pp. 222, August 1972.
- 86 P.V. Gilli, K. Fritz, J.M. Lippitsch, and G. Lurf, “Radial-Flow Heat Exchanger,” U.S. patent number 3712370, filing date Sept. 22, 1970, issue date January 23, 1973.
- 87 U.S. Nuclear Regulatory Commission, “Standard Review Plan, Section 5.4.2.2, Steam Generator Program,” NUREG-0800, Rev. 2, March, 2007.
- 88 P.F. Peterson and H. Zhao, “A Flexible Baseline Design For the Advanced High Temperature Reactor Utilizing Metallic Reactor Internals (AHTR-MI),” 2006 International Congress on Advances in Nuclear Power Plants (ICAPP '06), Reno, NV, Table 4, June 4-8, 2006.
- 89 G. Buster, N. Pardede, and T. Phan, “NE-170 Design, manufacture, modeling and testing of 316 SS diffusion bonded tube sheet joints for the Mk1 PB-FHR CTAHs,” Department of Nuclear Engineering, U.C. Berkeley, Report UCBTH-14-005, 2014.
- 90 R. B. Briggs, Molten Salt Reactor Program Semiannual Progress Report for the Period Ending January 31, 1963, ORNL-3419, p.65 (1963).
- 91 <http://www.arcmachines.com/industries-served/semiconductor/small-diameter-tubing> (accessed Oct. 1, 2013).
- 92 G. Buster, et al., 2014, *ibid.*
- 93 R.B. Briggs, “Molten-Salt Reactor Program Quarterly Progress Report For Period Ending August 31, 1966,” ORNL-4037, pg. 42 (1967).
- 94 L. E. McNeese, “Molten-Salt Reactor Program Semiannual Progress Report for the Period Ending February 29, 1976,” Oak Ridge National Laboratory, Oak Ridge, Tennessee, ORNL-5132, pg. 20, 1976.
- 95 R.E. Thoma, “Chemical Aspects of MSRE Operations,” ORNL-4658, p. 116 (1971).
- 96 IAEA, “Construction Technologies for Nuclear Power Plants,” International Atomic Energy Agency, Nuclear Energy Series No. NP-T-2.5, Vienna, pg. 60, 2011.
- 97 S. Fazluddin, K. Smit, and J. Slabber, “The Use of Advanced Materials in VHTR’s,” 2nd International Topical Meeting on High Temperature Reactor Technology, Paper E06, Beijing, China, Sept. 22-24, 2004.
- 98 <http://www.leedsvalve.com/Refractory-Lined-Butterfly-Valve.pdf>

-
- 99 C. Andreades, L. Dempsey, and P.F. Peterson, "Reheat Air-Brayton Combined Cycle (RACC) Power Conversion Off-Nominal and Transient Performance," *ASME Journal of Engineering for Gas Turbines and Power*, vol. 136, No. 7, doi:10.1115/1.4026612 (2014).
 - 100 A. T. Cisneros, "Development of Depletion Analysis Methods and Design Optimization Methods for Pebble Bed Reactors Applied to the Design of the Pebble Bed Fluoride Salt Cooled High Temperature Reactor (PB-FHR)," Ph.D. dissertation, University of California Berkeley, Berkeley, CA, Fig. 5-10, pg. 206, 2013.
 - 101 G. Cao, et al., "Fluoride-Salt-Cooled High Temperature Reactor (FHR) Materials, Fuels and Components White Paper: Integrated Research Project Workshop 3," U.C. Berkeley, UCBTH-12-003, Section 6.1, July 2013.
 - 102 P.J. Pappano and M.R. Rogers, "Method for producing dustless graphite spheres from waste graphite fines," US Patent 8173208, May 8, 2012.
 - 103 L.E. McNeese, "Semi-annual Progress Report for Period Ending August 31, 1974," Oak Ridge National Laboratory, ORNL-5011, pg. 30, 1974.
 - 104 R. B. Briggs, "Tritium In Molten-Salt Reactors," *Reactor Technology*, Vol. 14, No. 4, pp. 335-342, Winter 1971-1972.
 - 105 M.W. Rosenthal, "Molten-Salt Reactor Program Quarterly Progress Report For Period Ending February 28, 1970," ORNL-4548, pg. 10 (1970).
 - 106 M.W. Rosenthal, "Molten-Salt Reactor Program Quarterly Progress Report For Period Ending August 31, 1970," ORNL-4622, pg. xvii (1971).
 - 107 G.W. Hollenberg, E.P. Simonen, G. Kalinin, and A. Terlain, "Tritium/hydrogen barrier development," *Fusion Engineering and Design*, vol. 28, pp. 190-208 (1995).
 - 108 R. A. Causey, R. A. Karnesky, and C. S. Marchi, "Tritium Barriers and Tritium Diffusion in Fusion Reactors," *Comprehensive Nuclear Materials*, 2010, 511–549.
 - 109 G.W. Hollenberg, E.P. Simonen, G. Kalinin, and A. Terlain, "Tritium/hydrogen barrier development," *Fusion Engineering and Design*, vol. 28, pp. 190-208 (1995).
 - 110 <http://www.kantal.com/en/products/material-datasheets/strip/kanthal.af/>
 - 111 <http://www.kantal.com/en/products/material-datasheets/strip/alkrothal-14/>
 - 112 J.D. Fowler, D. Chandra, T.S. Elleman, A.W. Payne, and K. Verghese, "Tritium Diffusion in Al₂O₃ and BeO," *Journal of The American Ceramic Society*, Vol. 60, pp. 155-161, 1977.
 - 113 J. T. Bell, J. D. Redman, and H. F. Bittner, "Tritium Permeation Through Clean Incoloy 800 and Sanicro 31 Alloys and Through Steam Oxidized Incoloy 800," *Metallurgical Transactions A*, Vol. 11A, pp. 775-782, May 1980.
 - 114 P. Calderoni, P. Sharpe, M. Hara, Y. Oya, "Measurement of tritium permeation in flibe (2LiF-BeF₂)" *Fusion Engineering and Design*, v 83, n 7-9, p 1331-1334, December 2008.
 - 115 D. Caron, et al., "A Modular Pebble-Bed Advanced High Temperature Reactor," NE-170 Senior Design Project, UC Berkeley Thermal Hydraulics Laboratory, Report UCBTH-08-001, May 16, 2008.
 - 116 B. Keller, University of Wisconsin, personal communication, Sept. 13, 2013.
 - 117 C. Forsberg, MIT, personal communication, Oct. 6, 2013.
 - 118 L.E. McNeese, "Molten-Salt Reactor Program Quarterly Progress Report For Period Ending February 29, 1976," ORNL-5132, pg. 197 (1976).
 - 119 B. Kelleher, U.W. Madison, personal communication, Oct. 14, 2013.
 - 120 David Holcomb, Oak Ridge National Laboratory, personal communication, May 7, 2014.

-
- 121 M.W. Rosenthal, R.B. Briggs, and P.N. Haubenreich, "Molten-Salt Reactor Program: Semiannual Progress Report Period Ending August 31, 1971," Oak Ridge National Laboratory, ORNL-4728, Table 15.1, February 1972.
 - 122 M.W. Rosenthal, R.B. Briggs, and P.N. Haubenreich, "Molten-Salt Reactor Program: Semiannual Progress Report Period Ending February 28, 1971," Oak Ridge National Laboratory, ORNL-4676, Chapter 11, "Chemistry of Molten-Salt Reactor Fuel Technology, Section 1 Extraction of Rubidium and Cesium From BSBR Fuel Solvent into Bismuth by Reduction with Lithium at 650°C," p.129, August 1971.
 - 123 L.E. McNeese, "Semi-annual Progress Report for Period Ending August 31, 1974," Oak Ridge National Laboratory, ORNL-5011, pg. xiii, 1974.
 - 124 R.E. Thoma, "Chemical Aspects of MSRE Operations," ORNL-4658, p. 117 (1971).
 - 125 H. G. MacPherson, "Molten Salt Reactor Quarterly Progress Report for Period Ending January 31, 1958," Oak Ridge National Laboratory, ORNL-2474, pg. 99, 1958.
 - 126 H. G. MacPherson, "Molten Salt Reactor Quarterly Progress Report for Period Ending July 31, 1960," Oak Ridge National Laboratory, ORNL-3014, pg. 79-80, 1960.
 - 127 R.B. Briggs, "Molten Salt Reactor Quarterly Progress Report for Period from August 1, 1960 to February 28, 1961," Oak Ridge National Laboratory, ORNL-3122, pg. 96-97, 1961.
 - 128 V.G. Ivanchenko, "Phase equilibria and stability of the phase composition in chromium alloys with interstitial phases," *Powder Metallurgy and Metal Ceramics*, Vol. 35, 1996.
 - 129 E.L. Compere et al., "Fission Product Behavior in the Molten Salt Reactor Experiment," ORNL-4865, pg. 12 (1975),
 - 130 R. S. Sellers, Impact of Reduction-Oxidation Agents on the High Temperature Corrosion of Materials in LiF-NaF-KF," Masters Thesis, University of Wisconsin, Madison, 2012.
 - 131 S. Cantor, "Density and Viscosity of Several Molten Fluoride Mixtures," ORNL-TM-4308, pg. 9, 16-17 (1973).
 - 132 W.R. Grimes, "Molten-Salt Reactor Chemistry," Nuclear Applications and Technology, Vol. 8, pp. 137-155, 1970.
 - 133 A. Cisneros, et al., "Fluoride-Salt-Cooled, High-Temperature Reactor (FHR) Methods and Experiments Program White Paper," Department of Nuclear Engineering, U.C. Berkeley, Report UCBTH-12-002, May, 2013.
 - 134 M.W. Rosenthal, et al., Molten Salt Reactor Program Semiannual Progress Report for the Period Ending August 31, 1969, ORNL-4449, pp.168-170 (1970).
 - 135 B. Badro, C. Bailey, S. Kaplan, H. Lee, and M. Malek, "NE-170 Applications of Finite Element Modeling (FEM) and Experiments to Study the Mk1 PB-FHR Center Reflector," Department of Nuclear Engineering, U.C. Berkeley, Report UCBTH-14-004, 2014.
 - 136 D. Kovan, "Torness tackles biggest-ever outage," Nuclear News, pg. 43-48, April 2014.
 - 137 J. W. Koger, "Alloy Compatibility with LiF-BeF₂ Salts Containing ThF₄ AND UF₄," Oak Ridge National Laboratory, ORNL-TM-4286, December 1972.
 - 138 James Rushton, personal communication, October 6, 2013.
 - 139 J. R. Keiser, J. H. DeVan, and D. L. Manning, The Corrosion Resistance of 316 Stainless Steel to Li₂BeF₄," Oak Ridge National Laboratory, ORNL/TM-5782, April, 1977.
 - 140 "Material, Fabrication and Repair Considerations for Austenitic Alloys Subject to Embrittlement and Cracking in High Temperature 565 - 760°C (1050 – 1400°F) Refinery

-
- Services,” American Petroleum Institute, Draft API Technical Report (TR) 942-B, Rev B (Sept. 5, 2012).
- 141 J. Hau and A. Seijas, “Sigma Phase Embrittlement of Stainless Steel in FCC Service,” Corrosion NACEpo 2006, Paper No. 06578, 2006.
- 142 Y. Minami, H. Kimura, and Y. Ihara, “Microstructural changes in austenitic stainless steels during long-term aging,” *Materials Science and Technology*, Vol. 2, pp. 795-795, August 1986.
- 143 Y. Minami, et al., 1986, *ibid*.
- 144 Westinghouse, “NGNP and Hydrogen Production Preconceptual Design Report,” Westinghouse Electric Company, NNGP-IN-RPT-001, May 2007.
- 145 H.-W. Chi, “PBMR - Fuel Handling and Storage System (FHSS),” U.S. Nuclear Regulatory Commission, ML021960042, Sep. 2001.
- 146 J. G. Liu, H. L. Xiao, and C. P. Li, “Design and Full Scale Test of the Fuel Handling System,” *Nuclear Engineering and Design*, vol. 218, pp. 169–178, 2002.
- 147 H.-W. Chi, *ibid*.
- 148 J. G. Liu et. al., 2001, *ibid*.
- 149 IAEA, “Advances in High Temperature Gas Cooled Reactor Fuel Technology,” International Atomic Energy Agency, IAEA-TECDOC-CD-1674, pp. 240-256, 2012.
- 150 Westinghouse, “NGNP and Hydrogen Production Preconceptual Design Report,” Westinghouse Electric Company, NNGP-IN-RPT-001, May 2007.
- 151 IAEA, 2012, *ibid*.
- 152 M. Spencer, New Westinghouse safety system OK’d by the feds,” Sept. 19, 2013, <http://www.bizjournals.com/pittsburgh/blog/energy/2013/09/new-westinghouse-safety-system-okd-by.html>.
- 153 E. Blandford and P.F. Peterson, “A Buoyantly-driven Shutdown Rod Concept for Passive Reactivity Control of High Temperature Fluoride Salt-Cooled Reactors,” *Nuclear Engineering and Design*, vol. 262, pp. 600-610 (2013).
- 154 H. M. Hashemian and A. Kadri, “Wireless Technology Applications in Nuclear Power Plants,” presentation to the 23rd Biennial Meeting of the Technical Working Group of Nuclear Power Plant Instrumentation and Control (TWG-NPPIC), May 24-26, 2011.
- 155 C. Andreades, R.O. Scarlat, L. Dempsey, and P.F. Peterson, “Reheat Air-Brayton Combined Cycle (RACC) Power Conversion Design and Performance Under Nominal Ambient Conditions,” *ASME Journal of Engineering for Gas Turbines and Power*, vol. 136, No. 6, doi:10.1115/1.4026506 (2014).
- 156 C. Andreades, L. Dempsey, and P.F. Peterson, “Reheat Air-Brayton Combined Cycle (RACC) Power Conversion Off-Nominal and Transient Performance,” *ASME Journal of Engineering for Gas Turbines and Power*, vol. 136, No. 7, doi:10.1115/1.4026612 (2014).
- 157 S. R. Greene, et al., “Pre-Conceptual Design of a Fluoride- Salt-Cooled Small Modular Advanced High-Temperature Reactor (SmAHTR), Oak Ridge National Laboratory, ORNL/TM-2010/199, Fig. 8-1, p. 8-2, December 2010.
- 158 Turkey Point Units 6 & 7 COL Application Part 2 — FSAR 2.2-i Revision 5, Section 2.2: Nearby Industrial, Transportation, and Military Facilities, <http://pbadupws.nrc.gov/docs/ML1335/ML13357A337.pdf>.
- 159 James Rushton, personal communication, May 10, 2014.

-
- 160 F. Eltawila, letter to Kevin Borton, Excelon Generation, “Request for Additional Information (RAI) Related to Excelon’s March 15, 2002, Document Titled ‘Proposed Licesning Approach for the Pebble Bed Modular Reactor (PBMR) in the United States,’” dated June 3, 2002, <http://pbadupws.nrc.gov/docs/ML0215/ML021540306.pdf>.
- 161 F. Eltawila, letter to Kevin Borton, Excelon Generation, “Request for Additional Information (RAI) on High Temperature Materials Graphite; Control of Chemical Attack; and Design Codes and Standards for the Pebble Bed Modular Reactor (PBMR),” dated May 31, 2002, <http://pbadupws.nrc.gov/docs/ML0215/ML021510521.pdf>.
- 162 F. Eltawila, letter to Kevin Borton, Excelon Generation, “Request for Additional Information (RAI) on Analytical Codes and Software Control; Core Design and Heat Removal and; Operational Modes and States for the Pebble Bed Modular Reactor (PBMR),” dated May 31, 2002, <http://pbadupws.nrc.gov/docs/ML0215/ML021510354.pdf>.
- 163 F. Eltawila, letter to Kevin Borton, Excelon Generation, “Request for Additional Information (RAI) on Pebble Bed Modular Reactor (PBMR) Nuclear Fuel; Fuel Fabrication Quality Control Measures and Performance Monitoring Plans and; PBMR Fuel Qualification Test Program,” dated June 27, 2002, <http://pbadupws.nrc.gov/docs/ML0217/ML021790445.pdf>.
- 164 A. Cisneros, et al., “Fluoride-Salt-Cooled, High-Temperature Reactor (FHR) Subsystems Definition, Functional Requirement Definition, and Licensing Basis Event (LBE) Identification White Paper,” Department of Nuclear Engineering, U.C. Berkeley, Report UCBTH-12-001, August 2013.
- 165 A. Cisneros, et al., “Fluoride-Salt-Cooled, High-Temperature Reactor (FHR) Methods and Experiments Program White Paper,” Department of Nuclear Engineering, U.C. Berkeley, Report UCBTH-12-002, May, 2013.